University of Minnesota
St. Anthony Falls Hydraulic Laboratory

Project Report No. 329

Water Temperature Characteristics of Lakes Subjected to Climate Change

by

Midhat Hondzo

and

Heinz G. Stefan

Prepared for

ENVIRONMENTAL RESEARCH LABORATORY
U.S. ENVIRONMENTAL PROTECTION AGENCY
Duluth, Minnesota

August 1992
Minneapolis, Minnesota

Abstract

A deterministic, one dimensional, unsteady lake water temperature model was modified and validated to simulate the seasonal (spring to fall) temperature stratification structure over a wide range of lake morphometries, trophic and meteorological conditions. Model coefficients related to hypolimnetic eddy diffusivity, light attenuation, wind sheltering, and convective heat transfer were generalized using theoretical and empirical extensions.

Propagation of uncertainty in the lake temperature model was studied using a vector state-space method. The output uncertainty was defined as the result of deviations of meteorological variables from their mean values. Surface water temperatures were affected by uncertain meteorological forcing. Air temperature and dew point temperature fluctuations had significant effects on lake temperature uncertainty. The method presents a useful alternative for studying long-term averages and variability of the water temperature structure in lakes due to variable meteorological forcing.

The lake water temperature model was linked to a daily meteorological data base to simulate daily water temperature in several specific lakes as well as 27 lake classes characteristic for the north central US. Case studies of lake water temperature and stratification response to variable climate were made in a particularly warm year (1988) and a more normal one (1971). A regional analysis was conducted for 27 lake classes over a period of twenty-five years (1955–1979). Output from a global climate model (GISS) was used to modify the meteorological data base to account for a doubling of atmospheric CO_2. The simulations predict that after climate change: 1) epilimnetic water temperatures will be higher but will increase less than air temperature, 2) hypolimnetic temperatures in seasonally stratified dimictic lakes will be largely unchanged and in some cases lower than at present, 3) evaporative water loss will be increased by as much as 300 mm for the open water season, 4) onset of stratification will occur earlier and overturn will occur later in the season, and 5) overall lake stability will become greater in spring and summer.

Preface

This study addresses the question of how lake water temperatures respond to climate and climate changes. The study is conducted by model simulation. The chapters of this study are a collection of papers or manuscripts previously published or submitted for publication in professional journals. Each chapter has its own abstract and conclusions. Each chapter of this study deals with a subquestion of the problem.

Table of Contents

List of Figures

List of Tables

Acknowledgements

We are grateful to the U.S. Environmental Protection Agency, Office of Program Planning and Evaluation, Washington, D. C. and Environmental Research Laboratory—Duluth, Minnesota; and the International Student Work Opportunity Program (ISWOP), University of Minnesota for support of this study.

Staff members of the Environmental Research Laboratory, Duluth, provided information, constructive comments, and suggestions for the study. Special thanks goes to John Eaton, Kenneth Hokanson, Howard McCormick, and Brian Goodno. Finally we wish to thank those who provided field data for the study, especially Dennis Schupp and David Wright (Minnesota Department of Natural Resources), Richard Osgood (Metropolitan Council), Donald Baker, David Rushee (Soil Science Department University of Minnesota), Roy Janne, Dennis Joseph (Center for Atmospheric Research, Boulder), and Tom Winter (U.S. Geological Survey).

Last but not least, we extend our gratitude to members of the SAFHL research staff for assistance and support.

1. Introduction and Literature Review

1.1 Introduction

The concentrations of some gases (CO_2, H_2O, N_2O, CH_4) have been increasing in the atmosphere (Bolin and Doos, 1986; NRC, 1982; 1983; Houghton et al., 1990). These commonly called "greenhouse gases" are absorbing and reradiating energy at both long and short wavelengths. As a consequence, greenhouse gases are able to affect global climate possibly resulting in global mean warming of the earth's terrestrial and aquatic surface and the lower atmosphere (Bolin and Doos, 1986; NRC, 1982; 1983; Wanner and Siegenthaler, 1988; Waggoner, 1990).

Special attention has been paid to the increase of carbon dioxide because it is estimated that about half of the temperature change is due to the increase of atmospheric CO_2 alone. Mathematical models of global climate change lead to the conclusion that the increase in mean global equilibrium surface temperature for a doubling of CO_2 is most likely to be in the range of 1.5 to 5.5°C (Bolin and Doos, 1986, Waggoner, 1990). One of the uncertainties is due to the transfer of increased heat into the oceans (NRC, 1982; 1983, Waggoner, 1990). Surely due to their high heat capacity, oceans will act as a sink for heat and delay the warming.

The question which we want to address in this report is how freshwater lake temperatures respond to atmospheric conditions. Changes in lake water temperatures and temperature stratification dynamics may have a profound effect on lake ecosystems (Meisner et al., 1987; Coutant, 1990; Magnuson et al. 1990; Chang et al., 1992). Dissolved oxygen, nutrient cycling, biological productivity, and fisheries may be severely affected through temperature changes.

Considerable effort has gone into global climatological modeling with the objective to specify future climatic conditions in a world with high greenhouse gases. Some models use statistical analysis of past climatological data in order to provide analogies for future climatological changes. Unfortunately, all causes of past climate changes are not fully understood (Bolin and Doos, 1986; Waggoner, 1990), and predictions of future climates are difficult, especially on a regional basis. Nevertheless simulated climate conditions are and will be used in numerous effect studies. Another approach to finding both climatic trends and their effects is to examine long-term records. In few lakes, e.g. in the experimental lake area (ELA) in Ontario, Canada, weekly or biweekly vertical profiles of water quality and biological parameters have been collected over periods of 20 or more years and these records reveal e.g. rising average surface water temperatures, shorter ice cover periods, etc. (Schindler et al., 1990). A data record of more than 100 years for Lake Mendota was analyzed by Robertson (1989) and Magnuson et al. (1990).

To make generalizations to lakes of different geometries and latitudes, and to extrapolate to possible future climates, numerical simulation models (McCormick, 1990; Robertson and Ragotzkie, 1990) are useful. Herein the use of such a model is demonstrated by application to morphometrically different lakes with sparse data sets. The lakes are located near 45° northern latitude and 93° western longitude in the northcentral United States.

1.2 Previous Temperature Prediction Model

A one-dimensional lake water quality model, which has been successfully applied to simulate hydrothermal processes in different lakes and for a variety of meteorological conditions (Stefan and Ford, 1975; Stefan et al., 1980a; Ford and Stefan, 1980) was used in this study. The model was previously expanded to include suspended sediment (Stefan et al., 1982), light attenuation (Stefan et al., 1983), phytoplankton growth and nutrient dynamics (Riley and Stefan, 1987). Only the hydrothermal part of the model was applied in this study.

1.2.1 Model formulation

In the model the lake is described by a system of horizontal layers, each of which is well mixed. Vertical transport of heat is described by a diffusion equation in which the vertical diffusion coefficient $K_z(z)$ is incorporated in a conservation equation of the form:

$$A \frac{\partial T}{\partial t} = \frac{\partial}{\partial z} \left(K_z A \frac{\partial T}{\partial z}\right) + \frac{H}{\rho_w c_p} \tag{1.1}$$

where T(z,t) is water temperature as a function of depth (z) and time (t), A(z) is the horizontal area of the lake as a function of depth, H(z,t) is the internal distribution of heat sources due to radiation absorption inside the water column, ρ_w is the water density, and c_p is the specific heat of water.

The vertical temperature profile in the lake is computed from a balance between incoming heat from solar and longwave radiation and the outflow of heat through convection, evaporation, and back radiation. The net increase in heat results in an increase in water temperature. The heat balance equation (see also Fig. 1.1) is given by

$$H_n = H_{sn} + H_a + H_c + H_e + H_{br} \tag{1.2}$$

where H_n is net heat input at the water surface (kcal $m^{-2}day^{-1}$), H_{sn} is net solar (short wave) radiation, H_a is atmospheric long wave radiation, H_c is conductive loss (sensible heat), H_e is evaporative loss (latent heat), and H_{br} is back radiation. The heat budget components in equation (1.2) are computed as follows:

$$H_{sn} = (1 - r)(1 - \beta)H_s \tag{1.3}$$

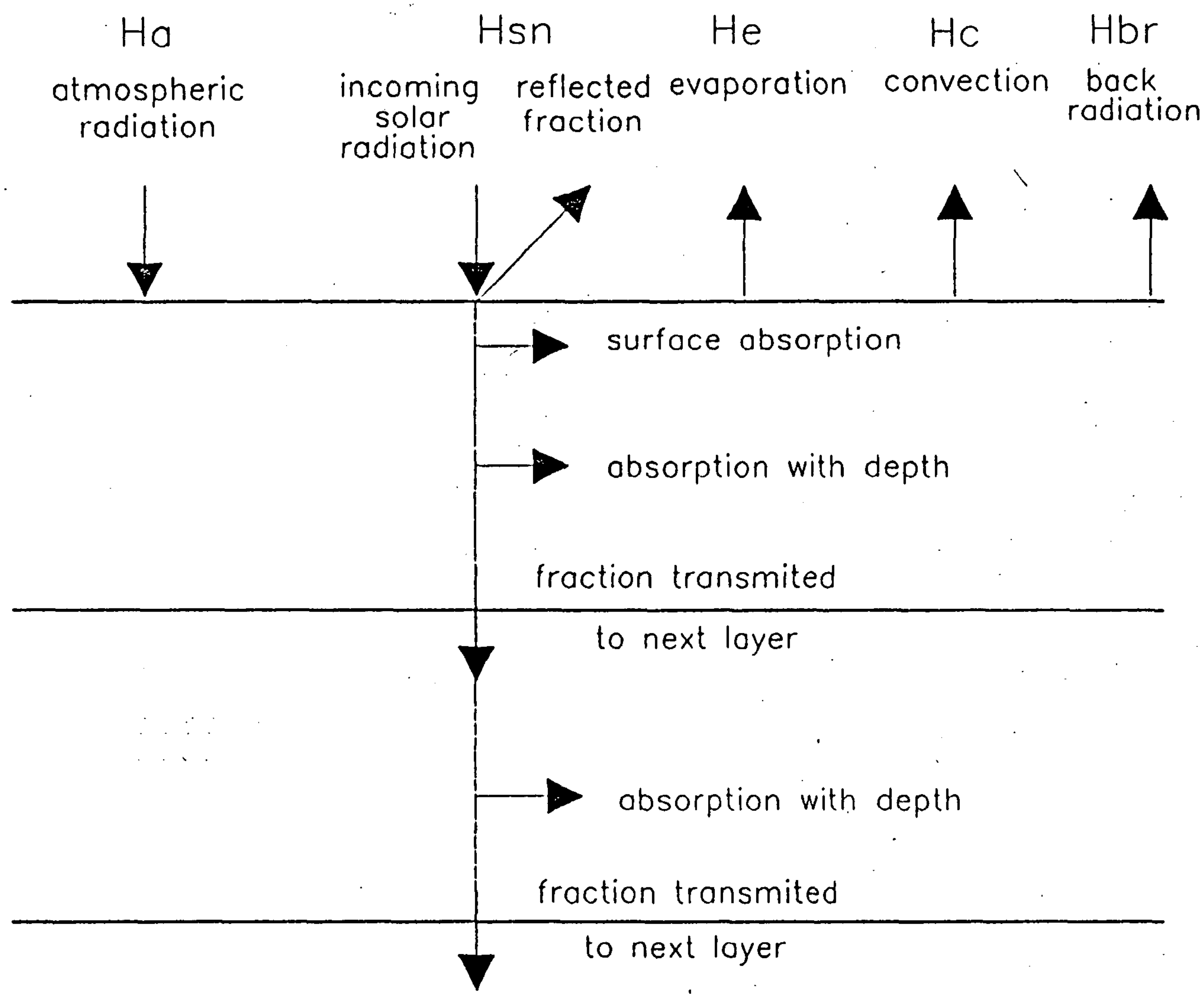

Fig. 1.1 Schematic diagram of source and sink terms in the heat budget model.

where H_s is incoming solar radiation (kcal $m^{-2}day^{-1}$), r is the reflection coefficient computed as a function of the angle of incidence and the concentration of suspended sediment in the surface layer (Dhamotharan, 1979; Stefan et al., 1982). β is the surface absorption factor (Dake and Harleman, 1969). The attenuation of solar radiation with depth follows Beer's law:

$$H_{sn}(i) = H_{sn}(i-1)\ \exp(-\mu\ \Delta z) \tag{1.4}$$

where $H_{sn}(i-1)$ is solar radiation at the top of a horizontal layer of water (kcal $m^{-2}day^{-1}$), $H_{sn}(i)$ is solar radiation at the bottom of a layer, Δ is thickness of a layer (m), μ is the extinction coefficient (m^{-1})

$$\mu = \mu_w + \mu_{ss}\cdot SS + \mu_{ch}Chla \tag{1.5}$$

where μ_w is the extinction coefficient of lake water (m^{-1}), μ_{ss} is the specific extinction coefficient due to suspended sediment (l $m^{-1}mg^{-1}$); SS is suspended inorganic sediment concentration (mg l^{-1}); μ_{ch} is the extinction coefficient due to chlorophyll ($m^2 \cdot g^{-1}$Chla)(Bannister, 1974), Chla is chlorophyll-a concentration (g m^{-3}).

$$H_a = \sigma\ \epsilon_a\ T_a^4 \tag{1.6}$$

where σ is Stefan-Boltzmann constant, T_a is absolute temperature (°K), ϵ_a is atmospheric emissivity (Idso and Jackson, 1969). Back radiation H_{br} follows the same formulation (6), but the emissivity is fixed at 0.975, and atmospheric temperature is replaced by water surface temperature T_s .

Aerodynamic bulk formulae were used to calculate surface wind shear τ, latent heat flux H_e, and the sensible heat flux H_c across the water surface (Keijman, 1974; Ford and Stefan, 1980; Strub and Powell, 1987; Sadhyram et al., 1988):

$$\tau = \rho_a\ \overline{u'\omega'} = \rho_a u_*^2 = \rho_a C_d\ U_a^2 \tag{1.7}$$

$$H_c = \rho_a c_p\ \overline{\theta'\omega'} = \rho_a c_p C_s u_*\ \theta_* = \rho_a c_p f(U_a)(T_s - T_a) \tag{1.8}$$

$$H_e = \rho_a L_v\ \overline{q'\omega'} = \rho_a L_v C_\ell q_* u_* = \rho_a L_v f(U_a)(q_s - q_a) \tag{1.9}$$

where τ is the surface wind stress, ρ_a is the density of the air, u' and ω' are turbulent fluctuations of velocity in horizontal and vertical direction; the overbar represents a time average; u_* is a velocity scale, U_a is the wind speed above the water surface, C_d is the momentum or drag coefficient (Wu, 1969),
θ' is turbulent fluctuation in temperature, θ_* is a temperature scale, C_s and C_ℓ are heat transfer and vapor transfer coefficients, respectively, and together

with u_* are expressed as a function of wind speed, $f(U_a)$, (Ford, 1976), T_s is water surface temperature, T_a air temperature above the water surface, L_v is latent heat of vaporization, q' is the specific humidity fluctuation, q_* is the specific humidity scale, q_a is the specific humidity above the water surface, q_s is the specific humidity at saturation pressure at the water surface temperature.

Turbulent kinetic energy supplied by wind shear and available for possible entrainment at the interface was estimated (Ford and Stefan, 1980) by

$$TKE = W_{str} \int_{A_s} U_* \, \tau \, dA \tag{1.10}$$

where A_s is lake surface area (m^2), U_* is shear velocity in the water (m day^{-1}), and W_{str} is the wind sheltering coefficient.

The model distributes the surface heat input in the water column using turbulent diffusion (Eq. 1) in response to wind and natural convection (Ford and Stefan, 1980). The numerical model is applied in daily timesteps using mean daily values for the meteorological variables. Initial conditions, model set-up parameters, and daily meteorological variables average air temperature (T_a), dew point temperature (T_d), precipitation (P), wind speed (U_a), and solar radiation (H_s) have to be provided to use the model.

1.2.2 Model coefficients

Model calibration coefficients needed for simulations of lake water temperatures are given in Table 1.1. These coefficients are kept at their initially specified value throughout the entire period of the simulation.

Table 1.1 List of calibration coefficients with ranges used in previous simulations.

Coefficient	Symbol	Units	Range of values: Previous Simulations	Range of values: Literature Values
Radiation extinction by water	μ_w	(m^{-1})	0.4–0.65	0.02–2.0
Radiation extinction by chlorophyll	μ_{ch}	($m^2\ g^{-1}$ Chla)	8.65–16.0	0.2–31.5
Wind sheltering	W_{str}	(–)	0.1–0.9	0.1–1.0
Wind function coefficient	c	(–)	20.0–30.0	20.0–30.0
Maximum hypolimnetic eddy diffusivity	K_{zmax}	($m^2\ day^{-1}$)	0.1–2.0	0.086–8.64

Radiation extinction coefficients by water (μ_w) *and chlorophyll* (μ_{ch}) specify the rate of attenuation of short-wave radiation energy as it penetrates through the water column. Both coefficients vary as a function of the wavelength. Usually these coefficients are reported by a single mean spectral value for a given lake. Smith and Baker (1981) measured a range of 0.02–2.0 (m^{-1}) for μ_w as a function of the wavelength. Values of μ_w in the range of 0.68 ± 0.35 (m^{-1}) have been reported by Megard et al. (1979). Chlorophyll extinction coefficient is species dependent. Values in the range of the 0.2–31.4 (m^2 g^{-1} Chla) with a mean spectral value of 16.0 have been reported by Bannister (1979; 1974) for μ_{ch} while Megard et al. (1979) reported values of 22 ± 5 (m^2 g^{-1} Chla) for the photosynthetically active radiation.

The wind sheltering coefficient (W_{str}) determines the fraction of turbulent kinetic energy from the wind applied at the lake surface and available for mixing. The coefficient can range from 0.1 to 1.0 depending on the size of the lake and the terrain surrounding the lake. The coefficient defines the "active" portion of the lake surface area on which wind shear stress contributes to the turbulent kinetic energy.

The wind function coefficient is defined for the neutral boundary layer above the lake surface. This condition occurs for the case of negligible atmospheric stratification. The wind speed function used is linear with the wind speed

$$f(U_a) = c\ U_a \tag{1.11}$$

where c is defined as a wind function coefficient. The atmosphere above natural water bodies is often nearly neutrally stable. A significant amount of experimental and theoretical research has been done in regard to wind function coefficient estimation (e.g. Dake, 1972, Ford, 1976, Stefan et al., 1980b, Adams et al., 1990). Different ranges of coefficients were reported depending on measurement location of the windspeed U_a relative to the lake surface. Herein the wind function coefficient is taken to be in the range 20–30 if wind speed is in mi h^{-1}, vapor pressure in mbar, and heat flux in kcal $m^{-2}day^{-1}$.

Maximum hypolimnetic eddy diffusivity is the threshold value for the turbulent diffusion under negligible stratification. In modeling this condition is assumed to be satisfied by small stability frequency e.g. $N^2 = 7.5*10^{-5}$ sec^{-2}. Maximum hypolimnetic eddy diffusivity ranges from 8.64 m^2 day^{-1} for large lakes (Lewis, 1983) to 0.086 m^2 day^{-1} for small lakes (Appendix A).

1.3 Overview of Study

The goal of this study is to develop an understanding of how freshwater lake temperatures respond to atmospheric conditions.

Chapter 2 presents the regional lake water temperature model development and validation. The lake water temperature model, which was originally developed for particular lakes and particular years has been generalized to a wide range of lake classes and meteorological conditions.

Chapter 3 presents a first order analysis of uncertainty propagation in lake temperature models. The source of the uncertainty is variable meteorological forcing which enters the lake temperature equations through the source term and boundary conditions. The analysis presents a useful alternative for the study of long-term averages and variability of temperature structures in lakes due to variable meteorological forcing.

Chapter 4 presents a lake water temperature model application to a particularly warm year (1988) and a normal year (1971) for comparison. The comparison is made for morphometrically different lakes located in the north central US. The analysis was a first step in quantifying potential thermal changes in inland lakes due to climate change.

Chapter 5 presents a lake water temperature model application to a representative range of lakes in Minnesota for past climate and a future climate scenario associated with doubling of atmospheric CO_2. Emphasis was on long term behavior and a wide range of lake morphometries and trophic levels. The base weather period (or reference) was for the years from 1955–1979. For future climate scenario the daily weather parameters were perturbed by the $2XCO_2$ GISS climate model output. The simulation results showed how water temperatures in different freshwater lakes responded to changed atmospheric conditions in a region.

Chapter 6 summarizes the results of the study.

2. Regional Lake Water Temperature Simulation Model Development

A lake water temperature model was developed to simulate the seasonal (spring to fall) temperature stratification structure over a wide range of lake morphometries, trophic and meteorological conditions. Model coefficients related to hypolimnetic eddy diffusivity, light attenuation, wind sheltering, and convective heat transfer, were generalized using theoretical and empirical model extensions. The new relationships differentiate lakes on a regional rather than individual basis. First order uncertainty analysis showed moderate sensitivity of simulated lake water temperatures to model coefficients. The proposed regional numerical model which can be used without calibration has an average 1.1°C root mean square error, and 93% of measured lake water temperatures variability is explained by the numerical simulations, over wide ranges of lake morphometries, trophic levels, and meteorological conditions.

2.1 Introduction

Changes in meteorological variables in the future "greenhouse" atmospheric conditions are usually specified through the global climate change models output on a regional rather than a local scale. Usually water temperature data are only available for a few lakes, not necessarily for "typical" lakes in order to calibrate lake water temperature model and to validate predictions. Some coefficients such as eddy diffusion coefficients or turbulence closure coefficients used in lake water temperature models are not universal due to their dependence on stratification, and the longer than subdaily time step of the simulations (Aldama et al., 1989).

The purpose of this chapter is to describe how a lake temperature model, which was described in Chapter 1, and which was initially developed for particular lakes and particular meteorological years, could be generalized to a wide range of lake classes and meteorological conditions. To do this, new functional relationships had to be introduced for the calibration coefficients which differentiate lakes on a regional rather than an individual basis. The generalized model can than be applied to lakes for which no measurements exist. Fortunately it can be demonstrated that the regional model makes prediction almost with the same order of accuracy as the validated previous calibrated to particular lakes. Therefore regional and long term lake temperature structure modeling rather than short time behavior of particular lakes can be accomplished with same confidence.

2.2 Model Generalization

In order to apply the lake water temperature numerical model to lakes for which there are no measurements, the model has to be generalized. This was accomplished by introducing functional relationships for the model coefficients which are valid for lakes on a regional rather than individual basis.

2.2.1 Hypolimnetic diffusivity closure

Although the hypolimnion is isolated from the surface (epilimnetic) layer by the thermocline and its associated density gradient, strong and sporadical local mixing events have been observed in the hypolimnion (Jassby and Powell, 1975; Imberger, 1985; Imberger and Patterson, 1989). Heat flux between water and lake sediments was found to be important in eddy diffusivity estimation for inland shallow (10 m maximum depth) lakes, representative for north central United States (Appendix A). Hypolimnetic eddy diffusivity dependence on stratification strength measured by buoyancy frequency has been pointed out consistently (Quay et al., 1980; Gargett, 1984; Gargett and Holloway 1984; Colman and Amstrong, 1987; Appendix A). Stability frequency is related to hypolimnetic eddy diffusivity by :

$$K_z = \alpha\,(N^2)^{\gamma} \tag{2.1}$$

where stability frequency $N^2=-(\partial\rho/\partial z)(g/\rho)$, in which ρ is density of water, and g is acceleration of gravity, γ is determined by the mode of turbulence production (narrow or broad band internal waves, local shear etc.), and α is determined by the general level of turbulence. For most inland lakes, coefficient γ ranges from 0.4 to 0.6 (Jassby and Powell, 1975; Quay et al., 1980; Gerhard et al., 1990; Ellis and Stefan, 1991, Appendix A).

Hypolimnetic eddy diffusivity estimations in five northern Minnesota lakes follow Eq. 2.1 as shown in Fig. 2.1. Lakes were selected from the regional prospective i.e. with different surface areas and maximum depths. Dimensionless analysis (Ward, 1977) suggests that lake surface area can provide the horizontal scale for the vertical eddy diffusivity estimation. The vertical scale (lake depth) is implicitly built into the stability frequency. The α coefficient in Eq. 2.1 can be interpreted as a measure of turbulence level and is plotted as a function of lake surface area in Fig. 2.2. A general relationship applicable to lakes on a regional scale was therefore summarized as:

$$K_z = 8.17 \times 10^{-4}\,(\text{Area})^{0.56}\,(N^2)^{-0.43} \tag{2.2}$$

where Area is lake surface area (km^2), N^2 is in sec^{-2}, and K_z is in $cm^2\ sec^{-1}$.

Maximum vertical hypolimnetic eddy diffusivity K_{zmax} was also correlated with lake surface area because turbulent mixing in non–stratified lakes depends strongly on kinetic wind energy supplied, which in turn depends on lake surface area. Maximum hypolimnetic eddy diffusivity versus lake surface area for eight different lakes is plotted in Fig. 2.3. Data are from Jassby and Powell (1975), Ward (1977), Lewis (1983), and from this study.

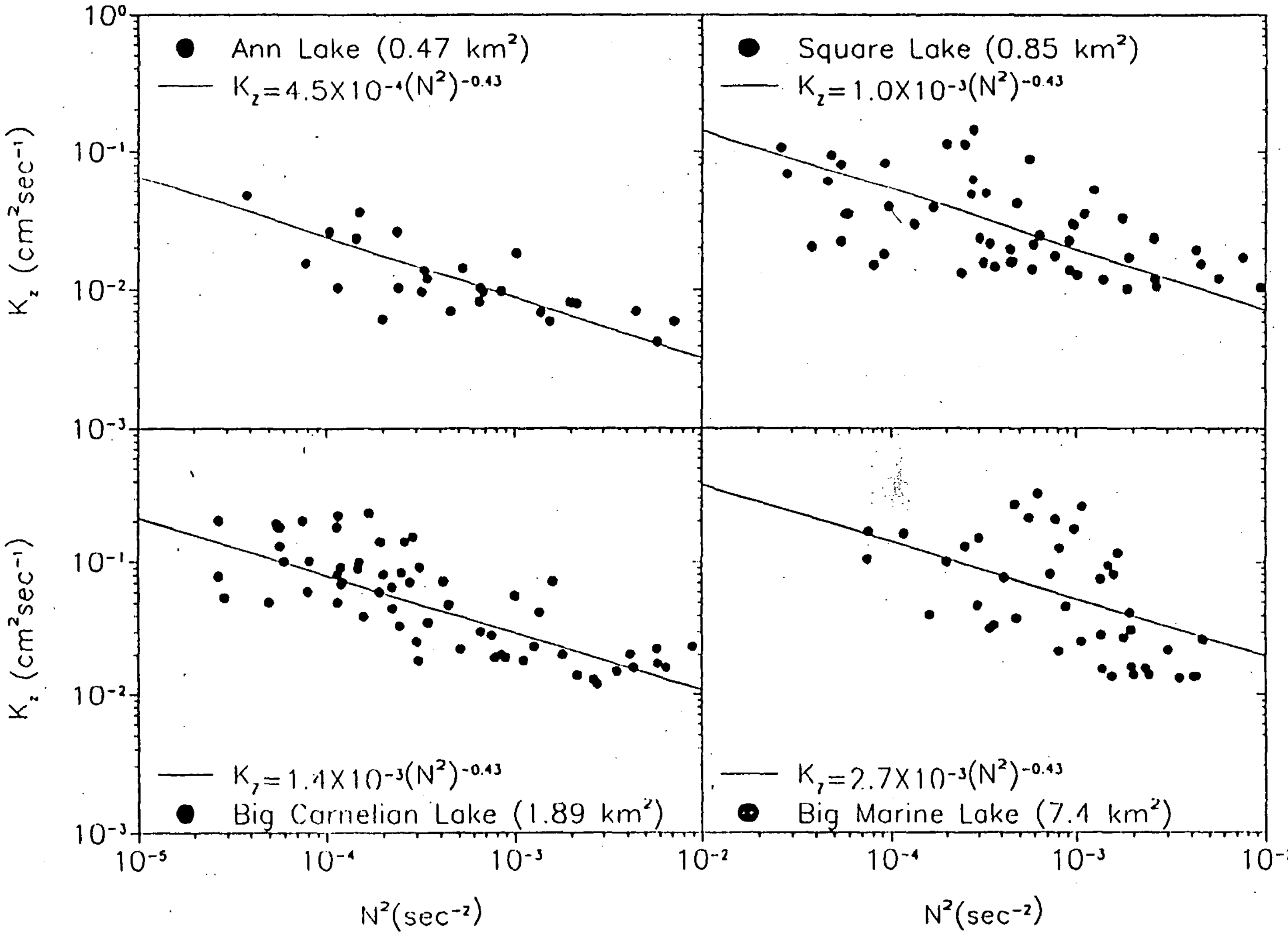

Fig. 2.1 Hypolimnetic eddy diffusivity dependence on lake surface area.

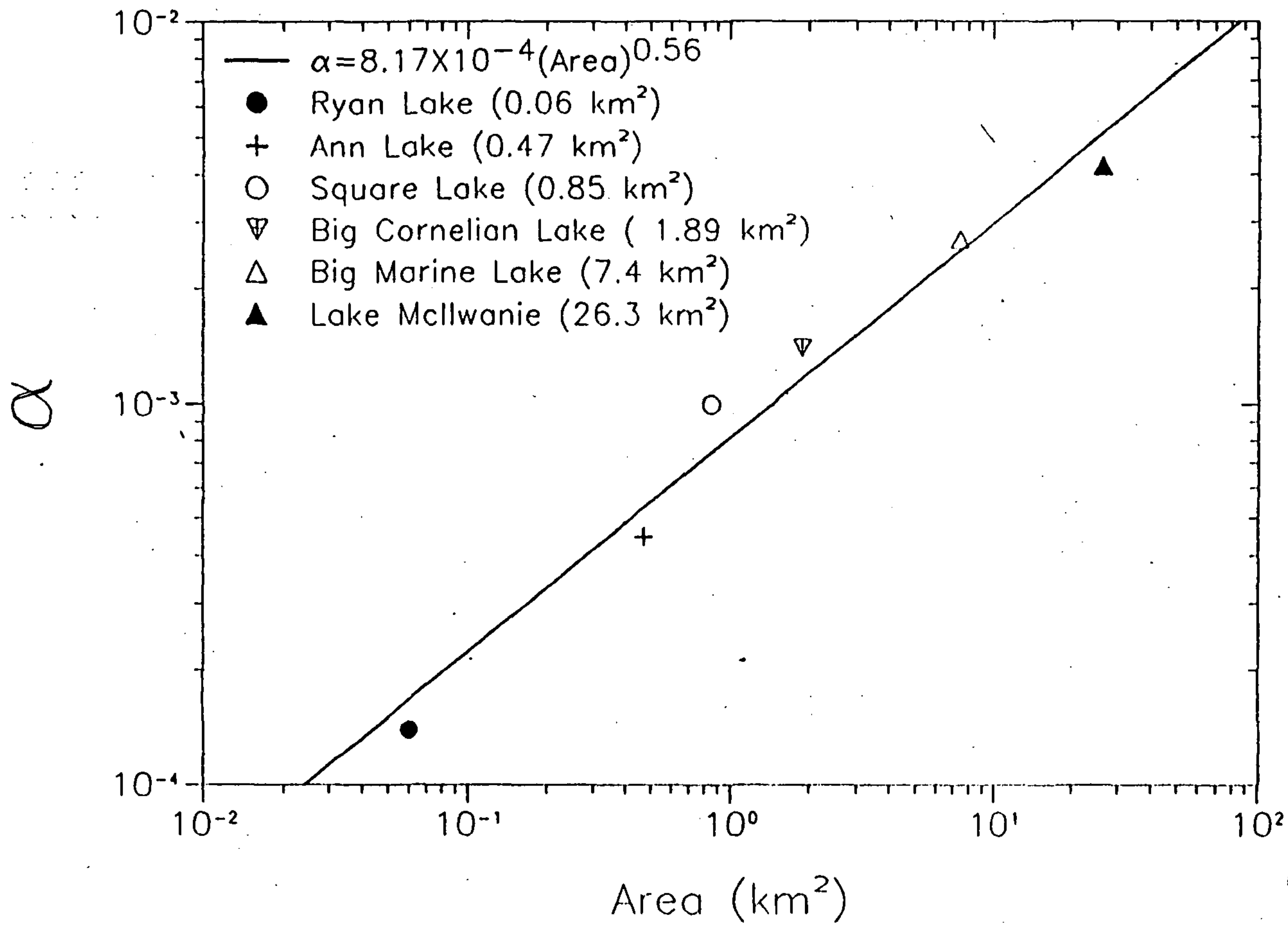

Fig. 2.2 Hypolimnetic eddy diffusivity forcing parameter (α) dependence on lake surface area.

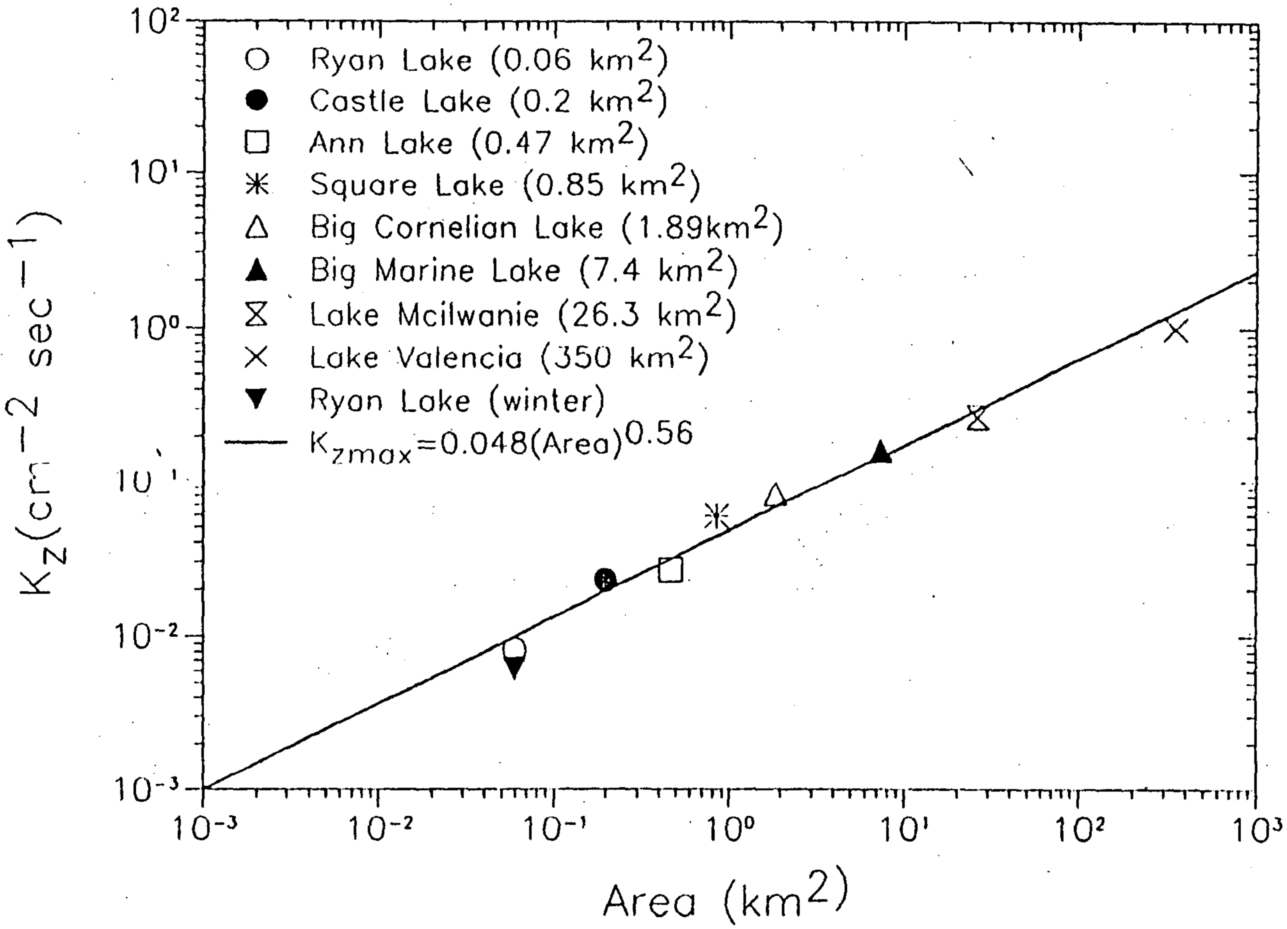

Fig. 2.3 Maximum hypolimnetic eddy diffusivity ($N^2=7.5*10^{-5}$ sec^{-2}) dependence on lake surface area.

Attenuation coefficient

The specific radiation attenuation coefficients for water and chlorophyll were replaced by the total attenuation coefficient. This was done following the parsimonious principle i.e. the fewer coefficients in the model, the less uncertain the model estimate. In addition uncertainty analysis showed that chlorophyll–a made a minor contribution to lake water temperature uncertainty. A relationship between total attenuation coefficient μ (m^{-1}) and Secchi depth z_{sd} (m) was obtained from measurements in 50 lakes in Minnesota (Osgood, 1990) and is plotted in Fig. 2.4.

$$\mu = 1.84\ (z_{sd})^{-1} \tag{2.3}$$

The form of this relationship has been found to be valid in inland waters in general (Idso and Gilbert, 1974) and in the ocean (Poole and Atkins, 1929).

2.2.3 Wind sheltering coefficient

The wind sheltering coefficient is a function of lake surface area (fetch). The turbulent kinetic energy computation (Eq. 1.10) uses a wind speed and direction taken from off–site weather station at 10 m elevation and adjusts that wind speed for fetch over the lake in the direction of the wind. As wind speed typically increases with fetch, the calculated downstream wind speed is an estimate of the maximum wind speed on the lake surface. Typically fetch on a lake is reduced by wind sheltering the upwind side of the lake where the wind makes a transition from a landbound turbulent velocity profile to the open water. This was explained by Ford and Stefan (1980). The reduction in fetch or surface area sheltered from direct wind access by trees or buildings along the shoreline will be more significant for small lake than a large one because a) a relatively larger portion of the total lake surface area will be wind sheltered b) the downwind maximum wind speed does not grow linearly with fetch and will on a large lake be near the real wind speed over a large portion of the lake surface area, and c) wind gusts will be less effective over a small lake surface than a large one because of spatial averaging. Also lake morphometry, i.e. distribution of area with depth will be a factor in the translation of wind energy into mixing. A maximum wind speed at the downwind end of a large lake will also be more representative for a large lake than a small one, especially if the lake morphometry is taken into consideration.

For all these reasons a very strong dependence of the wind sheltering coefficient (W_{str}) on lake surface area can be expected. A functional relationship was obtained by plotting the wind sheltering coefficient obtained by calibration in several previous numerical model simulations (Fig. 2.5). Biweekly temperature profile measurements in ten lakes and throughout the summer season were used to optimize the wind sheltering coefficients plotted in Fig. 2.5. The empirical relationship is

$$W_{str} = 1.0 - \exp(-0.3 * \text{Area}) \tag{2.4}$$

where Area is the lake surface area in km^2.

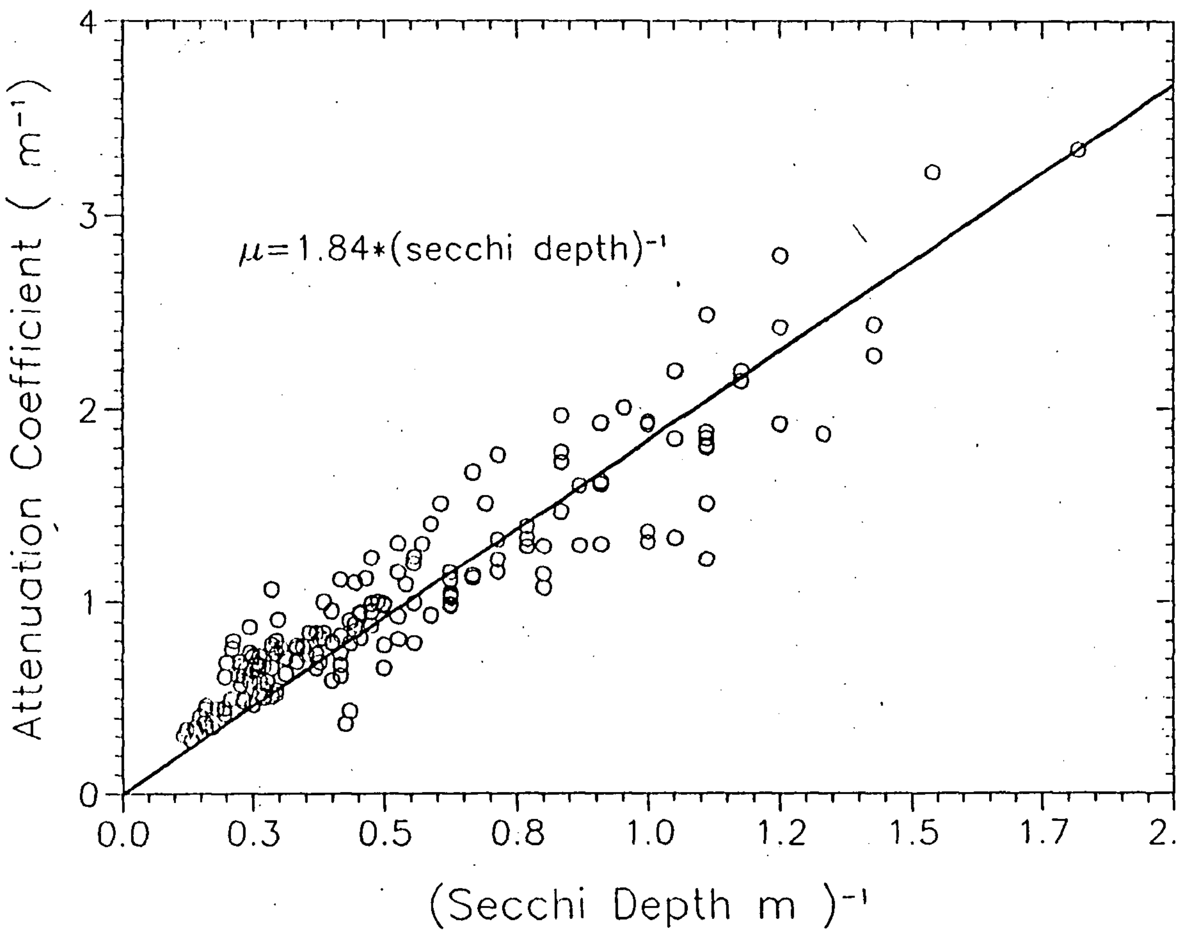

Fig. 2.4 Relationship between total attenuation coefficient and Sechi disk depth.

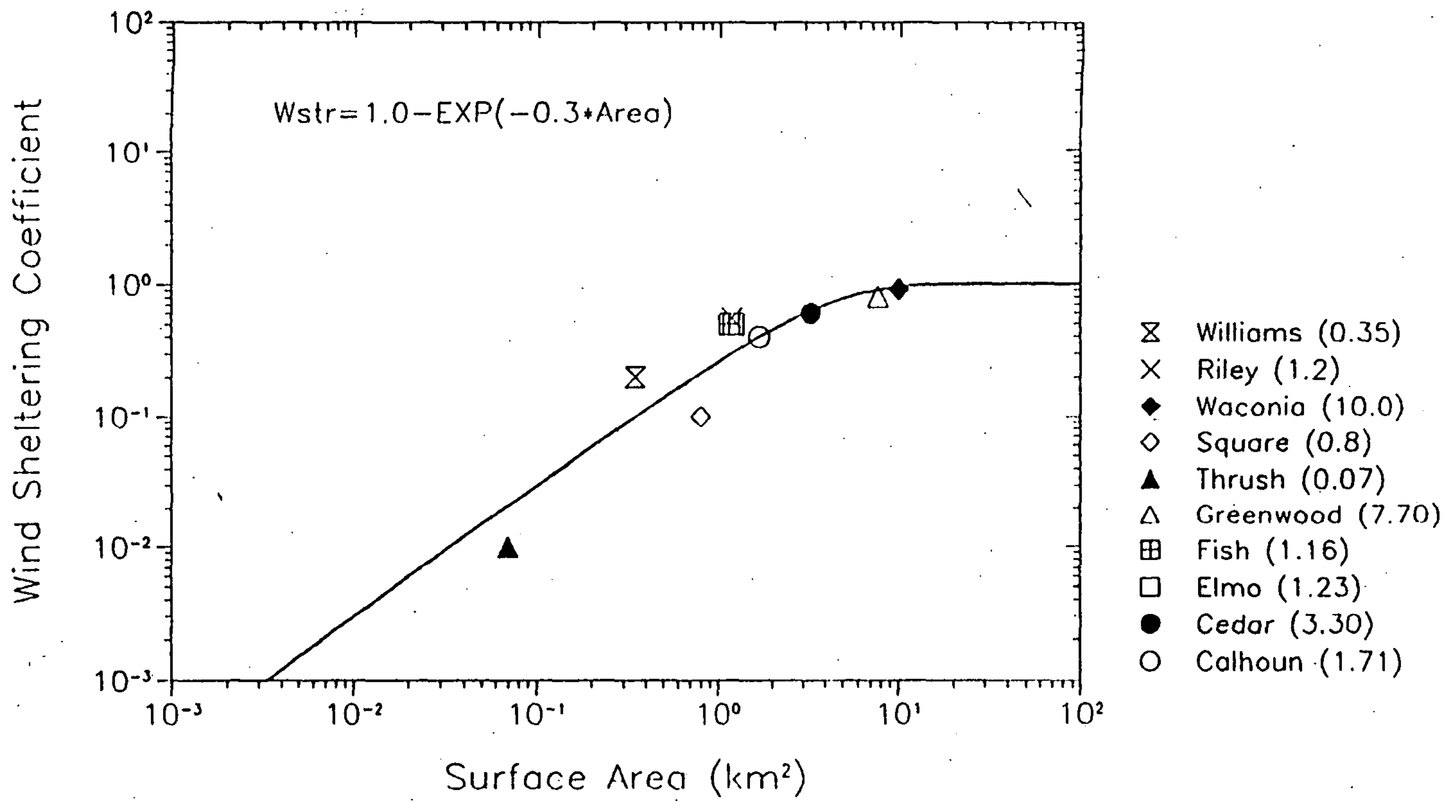

Fig. 2.5 Wind sheltering coefficient dependence on lake surface area.

The result in Fig. 2.5 seems to indicate that the modeling of wind mixing in lakes, especially small ones, depends more on a correct amount of energy supplied than on a energy dissipation. This is a new insight which appears to result from this study.

2.2.4 Wind function coefficient

Wind function coefficients (c) defined in Eq. 1.11 enters into the heat transfer relationships (1.8) and (1.9), and depends also on lake surface area (fetch) as was found by Harbeck (1962), Sweers (1976), and summarized by Adams et al. (1990). Harbeck (1962) analyzed data from several lakes of different sizes and pointed out that evaporation rates in small and large lakes might be the same. The fetch dependence is introduced mainly due to the wind speed increase over the water. As air flows from land to a smoother water surface, at a constant height above the water (e.g. 10 m), its velocity increases with fetch. In this numerical model off–lake wind speeds measured at permanent weather stations are are used, but they are adjusted for lake fetch (Ford and Stefan, 1980). Nevertheless, some residual wind function coefficient dependence on lake fetch is shown in Table 2.1. A functional relationship was obtained by plotting the wind function coefficient from several previous numerical model simulations against lake surface area (Fig. 2.6). The estimated relationship is

$$c = 24+\ln(\text{Area}) \tag{2.5}$$

where Area is again in km^2. This relationship shows only a week dependence of c on lake surface area, and can be viewed as a minor adjustment. The need for this adjustment can be explained by examining the wind boundary layer development over the surface of small and large lakes (see Fig. 2.7). Wind speed increases with fetch (distance from the leeward shore) but non–linearly. In our model wind speed is taken from an off–lake weather station and a maximum wind speed at the downwind end of the lake as shown in Fig. 2.7 (top) is computed for the use in the heat transfer equations (1.8) and (1.9). This calculated wind speed is an overestimate of the areal average wind speed over the lake surface. Because of the non–linearity of wind speed with distance the overestimate is more severe for small lakes than for large lakes. Therefore the wind function coefficient has to be smaller for smaller lakes in order to compensate for the wind velocity overestimate. If on the other hand, wind speeds are measured on the lake (middle of the lake) as shown in Fig. 2.7 (bottom) the situation is reversed. In that case the wind measurements on a small lake are severely underestimated relative to the areal average than on a big lake. For this reason the wind function coefficient has to decrease with fetch (surface area) to compensate for this non–representativeness of the wind speeds measured in midlake. This decreasing trend of wind function coefficient with lake surface area was found and reported by Harbeck (1962), Sweers (1976) and summarized by Adams et al. (1990). In addition Adams called upon increases in relative humidity with fetch over cooling ponds to justify the decrease in wind function coefficient with fetch.

It is concluded from all of the above that the wind function coefficient can increase or decrease with lake surface area depending on the location where wind speed is measured.

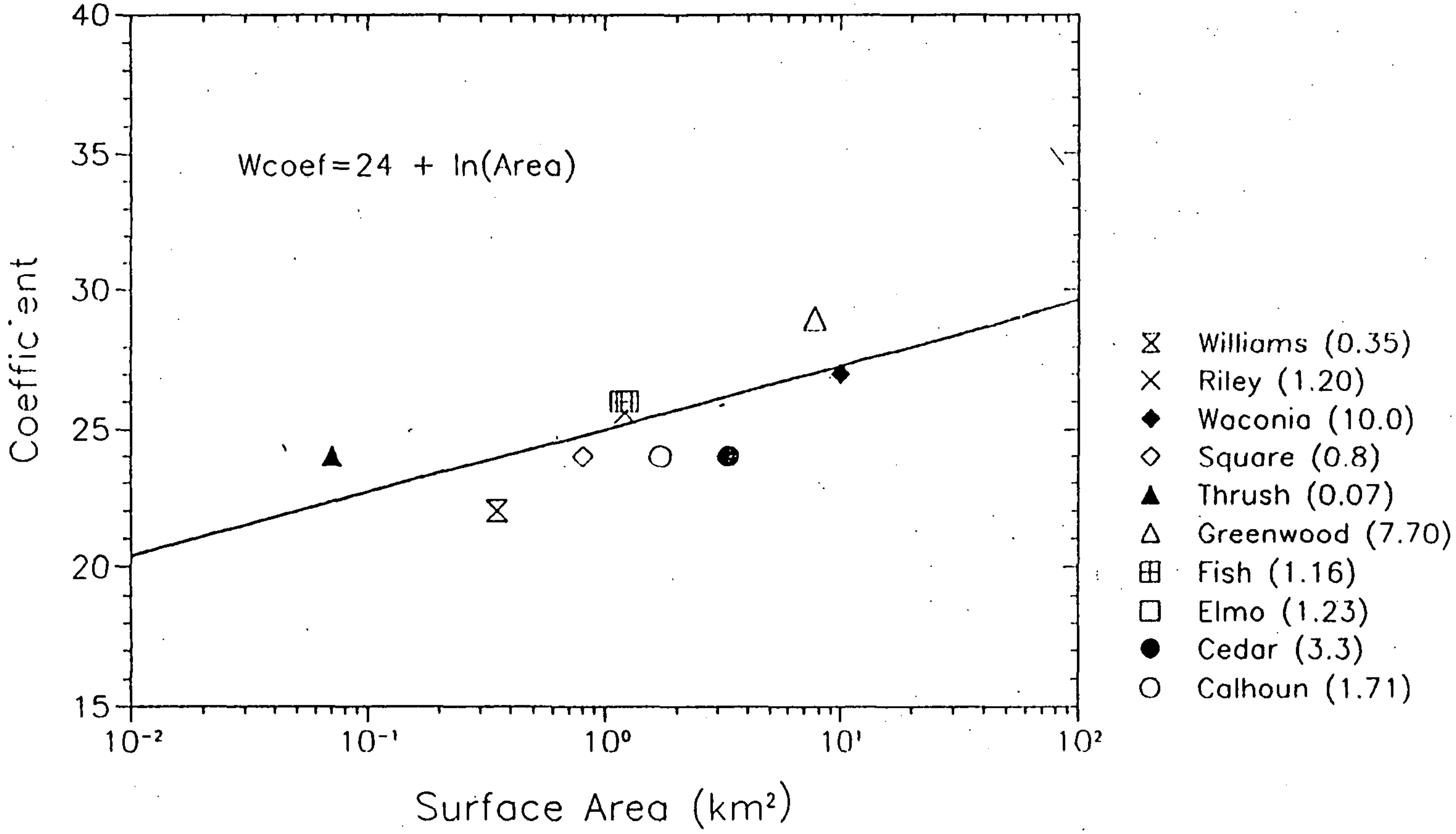

Fig. 2.6 Wind function coefficient dependence on lake surface area.

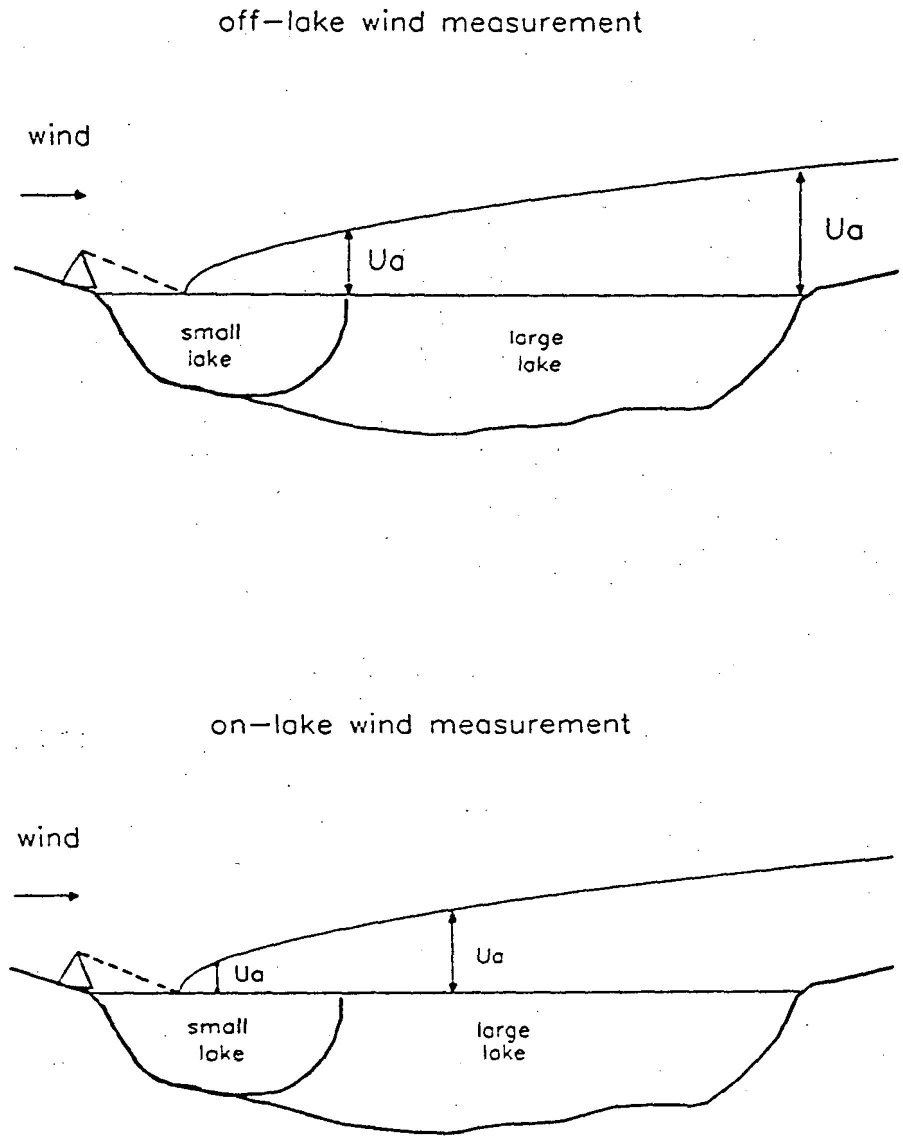

Fig. 2.7 Lake wind speed measurements.

2.3 Water Temperature Model Validation After Generalization of Hypolimnetic Eddy Diffusivity

The model was first modified by adding the hypolimnetic eddy diffusivity closure (Eq. 2.2). The number of calibration coefficients (Table 1.1) was thereby reduced from five to four. The modified numerical model than had to be validated with water temperature measurements in several selected lakes over a period of several years. Representative lakes in Minnesota were selected through an analysis of the state's extensive data bases. Differences between waterbodies in adjacent ecoregions were found too small to justify further subdivisions on this basis. The state was divided into a northern part, roughly coinciding with three ecoregions, and a southern part, roughly coinciding with three other ecoregions (Fig. 2.8) which also extended into Wisconsin, Iowa, and South Dakota. "Representative" lake meant either having values of lake surface area, maximum depth, and secchi depth near the median as identified in a state report by the Minnesota Pollution Agency (Heiskary et al., 1988) or being near the far ends of the respective frequency distributions for ecoregions. Selected representative lakes with their position on the cumulative frequency distribution curves for northern and southern Minnesota are given in Fig. 2.9. Lakes covered the entire range of maximum depths (shallow–medium–deep), surface area (small–medium–large), and trophic status (eutrophic–mesotrophic–oligotrophic). Geographical distribution of these lakes in Minnesota is given in Fig. 2.8.

To validate the model numerical simulations were started with isothermal conditions (4 °C) on March 1 and continued in daily timesteps until November 30. Ice goes out of Minnesota lakes sometime between the end of March and beginning of May. Dates of spring overturn vary with latitude and year. To allow for these variable conditions, a 4°C isothermal condition was maintained in the lake water temperature simulations until simulated water temperatures began to rise above 4°C. This method permitted the model to find its own date of spring overturn (4°C) and the simulated summer heating cycle started from that date.

Daily meteorological data files were assembled from Minneapolis/St. Paul, and Duluth, for southern and northern Minnesota respectively.

A quantitative measure of the success of the simulations for the nine representative lakes is given in Table 2.1. Different gauges of the simulation success are defined as: (a) volume weighted temperature averages

$$\hat{T}_s = \frac{\sum_{i=1}^{p} V_i\, T_{si}}{\sum_{i=1}^{p} V_i} \qquad \hat{T}_m = \frac{\sum_{i=1}^{p} V_i\, T_{mi}}{\sum_{i=1}^{p} V_i} \tag{2.6}$$

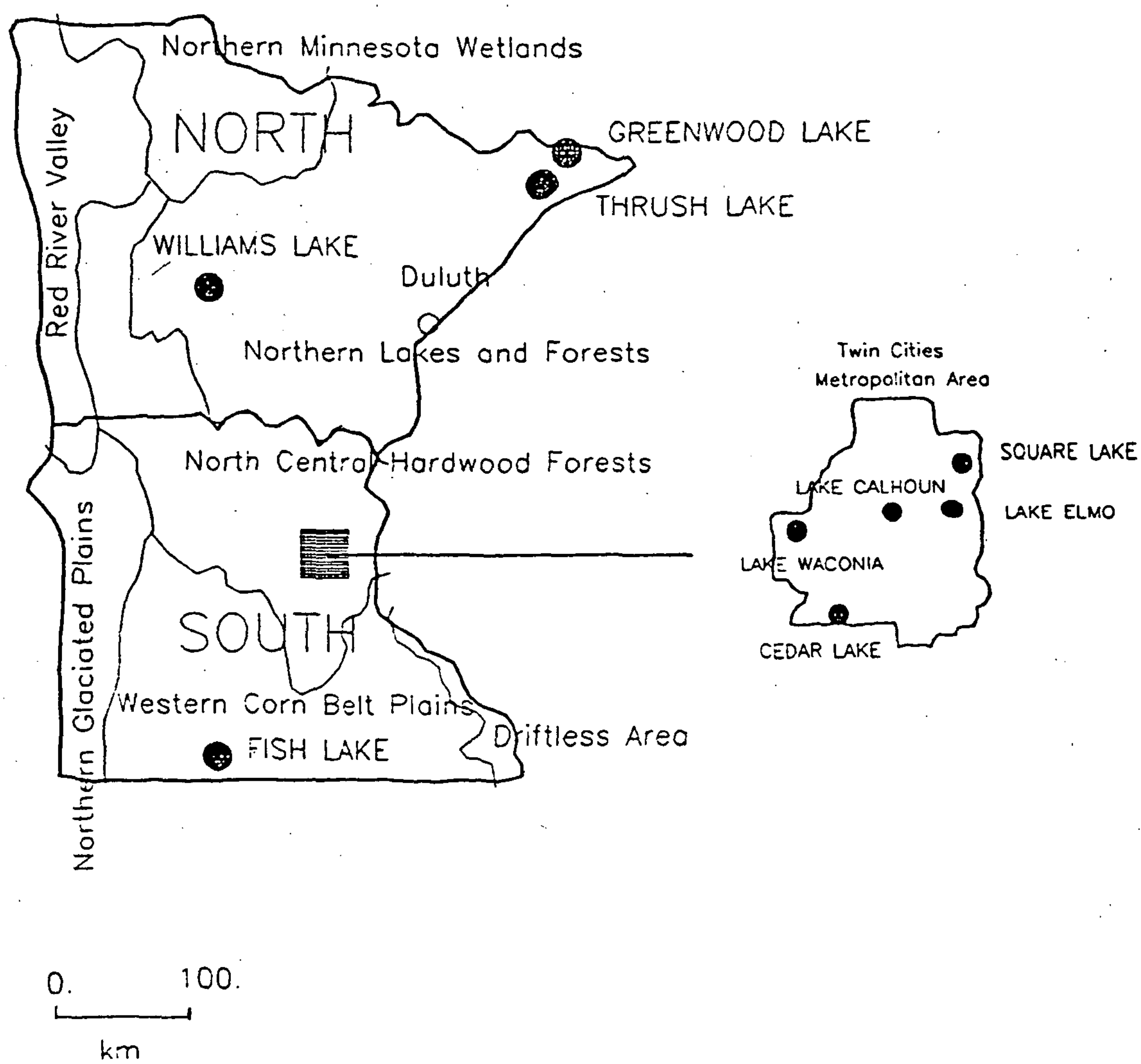

Fig. 2.8 Ecoregions and spatial distribution of selected lakes.

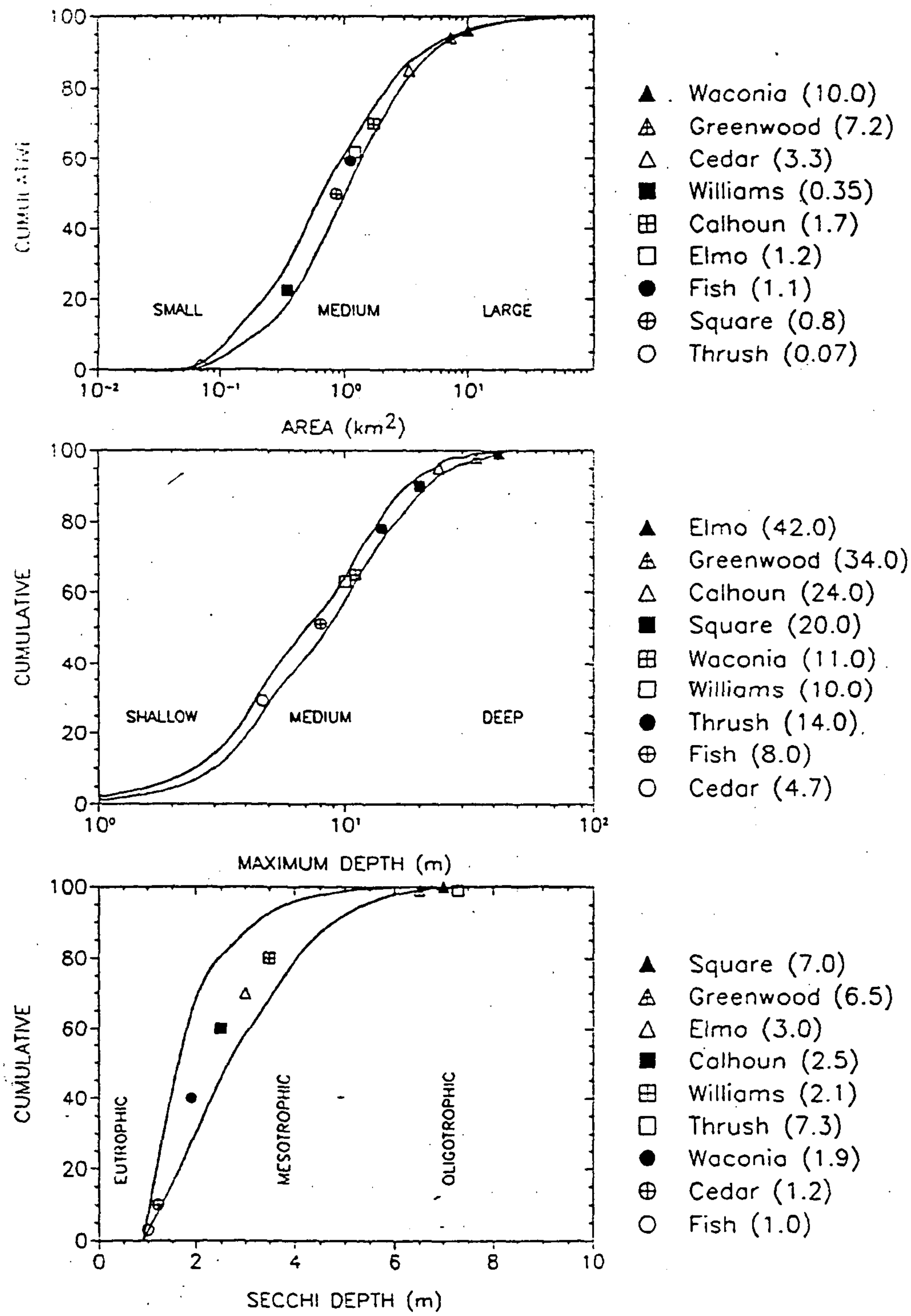

Fig. 2.9 Cumulative distributions (%) of lake parameters in Minnesota. Lakes selected for model validation are shown by symbols.

(b) temperature root mean square errors

$$E_1=\left[\frac{\sum_{i=1}^{p}(T_{si}-T_{mi})^2}{p}\right]^{0.5} \qquad E_2=\left[\frac{\sum_{i=1}^{p}V_i(T_{si}-T_{mi})^2}{\sum_{i=1}^{p}V_i}\right]^{0.5} \tag{2.7}$$

and (c) r^2 i.e. portion of the temperature measurements explained by the simulations (Riley and Stefan, 1987). In the above equations subscripts i, s, and m refer to the counting index, simulated, and measured temperature respectively. V_i is the water volume of a layer in the stratified lake. The above parameters are estimated by summing over lake depths. Overall seasonal average parameters are reported in Table 2.1. Examples of simulated and measured vertical lake water temperature profiles are given in Figs. 2.10, 2.11, 2.12, 2.13, and 2.14. The model simulates onset of stratification, mixed layer depth and water temperatures well.

Table 2.1 Quantitative measure of the success of the simulations–Validated model.

Lake	Year	$\hat{T}_m$ (oC)	$\hat{T}_s$ (oC)	E_1 (oC)	E_2 (oC)	r^2 (–)	Number of field data.
Calhoun	1971	14.37	14.52	0.86	0.79	0.97	136
Cedar	1984	20.64	20.86	0.94	0.99	0.93	20
Elmo	1988	13.94	14.09	1.77	1.80	0.92	214
Fish	1987	24.40	24.13	0.80	0.82	0.90	32
Square	1985	14.37	14.52	0.86	0.79	0.97	136
Waconia	1985	20.14	20.12	0.78	0.73	0.92	43
Greenwood	1986	11.80	11.97	0.89	0.79	0.93	46
Thrush	1986	11.97	11.91	0.90	0.91	0.96	114
Williams	1984	17.26	16.37	1.08	1.07	0.97	110
Average		16.54	16.49	0.97	0.96	0.94	95

$\hat{T}_m$ – measured volume weighted average temperature
$\hat{T}_s$ – simulated volume weighted average temperature
E_1 – temperature root mean square error
E_2 – volume weighted temperature root mean square error
r^2 – portion of the measured water temperature variability explained by the simulations

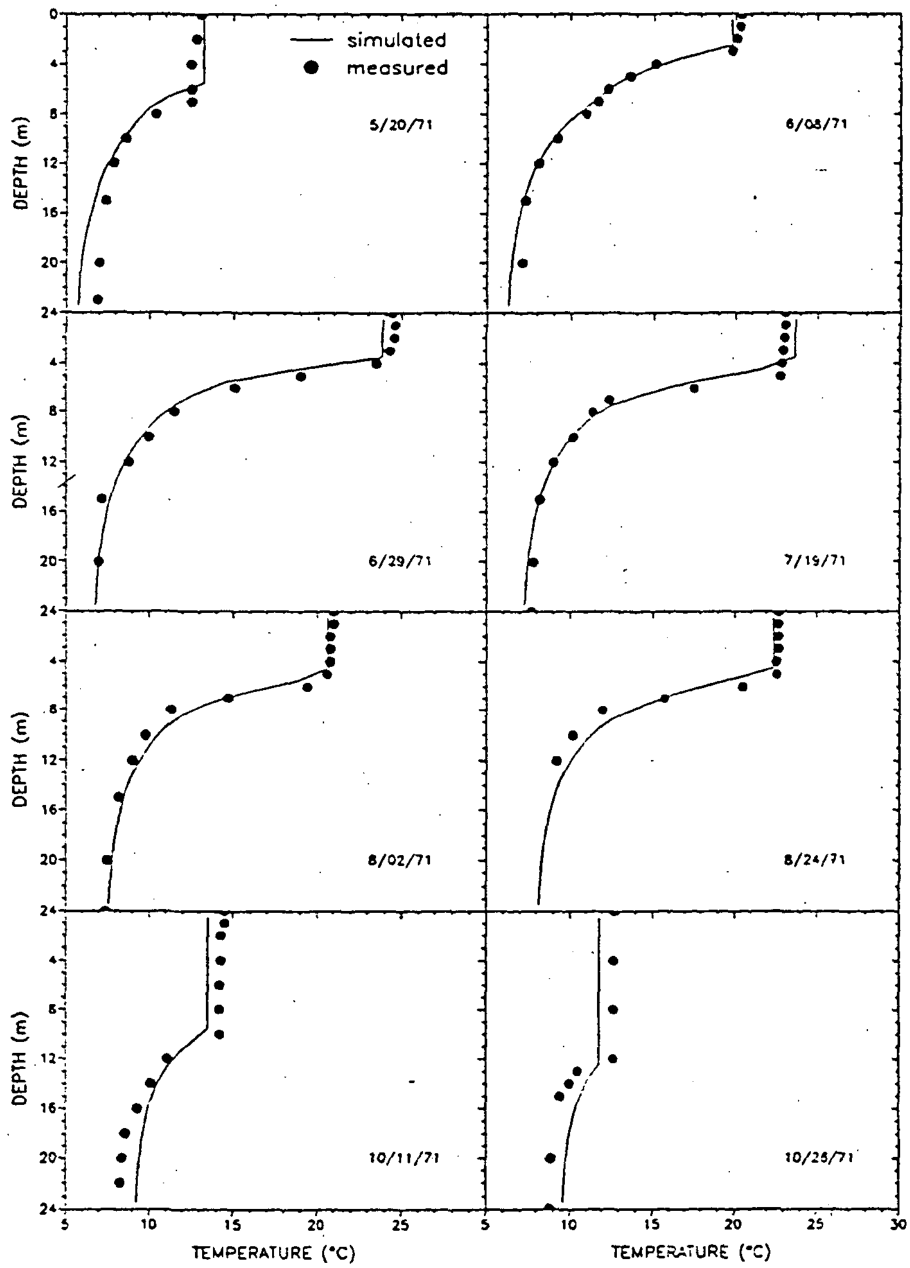

Fig. 2.10 Lake Calhoun water temperature profiles.

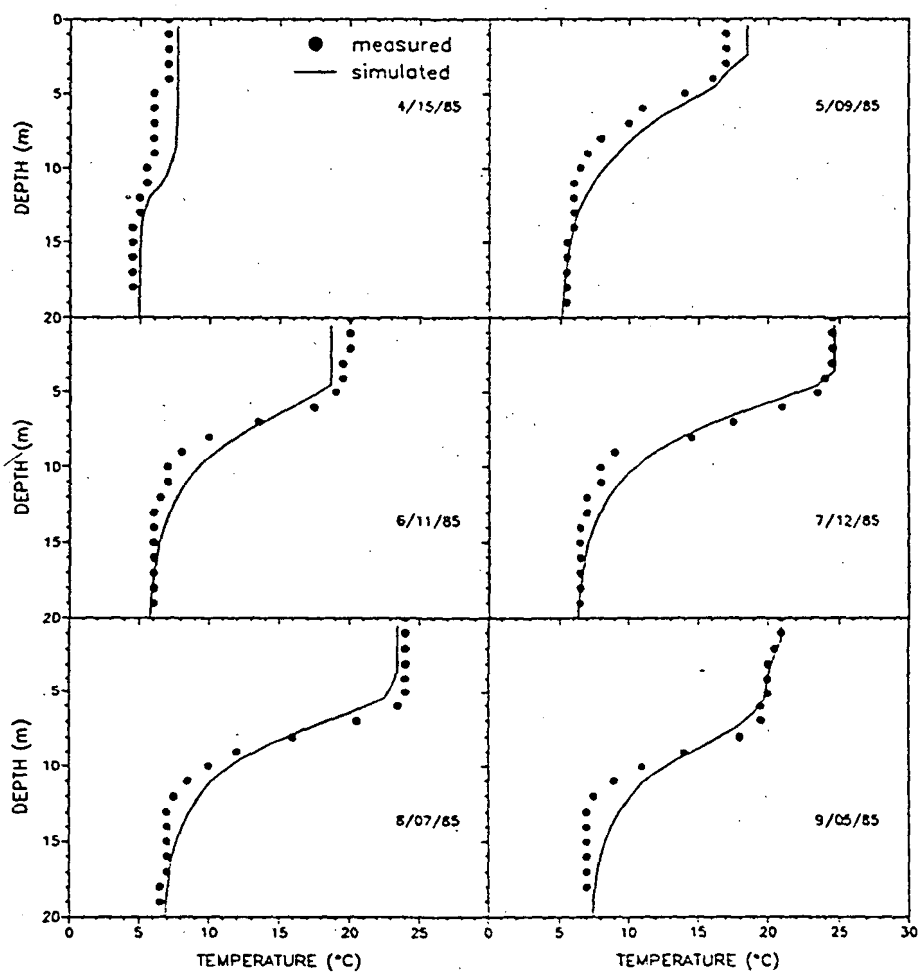

Fig. 2.11 Square Lake water temperature profiles.

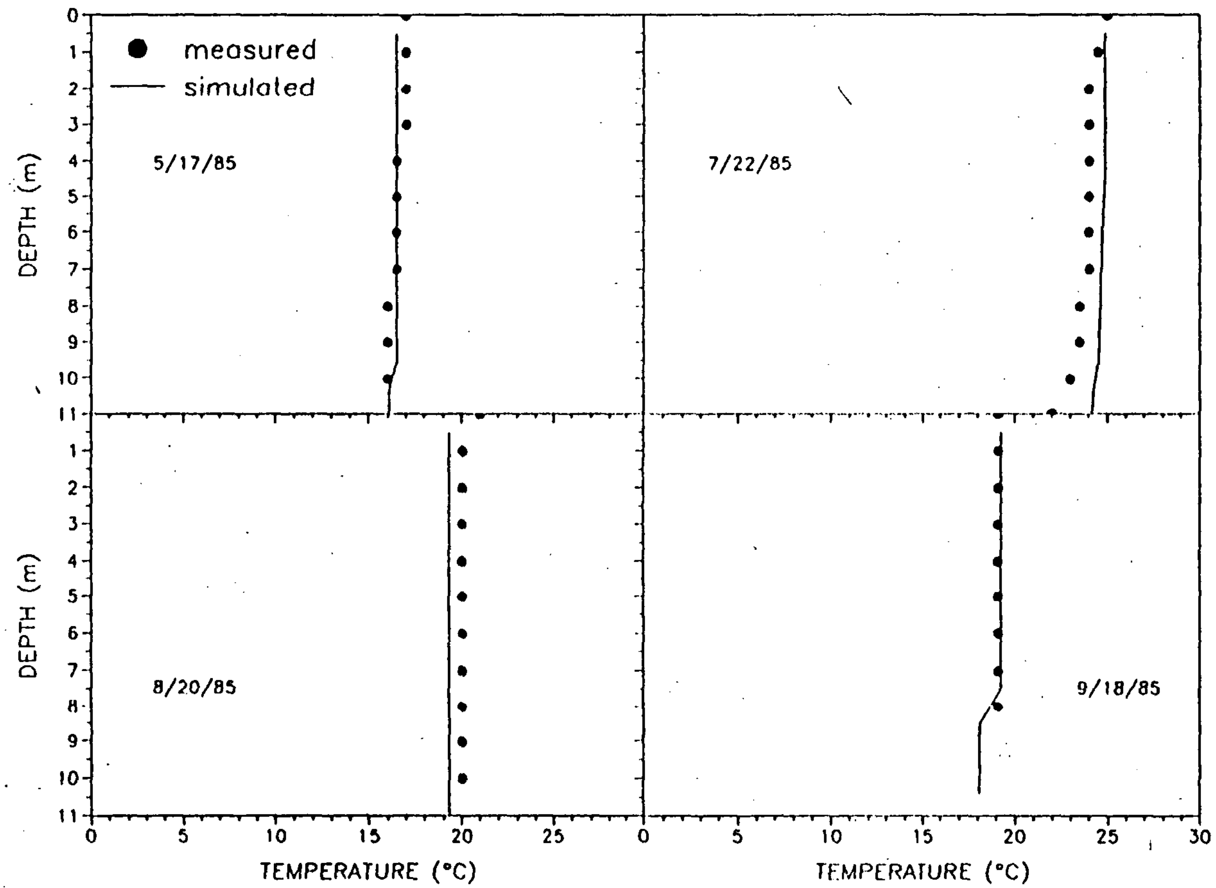

Fig. 2.12 Waconia Lake water temperature profiles.

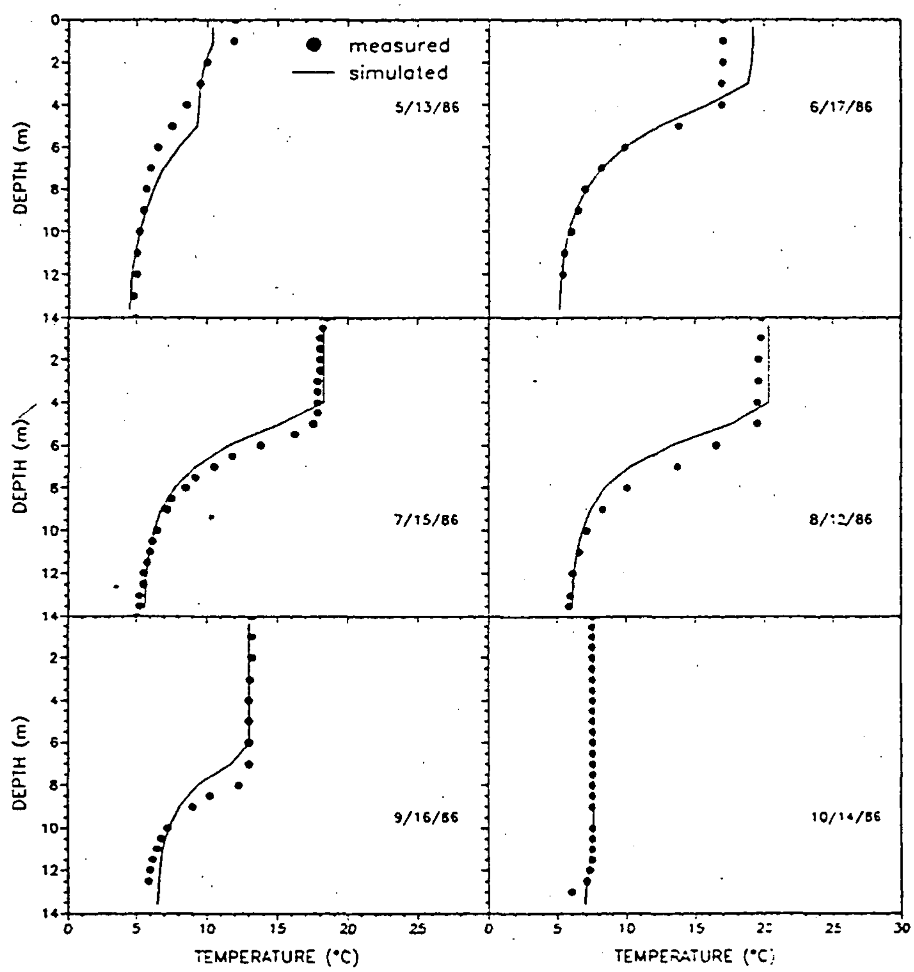

Fig. 2.13 Thrush Lake water temperature profiles.

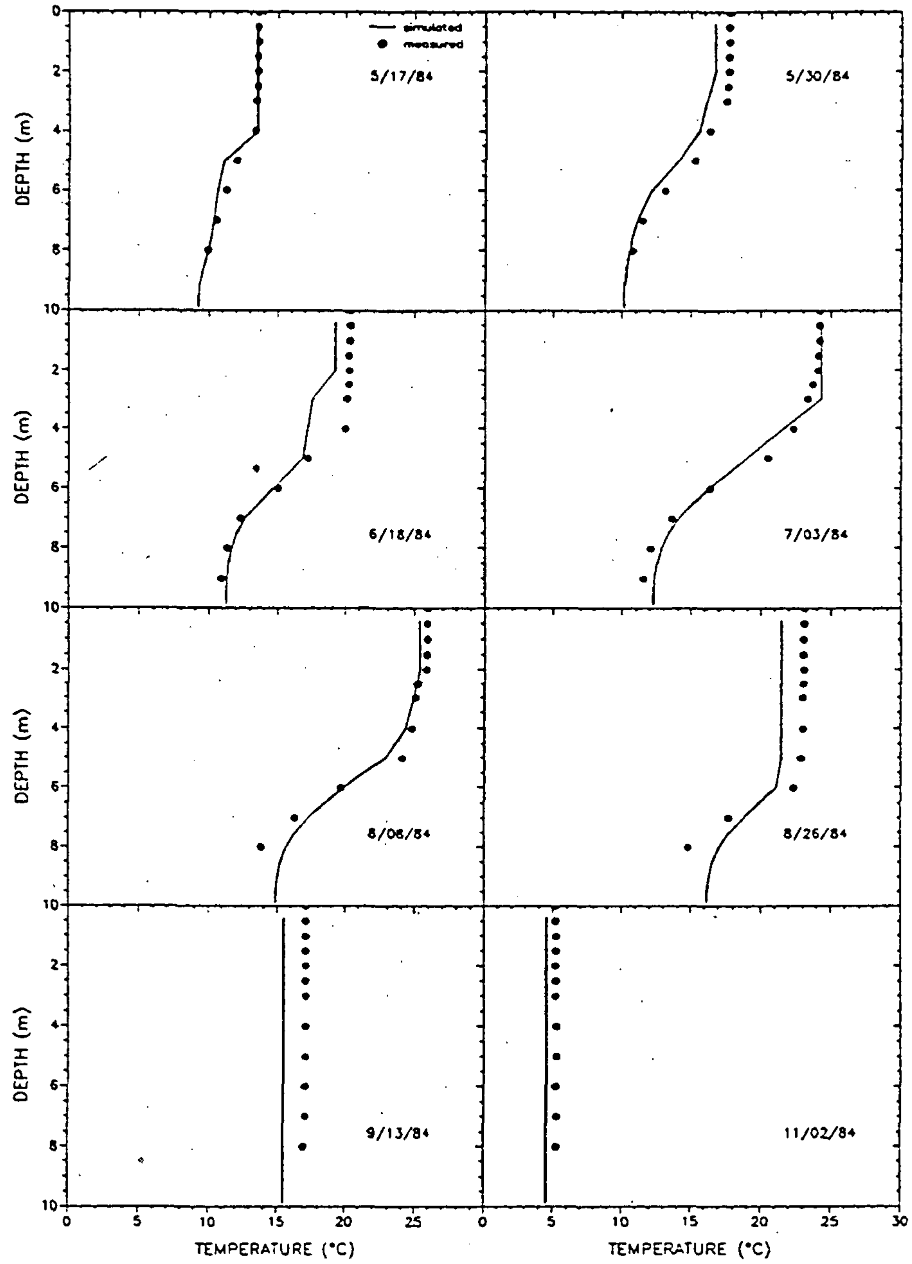

Fig. 2.14 Williams Lake water temperature profiles.

Volume weighted and unweighted root mean square error was less than 1°C for all lakes (Table 2.2) except the deepest (Lake Elmo has a maximum depth 40 m). This is mostly due to small differences in predicted thermocline depth for the deepest simulated lake. Difference between two estimated root mean square errors (E_1 and E_2) indicate the vertical position of the maximum simulation error. If E_2 is greater than E_1, than the difference between measured and simulated lake water temperatures are greater in the surface layers because E_2 values are volume weighted and E_1 values are not.

Table 2.2 Coefficients for calibration of water temperature model

Lake	Year	Max. depth H_{max} (m)	Surface area A_S (km²)	Wind funct. coeff. c (–)	Wind shelt. coeff. W_{str} (–)	Attenuation coefficient μ_w (m^{-1})	μ_{ch} (m^2g^{-1}Chl–a)	Chl–a (g m^{-3})
Calhoun	1971	24.0	1.71	24	0.40	0.65	8.65	4–37[1]
Cedar	1984	4.70	3.30	24	0.60	0.65	8.65	6–130[2]
Elmo	1988	41.8	1.23	26	0.50	0.65	8.65	3–8[3]
Fish	1987	8.20	1.16	26	0.50	1.00	8.65	18–48[4]
Square	1985	21.0	0.85	24	0.10	0.50	8.65	1–4[7]
Waconia	1985	11.0	10.0	27	0.90	0.65	8.65	11–34[8]
Greenwood	1986	34.0	7.70	29	0.80	0.65	8.65	1–3[5]
Thrush	1986	14.0	0.07	24	0.01	0.65	8.65	2–4[6]
Williams	1984	10.0	0.35	22	0.20	0.65	8.65	3–7[9]

Field data given by:

[1] Shapiro and Pfannkuch, 1973
[2] Osgood, 1984
[3,7,8] Osgood 1989
[4,5] Minnesota Pollution Control Agency, 1988
[6] Wright et al., 1988
[9] Winter, 1980

The average root mean square error for all lakes was 1°C, and 94% (r^2 = 0.94) of water temperature measurements variability was explained by the numerical model (Table 2.2).

Model coefficients used in the simulations are given in Table 2.2. These coefficients give minimum values of root mean square error, and highest value of r^2 between measurements and simulated lake water temperatures.

In the following sections the modified model with the hypolimnetic eddy diffusivity closure as described in this section will be referred to as the **validated** model.

2.4 Numerical Uncertainty of Model After Hypolimnetic Closure

Uncertainty in the lake water temperature simulations was considered in terms of all model coefficients except maximum hypolimnetic eddy diffusivity as specified in Table 1.1. To first-order the uncertainty in lake water temperature depends on the uncertainty in the model coefficients, and on the sensitivity of the lake water temperatures to changes in the coefficients:

$$
\begin{aligned}
P_T &= E\{[T - \hat{T}][T - \hat{T}]^{tr}\} \approx \\
&E\{[T(\hat{u}) + \frac{\partial T}{\partial u}(u - \hat{u}) - \hat{T}][T(\hat{u}) + \frac{\partial T}{\partial u}(u - \hat{u}) - \hat{T}]^{tr}\} = \\
&E\{[\frac{\partial T}{\partial u}(u - \hat{u})][\frac{\partial T}{\partial u}(u - \hat{u})]^{tr}\} = \\
&\frac{\partial T}{\partial u} E\{(u - \hat{u})][(u - \hat{u})]^{tr}\} \frac{\partial T^{tr}}{\partial u} = \\
&\frac{\partial T}{\partial u} P_u \frac{\partial T^{tr}}{\partial u}
\end{aligned}
\qquad (2.8)
$$

where P_T is the (m x m) covariance matrix of the simulated lake water temperatures, m is the total number of discritized lake control volumes, E{.} is the mathematical expectation, $\hat{T}$ is the mean lake water temperature, (^{tr}) is the transpose, u is the vector of the n coefficients, P_u is the (n x n) covariance matrix of system coefficients, $\frac{\partial T}{\partial u}$ is the (m x n) sensitivity matrix of partial derivatives of the lake water temperatures with respect to the coefficients. Sensitivity matrix is estimated using the influence coefficient method (Willis and Yeh, 1987).

Data for the system coefficients covariance matrix are given in Table 2.3. These values were chosen to be in the range of theoretical and simulated values (Tables 1.1 and 2.2), and to have coefficients of variation (standard deviation/mean) equal to 0.3. This value is chosen because first-order uncertainty analysis could be questionable when the coefficient of variation of a nonlinear function increases above 0.3.

Table 2.3 Coefficients for uncertainty analysis

Coefficient	Lake Calhoun		Williams Lake		Cedar Lake	
	mean	st. dev.	mean	st. dev.	mean	st. dev.
μ_w (m^{-1})	0.65	0.20	0.65	0.20	0.65	0.20
μ_{ch} ($m^2 g^{-1}$Chla)	8.65	2.65	8.65	2.65	8.65	2.65
W_{str}	0.60	0.18	0.20	0.06	0.60	0.18
c	24.0	7.20	20.0	6.00	24.0	7.20

Three lakes are selected for the lake water temperature uncertainty estimation. Lake Calhoun is a eutrophic, deep (24 m maximum depth) lake, Williams Lake is oligotrophic, and has maximum depth close to the median depth of 3002 lakes in Minnesota (Fig. 2.9), and Cedar Lake is a highly eutrophic shallow (4.7 m maximum depth) lake.

Standard deviations of smoothed simulated epilimnion and volume weighted average hypolimnion temperatures are given in Figures 2.15, 2.16, and 2.17. Although high variability in model coefficients was imposed, maximum standard deviation in epilimnion temperatures was less than 1°C, and less than 1.5°C for the hypolimnion temperatures. Epilimnion temperatures are most sensitive to the wind function coefficient for all three lakes. In the shallow and well mixed Cedar Lake the wind function coefficient is the only one that significantly contributes to lake water temperature uncertainty. The lowest variability of lake water temperature uncertainty is associated with radiation attenuation by phytoplankton (Chlorophyll–a). Variability in water attenuation and wind sheltering contribute less to uncertainty in epilimnion lake water temperatures than the wind function coefficient. Volume weighted hypolimnion temperatures displayed higher uncertainty than epilimnion temperatures. For Williams Lake and Lake Calhoun, all three coefficients i.e. water attenuation, wind sheltering and wind function coefficient significantly contributed to the lake water temperature uncertainty. Schindler (1988) pointed out that in oligotrophic lakes dissolved organic carbon is one of the major light attenuating factors.

2.5 Accuracy of the Regional Model After Implementation of all Changes

The Number of calibration coefficients was reduced from four to zero. Functional relationships substituted into the model in Equations 2.2, 2.3, 2.4, and 2.5. The model output was compared with water temperature measurements in nine selected representative lakes. Simulations started with isothermal conditions (4°C) on March 1 and progressed in daily time steps until November 30. Quantitative measure of the success of the simulations and differences between the regional model and the validated model of section 2.3 and 2.5 are given in Table 2.4. The average weighted and unweighted root mean square error was 1.1 °C (16.5 °C average measured lake water temperature). Ninty three percent of measured lake water temperature variability was explained by the numerical simulations (r^2=0.93). The regional model has in average 0.15°C higher temperature root mean square error.

One example of the daily simulated isotherms for the regional and validated model (section 2.3) is given in Fig. 2.18. Both models simulate onset of stratification, mixed layer depth and water temperatures in a virtually identical way.

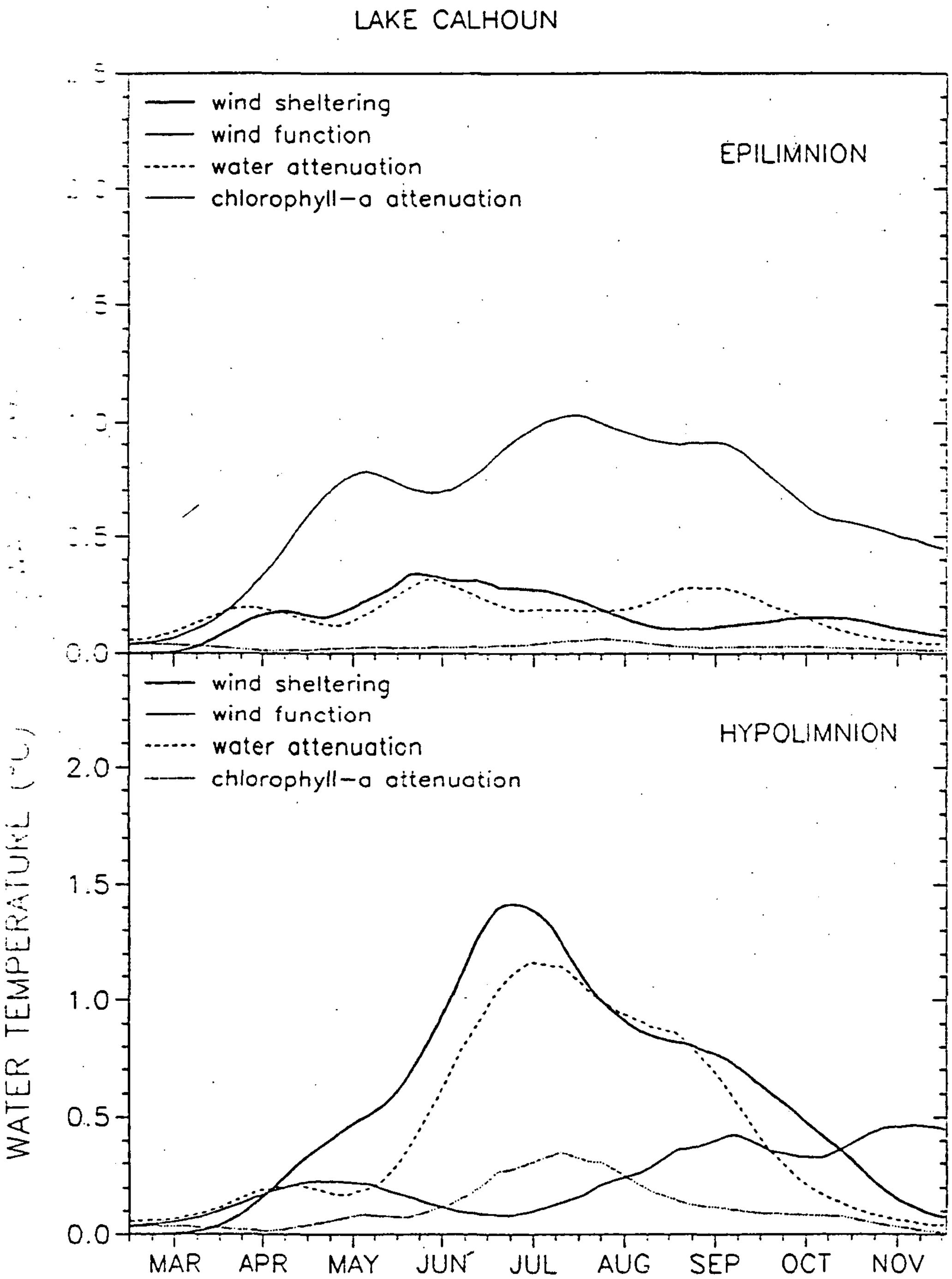

Fig. 2.15 Standard deviations of estimated lake water temperature uncertainties.

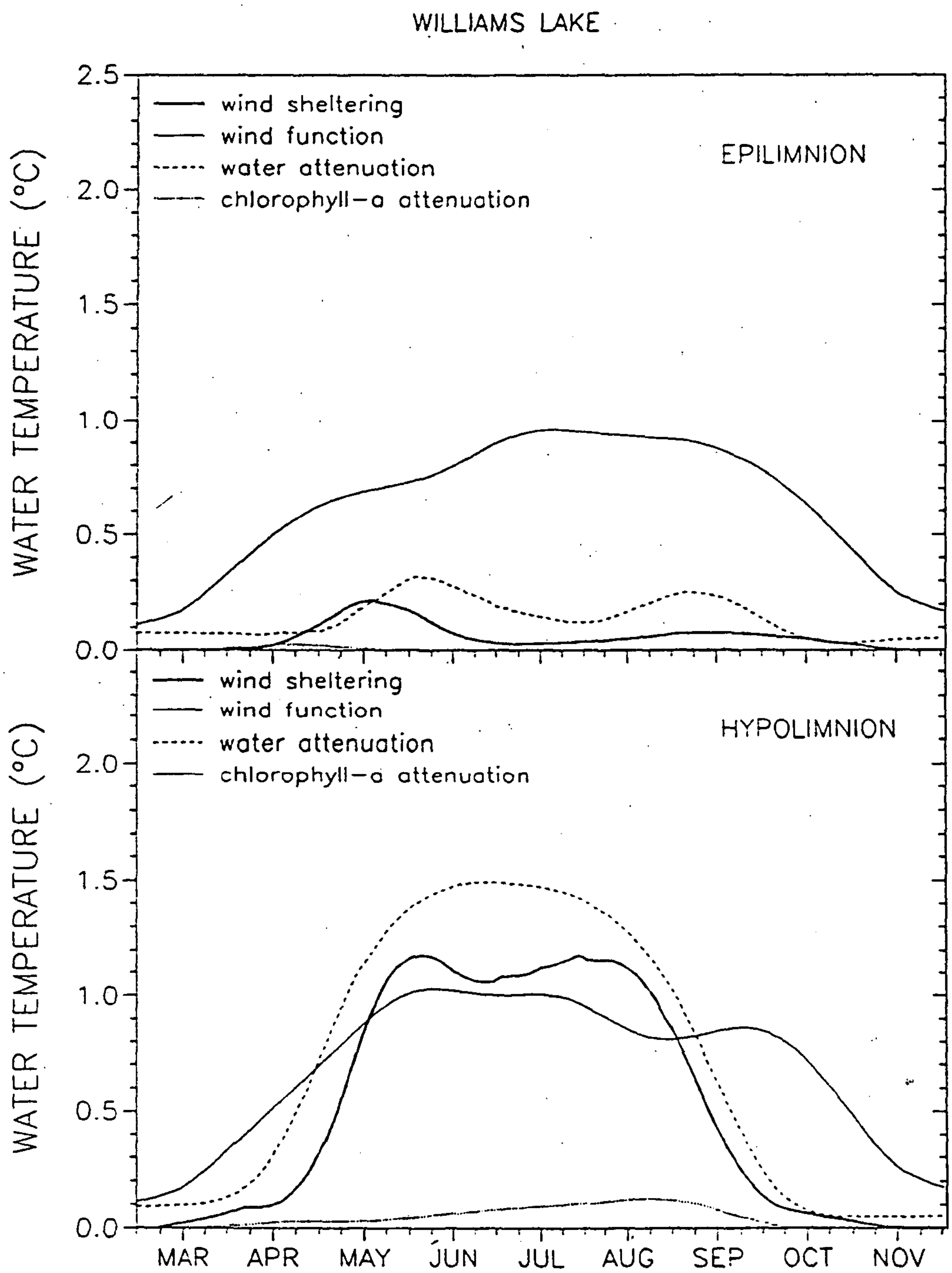

Fig. 2.16 Standard deviations of estimated lake water temperature uncertainties.

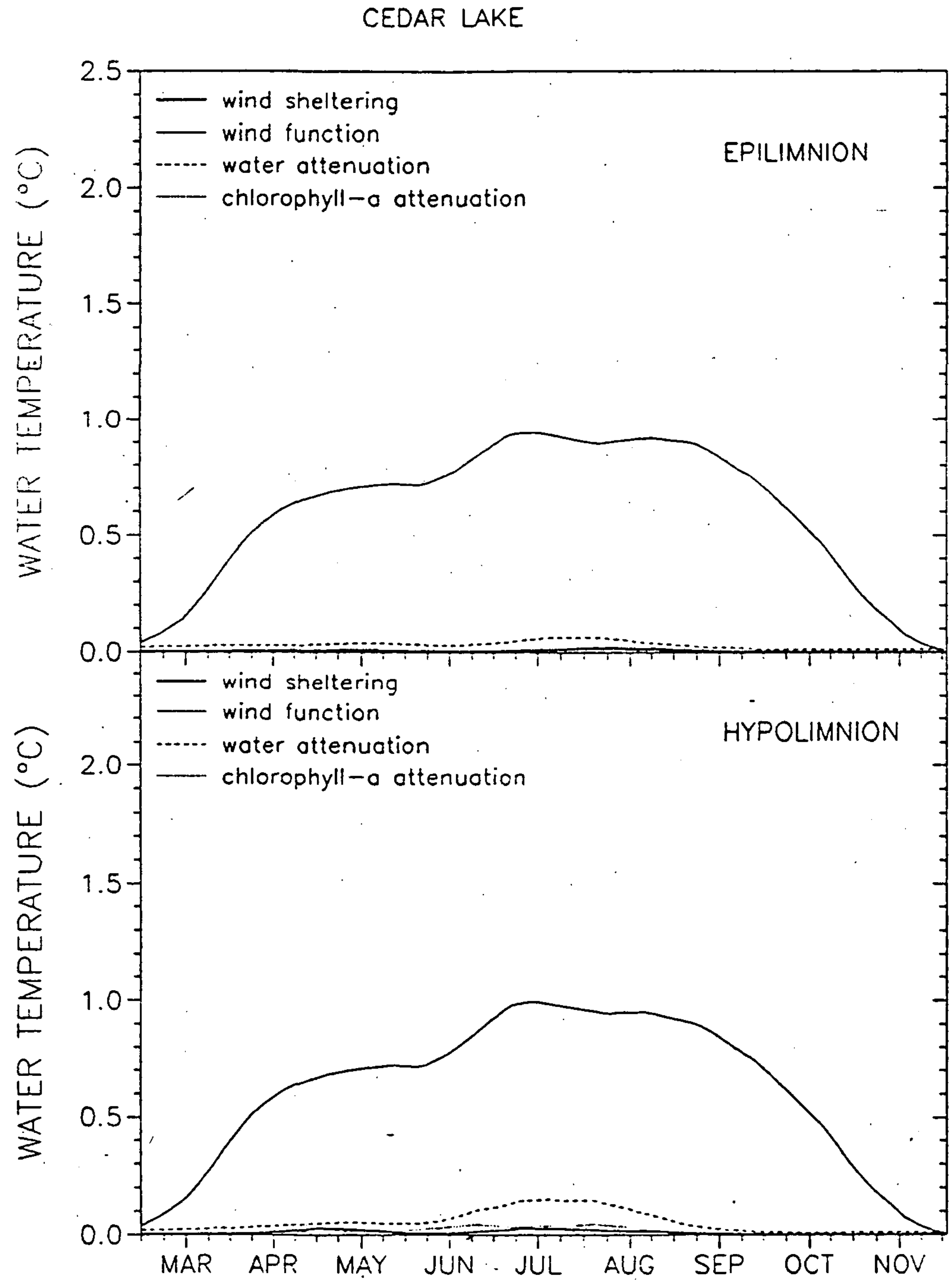

Fig. 2.17 Standard deviations of estimated lake water temperature uncertainties.

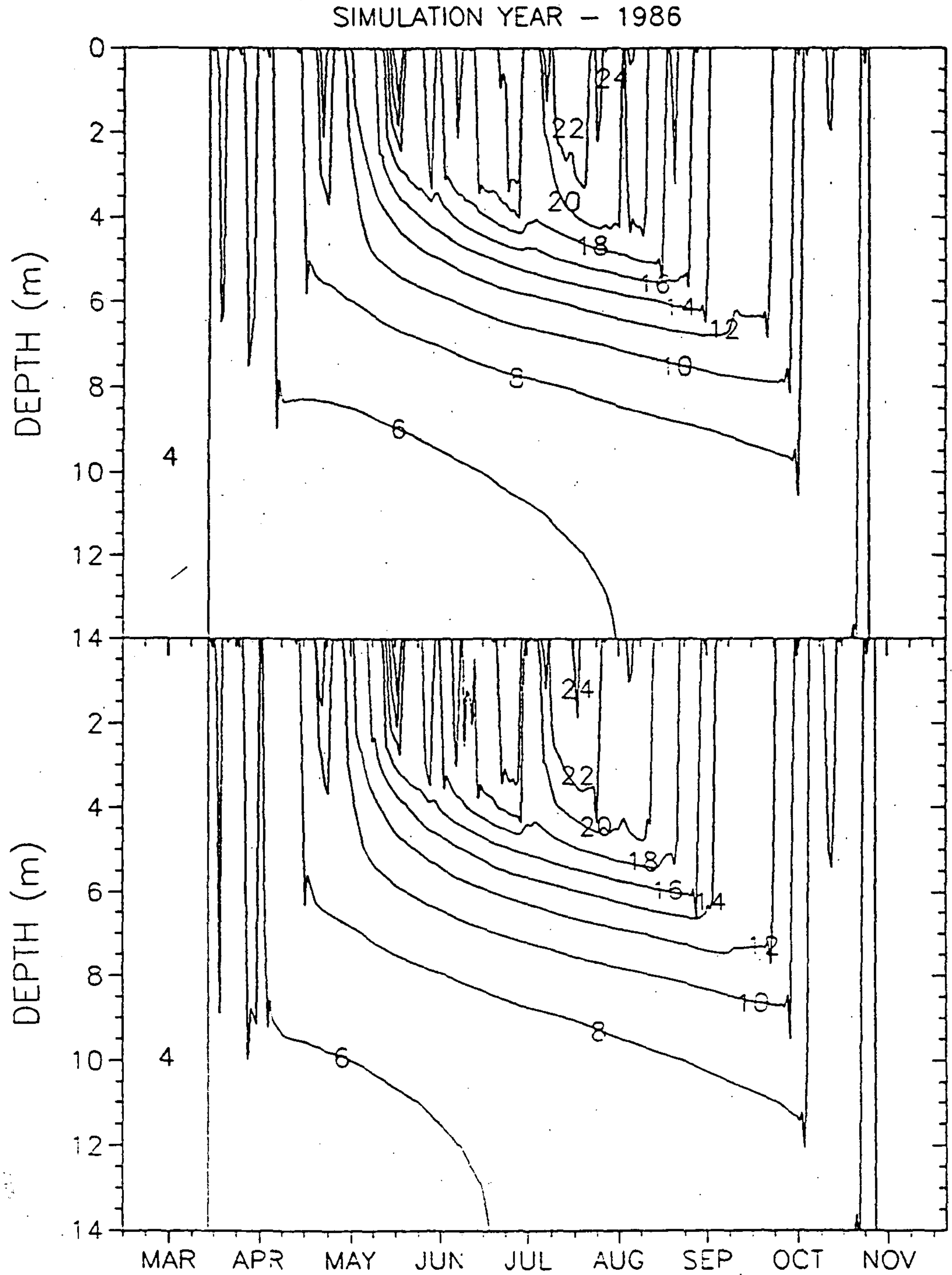

Fig. 2.18 Simulated temperature (isotherm) structure in Thrush Lake. Top shows results from validated model and bottom shows results from regional model.

Table 2.4 Quantitative measure of the success of the simulations – Regional model

Lake	Year	Regional model					Differences regional model – validated model			
		$\hat{T}_m$ (°C)	$\hat{T}_s$ (°C)	E_1 (°C)	E_2 (°C)	r^2 (–)	$\Delta\hat{T}_s$ (°C)	ΔE_1 (°C)	ΔE_2 (°C)	Δr^2 (%)
Calhoun	1971	14.37	14.44	1.02	0.89	0.96	–0.08	0.16	0.10	–1
Cedar	1984	20.64	20.68	1.07	1.15	0.91	–0.18	0.13	0.16	–2
Elmo	1988	13.94	14.31	1.83	1.93	0.90	0.22	0.06	0.13	–2
Fish	1987	24.40	23.90	0.87	0.89	0.89	–0.23	0.07	0.07	–1
Square	1985	14.37	14.90	1.24	1.03	0.95	0.38	0.38	0.24	–2
Waconia	1985	20.14	20.09	0.68	0.68	0.94	–0.03	–0.10	–0.05	2
Greenwood	1986	11.80	12.61	1.24	0.99	0.92	0.64	0.35	0.20	–1
Thrush	1986	11.91	12.54	0.95	0.97	0.95	0.63	0.05	0.06	–1
Williams	1984	17.26	16.57	1.26	1.25	0.95	0.20	0.18	0.18	–1
Average		16.54	16.67	1.13	1.10	0.93	0.17	0.14	0.12	–1

2.6 Conclusions

A lake specific water temperature model was generalized for the application to a wide range of lake classes and meteorological conditions. Functional relationships which differentiate lakes on a regional rather than on an individual basis were developed.

Hypolimnetic eddy diffusivity was estimated as a function of lake surface area, and stability frequency. Equation 2.2 extends Ward's (1977) analysis to a wider range of lake geometries. Although the proposed relationship is a significant simplification of the turbulent diffusion processes taking place in the hypolimnion, it was found to be useful in the seasonal lake water temperature modeling.

Total attenuation coefficient was estimated as a function of Secchi depth (Fig. 2.4). Secchi depth is chosen because it can be measured easily and values are commonly available.

Wind sheltering and wind function coefficient increase with surface area (fetch) of the lake (Figs. 2.5 and 2.6). The wind function coefficient increase is very likely an additional adjustment of the wind velocity coming from land over the lake surface.

Uncertainty analysis revealed moderate sensitivity of simulated lake water temperatures to the variability of individual model coefficients. This could be due to the high thermal inertia of the water especially for the seasonal lake water temperature modeling. Nevertheless epilimnion temperatures showed 1°C standard deviations due to the wind function coefficient variability. Water attenuation, wind function and wind sheltering coefficients equally contribute to the hypolimnetic temperatures variability in an oligotrophic lake.

The proposed model has practical application in lake water temperature modeling, especially in lakes where measurements are not available. The regional model simulates onset of stratification, mixed layer depth, and water temperatures well. Average temperature mean square error was 1.1°C, and 93% of measured lake water temperature variability was explained by the numerical simulations over a wide range of lake classes and trophic levels.

3. Propagation of Uncertainty Due to Variable Meteorological Forcing in Lake Temperature Models

Propagation of uncertainty in lake temperature models is studied using a vector state–space method. The output uncertainty is defined as the result of deviations of the meteorological variables from their mean values. The analysis is applied to systems with correlated and uncorrelated meteorological variables. Surface water temperatures are strongly affected by uncertain meteorological forcing. Air temperatures and dew point temperature fluctuations have significant effect on lake temperature uncertainty. Ignoring correlation in meteorological variables underestimates uncertainties in lake temperature estimates. Long–term average water temperature structure in lakes can be estimated by computer model simulation for just one year when results from a statistical analysis of meteorological variables are used as input. The analysis presents a useful alternative for the study of long–term averages and variability of water temperature structures in lakes due to variable meteorological forcing.

3.1 Introduction

It was shown in Chapters 1 and 2 that vertical water temperature profiles in lakes are related to meteorological variables by heat transport equations which apply basic conservation principles. Atmospheric conditions are the driving force for heat transfer through a lake water surface. Surface water temperatures of lakes are primarily related to the meteorological forcing and secondarily to lake morphometries (Ford and Stefan, 1980a).

Observed meteorological variables used in lake water temperature modeling (Harleman and Hurley, 1976; Ford and Stefan, 1980b) such as solar radiation, air and dew point temperature, and wind speed are usually single realizations of the weather process for a particular year. For lake management purposes and decision analysis we are interested in mean temperatures as well as expected ranges of water temperature variation due to the weather variability over a longer period of time. Deterministic lake water temperature models cannot provide such information from a single model simulation for a particular year. The stochastic alternative is to consider meteorological variables as random variables with estimated statistical properties in terms of first and second moments, and correlation structure. First and second moment of lake temperatures can then be predicted from a single mode simulation.

Lake water temperature models are nonlinear dynamic systems. Approximation techniques for obtaining the second moment of a dynamic system output from the moments of its input have been employed in the area of groundwater hydrology (Dettinger and Wilson, 1981; McLaughlin, 1985; Townley and Wilson, 1985; Protopapas and Bras, 1990; McKinney, 1990).

Generally, three techniques are available i.e. (1) Monte Carlo, (2) derived distribution, and (3) perturbation approach techniques. Monte Carlo methods have been proposed in lake water quality modeling of phytoplankton, herbivores, nitrate, and available phosphorus (Scavia et al., 1981; US Army Corps of Engineers, 1986; Canale and Effler, 1989). Although simple, limitations of this approach have been related to the large number of simulations. In addition, the prescribed probability distribution for the coefficients could change in time–varying systems. The derived distribution approach is not applicable because of the complex relationship between inputs (meteorological variables) and outputs (lake temperatures). The perturbation approach utilizes generally two methods: time domain (state–space) methods of the Taylor series expansion type, and spectral (frequency domain) methods. As pointed out by Protopapas and Bras (1990), state space methods are advantageous for the time variable boundary conditions.

In this Chapter we employed the perturbation vector state–space approach to propagate uncertainty of meteorological input variables into a lake temperature model. This study follows the work of Protopapas (1988) who used the state–space approach for uncertainty propagation of meteorological inputs in a soil/plant model.

The question we want to address in this Chapter is how to predict the lake temperature uncertainty due to the variability of the meteorological forcing in time. This analysis quantifies contribution of each meteorological variable to temperature uncertainty separately. Secondly, we will demonstrate that a long–term average thermal structure in a lake can be obtained without running a water temperature model for several years of meteorological data.

3.2 Numerical Model

In this study a one–dimensional lake water temperature model, which has been previously described in Chapter 1, was used. Lake temperature is represented by a nonlinear partial differential equation (1.1). Nonlinearity comes through the boundary conditions and hypolimnetic eddy diffusivity. Analytical solution of this equation is possible only under certain approximations (Dake and Harleman, 1969). Equation (1.1) is discretized numerically (Appendix B) using an implicit control volume method. This leads to a system of equations in the form

$$A_c(K(k),G)\ T(k+1) = T(k) + H(k) \tag{3.1}$$

where A_c is a system (mxm) tridiagonal matrix, m is the number of discretized control volumes, T(k+1) is a (mx1) vector with lake temperatures at time step k+1, K(k) is a (mx1) vector with lake eddy diffusivity parameters; note that $K(k) = f(T(k), W_s(k))$, W_s is a wind speed, H(k) is a (mx1) vector function with source term parameters, and G is a (mx1) vector with lake geometry parameters. Boundary conditions are treated through the source term. The control volume approach, satisfies the heat balance in the computational domain regardless of the number of discretized control volumes (Patankar, 1988).

The numerical model is applied in daily time steps using mean daily values for the meteorological variables. The required meteorological variables are solar radiation, air temperature, dew point temperature, wind speed and direction. Initial conditions, model setup parameters, have to be provided to the model.

Taylor series expansion is commonly used for the linearization of functional relations around nominal values. The function and its first derivative must be defined at the nominal point. Expanding equation (3.1) in a Taylor's series around the nominal value and keeping first order terms, gives a linear perturbation temperature equation.

$$\hat{A}_c(k)\ T'(k+1) = \hat{B}(k)\ T'(k) + \hat{F}(k)\ C'(k) \tag{3.2}$$

Nominal (mean) values and first order derivatives evaluated at these values are denoted by circumflex. Perturbations of the water temperatures $T'(k)$, and meteorological variables $C'(k)$ are denoted by primes are defined as:

$$T'(k) = T\ (k) - \hat{T}\ (k),\ C'(k) = C(k) - \hat{C}(k) \tag{3.3}$$

The tridiagonal matrix $\hat{A}_c(k)$ is equivalent to the matrix $A_c(k)$ of the deterministic temperature model. Matrices $\hat{B}(k)$ and $\hat{F}(k)$ require evaluation of the first order derivatives of all terms in equation (3.1) which contains lake temperature and meteorological variables at time step k respectively. Details about entries in matrices $\hat{A}_c(k)$, $\hat{B}(k)$, and $\hat{F}(k)$ are given in Appendix C. Terms with the same perturbation parameter are collected before entries into the matrices. Equation (3.2) can be rewritten as

$$T'(k+1) = \phi(k)\ T'(k) + \psi(k)\ C'(k) \tag{3.4}$$

where $\phi(k)$ is transition matrix $\phi(k)=\hat{A}_c^{-1}(k)\ \hat{B}(k)$, and $\psi(k)=\hat{A}_c^{-1}(k)\hat{F}(k)$.

The first term in equation (3.4) describes unforced dynamics of the system while the second term describes the variation of the meteorological forcing function. A schematic illustration of the lake temperature perturbation system is given in Fig. 3.1. Air temperature (T_a), dew point temperature (T_d), solar radiation (H_s), and wind speed (W_s) are forcing meteorological functions. A transition matrix $\phi(k)$ connects the state of the system between time steps.

3.3 First and Second Moment Development

Taking the expected value of equation (3.1) yields the first order estimate of the mean of water temperature

$$E\ [T(k+1)] = \bar{T}(k+1) = \hat{A}_c^{-1}(k)\ (\bar{T}(k) + \hat{H}(k)) \tag{3.5}$$

Notice that the first order estimate of the mean water temperature is exactly the value obtained through the deterministic approach.

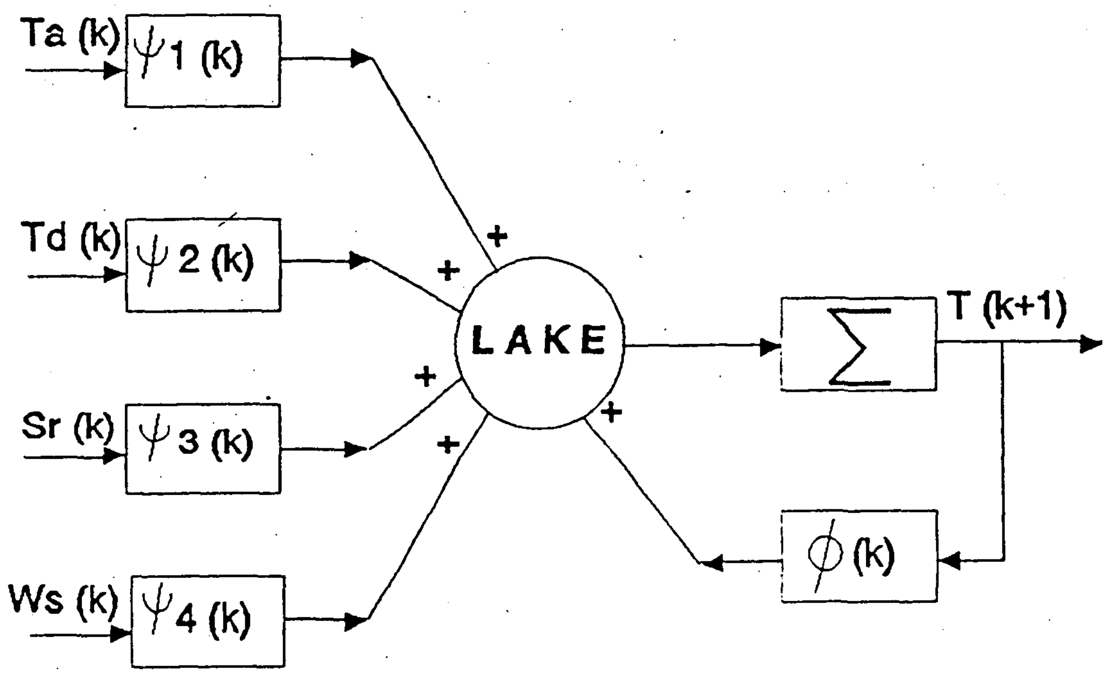

Fig. 3.1 Schematic illustration of the lake temperature perturbation system.

A recursive, solution of equation (3.4) is

$$T'(k) = \phi(k,0)T'(0) + \sum_{n=0}^{k-1} \phi(k,n+1)\ \psi(n)\ C'(n); \qquad T'(0)=0$$

$$T'(k) = \sum_{n=0}^{k-1} \phi(k,n+1)\ \psi(n)\ C'(n) \qquad (3.6)$$

Initial conditions are assumed to be known with certainty i.e. $T'(0)=0$, $\phi(k,s)=\phi(k-1)\phi(k-2)...\phi(s)$, and $\phi(k,k)$ is an identity matrix. Equation (3.6) says that temperature perturbation at time step k is a linear combination of the meteorological forcing perturbations $C'(k)$, $C'(k-1)$,...,$C'(1)$.

The *first order estimate of the mean and covariance temperature* perturbations are obtainable from equation (3.6) (Protopapas, 1988). In the difference equation form

$$\bar{T}'(k+1) = \phi(k)\ \bar{T}'(k) \qquad (3.7)$$

$$\begin{aligned}\Sigma_{T'T'}(k+1) &= E\ [(T'(k+1) - \bar{T}'(k+1))(T'(k+1) - \bar{T}'(k+1))^T] = \\ &\phi(k)\ E\ [(T'(k) - \bar{T}'(k))(T'(k) - \bar{T}'(k))^T]\ \phi(k)^T + \\ &\phi(k)\ E\ [(T'(k) - \bar{T}'(k))\ C'(k)^T]\ \psi(k)^T + \\ &\psi(k)\ E\ [C'(k)(T'(k) - \bar{T}'(k))^T]\ \phi(k)^T + \\ &\psi(k)\ E\ [C'(k)\ C'(k)^T]\ \psi(k)^T \end{aligned} \qquad (3.8)$$

$E\ [T'(k)] = \bar{T}'(k) = 0$ since $E\ [C'(k)] = 0$, and $E\ [T'(0)] = \bar{T}'(0) = 0$. Assuming that perturbations have the following properties

$E\ [C'(k)\ C'(k)^T] = M(k,k)$; $E\ [T'(0)^T]\ E\ [C'(k)] = 0$ yields

$$\begin{aligned}\Sigma_{T'T'}(k+1) &= \phi(k)\Sigma_{T'T'}(k)\phi(k)^T + \psi(k)M(k,k)\psi(k)^T + \\ &\phi(k)\ E\ [T'(k)\ C'(k)^T]\ \psi(k)^T + \psi(k)\ E\ [C'(k)^T\ T'(k)]\ \phi(k)^T\end{aligned} \qquad (3.9)$$

where $M(k,k)$ is a covariance matrix of the perturbed meteorological parameters, and superscript T is the transpose. Since $T(k) = T'(k) + \hat{T}(k)$ then the covariance of the temperature perturbations is equal to the temperature covariance $\Sigma_{T'T'}(k) = \Sigma_{TT}(k)$.

If it could be assumed that weather perturbations are not correlated between successive days (the time step of the water temperature model is one day), nor among themselves, on the same day, equation (3.9) could be simplified by dropping the third and fourth term. Covariance of the water temperature then could be written as

$$\Sigma_{T'T'}(k) = \sum_{n=0}^{k-1} \phi(k,n+1)\psi(n)M_{uc}(k,k)\psi(n)^T\phi(k,n+1)^T; \ \Sigma_{T'T'}(0) = 0,$$

or in difference equation form

$$\Sigma_{T'T'}(k+1) = \phi(k)\ \Sigma_{T'T'}(k)\ \phi(k)^T + \psi(k)M_{uc}(k,k)\psi(k)^T \tag{3.10}$$

where the covariance matrix $M_{uc}(k,k)$ has diagonal terms equal to the variances of the perturbed meteorological variables (Appendix C).

If weather perturbations are correlated between successive days, cross terms (third and fourth) in equation (3.9) have to be evaluated. If we define a disturbance covariance matrix as

$$M(n,k) = E\ [\ C'(n)\ C'(k)^T] = S(n)M_cS(k)^T$$

then

$$E\ [T'(k)\ C'(k)^T] = \sum_{n=0}^{k-1} \phi(k,n+1)\psi(n)S(n)M_cS(k)^T \tag{3.11}$$

where M_c is a correlation matrix between successive days, and $S(n)$, $S(k)$ are "standard deviations" of the covariance matrix $M(n,k)$. If we define $N(k)$ as:

$$\begin{aligned} N(k) &= \sum_{n=0}^{k-1} \phi(k,n+1)\psi(n)S(n) \\ &= \phi(k-1)N(k-1) + \psi(k-1)S(k-1) \end{aligned} \tag{3.12}$$

additional cross terms can be written in difference equation form:

$$\begin{aligned} P_1(k) &= \phi(k)N(k)M_cS(k)^T\psi(k)^T \\ P(k) &= P_1(k) + P_1(k)^T \end{aligned} \tag{3.13}$$

The water temperature covariance (Eq. 3.9) could be written in the difference equation form as

$$\Sigma_{T'T'}(k+1) = \phi(k)\Sigma_{T'T'}(k)\phi(k)^T + \psi(k)M(k,k)\psi(k)^T + P(k) \tag{3.14}$$

Entries of the correlation matrix M_c, $S(k)$, $S(n)$, and the covariance matrix $M(k,k)$, for the case of correlated weather perturbations for successive days as well as cross correlation for the same day, are given in Appendix D.

The first order estimate of the mean and covariance of lake temperatures can only be properly applied if the variations of the normalized input meteorological variables are a small fraction of one.

Lake temperature covariance propagation is calculated in the following steps: (1) Set isothermal (4°C) initial steady state conditions for lake water temperatures in spring, initialize covariance matrix of meteorological perturbations; (2) read meteorological variables, mean and perturbation values, for the next time step; (3) using mean values for meteorological variables, compute first moment of lake temperature profile for the next time step (Equation (3.5), store matrix $A_c(k)$; (4) compute matrices $\hat{B}(k)$, $\hat{F}(k)$, i.e. first order derivatives with respect to the perturbed meteorological variables and estimated lake temperatures (Appendix C); (5) calculate matrix $N(k)$ for the correlated case (Equation 3.12); (6) compute transition matrix $\phi(k)$, and $\psi(k)$; (7) calculate additional term $P(k)$ (Equation 3.13) for the correlated case; (8) propagate and store temperature covariance matrix $\Sigma_{T'T'}$ for the next time step (correlated case Equation 3.14, uncorrelated Equation 3.10); (9) store transition matrix $\phi(k)$, and $\psi(k)$, if correlated case, store in addition $P(k)$, and $S(k)$; (10) go to step 2 if last day of simulation is not reached.

3.4 Lake Calhoun – Application

The test lake, Lake Calhoun, is a temperature zone dimictic lake. The lake is eutrophic with maximum depth of 24 m, and surface area of 1.7 km^2. Meteorological data used are from the Minneapolis St. Paul International Airport, located 10 km from the lake.

Daily meteorological data time series (1955–1979), averaged over 25 years, are given in Fig. 3.2. Long term means of solar radiation, dew point temperature, and air temperature display typical seasonal cycles. Means are increasing till the end of summer and decreasing towards fall. Perturbations (standard deviations) for meteorological forcing variables are also obtained by direct data processing. They describe weather variability over 25 years for a particular day. Standard deviations were higher in spring and fall than in summer (Fig. 3.2).

The time series for each meteorological variable is reduced to a residual series by removing periodic means and standard deviations as pointed out by Richardson (1981). The dependence among the meteorological variables was described by calculating cross correlation coefficients of the residual time series. The serial correlation coefficients for time lags up to 3 days are given in Table 3.1. The serial correlation coefficients for the one day lag were significant for air temperature (0.69) and dew point temperature (0.66). A significant cross correlation coefficient (0.8) was calculated for zero time lag (the same day) between dew point temperature and air temperature. Other meteorological variables were uncorrelated for the same day.

The first order estimate of the mean and covariance temperatures is constrained to parameter perturbations within only the linear region about the model trajectories. Linear approximation could be questionable when the coefficient of variation for the parameter of a highly nonlinear function increases above 0.3 (Gardner et al., 1981). Average coefficients of variation for input meteorological variables are: air temperature 0.13, dew point temperature 0.17, wind speed 0.33, and solar radiation 0.37. Although the

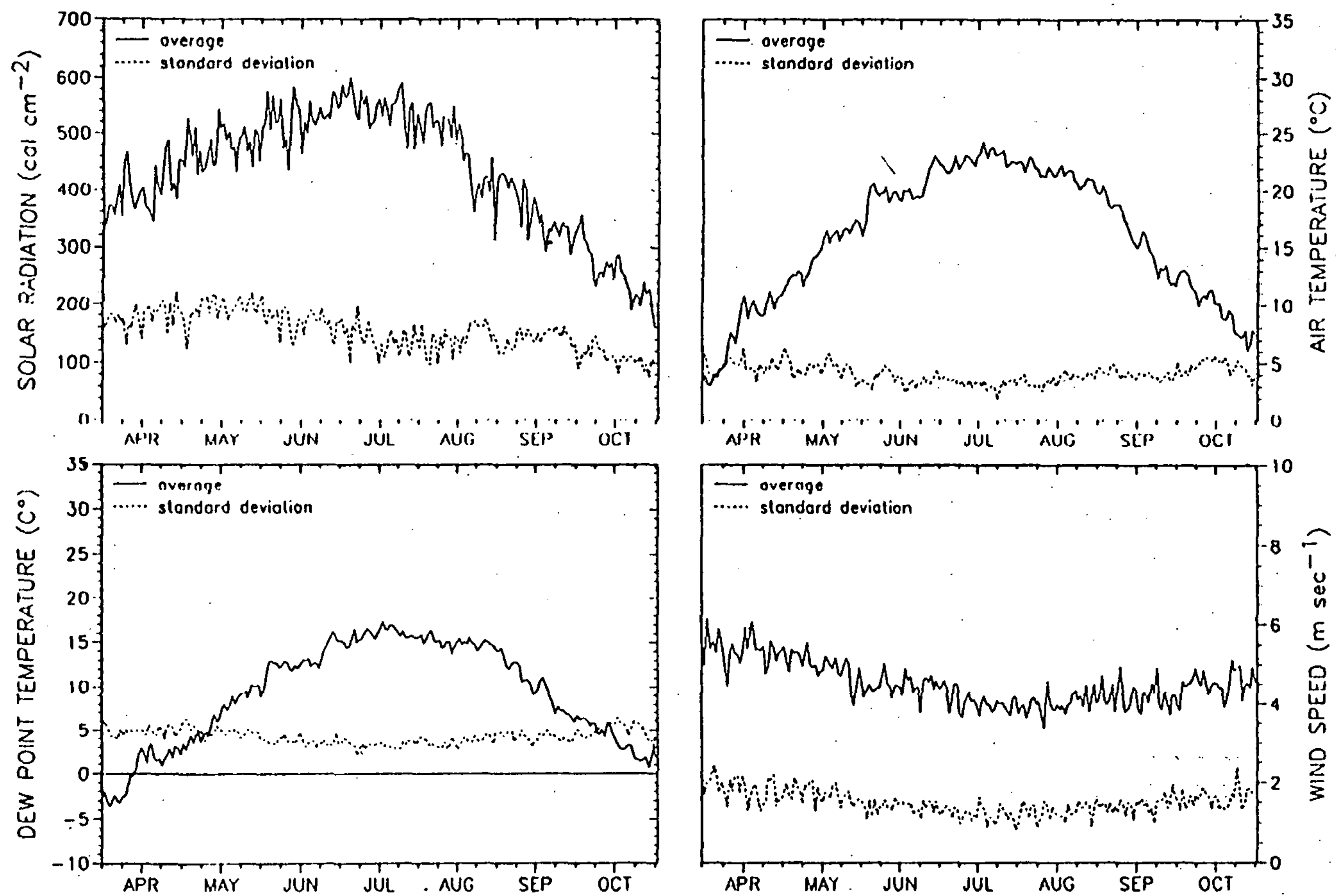

Fig. 3.2 Meteorological variables at Minneapolis/St. Paul. Daily means and standard deviations for the period 1955–1979.

Table 3.1 Correlation coefficients of daily meteorological variables for Minneapolis–St. Paul, 1955–1979.

	Solar Radiation			Air Temperature			Dew Point Temperature			Wind Speed		
	Time Lag (days)			Time Lag (days)			Time Lag (days)			Time Lag (days)		
	0	1	2	0	1	2	0	1	2	0	1	2
Solar Radiation	1.00	0.39	0.14									
Air Temperature	0.18	0.17	0.11	1.00	0.69	0.38	0.80	0.58	0.29			
Dew Point Temperature	–0.25	–0.14	–0.06	0.80	0.54	0.26	1.00	0.66	0.33			
Wind Speed	–0.16	–0.05	–0.04	0.11	0.08	0.07	0.09	0.07	0.06	1.00	0.38	0.18

solar radiation had the highest variability note that it is linearly related through the source term to the water temperature equation (Equations 1.1, 1.2, 1.3, and 1.4)

3.4.1 First moment analysis

The nonlinear lake temperature model was used for the first moment temperature estimation. Model setup parameters which are basically related to lake geometry have been estimated by comparing model simulations with measurements (Chapter 2). The standard error between measurements and simulations was about 1.0 °C. The error is mostly associated with small differences between measured and predicted thermocline depths.

Long term average temperature structure in Lake Calhoun was obtained using two different methods. In the first method, the lake temperature model computed the vertical temperature structure in the lake for each of twenty five years (1955–1979), separately using daily values for meteorological data. The results of these twenty five years of simulated lake temperatures were statistically analyzed in terms of mean (T_{eav}) and standard deviation (σ_{eav}) for the particular day. In the second method, twenty five years of daily meteorological data were first statistically analyzed to provide daily means and standard deviations. This averaged meteorological year was used in a single simulation run to obtain the average daily water temperature (T_{av}) throughout a season.

Epilimnetic and hypolimnetic lake temperatures obtained by these two methods are compared in Fig. 3.3. Epilimnion temperature is defined as the temperature of the upper isothermal (mixed) layer. Hypolimnetic temperature is a volume weighted average temperature below the upper isothermal layer down to the lake bottom (Equation 2.5). Nearly identical temperature distributions were obtained by the two methods. Maximum difference was less than 1°C at any time of the season. Isotherms obtained by the two methods are compared for the entire period of simulation in Fig. 3.4. Onset of stratification and mixed layer depths can be seen to be nearly identical.

3.4.2 Second moment analysis

Uncertainty in the lake temperatures is measured by the variance of the model output. Temperature covariance propagation was calculated by using the proposed vector state–space perturbation model. Two cases were considered: (1) uncorrelated meteorological variables, (2) correlated meteorological variables. "Uncorrelated" means that daily meteorological variables were independent of each other at any time. "Correlated" means that a correlation between air and dew point temperature at zero and one day time lag existed. These two meteorological variables were considered because they had significant correlation, and as will be shown later, this resulted in a significant contribution to lake temperature uncertainty.

The Long–term average temperature structure in the lake was calculated using the second method in the first moment analysis. Perturbations for meteorological forcing variables are given in Fig. 3.2.

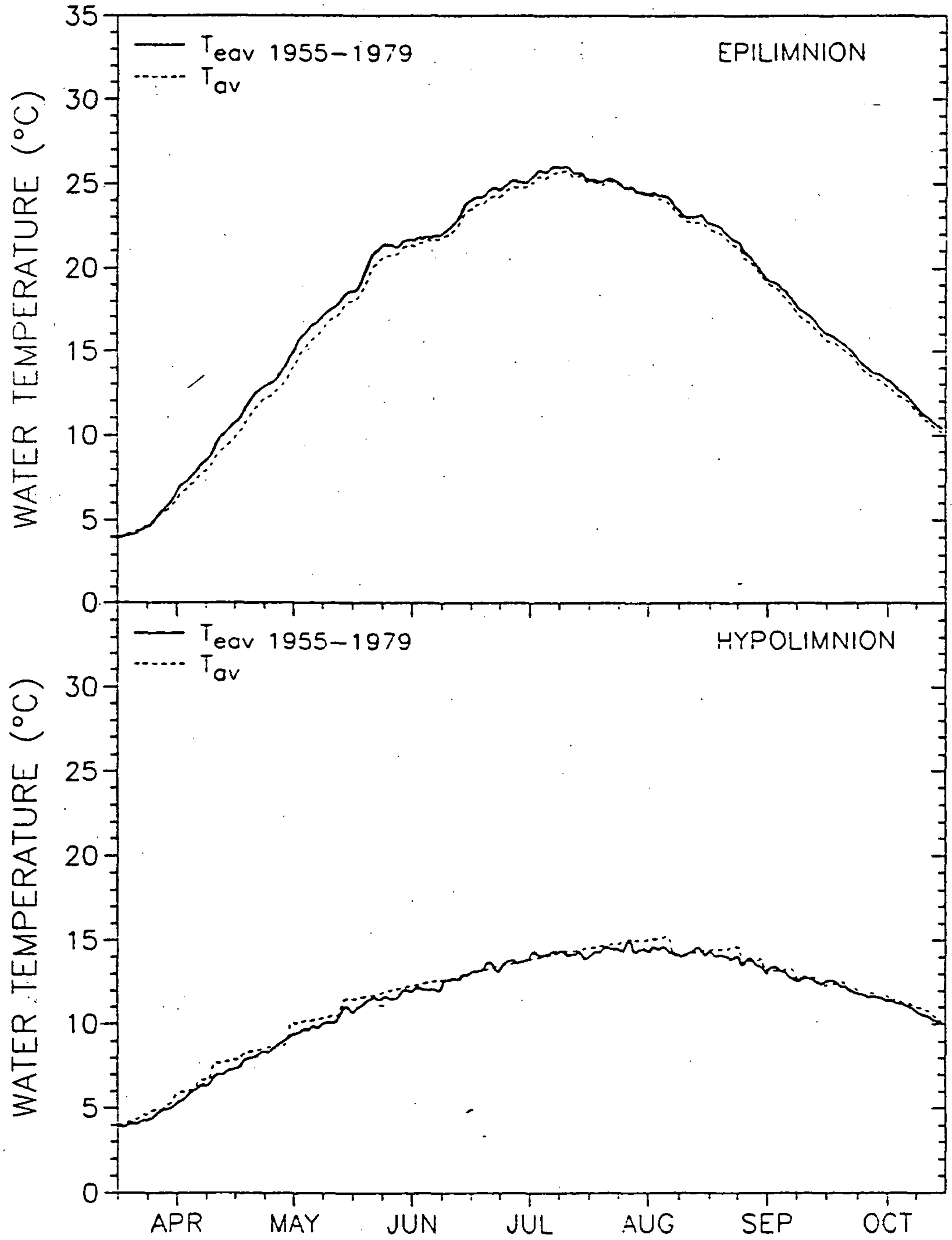

Fig. 3.3 Estimated long–term average epilimnion and hypolimnion temperatures.

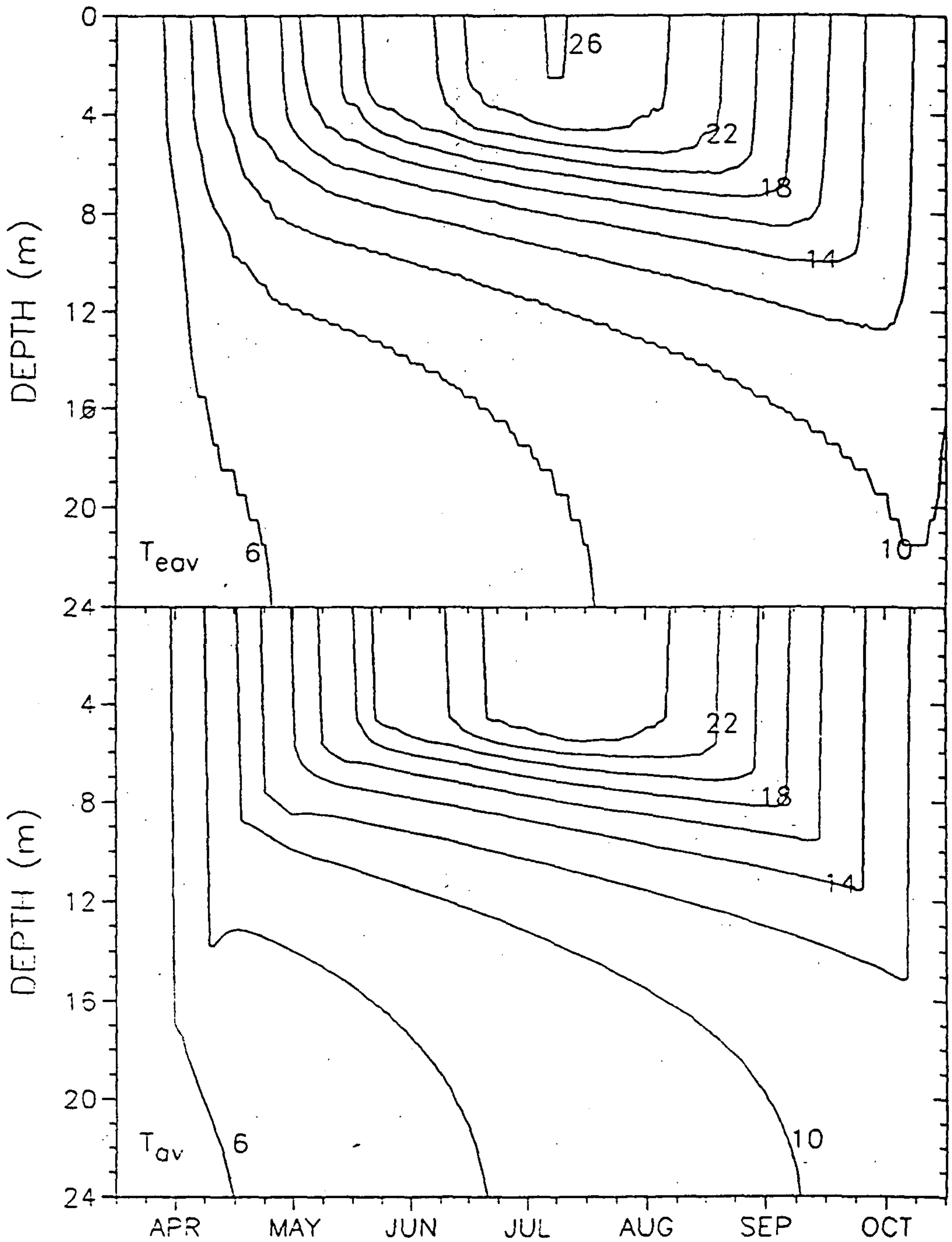

Fig. 3.4 Long-term average isotherms in Lake Calhoun.

Standard deviations of simulated epilimnion and hypolimnion temperatures are given in Figs. 3.5 and 3.6, respectively. Contributions by perturbations of individual meteorological variables perturbations as well as the total contribution of all perturbation variables were calculated with correlated and uncorrelated input variables at a daily timestep. Air and dew point temperature contributed the most to the temperature uncertainty, while solar radiation and wind speed had smaller effects. Furthermore, the overall uncertainty in water temperature was found to be larger in the case of the correlated daily process than in the uncorrelated one. Uncertainty in lake water temperature varies with time, since sources of uncertainty vary with time. These sources are, the sensitivity of lake temperatures to meteorological variables as well as the amount of the uncertainty concerning these variables. At the beginning of the simulated period uncertainty was set to zero since initial conditions were considered perfectly known. Isothermal initial conditions of 4°C (after ice thaw) April 1 are appropriate for the 45° latitude. Although isothermal water at 4°C may not exactly exist on April 1, thermal inertia of the water makes summer predictions insensitive to initial conditions if a starting date at or before "ice-out" is chosen (Chapter 2). Three periods can be distinguished in Fig. 3.5 : a steep rise in temperature uncertainty in spring, more or less constant uncertainty after onset of stratification in summer, and decreasing uncertainty in fall when lake temperature is driven towards isothermal conditions. Temperature uncertainty is decreasing in fall when observed meteorological variables and estimated lake water temperatures are both decreasing. First order derivatives with respect to the lake temperatures and meteorological variables are evaluated at these observed and estimated values respectively. Thus, they have less weight in uncertainty propagation.

Uncertainty propagation for deep hypolimnetic temperature (1m above lake sediments) is given in Fig. 3.6. In spring and fall, during well-mixed conditions (overturn periods), standard deviations of 0.4 °C (correlated case) and 0.3 °C (uncorrelated case) are calculated. During stable stratification, uncertainty was not significant. This is a result of the fact that Lake Calhoun has no significant continous point inflows (tributaries). Summer temperature in the hypolimnion was determined by mixing events in spring, and remained almost constant throughout the fall overturn (Ford and Stefan, 1980a). In lakes with point inflows this would not be the case, due to plunging flow phenomena.

Vertical profiles of the first moment lake temperatures, plus or minus one standard deviation interval, are shown in Fig. 3.7. Spring (April) and fall (October) indicated periods when uncertainty propagates throughout the entire lake depth. These are the periods of weak stratification or well mixed conditions. Uncertainty was decreasing with depth. After the onset of stratification estimated uncertainty was much more significant for the epilimnetic layer than for the hypolimnetic layer. For the same period of time, deep water had insignificant lake temperature uncertainty.

The first moment epilimnion temperature estimates plus or minus one standard deviation obtained by two different approaches for the 1955–1979 period are compared in Fig. 3.8. In the first approach the deterministic water temperature model was run for 25 years using daily meteorological

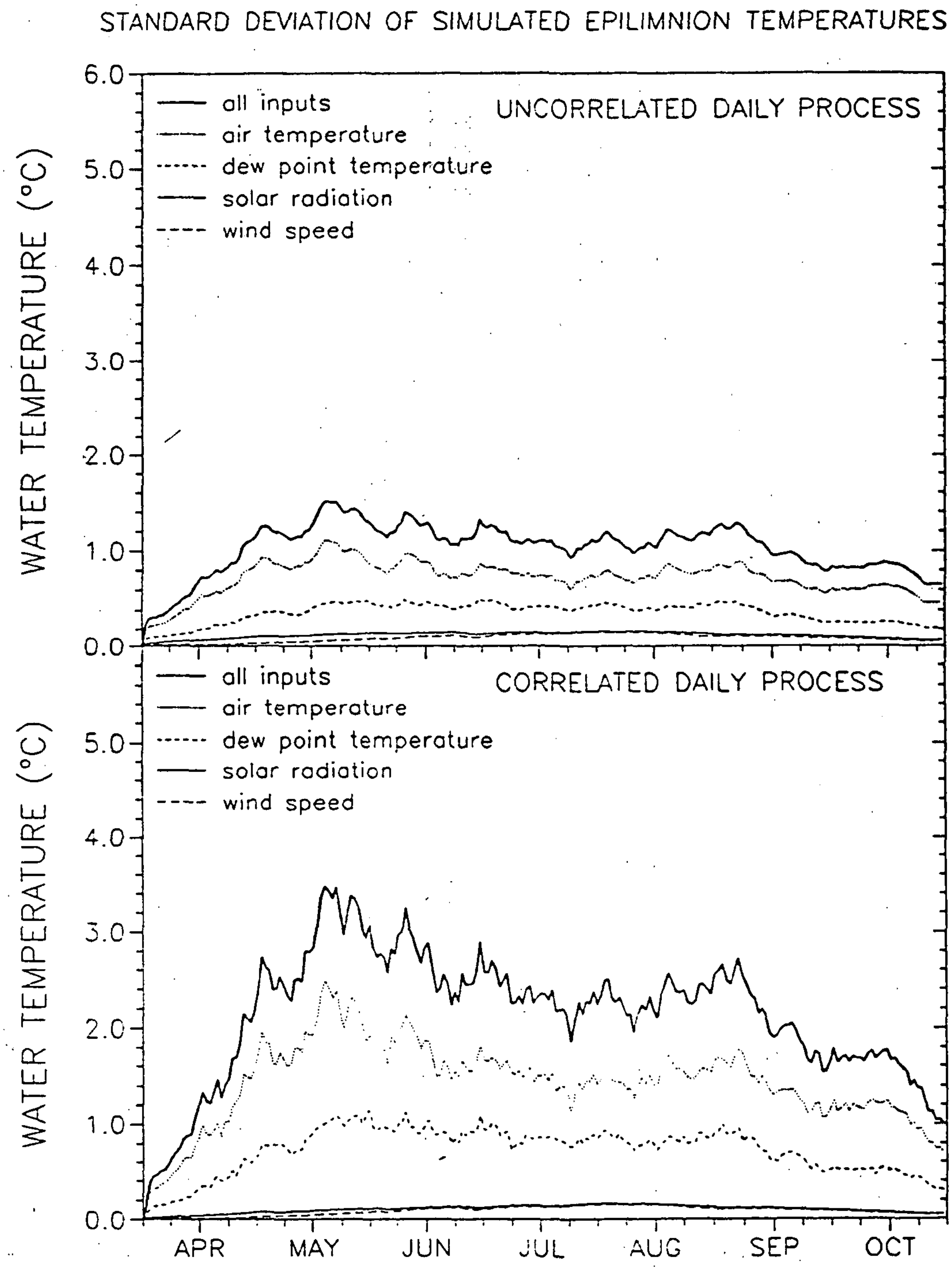

Fig. 3.5 Standard deviations of estimated epilimnion temperature uncertainties. Contributions by several meteorological variables and totals are shown.

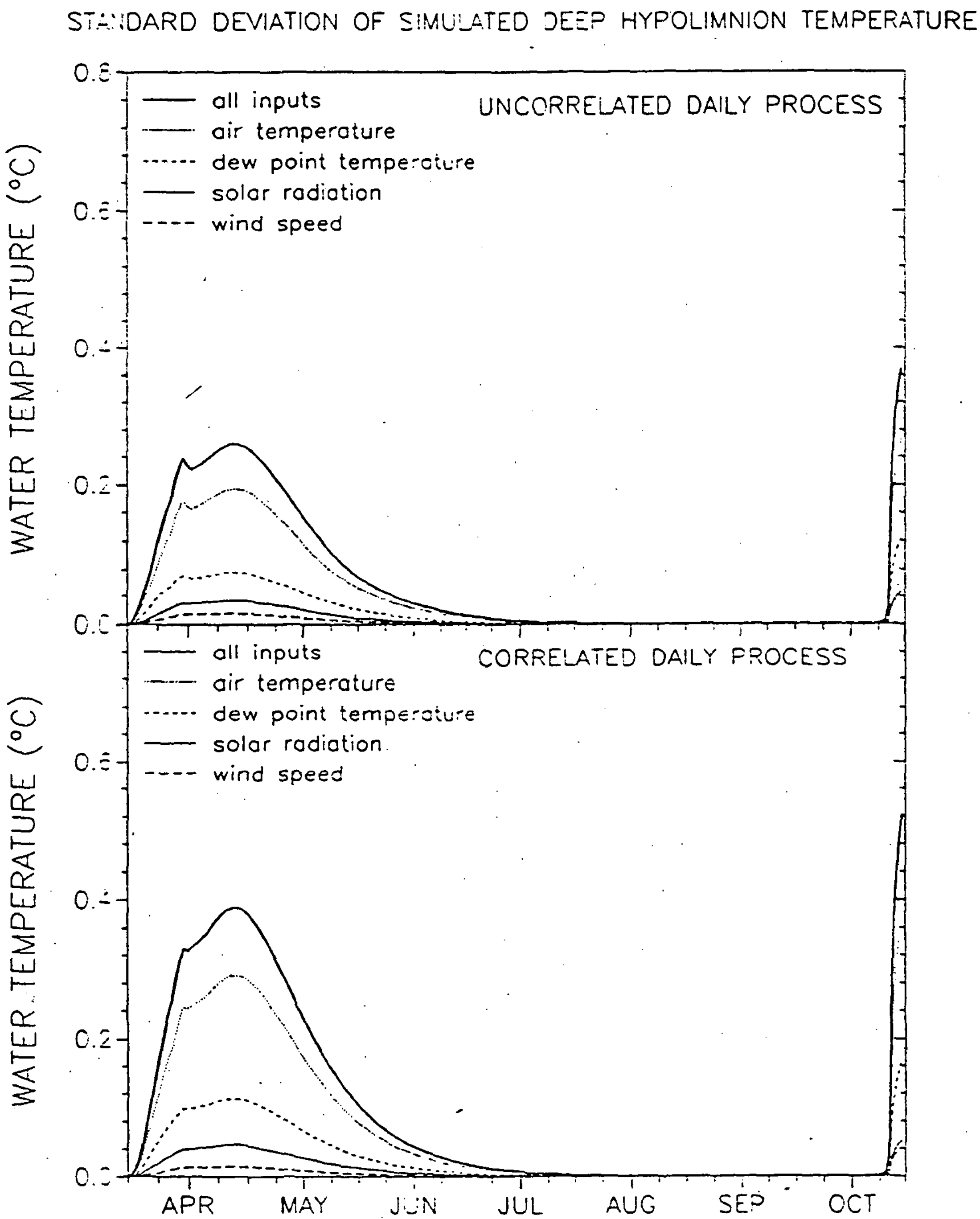

Fig. 3.6 Standard deviations of estimated deep water temperature uncertainties. Contributions by several meteorological variablesand totals are shown.

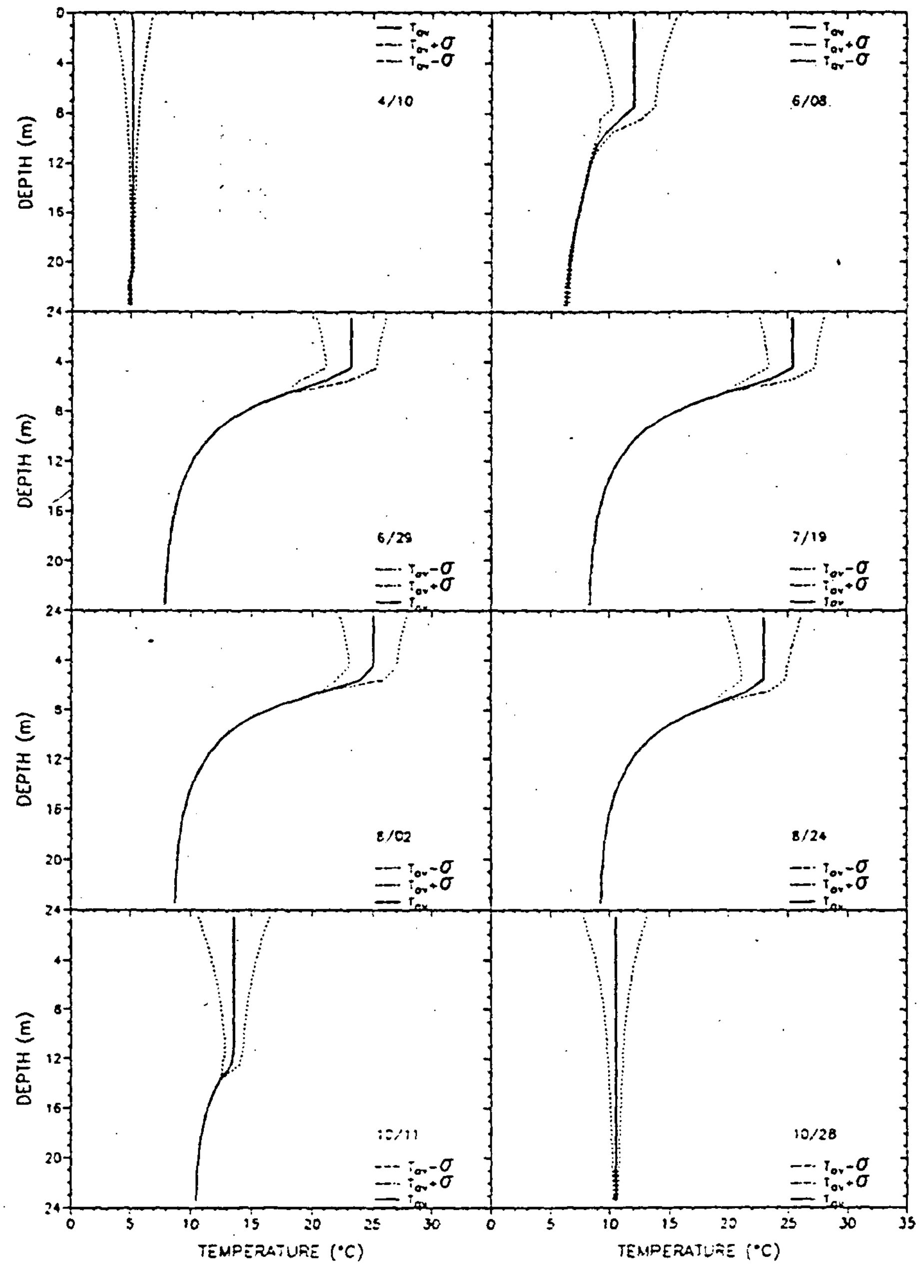

Fig. 3.7 Long–term average temperature profiles plus or minus one standard deviation in Lake Calhoun.

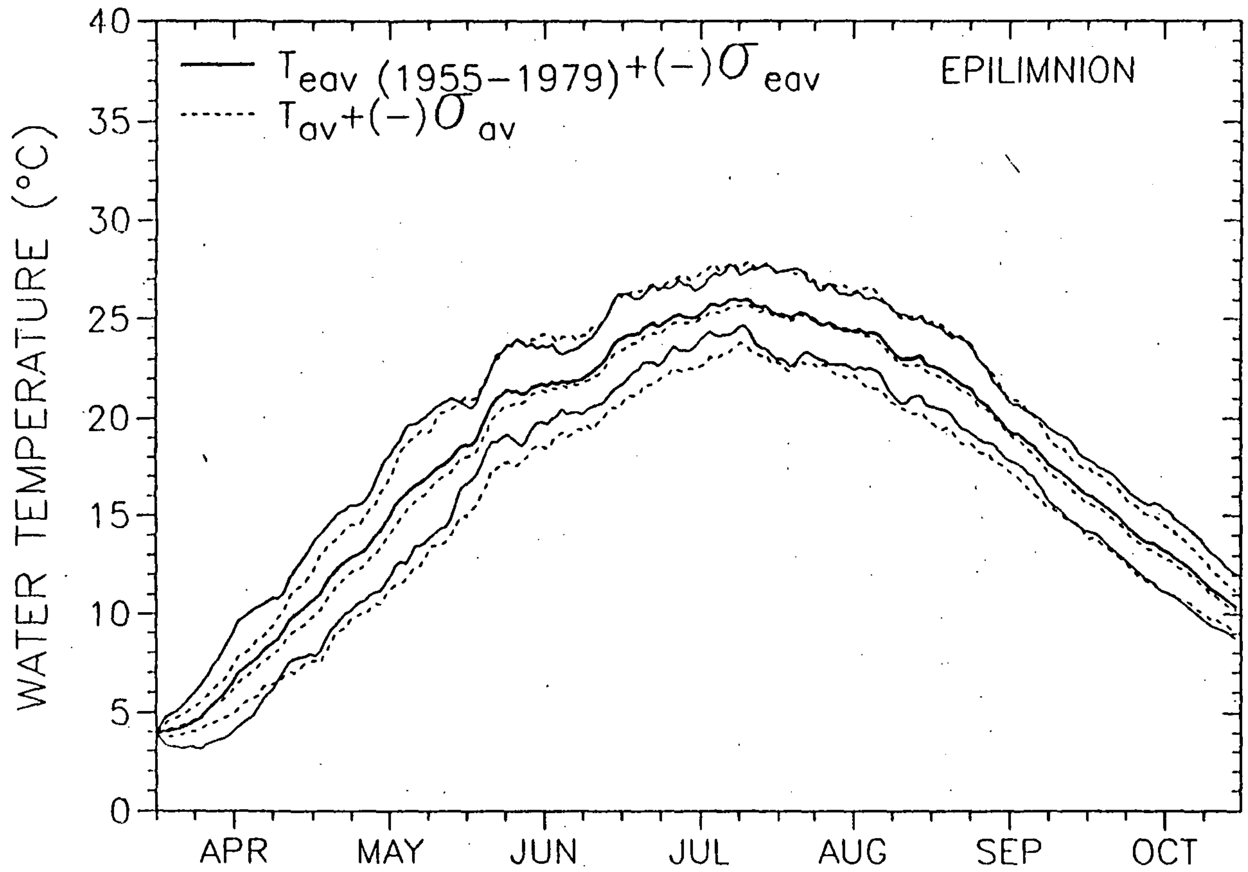

Fig. 3.8 Epilimnion temperature long-term average plus or minus one standard deviation.

data. Long term average (T_{eav}) and standard deviations (σ_{eav}) were estimated from the simulated lake water temperatures over the 25 year period. In the second approach the long term average (T_{av}) temperature structure in the lake was estimated using the method described in Section 5.1. Water temperature variability (σ_{av}) was estimated using the proposed perturbation model. Results shown are for correlated meteorological perturbation variables. The maximum difference was less than 2°C for the range of 23°C variability.

3.5 Conclusions

A first order analysis of uncertainty propagation in lake temperature modeling has been made. The source of the uncertainty is variable meteorological forcing which enters the lake temperature equations through the source term and boundary conditions. The analysis presents a useful alternative for the study of long–term averages and variability of temperature structures in lakes due to variable meteorological forcing.

The analysis applied herein can be applied to systems with correlated and uncorrelated meteorological parameters. The main findings are:

(1) Long–term average temperature structure in lakes can be estimated by using the results of a statistical analysis of long–term meteorological variables as input in a computer model simulation for just one year.

(2) Air temperature and dew point temperature have significant effect on lake temperature uncertainty.

(3) Epilimnetic temperature uncertainty has three distinct periods : steep rising uncertainty in spring, steady uncertainty in summer, and falling uncertainty in fall. The maximum standard deviation of 4°C of epilimnetic temperature uncertainty was estimated in the summer for the 25 year a period.

(4) Hypolimnetic temperatures were not strongly affected by uncertain meteorological forcing. Standard deviations of less than 1°C were estimated in spring and fall during the overturn periods.

(5) Ignoring the correlation of air and dew point temperatures underestimates uncertainties in lake temperature estimates. Accounting for correlations gives better agreement with lake water temperatures obtained by 25 years of estimated lake temperatures.

4. Case Studies of Lake Temperature and Stratification Response to Warmer Climate

The impact of climatic warming on lakes will most likely have serious implications for water resources and water quality. Rather than using model predictions of greenhouse warming, this chapter looks at the changes in heat balance and temperature profiles in a particularly warm year (1988) compared to a more normal one (1971). The comparisons are made for three different morphometrically different lakes located at 45° north latitude and 93° west longitude (North Central USA) and for the summer period (April 1 to October 31). Water temperatures are daily values simulated with a model driven by daily weather parameters and verified against several sets of measurements. The results show that in the warmer year epilimnetic water temperatures were higher, evaporative water loss increased, and summer stratification occurred earlier in the season.

4.1 Introduction

A validated one-dimensional lake water temperature model, which has been described in Chapters 1 and 2, was used to study the changes in a lake as a result of different weather conditions. In this chapter use of such a model is demonstrated by application to three different morphometrically lakes with sparse data sets. The lakes are located near 45° northern latitude and 93° western longitude in northcentral United States. The lakes are Lake Calhoun, Lake Elmo, and Holland Lake in the Minneapolis/St. Paul metropolitan area.

In the summer of 1988, the northcentral region of the United States experienced very dry and hot weather and this was selected to represent a "warm climate" in this study, while for "normal" conditions, the year 1971 was chosen. 1988 tied for the warmest year in the 100-year global record of instrumentally recorded air temperatures (Kerr, 1989). Uncertainty analysis of the effects of variable meteorological forcing on lake temperature models indicates that air temperature has the most significant effect on lake temperature uncertainty (Henderson-Sellers, 1988; Chapter 3). 1971 was normal in the sense that mean air temperature from May to September was only 0.2°C below the normal from 1941 to 1970. The effects of the 1988 (warmer) and the 1971 (normal) summer climate on temperatures and stratification in the three lakes are reported herein.

4.2 Method of Lake Temperature Modeling

The test lakes, Lake Calhoun, Lake Holland, and Lake Elmo, are three temperature zone dimictic lakes. Water temperature data were collected in Lake Calhoun in 1971 (Shapiro and Pfannkuch, 1973) and used to validate the model for normal weather conditions. For warmer conditions (1988) the model was validated with data from Lake Elmo and Lake Holland (Osgood, 1989). The terrain in which the lakes and weather stations are located is flat and quite uniform with respect to land use (residential and park land). Morphometric characteristics, Secchi–depths and chlorophyll–a measurements for all three lakes in 1984 (Osgood, 1984) are given in Table 4.1. Lake Elmo surface area is equal to the median value of 970 statistically analyzed lakes in the North Central Harwood Forests ecoregion in Minnesota (Heiskary and Wilson, 1988). Lake Calhoun and Holland Lake have a larger and smaller surface area than the median, respectively. All three lakes were classified as eutrophic. Secchi depths and chlorophyll–a were close to the median values of the lakes in the ecoregion.

Table 4.1 Lake data

Lake	Mean depth [m]	Max depth [m]	Surface area [km^2]	Volume [$10^6 m^3$]	Secchi Depth [m]	Typical Summer, Chla [$g\ m^{-3}$]
Calhoun	10	24.0	1.71	17.1	2.5	20
Elmo	13.4	41.8	1.23	16.5	2.8	8
Holland	4.6	18.8	0.14	0.65	2.2	28

Meteorological data used are from the Minneapolis–St. Paul International Airport located 5 to 18 miles from the studied lakes. The meteorological data file contains measured daily values of average air temperature (T_a), dew point temperature (T_d), precipitation (P), wind speed (U_a) and solar radiation (H_s). Mean and standard deviations (S.D.) for those parameters averaged over the simulation period, from May through September, are given in Table 4.2. Mean summer air temperature in 1988 (21.6 °C) was 2.9°C higher than in 1971 (18.7 °C). May to September is the main period of interest. Mean April air temperature was about the same in 1971 and 1988, but October 1988 was much colder than normal. Wind, the most important external hydrodynamic force causing mixing in the lake, had similar values for both periods in terms of mean and standard deviation. Mean solar radiation was 18% higher in 1988 than in 1971.

The model assumes isothermal initial conditions of 4°C on April 1. This is appropriate for the 45° latitude. Dates of ice formation, thaw and duration have been continuously recorded on Lake Mendota (Wisconsin, 43° latitude) since 1855. The mean date of ice thaw was April 5 with 11 days standard deviation (Robertson, 1989). Model sensitivity to the date of the initial isothermal conditions is summarized in Table 4.3. Epilimnetic temperatures are very well simulated throughout the entire summer period

Table 4.2 Mean Monthly Meteorological Data

	T_a [°C] Max	Min	Aver.	Diff. from Normal*	T_d [°C]	P [mm]	W [ms^{-1}]	HS [cal $cm^{-2}d^{-1}$]
Year 1971								
APR	14.9	1.7	8.3	0.6	−1.7	0.9	5.1	411
MAY	19.4	6.5	13.0	−1.3	2.8	2.6	4.6	482
JUN	27.4	16.5	21.9	2.0	15.0	3.0	4.0	450
JUL	26.5	14.3	20.4	−2.3	12.8	3.2	4.1	563
AUG	27.5	14.2	20.9	−0.8	12.2	1.4	3.8	479
SEP	22.9	11.3	17.1	1.2	10.0	2.3	4.1	338
OCT	15.7	5.8	10.8	0.5	6.7	4.6	4.5	192
MEAN(MAY to SEPT)	24.7	12.6	18.7	−0.2	10.6	2.5	4.1	462
σ (MAY to SEPT)	3.15	3.45	3.26	1.60	4.20	0.63	0.26	72.7
Year 1988								
APR	15.1	2.0	8.5	0.8	−2.4	1.3	4.6	469
MAY	25.7	11.4	18.5	4.2	7.1	1.4	5.1	584
JUN	30.5	16.6	23.5	3.6	12.3	0.2	4.8	654
JUL	32.3	18.8	25.6	2.9	14.5	0.9	4.4	610
AUG	29.3	17.3	23.3	1.6	15.3	3.5	4.8	497
SEP	22.8	10.9	16.9	1.0	9.8	2.4	4.8	331
OCT	12.5	0.8	6.7	−3.6	−0.6	0.7	4.7	284
MEAN(MAY – SEPT)	28.2	15.0	21.6	2.7	11.8	1.7	4.8	535
σ (MAY – SEPT)	3.42	3.23	3.29	1.20	3.03	1.16	0.23	114

*Normal is the 30–year average from 1941 to 1970

σ = standard deviation

Table 4.3 Differences (°C) in simulated mean daily epilimnetic and hypolimnetic temperatures for different starting dates of the model (April 1 reference)

	Epilimnion							Hypolimnion						
	MAY	JUN	JUL	AUG	SEP	OCT	SEASON	MAY	JUN	JUL	AUG	SEP	OCT	SEASON
Year 1971														
MAR 1	–0.05	–0.07	0.00	0.00	0.00	0.00	–0.02	–0.19	–0.24	–0.28	–0.30	–0.32	–0.33	–0.28
MAR 12	–0.09	–0.08	0.00	0.00	0.00	–0.01	–0.03	–0.29	–0.34	–0.39	–0.41	–0.43	–0.45	–0.39
MAR 22	–0.09	0.07	0.01	–0.01	–0.05	–0.03	–0.02	–0.18	–0.18	–0.18	–0.19	–0.19	–0.19	–0.18
APR 10	0.05	0.01	0.00	0.00	0.00	0.00	0.01	0.08	0.03	0.01	0.00	0.00	0.01	0.02
APR 20	0.91	–0.03	0.00	0.00	0.02	0.08	0.16	1.77	1.59	1.46	1.35	1.26	1.20	1.44
Year 1988														
MAR 1	0.14	0.00	0.00	0.00	0.01	0.03	0.03	0.48	0.49	0.51	0.52	0.52	0.44	0.49
MAR 12	0.07	0.00	0.00	0.00	0.00	0.01	0.01	0.01	0.13	0.10	0.10	0.10	0.08	0.10
MAR 22	0.07	0.00	0.00	0.00	0.00	0.01	0.01	0.29	0.30	0.32	0.33	0.33	0.28	0.31
APR 10	0.70	0.03	0.00	–0.02	–0.04	–0.06	0.10	1.42	1.46	1.44	1.43	1.42	1.40	1.43
APR 20	1.60	0.08	0.00	–0.03	–0.07	–0.15	0.24	3.14	2.93	2.79	2.77	2.67	2.59	2.82

regardless of the starting date of the model. Surface water temperatures "catch up" in time. Hypolimnetic summer water temperatures are good as long as the model is started before seasonal stratification sets in. Better results are obtained if temperature is not allowed to drop below 4°C after start of the simulation. Although isothermal water at 4°C may not exactly exist on April 1, thermal inertia of the water make summer predictions insensitive to initial conditions if a starting date at or before "ice-out" is chosen.

4.3 Model Validation

The model was validated with water temperatures measured in Lake Elmo and Holland Lake in 1988. Eight examples of measured and calculated water temperature profiles for these lakes are given in Figs. 4.1 and 4.2. Actually 16 profiles were measured in each lake. Simulations started with isothermal conditions (4°C) on April 1 and progressed in daily timesteps until October 31. Model coefficients were kept at their initially specified value throughout this period. The model simulates onset of stratification, mixed layer depth and water temperatures well. Standard error between measurements and simulations was 2.0 °C and 1.5 °C for Elmo and Holland, respectively. This is mostly due to small differences in the predicted thermocline depth. A model validation for Lake Calhoun was made for 1971. Measured and calculated water temperature profiles are given in Fig. 4.3. Comparison shows that the onset of stratification, mixed layer depth and temperature were well predicted. Standard error was 1.4°C.

4.4 Results and Discussion

4.4.1 Thermal energy budget

Mean monthly heat balance terms for 1971 and 1988 are given in Table 4.4. Short wave solar radiation (H_{sn}) and longwave atmospheric radiation (H_a) increase the water temperature, while evaporation (H_e), and back radiation (H_{br}) cool the water. Conductive heat transfer (H_c) can either heat or cool the water. These five mechanisms, mainly responsible for the net heat energy input to the water, changed from month to month and from year (1971) to year (1988). Solar radiation (H_{sn}) and atmospheric radiation (H_a) are only given once because they are the same for all three lakes. Cumulative heat balance terms for both simulated periods are given in Table 4.5.

Under warmer conditions (1988) more solar radiation reached the lake surfaces. The cumulative difference at the end of the simulation period was 5000 kcal m^{-2}. The additional available solar radiation increased the surface–water temperature and stability (defined as a density difference between adjacent layers) of the water column (Spigel et al., 1986) as will be shown.

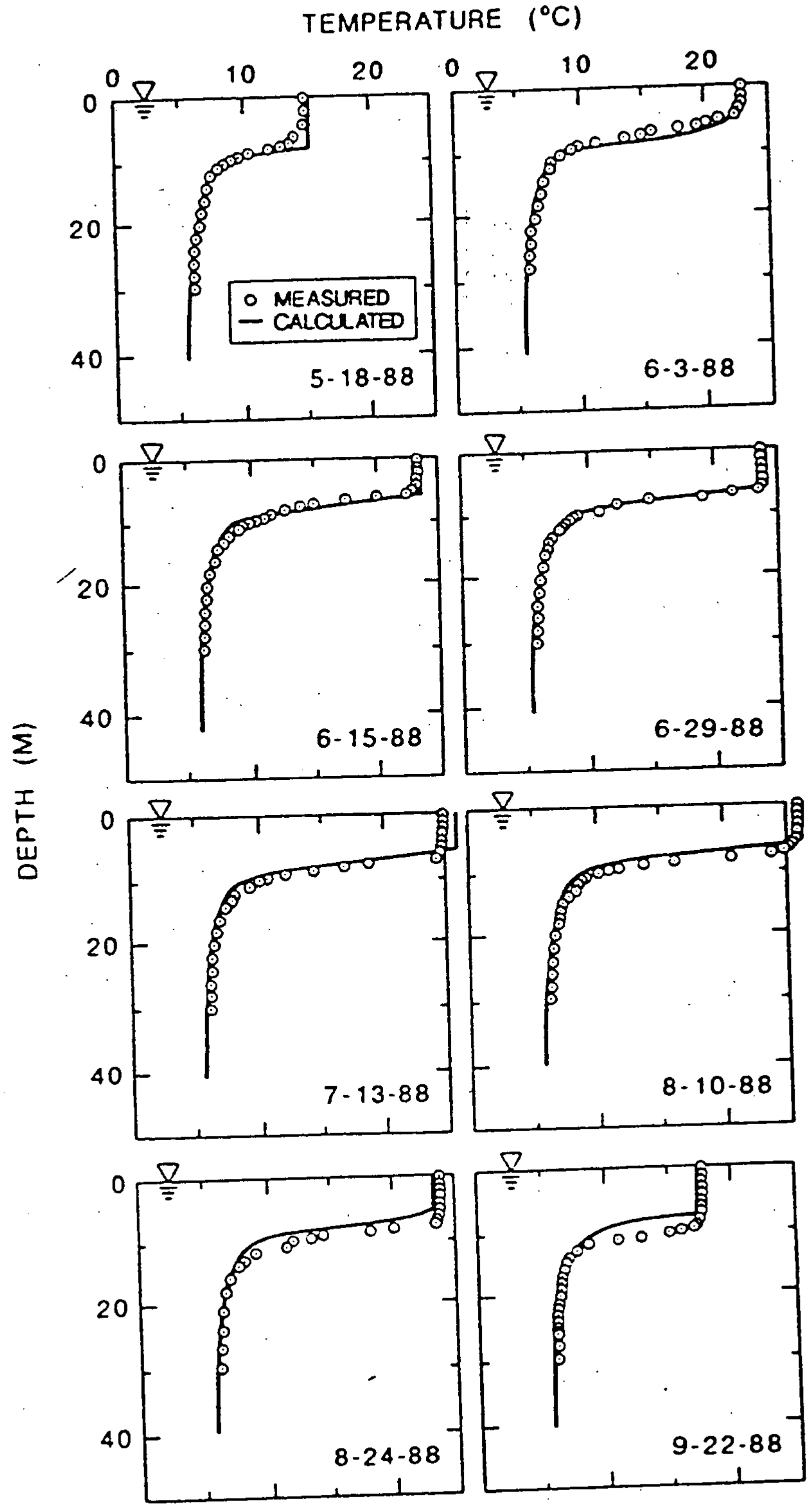

Fig. 4.1 Lake Elmo water temperature profiles.

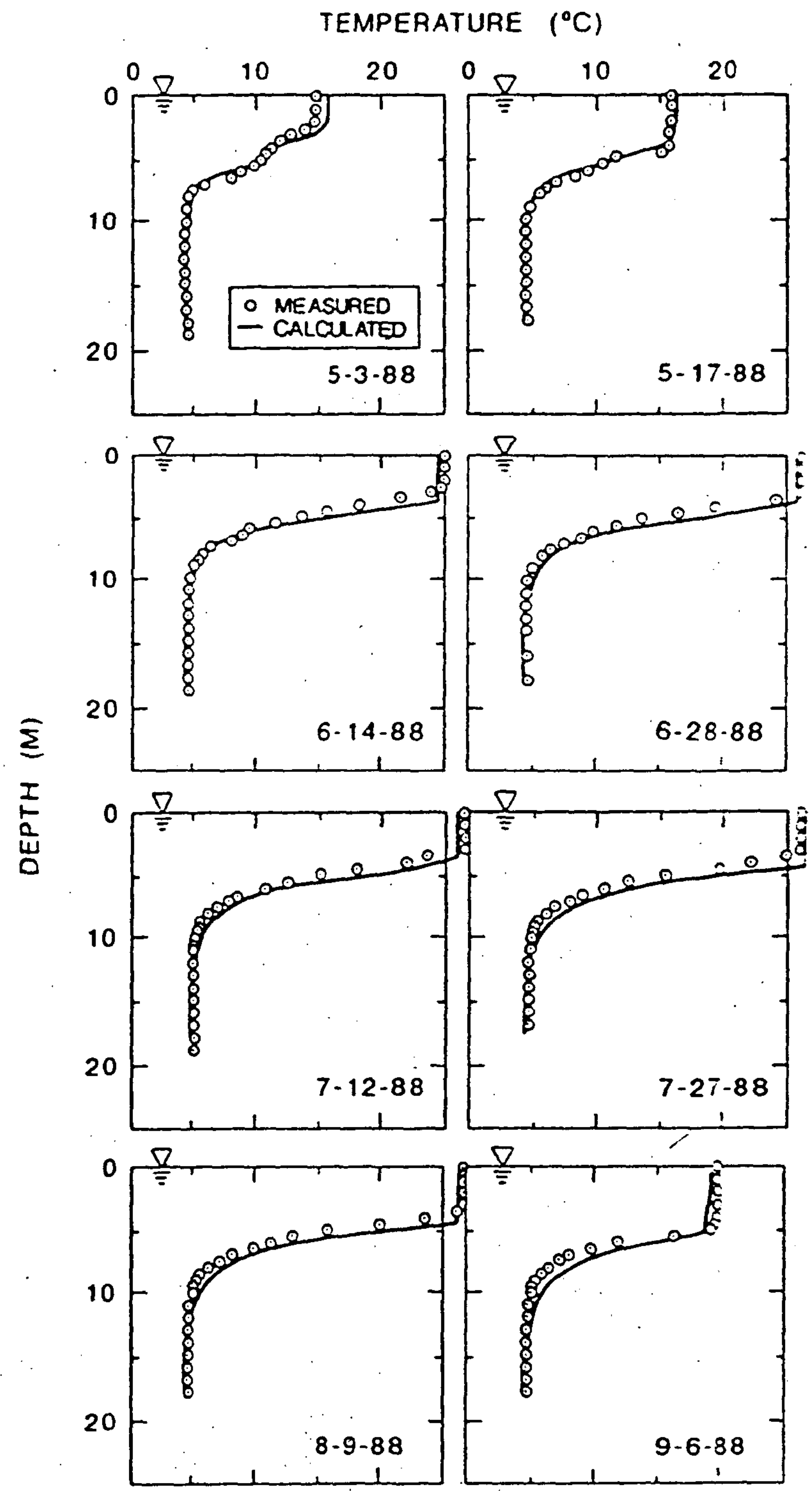

Fig. 4.2 Lake Holland water temperature profiles.

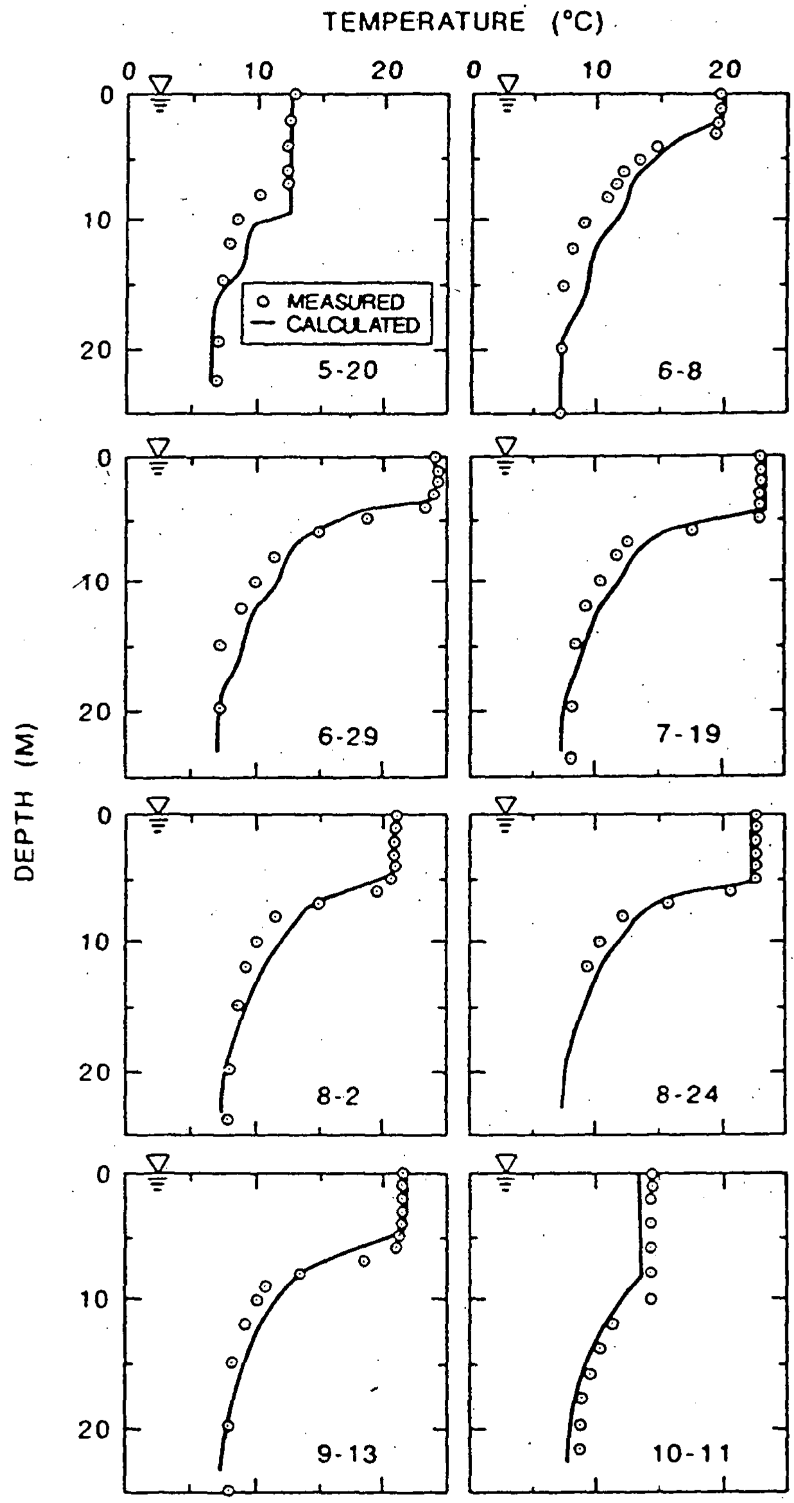

Fig. 4.3 Lake Calhoun water temperature profiles in 1971.

Table 4.4 Monthly averages of daily heat balance components [1000 kcal m^{-2}day^{-1}]

	Lake Calhoun						Lake Elmo				Lake Holland			
	H_{sn}	H_a	H_{br}	H_e	H_c	H_n	H_{br}	H_e	H_c	H_n	H_{br}	H_e	H_c	H_n
Year 1971														
APR	3.89	5.76	−6.92	−1.04	0.34	2.03	−6.88	−1.04	0.44	2.17	−7.03	−1.37	0.17	1.41
MAY	4.60	6.27	−7.64	−1.86	−0.08	1.28	−7.49	−1.65	0.13	1.85	−7.76	−2.22	−0.25	0.64
JUN	4.27	7.44	−8.58	−2.00	0.07	1.20	−8.44	−1.74	0.25	1.77	−8.63	−2.24	0.01	0.84
JUL	5.37	7.11	−8.85	−3.30	−0.46	−0.13	−8.82	−3.47	−0.46	−0.27	−8.83	−3.38	−0.45	−0.19
AUG	4.54	7.20	−8.71	−2.68	−0.20	0.15	−8.67	−2.76	−0.17	0.13	−8.71	−2.79	−0.21	0.04
SEP	3.18	6.87	−8.36	−2.14	−0.25	0.70	−8.35	−2.26	−0.25	−0.81	−8.30	−2.10	−0.19	−0.54
OCT	1.83	6.18	−7.69	−1.39	−0.42	−1.49	−7.71	−1.55	−0.49	−1.75	−7.49	−1.09	−0.15	−0.73
MEAN (MAY to SEPT)														
	4.39	6.98	−8.43	2.39	−0.18	0.36	−8.35	−2.38	−0.10	0.53	−8.45	−2.55	−0.22	0.16
Year 1988														
APR	4.46	5.76	−7.08	−1.29	0.16	2.01	−6.96	−1.15	0.39	2.49	−7.25	−1.71	−0.12	1.13
MAY	5.57	6.84	−8.06	−2.49	0.32	2.18	−7.84	−2.00	0.71	3.28	−8.21	−3.07	0.10	1.23
JUN	6.27	7.52	−8.99	−4.40	−0.18	0.22	−8.87	−4.29	−0.04	0.59	−9.01	−4.63	−0.20	−0.06
JUL	5.83	7.84	−9.17	−4.06	0.03	0.47	−9.11	−4.14	0.11	0.52	−9.14	−4.15	0.05	0.43
AUG	4.72	7.56	−9.00	−3.74	−0.21	−0.67	−8.99	−3.98	−0.21	−0.89	−8.95	−3.70	−0.15	−0.52
SEP	3.11	6.79	−8.23	−2.32	−0.27	−0.92	−8.24	−2.55	−0.31	−1.20	−8.16	−2.21	−0.18	−0.65
OCT	2.69	5.54	−7.50	−1.97	−0.79	−2.03	−7.39	−1.86	−0.47	−1.44	−7.30	−1.65	−0.48	−1.21
MEAN (MAY to SEPT)														
	5.10	7.31	−8.69	−3.40	−0.06	0.26	−8.61	−3.39	0.05	0.46	−8.69	−3.55	−0.08	0.09

Atmospheric long wave radiation and back radiation from the water surface are proportional to the fourth power of absolute temperatures. Both were higher under warmer conditions. Higher back radiation was an indication of higher surface water temperatures under increased air temperatures and solar radiation.

Cumulative evaporative losses resulting from the average 2.9°C air temperature increase are plotted in Fig. 4.4. Cumulative evaporative loss was higher by about 180,000 kcal m^{-2} for the 1988 season compared to 1971. This translates into an additional water loss of about 0.3 m in 1988 compared to 1971. This loss occurred in each of the three lakes despite their differences in size and depth. Increased evaporation not only represents an additional water loss but also contributes to increased natural convection due to surface cooling.

Conductive heat transfer through the lake surface made only a small contribution to the heat budget. The cumulative conductive heat input was not significantly different during the two years, but the onset of cooling by convection was delayed until August in 1988.

Net heat fluxes on a monthly time scale are shown in Table 4.4, and on a cumulative basis in Table 4.5. Cumulative net heat flux (H_n) from the atmosphere to the water increased from April to June in 1971 and from April to July in 1988, and then began to decrease indicating that the lakes received heat for a longer period in 1988 than in 1971. The net cumulative heat input is also a measure of heat content relative to April 1. The maxima of the net cumulative heat input were only slightly different in 1971 and 1988 (see Table 4.5), but very different among the three lakes because of the effect of depth especially surface mixed layer depth. Normalized values with respect to depth are given in Table 4.6. The trend is from higher to lower values as the depth increases. This reflects the thickness of the surface mixed layer depth relative to the total lake depth.

4.4.2 Equilibrium temperatures

Equilibrium temperature is defined as that water temperature at which the net rate of heat exchange through the water surface is zero and continually changes in response to the meteorological conditions. Mean monthly equilibrium temperatures for Lake Calhoun are shown in Fig. 4.5. These values were obtained by a separate calculation setting the net heat transfer rate H_n equal to zero. Calculations were carried out for the entire year (12 months) to see how the dates of the 0°C crossings and hence the date of ice formation might shift from year to year. Under warmer conditions equilibrium temperature was higher from March to August. From August up to the ice formation in November no difference between the colder and the warmer year was noticed probably because the fall of 1988 was cooler than in 1971 (see Table 4.2). The 0°C crossings in Fig. 6 occurred at about the same time in 1988 and 1971 indicating that dates of ice formation and ice thaw were not significantly affected by the heat in July and August. There could be a larger change in ice thaw and freeze-over dates if air temperatures were changed year-around, not only in summer as in this case study.

Table 4.5 Cumulative heat balance components [1000 kcal m^{-2}]

	Lake Calhoun						Lake Elmo		Lake Holland	
	H_{sn}	H_a	H_{an}	H_e	H_c	H_n	H_e	H_n	H_e	H_n
Year 1971										
APR	117	173	–208	–31	10	61	–31	65	–41	42
MAY	259	367	–444	–89	8	101	–82	122	–110	62
JUN	387	590	–702	–149	10	137	–135	175	–177	87
JUL	554	810	–976	–251	–4	132	–242	167	–282	81
AUG	694	1034	–1246	–334	–11	137	–328	171	–369	82
SEP	790	1240	–1497	–398	–18	116	–396	147	–431	66
OCT	846	1431	–1735	–441	–31	70	–444	93	–465	44
Year 1988										
APR	134	173	–212	–39	5	60	–35	75	–51	34
MAY	306	385	–462	–116	15	128	–97	176	–147	72
JUN	495	610	–732	–248	9	134	–225	194	–286	70
JUL	675	853	–1016	–374	10	149	–354	210	–414	84
AUG	822	1088	–1295	–490	4	128	–477	183	–529	68
SEP	915	1291	–1542	–559	–4	101	–553	147	–595	48
OCT	998	1463	–1775	–620	–29	38	–611	102	–647	11

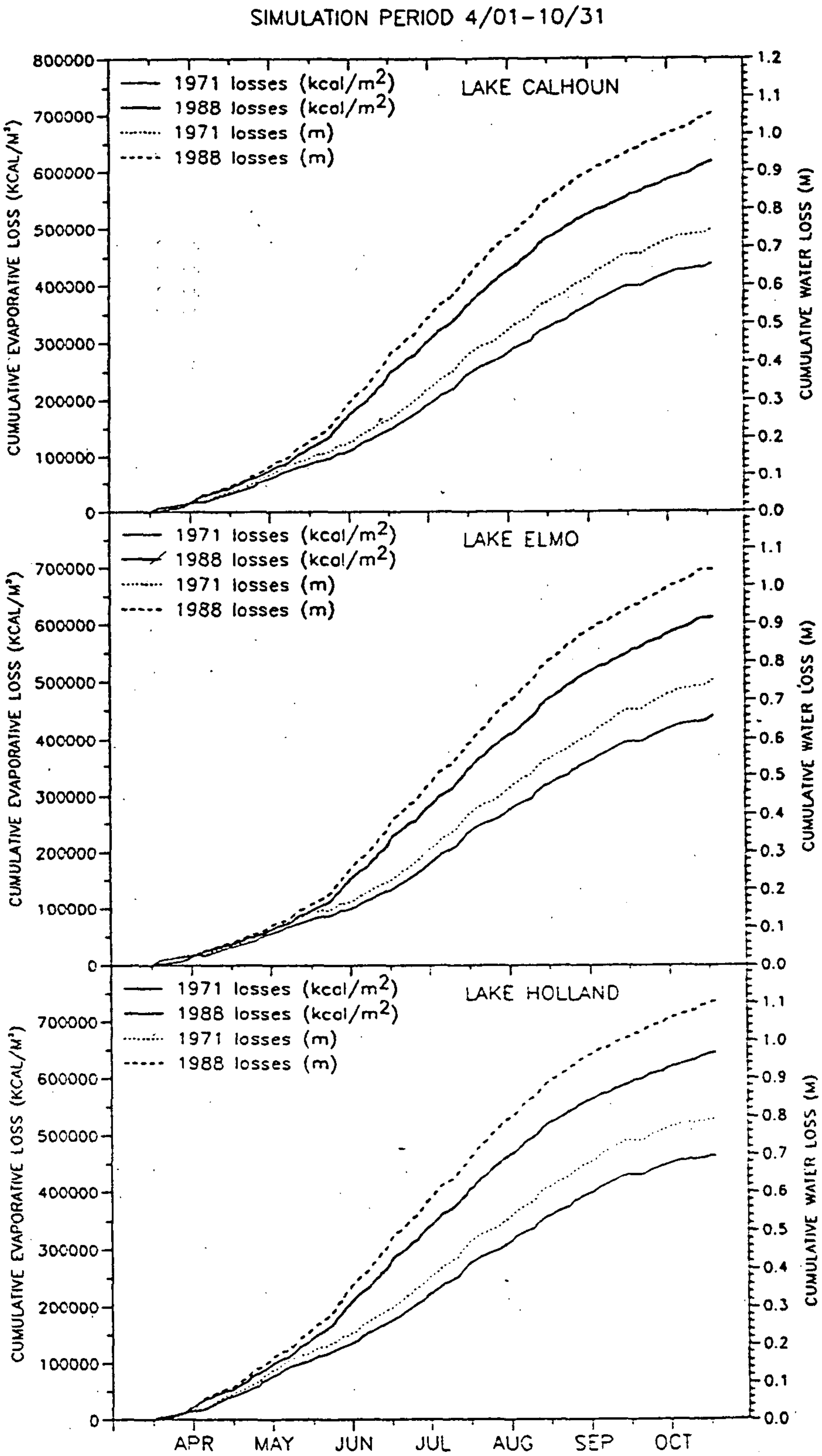

Fig. 4.4 Cumulative evaporative losses (simulated).

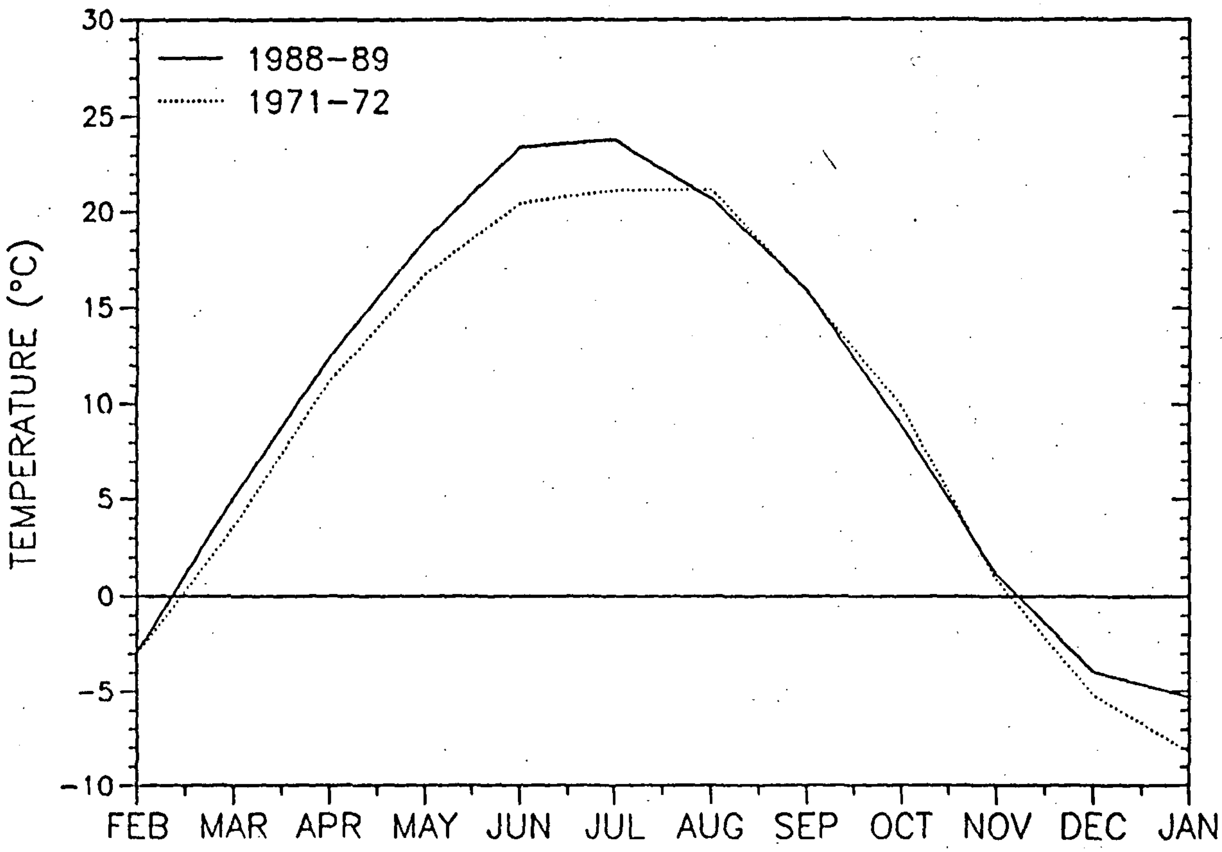

Fig. 4.5 Mean monthly equilibrium temperatures (simulated).

Table 4.6 Net cumulative heat input (content) per meter of average depth (1000 kcal m^{-1})

	Lake Holland (4.6 m)	Lake Calhoun (10 m)	Lake Elmo (13.4 m)
		Year 1971	
APR	11	6	5
MAY	16	10	10
JAN	22	14	14
JUL	20	13	13
AUG	21	14	14
SEP	17	12	12
OCT	11	7	7
		Year 1988	
APR	8	6	6
MAY	18	13	14
JUN	18	13	16
JUL	21	15	17
AUG	17	13	15
SEP	12	10	12
OCT	3	4	8

4.4.3 Vertical mixing/onset of stratification

Surface mixed layer depths are shown in Fig. 4.6. The mixed layer depth is defined as the thickness of the upper isothermal layer. Large mixed layer depths at the beginning and at the end of the simulated period indicate spring and fall overturns. After ice-out in spring, mixing depths were high, i.e. temperature was uniformly distributed throughout the entire lake. That was also the justification for selecting April as the initial time for numerical simulations.

In summer mixed layers were deeper in two of the three lakes under warmer (1988) conditions. Increased net heat flux to the lake caused a slightly earlier onset of stratification. The simulated onset of stratification is first observed in the smallest lake (Holland Lake). Lake Calhoun and Lake Elmo started to stratify later and showed similar mixing events on a daily timescale. Vertical mixing is caused by wind and natural convection. Surface mixed layers were deeper in Lake Elmo, mainly because more wind energy was available for entrainment at the thermocline due to the longer fetch (greater surface area) of the lake. Natural convection is mainly driven by net surface (evaporative, conductive) heat loss. Under warmer conditions evaporative loss was much higher, and 1 to 2 m deeper mixed layers were probably produced in this way.

Fall overturn occurred earlier after the warmer 1988 summer because lower fall temperatures produced stronger cooling and surface water instabilities, i.e. thermals and convective negatively buoyant (cold) currents earlier (Horsch et al.,1988). In the presence of convective cooling, less turbulent kinetic energy, supplied by the wind, is needed for the deepening of the thermocline.

4.4.4 Water temperatures

Daily epilimnetic temperatures at a depth of 1.5 m are shown in Fig. 4.7. Although lakes have different morphometries, similar temperature patterns were observed. This is in agreement with field measurements made by Ford and Stefan (1980) in 1974 and 1975. In both 1971 and 1988 the surface temperatures of the three lakes exhibited similarities and parallel trends which are predominantly related to weather phenomena and only secondarily to lake morphometry (Ford and Stefan, 1980). From April through August epilimnion water temperatures were higher in 1988 (average water temperature increase ≈ 3°C compared to 3°C in air temperature change) and lower after the lake started cooling.

Daily hypolimnetic temperatures are shown in Fig. 4.8. Values are at depths well below the thermocline, and water temperatures are nearly isothermal below that depth. Lake Calhoun and Lake Elmo received additional heat during the spring turnover periods (Fig. 3.6) when the climate was warmer (1988). Average hypolimnion temperature was 0.6 and 1.4°C higher in 1988 in Lake Calhoun and Lake Elmo, respectively, than in 1971. Lake Holland experienced an opposite trend. The lake started to stratify earlier too, but due to the increased stability and small lake surface area, wind mixing throughout the entire lake in spring under warmer conditions was weaker. Average hypolimnion temperature was 1.2°C lower under warmer conditions. Once a stable stratification was established, the hypolimnetic temperature was almost constant throughout the summer for all three lakes.

As is typical for dimictic lakes in temperate regions, the summer temperature in the hypolimnion was determined by mixing events in spring and remained almost constant throughout the rest of the simulation period. Lake Elmo, although twice as deep as Lake Holland, had a higher hypolimnetic temperature. Point inflows in these lakes were not significant, and the hypolimnetic temperature difference is therefore related to the differences in spring mixing dynamics, which through wind fetch, is related to the surface areas of the lakes. Greater wind shear stresses and hence wind energy inputs are usually associated with larger lake surface area (longer fetch).

4.5 Conclusions

A validated one-dimensional and unsteady lake water quality model can be used to study the changes in a lake as a result of different weather conditions including global warming. The analysis described herein is a first step in quantifying potential thermal changes in inland lakes due to climate change. Water temperatures in three lakes in a sensitive latitude have been simulated with weather from two very different summers. Mean lake depths were 4.8, 10, and 13.4 m.

The main findings are:

(1) Simulated epilimnetic water temperatures responded strongly to atmospheric changes.

(2) Simulated hypolimnetic temperatures responded less strongly and inconsistently (plus or minus) to atmospheric changes. They were determined by mixing events in spring, and lake morphometries.

(3) Simulated evaporative heat losses increased about 40 percent in the warmer summer. Evaporative water losses increased by about 300 mm out of 800 mm or about 40 percent.

(4) Dates of ice formation in fall seemed only weakly affected by the hot midsummer weather. Dates shifted by a few days. This may not be typical because of the cool fall.

(5) Simulated conductive heat transfer had a negligible effect on heat budget changes.

(6) Higher atmospheric radiation due to higher air temperature was compensated by higher backradiation from the water.

(7) Simulated surface mixed- layer depths increased slightly (by 1 to 2 m) in the warmer summer, probably due to stronger convective mixing.

(8) Simulated stratification onset occurred slightly earlier in the warmer year.

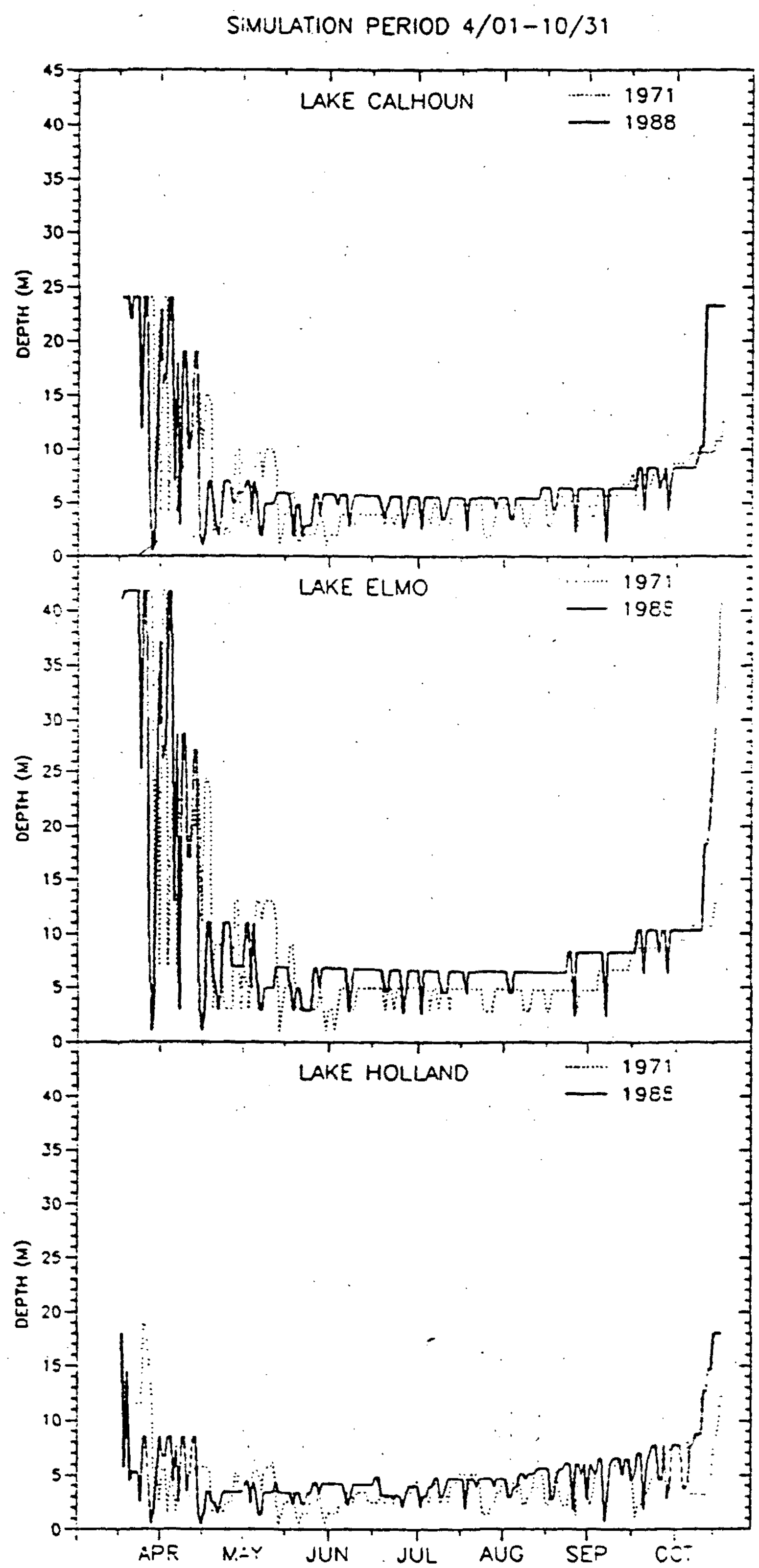

Fig. 4.6 Mixed layer depths (simulated).

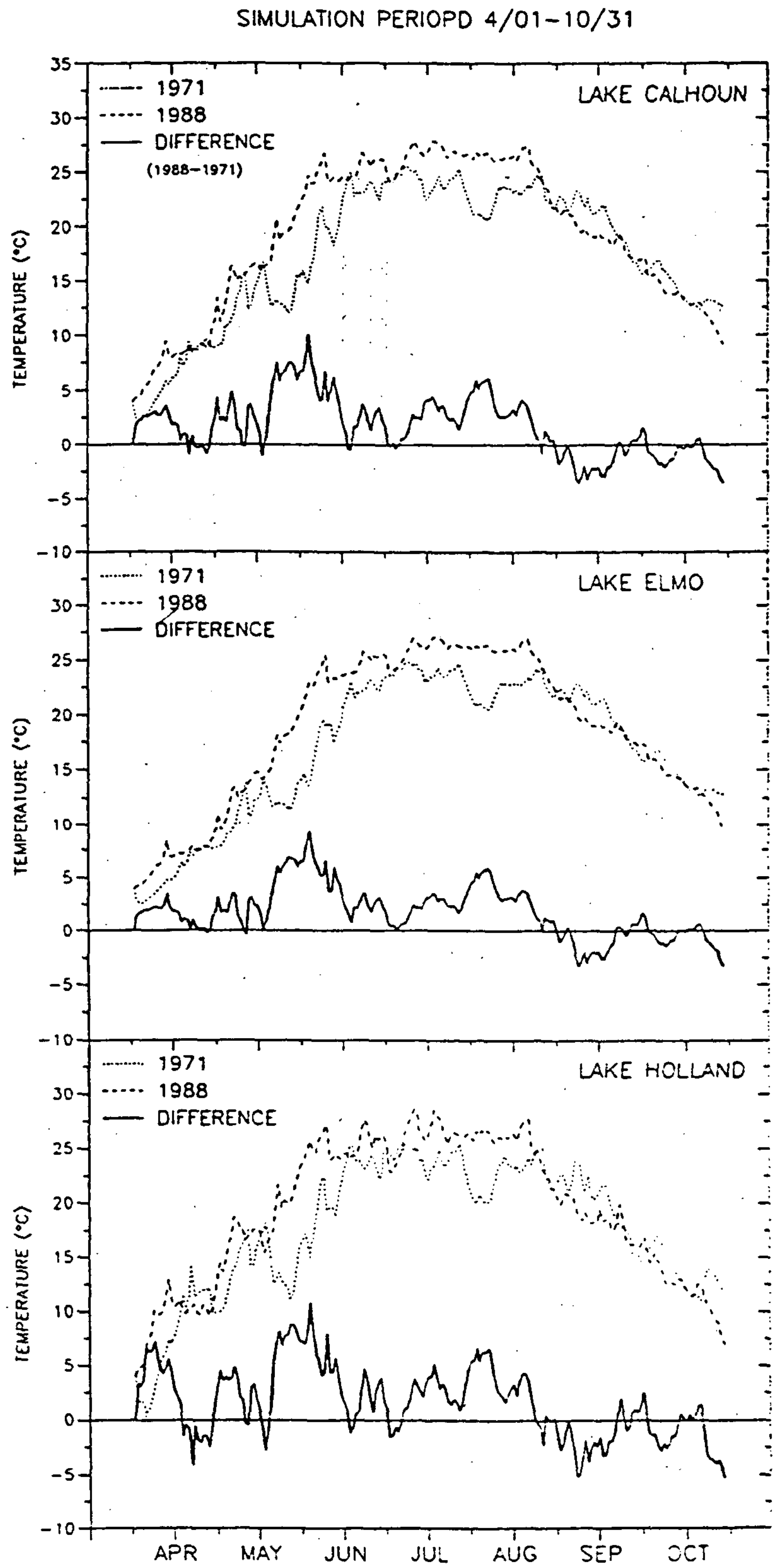

Fig. 4.7 Simulated epilimnion temperatures.

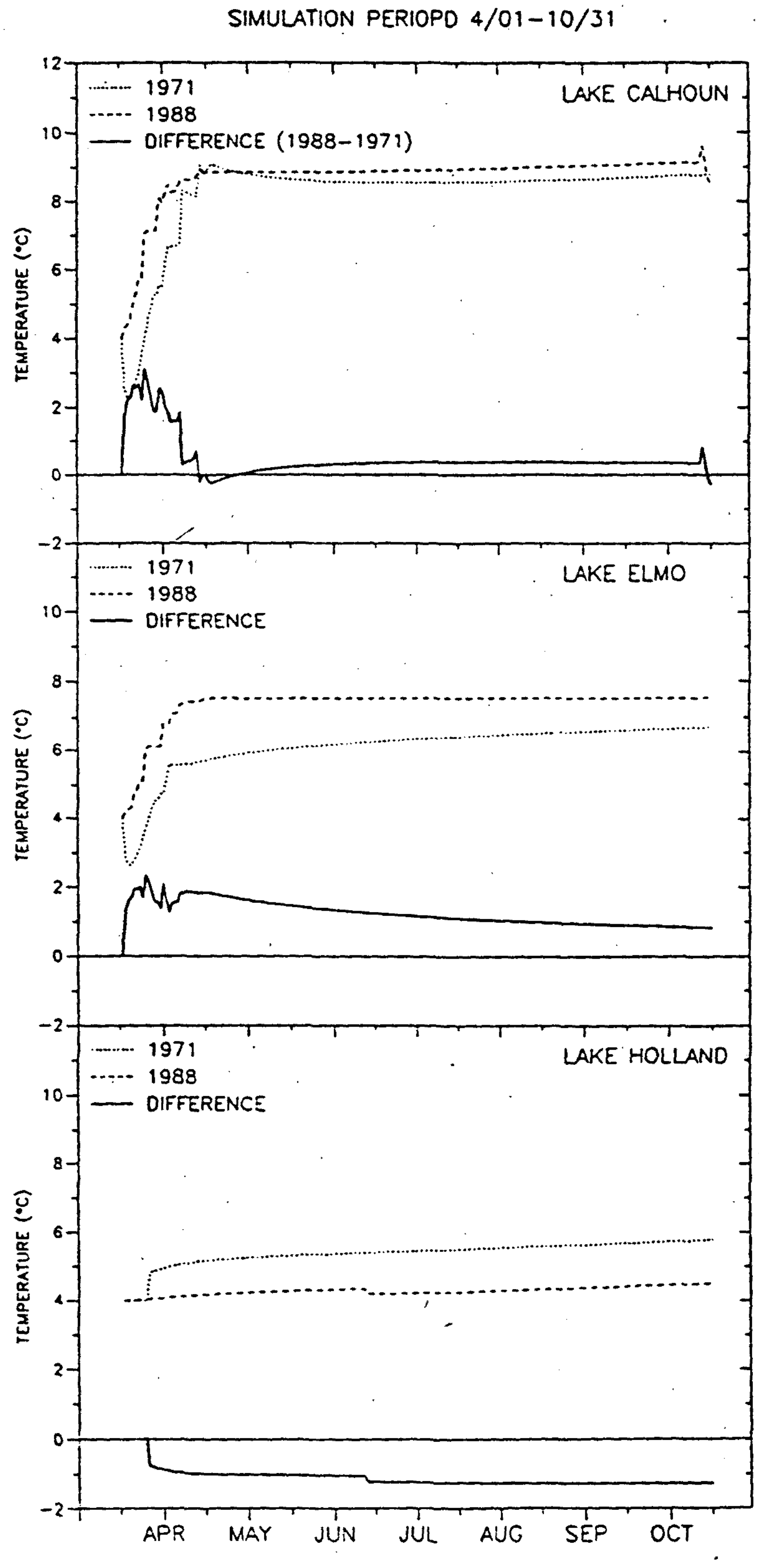

Fig. 4.8 Simulated hypolimnion temperatures.

5. Water Temperature Characteristics of Minnesota Lakes Subjected to Climate Change

A deterministic, validated, one–dimensional, unsteady–state lake water quality model was linked to a daily weather data base to simulate daily water temperature profiles in lakes over a period of twenty–five (1955–79) years. 27 classes of lakes which are characteristic for the north–central US were investigated. Output from a global climate model (GISS) was used to modify the weather data base to account for a doubling of atmospheric CO_2. The simulations predict that after climate change epilimnetic temperatures will be higher but increase less than air temperature, hypolimnetic temperatures in seasonally stratified dimictic lakes will be largely unchanged or even lower than at present, evaporative water loss will be increased by as much as 300 mm for the season, onset of stratification will occur earlier and overturn later in the season, and overall lake stability will become greater in spring and summer.

5.1 Introduction

This Chapter deals with the question of how climate change may affect thermal aquatic habitat in lakes. A regional perspective is taken, and the scope is to estimate temperature changes in lakes of different morphometric and trophic characteristics in a region. Southern Minnesota is chosen as an example because an extensive lake database is available (ERLD/MNDNR, 1990). The geographic boundaries of Southern Minnesota are defined in Figure 5.1.

Herein a dynamic and validated regional lake water temperature model (Chapter 2) will be applied to a representative range of lakes in a region for past climate and one future climate scenario. Rather than analyzing particular years and lakes, emphasis is on long term behavior and a wide range of lake morphometries and trophic levels. In this study the base period (or comparable reference) was from 1955 – 1979. For the same period of time weather parameters were perturbed by the $2XCO_2$ GISS (Goddard Institute for Space Studies) climate model output. The regional impact of these climates on different lake classes in southern Minnesota is reported herein. The simulated water temperatures, past and future, will be presented, interpreted and related to the lake characteristics and climate characteristics. The results will show how water temperatures in different freshwater lakes respond to changed atmospheric conditions in a region.

Lake levels will be largely controlled by the water budget including evaporation and runoff. The response of watershed (surface) runoff to climate change is the subject of other investigations not included herein. Lake depths

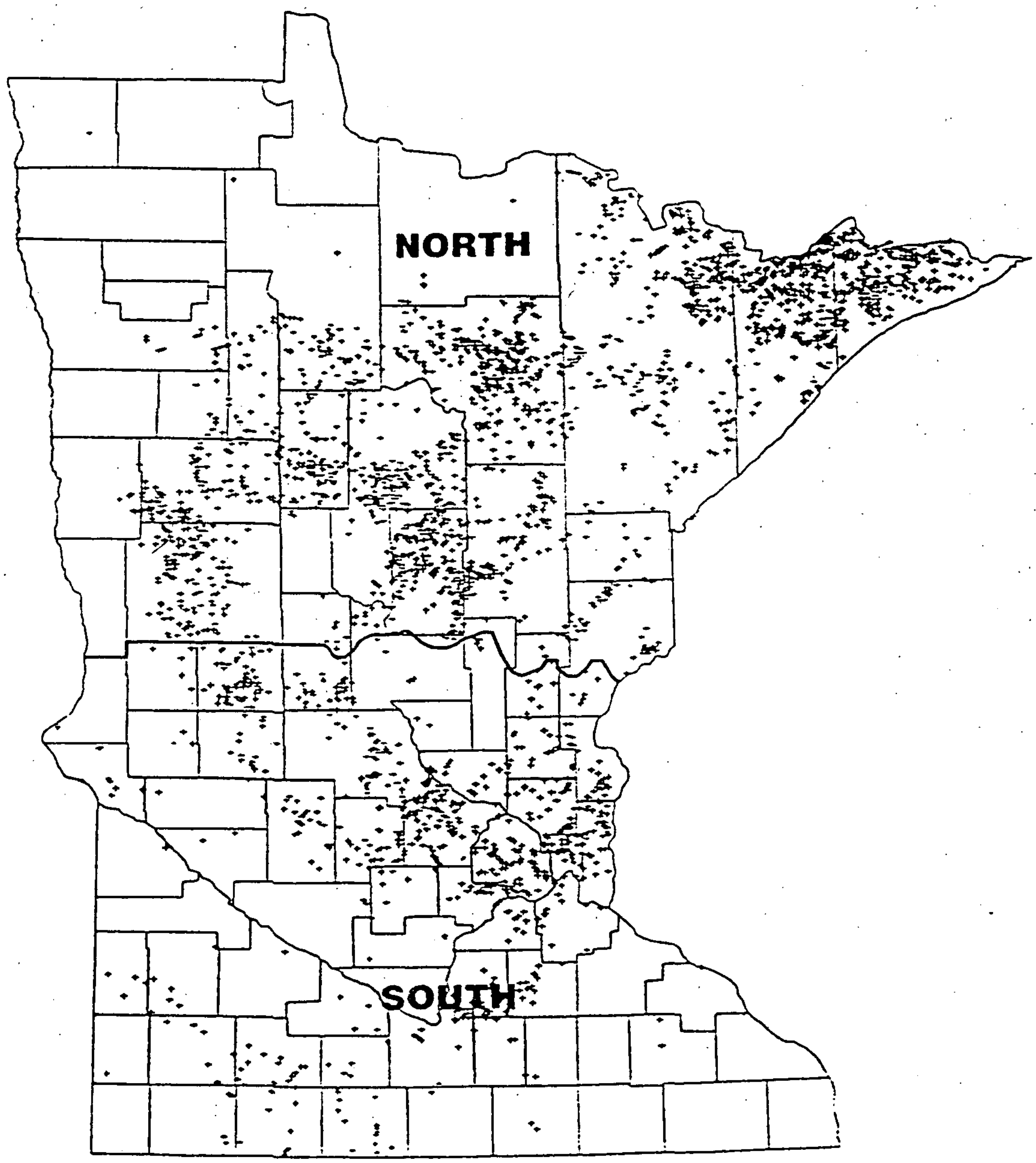

Fig. 5.1 Regional boundaries and geographic distribution of lakes in MLFD database.

will therefore be treated herein as either invariant or be lowered to account for increased evaporative water losses, where applicable. Changes in the watershed may affect nutrient loadings and hence primary productivity and transparency of the water. Such secondary effects, also were not investigated, but a sensitivity analysis indicates that water temperature predictions for the types of lakes studied herein are usually not sensitive to transparency (Chapter 2).

5.2 Method of Lake Temperature Modeling

The numerical model is applied in daily timesteps using mean daily values for the meteorological variables. The required weather parameters are solar radiation, air temperature, dew point temperature, wind speed, wind direction, and precipitation. Initial conditions, lake morphometry (area–depth–volume), and Secchi depth have to be provided to use the model. Simulations were made from spring overturn to fall overturn. Since the date of spring overturn is unknown, the initial conditions were set at 4°C on March 1, and water temperature was not allowed to drop below 4°C (well mixed conditions). Although isothermal water at 4°C may not exactly exist on March 1, the isothermal 4° condition continues until the model simulates warmer temperatures and the onset of stratification. The summer predictions are thus made quasi-independent of initial conditions and match measurements well (Chapter 3). The model is one-dimensional in depth and unsteady, i.e. it simulates water temperature distributions over depth in response to time variable weather. Vertical water temperature simulations are made over an entire season (March 1 to November 30) and in time steps of one day. The calculated daily water temperature profiles are analyzed statistically and presented graphically.

The regional water temperature simulation model was validated against data from nine Minnesota lakes for several years (Chapter 2). The model simulates onset of stratification, mixed layer depth, and water temperature well. Root mean square error is 1.2°C, and 93% of measured lake water temperatures variability is explained by the numerical simulations, over wide range of lake morphometries and trophic levels.

5.3 Climate Conditions Simulated

Meteorological data from the Minneapolis–St. Paul International Airport (93.13° longitude, 44.53° latitude) were used. The meteorological data file assembled contains measured daily values of average air temperature, dew point temperature, precipitation, wind speed, and solar radiation from 1955 to 1979 (March – November). The period from 1955 to 79 was chosen because it is long enough to give a representative average of base conditions before climate warming. In the 1980s warmer than average air temperatures were observed (Jones et al., 1986; Kerr, 1989), and therefore this period is excluded. Sources of climate data were as follows:

Climate scenarios were selected following EPA guidelines on global climate change effect studies (Robinson and Finkelstein, 1990). Climate projections by four different models (GISS, GFDL, OSU, UMKO) for the doubling of atmospheric CO_2 were provided by NOAA (1990). The monthly climate projections by the four models are different from each other and their explicit effects on water temperature dynamics can be studied for each model separately. In this study only the GISS projections for the grid point closest to Minneapolis/St. Paul were used (Table 5.1), as suggested by EPA for effect studies. The geographical location of this grid point is given in Figure 5.2. A comparison of the mean monthly weather parameter values (for Minneapolis/St. Paul) projected by the four models shows that the GISS projections are not substantially different from GFDL and OSU, except for wind speeds in November. No adjustments were made to those wind speeds, however, for a lack of a rational basis and because late fall winds do not affect the summer water temperature dynamics. No interpolations between grid points were made, following explicit EPA recommendations.

Table 5.1 Weather parameters changes projected by the $2XCO_2$ climate model output for Minneapolis/St. Paul.

MONTH	AIR. TEMP (diff.°C)*	SOL. RAD. (Ratio)‡	WIND S. (Ratio)‡	REAL. HUM. (Ratio)‡	PRECIP. (Ratio)‡
JAN	6.20	0.92	0.92	1.16	1.17
FEB	5.50	1.04	1.12	1.01	1.03
MAR	5.20	0.98	0.47	1.13	1.28
APR	5.05	1.03	0.69	1.00	1.03
MAY	2.63	1.00	0.67	1.09	1.12
JUN	3.71	0.99	0.85	1.01	1.08
JUL	2.15	0.98	0.93	0.93	1.10
AUG	3.79	1.04	1.00	1.02	0.98
SEP	7.02	1.04	1.07	0.90	0.70
OCT	3.73	1.12	2.23	0.95	0.88
NOV	6.14	1.03	5.00	1.00	0.99
DEC	5.85	0.99	0.77	0.98	1.24

* Difference = $2XCO_2$ GISS − PAST
‡ Ratio = $2XCO_2$ GISS/PAST

The uncertainty of the climate predictions is not the subject of this paper. It is understood that relative humidity and wind speeds are not well predicted at the local scale by global climate models. Fortunately, uncertainty analysis of the effects of variable meteorological forcing on lake temperature models indicates that air temperature has the most significant effect in lake temperature uncertainty (Henderson-Sellers, 1988; Chapter 3), and that parameter is better predicted than others.

Seasonal distributions of the 25-year average of observed weather parameters (which were used as model inputs) are shown in Figure 5.3. Past climate and the $2XCO_2$ GISS scenario were used as inputs to the water temperature simulations.

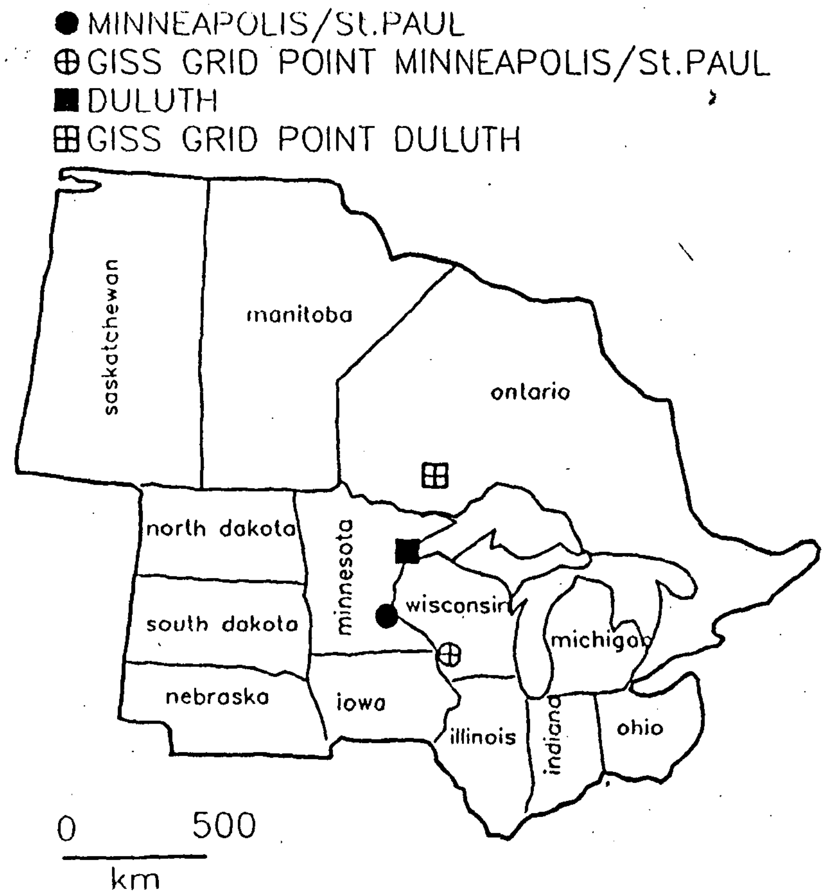

Fig. 5.2 Geographical location of the closest GISS grid points for Minneapolis/St. Paul and Duluth.

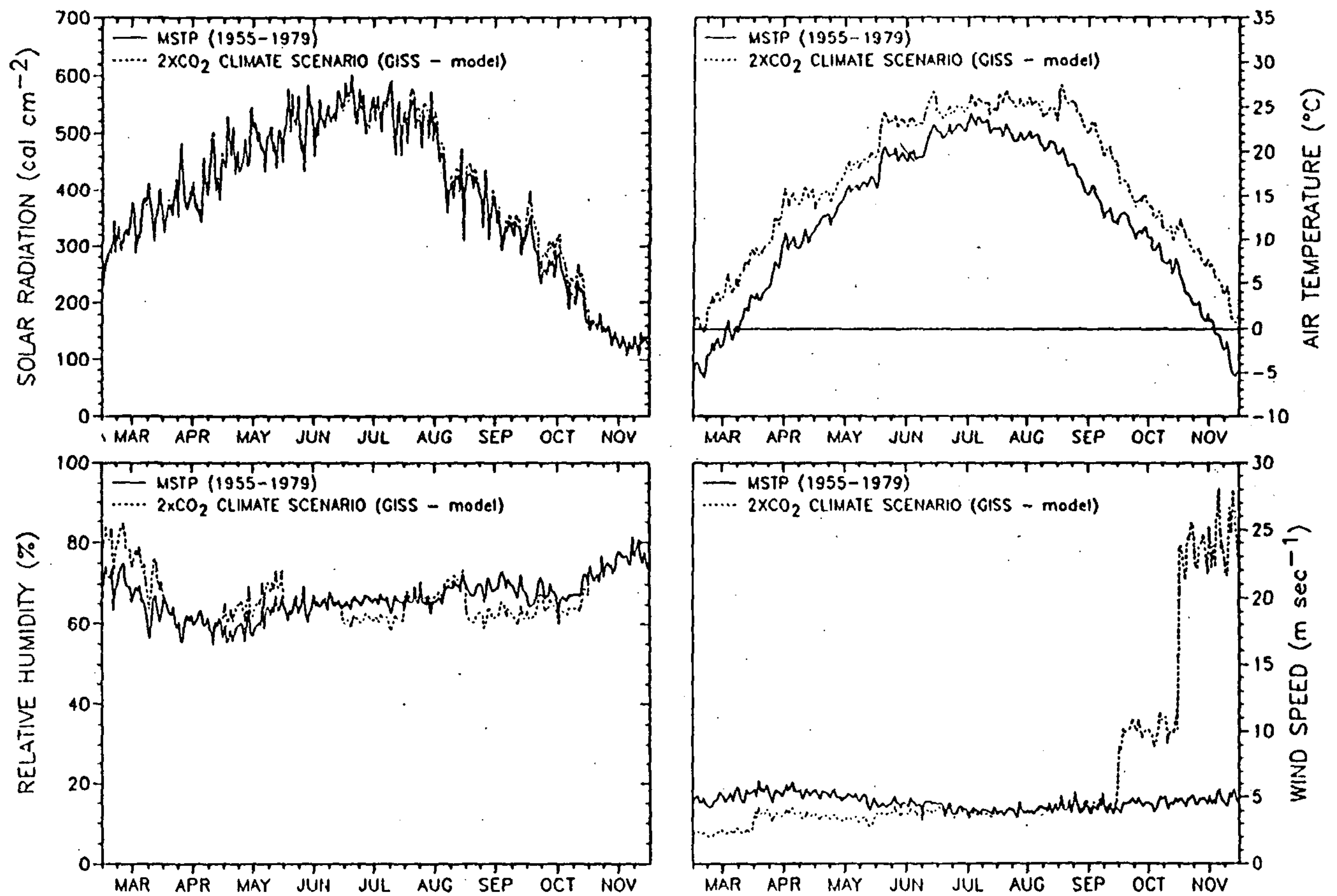

Fig. 5.3 Climate parameters a Minneapolis/St. Paul in the past and under a 2xCO_2 (GISS) climate scenario.

5.4 Regional Lake Characteristics

Regional classification of lakes was approached in a variety of ways. The ecoregion approach was considered first, but found to give too detailed a picture. The entire state was considered as a regional entity but rejected as too large because of the diversity of climate. Dividing the state into a northern and southern region was considered appropriate and not as arbitrary as might seem because there is a significant gradient in geological, topographic, hydrological climatological and ecological parameters across the mid-section of the state (Baker et al., 1985, Heiskary et al., 1987). The southern and northern regions are about equal in size (Fig. 5.1).

The Minnesota Lakes Fisheries Database, MFLD (ERLD/MNDNR, 1990), which contains lake survey data for 3002 Minnesota lakes, is for the southern region. The MLFD database includes 22 physical variables and fish species. Nine primary variables explain 80 percent of the variability between lakes. These nine variables include surface area, volume, maximum depth, alkalinity, secchi depth, lake shape, shoreline complexity, percent littoral area, and length of growing season. For regional classification of the lakes in this study, the possible thermal structure (i.e. whether lakes are stratified or not) and trophic status are of primary concern. Observations in the northern hemisphere show that onset and maintenance of stratification in lakes is dependent on surface area and maximum depth (Gorham and Boyce, 1989) as well as climatological forcing i.e. solar radiation and wind (Ford and Stefan, 1980). Lake trophic status contributes to solar radiation attenuation and oxygen balance. Trophic status was assessed by using a Secchi depth scale (Heiskary and Wilson, 1988) related to Carlson's Trophic State Index (Carlson, 1977). Secchi depth information was available in the MLFD.

A statistical analysis of southern and northern Minnesota Lakes in the MLFD in terms of surface area, maximum depth and Secchi depth was made. The geographic distribution of different classes of lakes in Minnesota is given in Figure 5.4. Cumulative frequency distributions shown in Figure 5.5 were used to subdivide all lakes into three ranges of surface area, maximum depth and Secchi depth, as shown in Table 5.2. These represent 27 classes of lakes in each of the two regions of the state.

Table 5.2 Lake classification

Lake Key Parameter	Range	Cumulative Frequency	Class	Description Value
Area (km^2)	< 0.4	Lower 30%	0.2	Small
	0.4 – 5	Central 60%	1.7	Medium
	> 5	Upper 10%	10	Large
Maximum Depth (m)	< 5	Lower 30%	4	Shallow
	5 – 20	Central 60%	13	Medium
	> 20	Upper 10%	24	Deep
Secchi Depth (m)	< 1.8	Lower 20–50%	1.2	Eutrophic
	1.8 – 4.5	Central 20–50%	2.5	Mesotrophic
	>4.5	Upper 0–10%	4.5	Oligotrophic

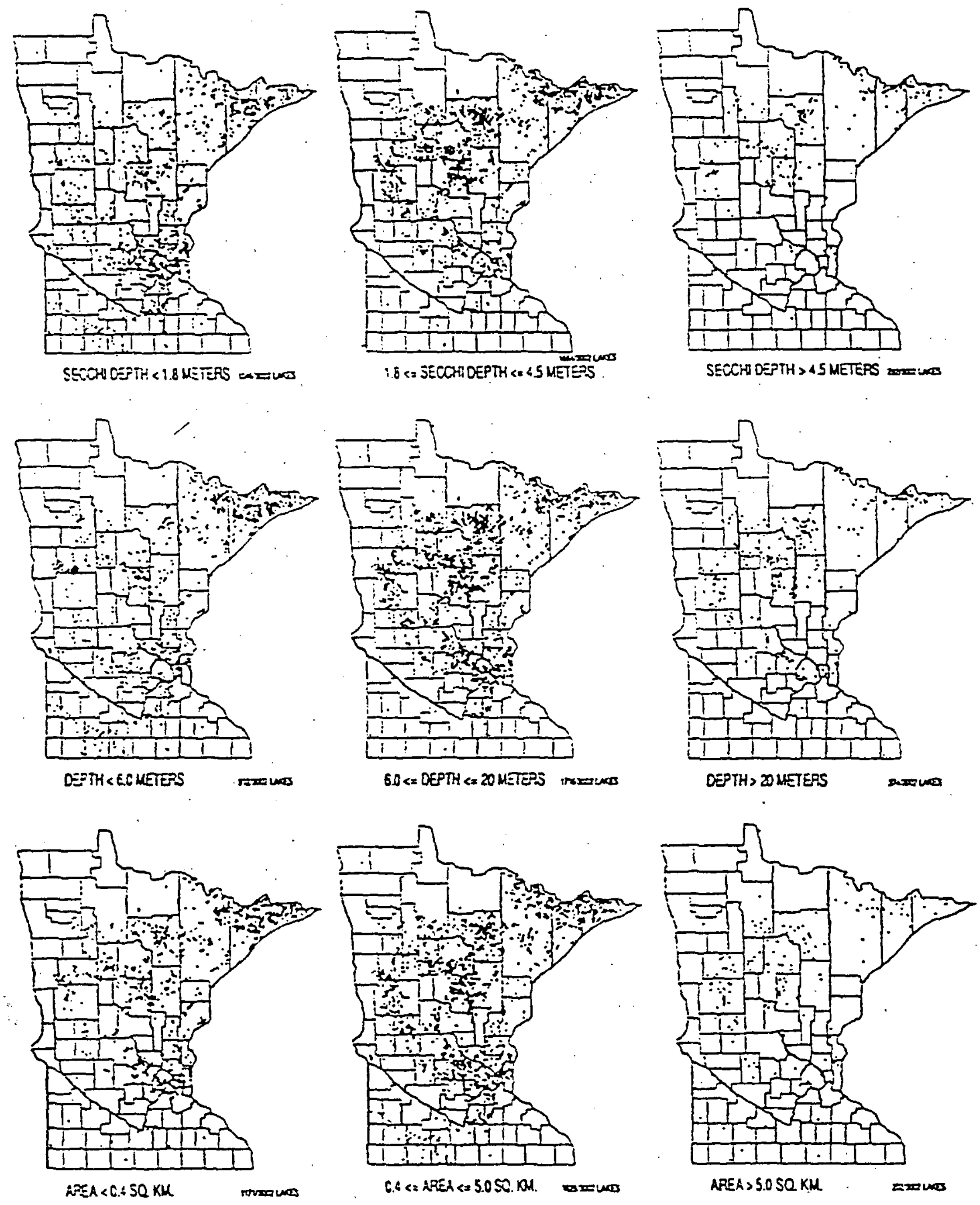

Fig. 5.4 Geographic distribution of lakes according to key parameters: Secchi depth, maximum depth, and surface area.

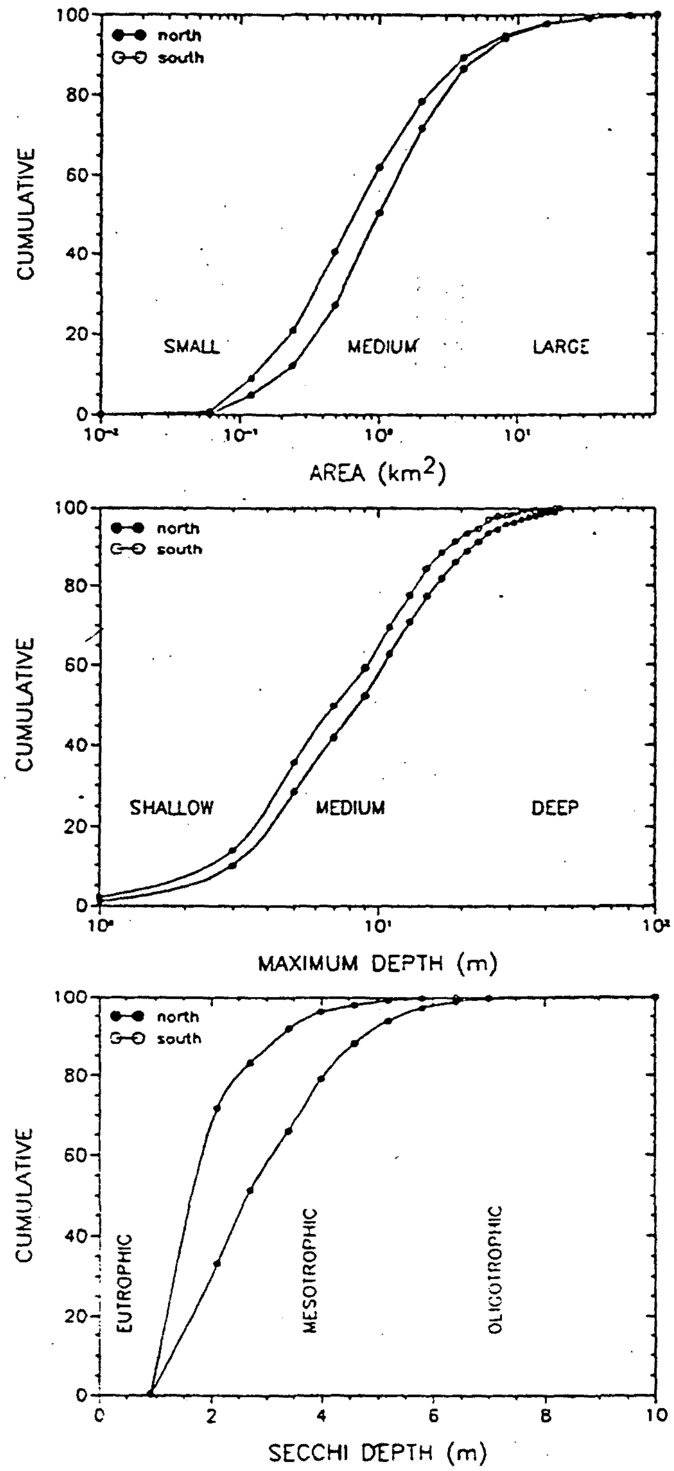

Fig. 5.5 Cumulative distributions (%) of key parameters in Minnesota lakes (from MLFD database).

A representative value for surface area, maximum depth and Secchi depth was chosen in each lake class as input to the model simulation. Those values are shown under the heading "class" in Table 5.2.

Representative area–depth relationships for three different lake classes (by surface area) were obtained from 35 lakes which covered the entire range of distributions in a set of 122 lakes (Figure 5.6).

After areas are expressed as fractions of surface area and depths are expressed as fractions of maximum depth, an equation of the form

$$\text{Area} = a \cdot \exp(b \cdot \text{Depth}) + c \tag{5.1}$$

is fitted to the data and subsequently used in the simulation as a representative area–depth relationship. Coefficients a, b, c, calculated by regression analysis are given in Table 5.3. This procedure is equivalent to self–similarity of depth–area relationships within a given class.

Table 5.3 Morphometric regression coefficients in the area vs. depth relationship.

Area	a	b	c
Small	1.19	–1.76	–0.20
Medium	1.14	–2.10	–0.15
Large	1.14	–2.91	–0.08

Lake basin shape was assumed circular for the purpose of wind fetch calculation. The water temperature simulation results were shown to be insensitive to these assumptions of morphometric self–similarity and basin shape.

5.5 Simulated lake water temperature regimes for historical and future weather

5.5.1 Water temperatures

Simulations of daily water temperature profiles from March 1 to November 30 (275 days) in each year from 1955 to 1979 (25 years) were made for each of the 27 lake classes. In addition to lake morphometric input, i.e. surface area, maximum depth and depth–area relationship, these simulations used actually recorded daily values of weather parameters, i.e. solar radiation, air temperature, dew point temperature, wind speed, and precipitation for each day simulated. A massive weather–database had to be developed prior to the simulations. The calculated output of 185,625 vertical water temperature profiles, each consisting of 24 water temperature values, provided base line information on lake characteristics during a period of the past when little climate change occurred.

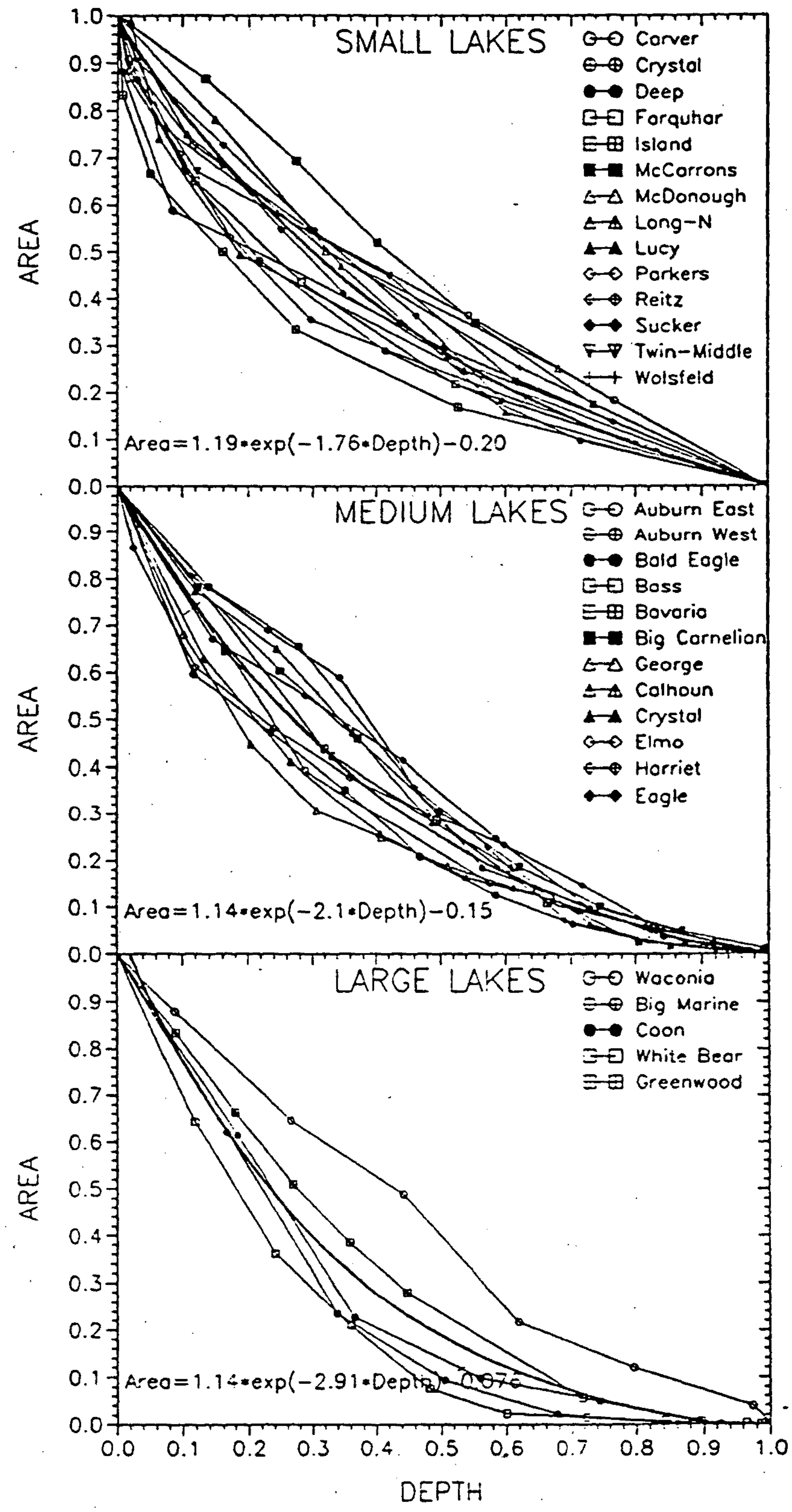

Fig. 5.6 Horizontal area vs. depth relationship for lakes. Area and depth are normalized.

To simulate possible future water temperature regimes, the monthly corrections specified by the $2XCO_2$ GISS model scenario were applied to the weather data base and the simulations were repeated.

From these simulated water temperature data bases under historical and future climates, each consisting of 4,455,000 water temperature values, the following characteristics were extracted.

Epilimnetic water temperatures were defined as water temperatures at 1.0 m below the water surface regardless whether maximum-depth is 4 m, 13 m or 24 m, respectively. The seasonal course of epilimnetic temperatures, averaged weekly over 25 years is shown in Figure 5.7 for both past climate and the $2XCO_2$ GISS climate scenario. The difference between the two is also shown in Figure 5.7; the associated air temperature increments due to climate change were presented in Table 5.1. The largest change in weekly water temperature change in response to climate change, is on the order of 6 to 7°C, and occurs in spring (April), the minimum is on the order of 0 to 2°C and occurs either in fall (October and November), or in July.

The GISS scenario gives a seasonal surface water temperature pattern different from that for the past. The cooling phase, for example, commences later and has stronger water temperature gradients. Maximum weekly surface water temperatures and the time of their occurrence are given in Table 5.4. The highest surface water temperatures, 27.4°C (± 0.1°C) were calculated for the shallow lakes and the lowest, 26.2°C (± 0.1°C) for the deep lakes. With climate change the predicted rise in the seasonal surface water temperature maxima is 1.9 to 2.2°C, which is small compared to air temperature changes in Table 5.1. The occurrence of the maximum water surface temperatures is shifted by 11 to 20 days towards the fall with the climate change.

Surface water temperatures are fairly independent of lake morphometry within the range of lakes investigated. Extreme values in lakes of different geometry vary by no more than 4°C on any given day. Maximum differentials occur in spring and fall. From June through September, i.e. during the period of seasonal water temperature stratification, surface water temperatures in lakes of different morphometic characteristics (depth and area) are very similar (within 1.0°C). In very large lakes (e.g. the North American Great Lakes) the significantly greater water volumes and mixed layer depths cause a substantial lag in heating and cooling leading to water temperature differences larger than 4°C.

Weekly averages of 25 years of simulated hypolimnetic temperatures are shown in Figure 5.8. Values are 1 m above the lake bottom (maximum depth). Hypolimnetic temperature responses to climate change show wider variability than epilimnetic responses. In shallow (polymictic) lakes, the hypolimnetic and epilimnetic water temperature rise is very similar in magnitude and time of occurrence. In deep small lakes hypolimnetic temperatures are as much as 3.5°C colder after climate change than before. Hypolimnetic warming during the summer is dependent on vertical turbulent diffusion and therefore wind fetch and hence surface area. Dependence of hypolimnetic temperatures on lake morphometry is very evident in Figure 5.8. The seasonal pattern of hypolimnetic water temperatures was altered by climate change most significantly in shallow lakes. All others showed typical seasonal warming patterns in response to vertical diffusion.

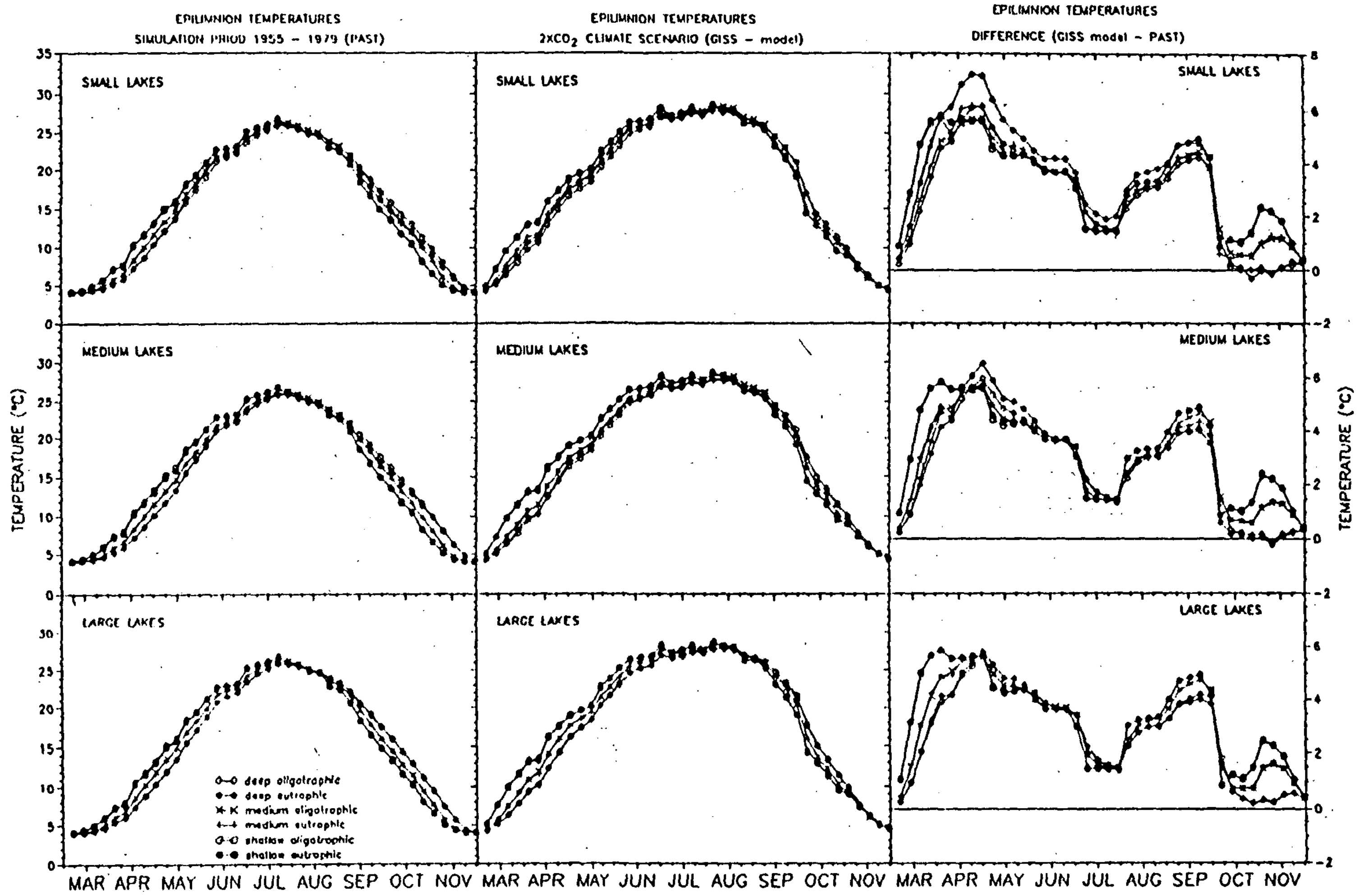

Fig. 5.7 Simulated weekly epilimnion temperatures.

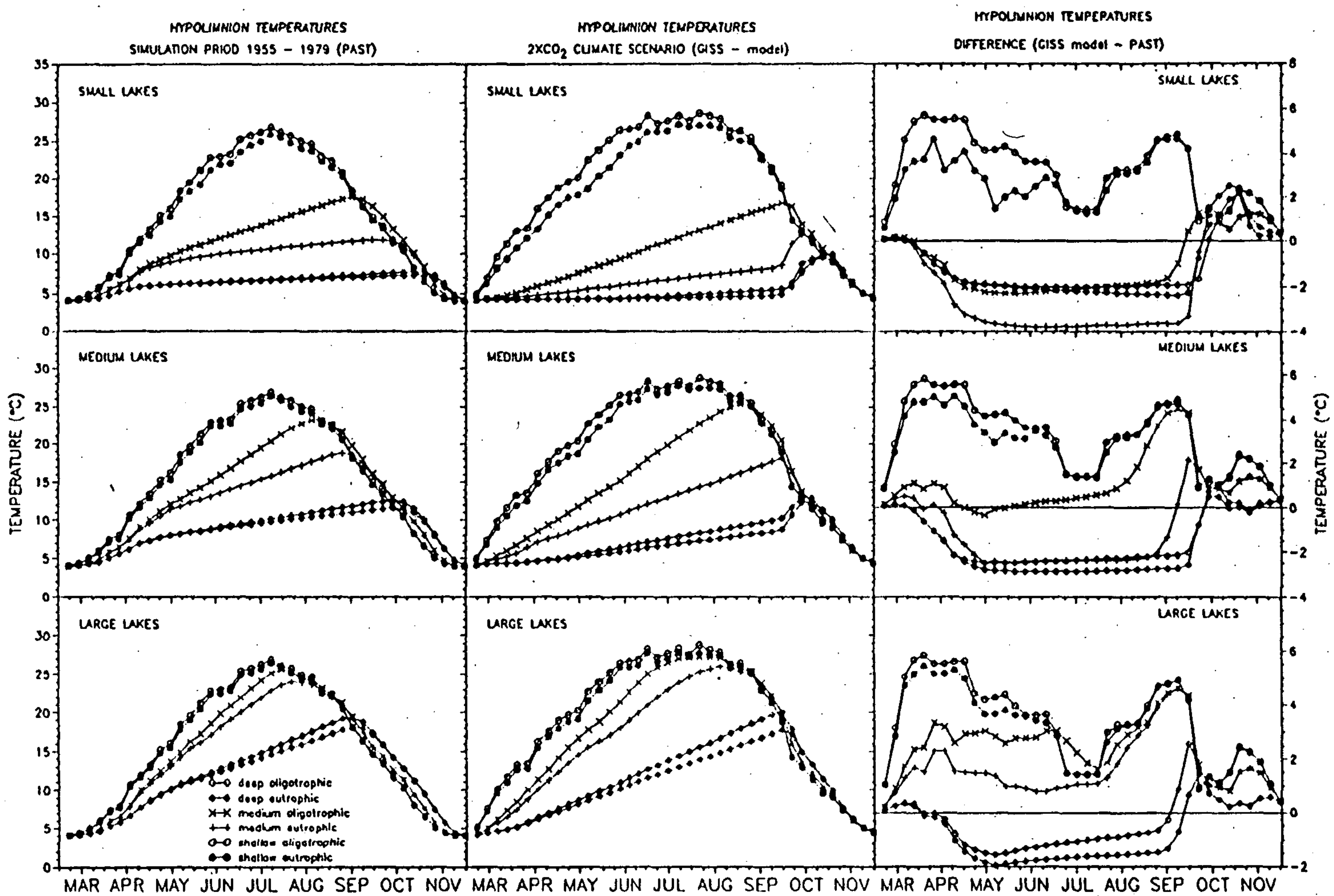

Fig. 5.8 Simulated weekly hypolimnion temperatures.

Table 5.4 Maximum temperatures of southern Minnesota lakes

Maximum Depth m	Area km^2	Trophic Level	PAST 1955–1979 Epilimnion °C	day	PAST 1955–1979 Hypolimnion °C	day	GISS–2XCO$_2$ Epilimnion °C	day	GISS–2XCO$_2$ Hypolimnion °C	day	DIFFERENCE (GISS–PAST) Epilimnion °C	DIFFERENCE (GISS–PAST) Hypolimnion °C
SHALLOW (4.0)	SMALL (0.2)	eutrophic	27.5	203	24.9	206	29.4	217	26.2	229	1.9	1.3
		mesotrophic	27.4	203	26.8	204	29.4	217	28.3	218	2.0	1.5
		oligotrophc	27.3	203	27.0	203	29.3	217	29.2	217	2.0	2.2
	MEDIUM (1.70)	eutrophic	27.4	203	26.2	204	29.4	217	27.5	205	2.0	1.3
		mesotrophic	27.4	203	27.0	203	29.5	217	29.1	181	2.1	2.1
		oligotrophic	27.3	203	27.1	203	29.4	217	29.4	217	2.1	2.3
	LARGE (10.0)	eutrophic	27.4	203	26.5	203	29.5	217	28.3	181	2.1	1.8
		mesotrophic	27.4	203	26.9	203	29.6	217	29.1	181	2.2	2.2
		oligotrophic	27.3	203	27.1	203	29.5	217	29.4	217	2.2	2.3
MEDIUM (13.0)	SMALL (0.2)	eutrophic	26.6	203	11.9	278	28.7	217	12.6	289	2.1	0.7
		mesotrophic	26.5	206	12.8	277	28.7	218	13.0	284	2.2	0.2
		oligotrophc	26.6	203	17.5	261	28.7	218	17.5	276	2.1	0.0
	MEDIUM (1.70)	eutrophic	26.4	204	18.7	254	28.5	218	18.2	274	2.1	–0.5
		mesotrophic	26.4	207	19.9	252	28.6	218	20.3	271	2.2	0.4
		oligotrophic	26.5	207	23.0	233	28.7	218	25.3	248	2.2	2.3
	LARGE (10.0)	eutrophic	26.5	203	24.0	220	28.6	223	26.0	233	2.1	2.0
		mesotrophic	26.5	206	24.6	218	28.7	218	26.6	224	2.2	2.0
		oligotrophic	26.6	207	25.5	211	28.7	218	27.3	218	2.1	1.8
DEEP (24.0)	SMALL (0.2)	eutrophic	26.4	206	7.3	308	28.5	217	10.3	305	2.1	3.0
		mesotrophic	26.3	204	7.4	308	28.3	218	10.4	305	2.0	3.0
		oligotrophc	26.1	207	7.8	308	28.10	220	10.6	305	2.0	2.8
	MEDIUM (1.70)	eutrophic	26.2	206	11.6	294	28.2	218	12.8	291	2.0	1.2
		mesotrophic	26.2	206	11.8	293	28.1	223	12.9	291	1.9	1.1
		oligotrophic	26.1	206	12.6	291	28.1	223	13.3	291	2.0	0.7
	LARGE (10.0)	eutrophic	26.1	206	18.2	261	28.1	223	18.4	276	2.0	0.2
		mesotrophic	26.1	206	18.4	263	28.1	223	18.7	276	2.0	0.3
		oligotrophic	26.1	207	19.4	259	28.2	218	20.1	273	2.1	0.7

day = Julian day when maximum temperature occur

The highest hypolimnetic water temperatures (27.1°C) were calculated for shallow oligotrophic lakes which are typically polymictic or well–mixed for the entire simulation period. The lowest maximum hypolimnetic temperatures (7.3°C) occurred in small and deep eutrophic lakes. Climate change raised by 0° to 3°C the maximum hypolimnetic water temperature or lowered it by as much as 3.5°C, depending on the particular stratification dynamics of a lake.

In addition to long–term changes of water temperatures (Figures 5.7 and 5.8) variations from year to year are also of interest. Unfortunately weather parameters for the GISS climate scenario were only given as long term monthly averages. Therefore variability on an annual basis could not be explored for the GISS scenario. On the other hand, annual weather information was available for the 1955–79 period, and therefore could be used to give the range of simulated daily water temperatures. Bands of water temperatures within the 95% confidence interval are shown in Figure 5.9. The spread is significant and on the order of ± 3 to 5°C around the mean. This range is about twice as wide as that due to differences in lake morphometry (Figures 5.7 and 5.8). This is in agreement with field measurements by Ford and Stefan (1980) and has some bearing on habitat. Examples of water temperature structures in typical lakes are given in Figure 5.10.

5.5.2 Thermal energy fluxes

The water temperatures discussed above are, of course, the result of net heat energy input or losses through the water surface, and vertical distributions of that heat within the lake. For better understanding of the water temperatures, it is therefore appropriate to consider, at least, briefly heat fluxes and stratification dynamics. Simulated net heat flux through the water surface is plotted in Figure 5.12 for past and future (GISS) climate conditions.

Five heat transfer processes are responsible for heat input into the water: short wave solar radiation, long wave atmospheric radiation, conductive heat transfer, evaporation, and back radiation. Short wave solar radiation and atmospheric radiation increase the water temperature, while evaporation and back radiation cool the water. Conductive heat transfer can either heat or cool the water. All five fluxes together comprise net heat flux at the water surface.

Individual daily heat fluxes vary dramatically with weather as is illustrated in Figure 5.11. To keep track of the extraordinary dynamics and to explain them would take more space than available here, and may not be particularly fruitful. As a summary, the cumulative net heat fluxes are presented in Figure 5.12 for past and future (GISS) climate. The difference between the two is also shown in Figure 5.12. Lakes with large surface areas will receive more net heat input (up to 30%) than smaller ones, and in extremely small lakes the difference is even negative, meaning less heat will be transferred through the water surface and stored in the lake! All net heat fluxes are per unit surface area of a lake, not total values.

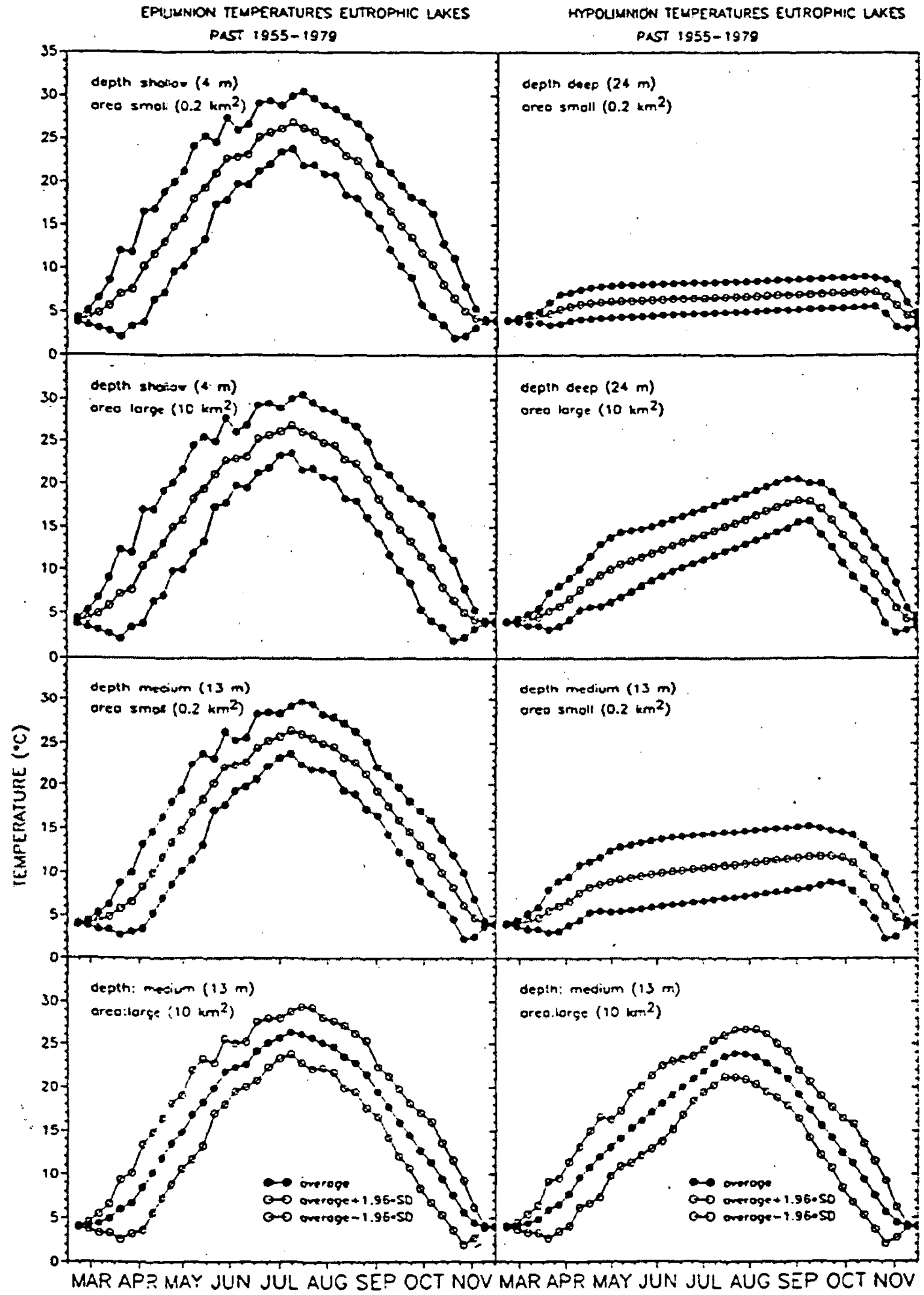

Fig. 5.9 Examples giving range of epilimnetic and hypolimnetic temperatures over a 25 year period (95% confidence interval).

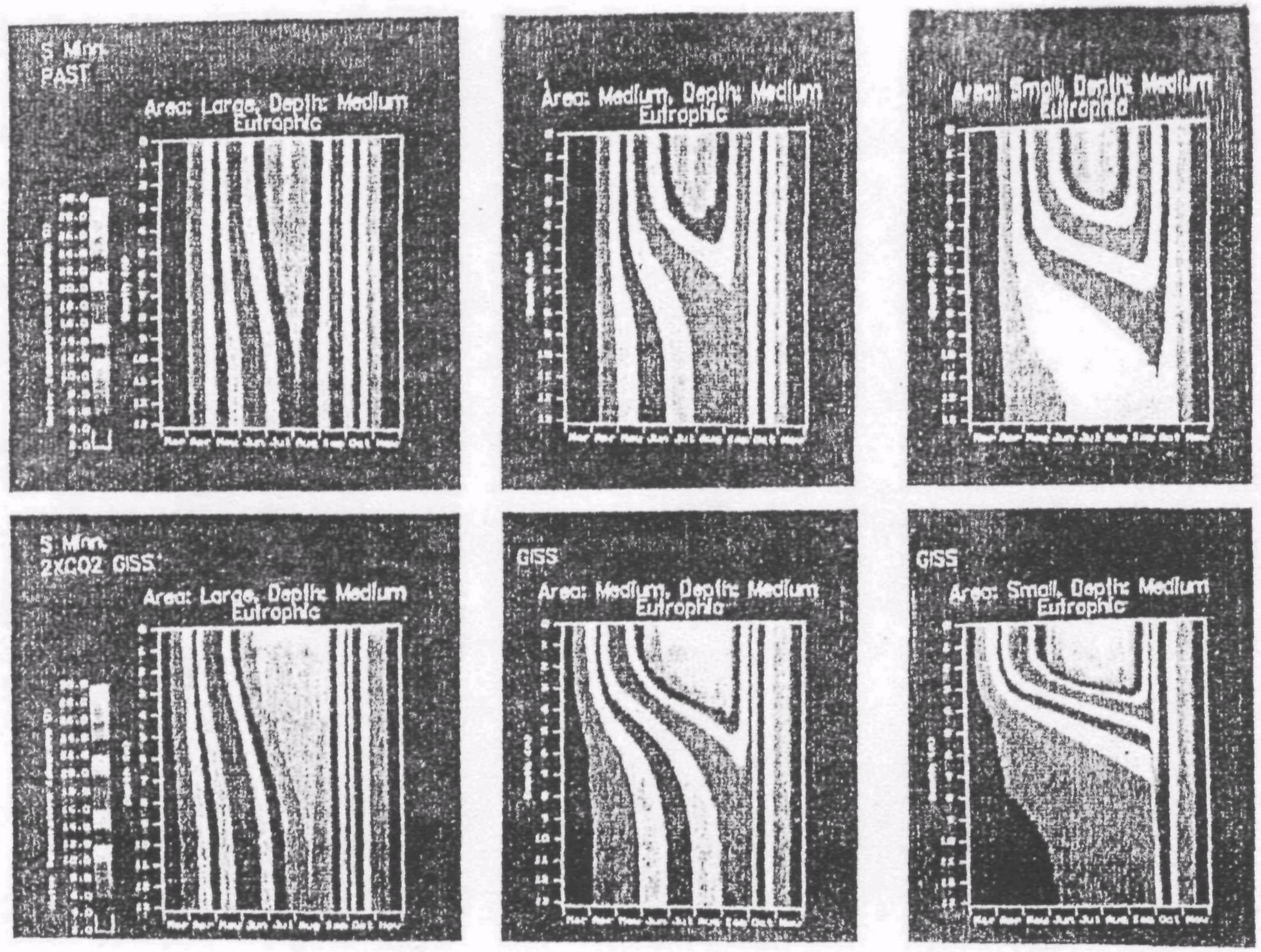

Fig.5.10a Simulated temperature (isotherm) structure in three medium deep (13 m maximum depth) lakes of large (10 km^2), medium (1.7 km^2) and small (0.2 km^2) surface area. Isotherm bands are in increments of 2°C. Simulated water temperatures are for past climate (1955–79) (top) and the $2XCO_2$ GISS climate scenario (bottom).

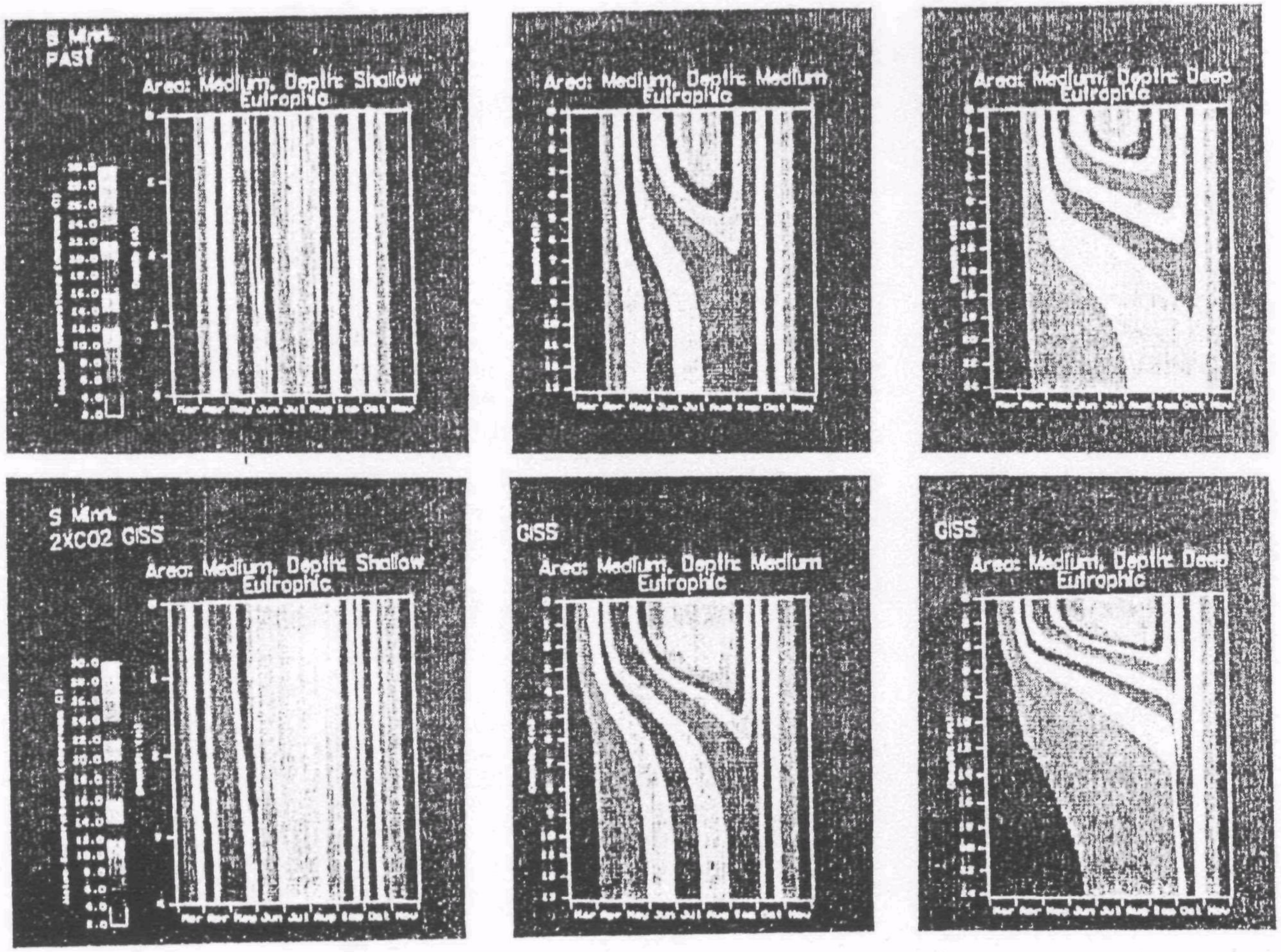

Fig.5.10b Simulated temperature (isotherm) structure in three medium area (1.7 km^2) lakes of different maximum depths: shallow (4 m), medium (13 m) and deep (24 m). Isotherm bands are in increment of 2°C. Simulated water temperatures are for past climate (1955–79) (top) and the 2XCO$_2$ GISS climate scenario (bottom).

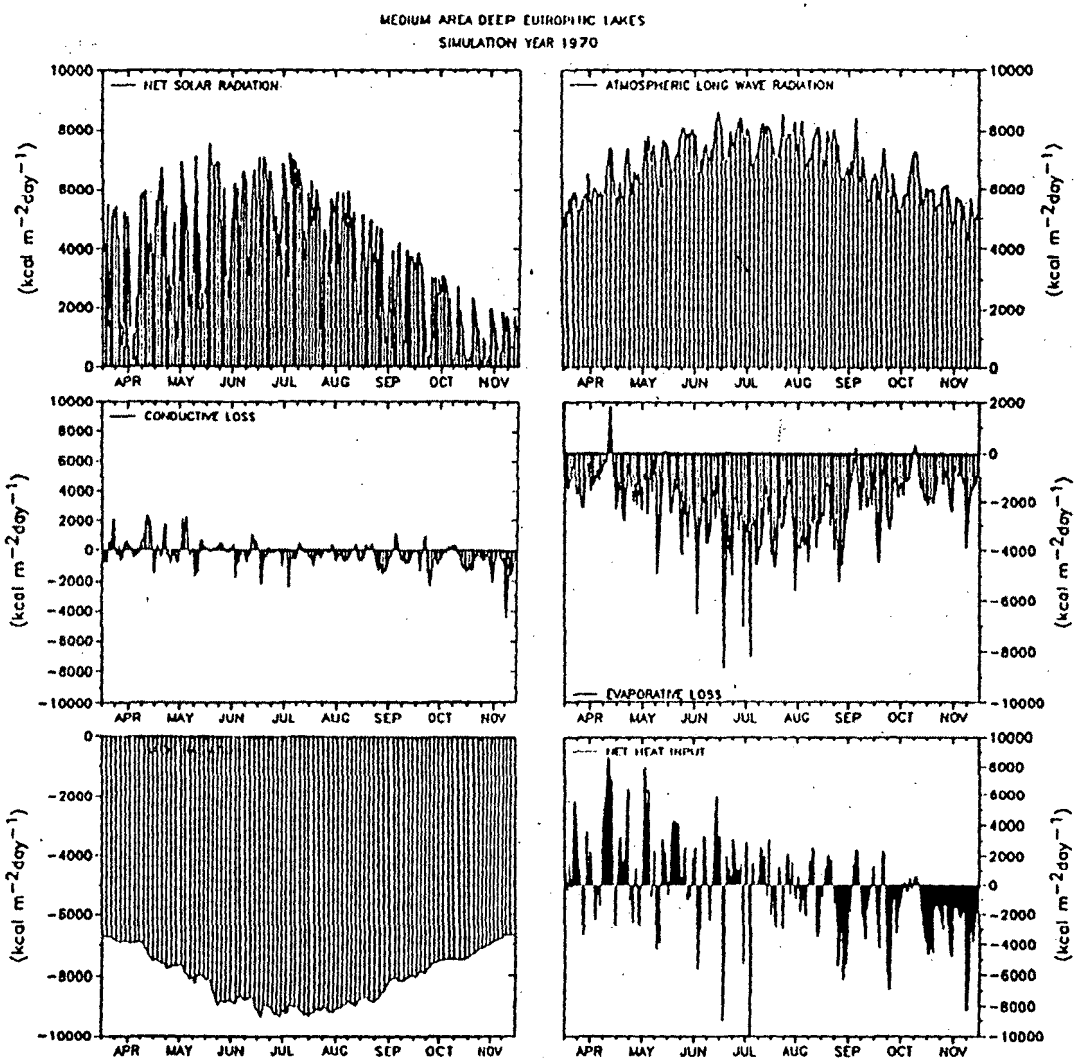

Fig. 5.11 Examples of individual surface heat flux components.

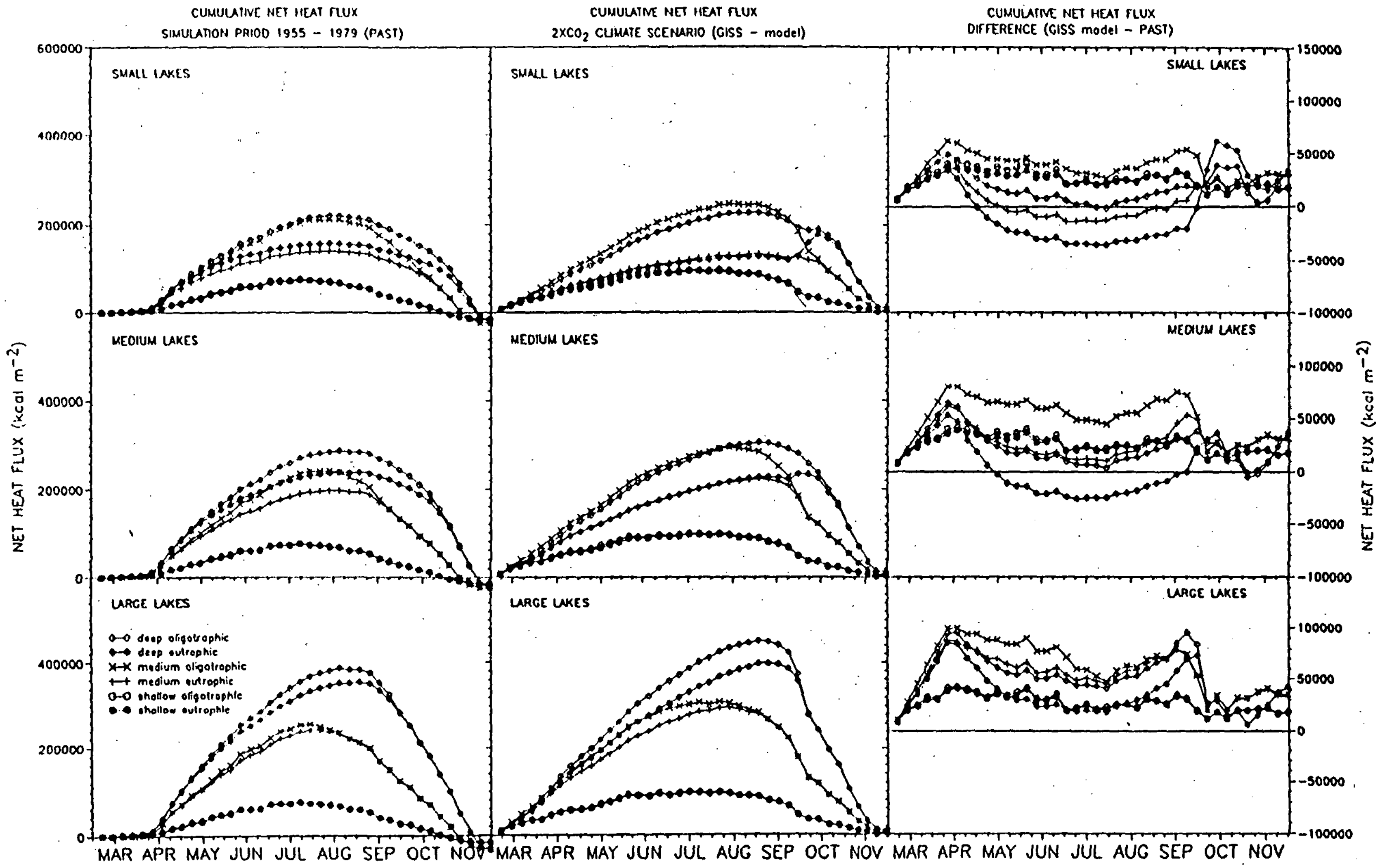

Fig. 5.12 Simulated cumulative net heat flux.

Back radiation and evaporation are the main processes by which lakes lose heat in the summer. Evaporative losses were found to be significantly increased after climate change (GISS). In all lakes, regardless of depth, surface area and trophic status, the computed evaporation water losses were uniformly 0.30 m (± 0.01 m) higher (Figure 5.13). In other words, lake water budgets will be put under significant stress. This increased evaporation also explains why the water temperature increases after climate change remains at a relatively moderate 2°C, when air temperature increases by an average seasonal simulation (March 1 – November 30) value of 4.4 °C. Evaporative cooling is a key to the understanding of the temperature responses to changed climate.

5.5.3 Vertical mixing/Stratification/Stability

Vertical mixing and stratification affect lake water temperature dynamics. A surface mixed layer depth is defined here as the thickness of the isothermal layer from the water surface downward. Surface mixed layer depths are calculated daily by the wind mixing algorithm in the model and averaged over a week (Figure 5.14). Mixed layer depths at the beginning and before the end of simulation are equal to the total lake depth and indicate spring and fall overturns. The most shallow mixed layer depths were calculated for small, deep, eutrophic lakes based on the classification in Table 5.2. Vertical mixing is caused by wind and natural convection. Surface mixed layer depths were the shallowest for small lakes because of short fetch. Smaller wind stresses and hence wind energy inputs are usually associated with smaller lake surface area (shorter fetch). In these lakes the smallest amount of turbulent kinetic energy is available for entrainment of the thermocline. Wind energy required for entrainment of layers at the thermocline is inversely proportional to the stability (defined as a density difference between adjacent layers) of the water column and depth of the mixed layer. The lowest hypolimnetic temperatures and the highest temperature (density) gradients were calculated for small, deep, eutrophic lakes. That was the reason for the smallest mixed layer depths calculated for these lakes.

For the same morphometric lake characteristics, oligotrophic lakes had deeper surface mixed layers than eutrophic lakes because of higher penetration depth of irradiance.

Climate change will impose higher positive net heat fluxes at the lake surface earlier in the season than in the past. That causes an earlier onset of stratification. This is in agreement with a conclusion derived by Robertson (1989) from field data for Lake Mendota. In the period from the onset of stratification until September, mixed layer depths were projected in the average 1.2 m smaller than in the past. From the end of September, mixed layer depths were deeper after climate change, mainly due to stronger natural convection and higher winds caused by climate change. In spring and summer evaporative losses were also increased by climate change but no significant persistent cooling occurred because of net heat input from radiation and convection. The earlier onset of stratification in spring and the mixed layer depth increase in fall were also found by Schindler et al. (1990) in his analysis of observations in the ELA. In the ELA mixed layer depths increased due to transparency increase and increased winds due to reduced forest cover resulting from increased incidence of forest fires.

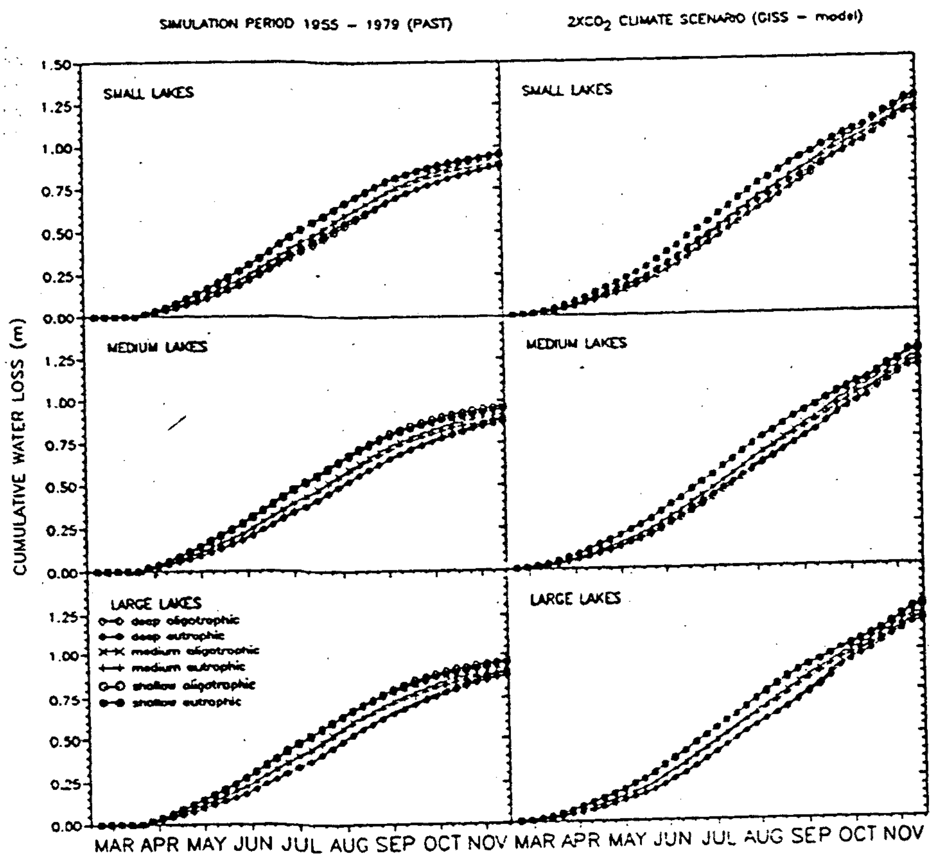

Fig. 5.13 Simulated cumulative evaporative losses.

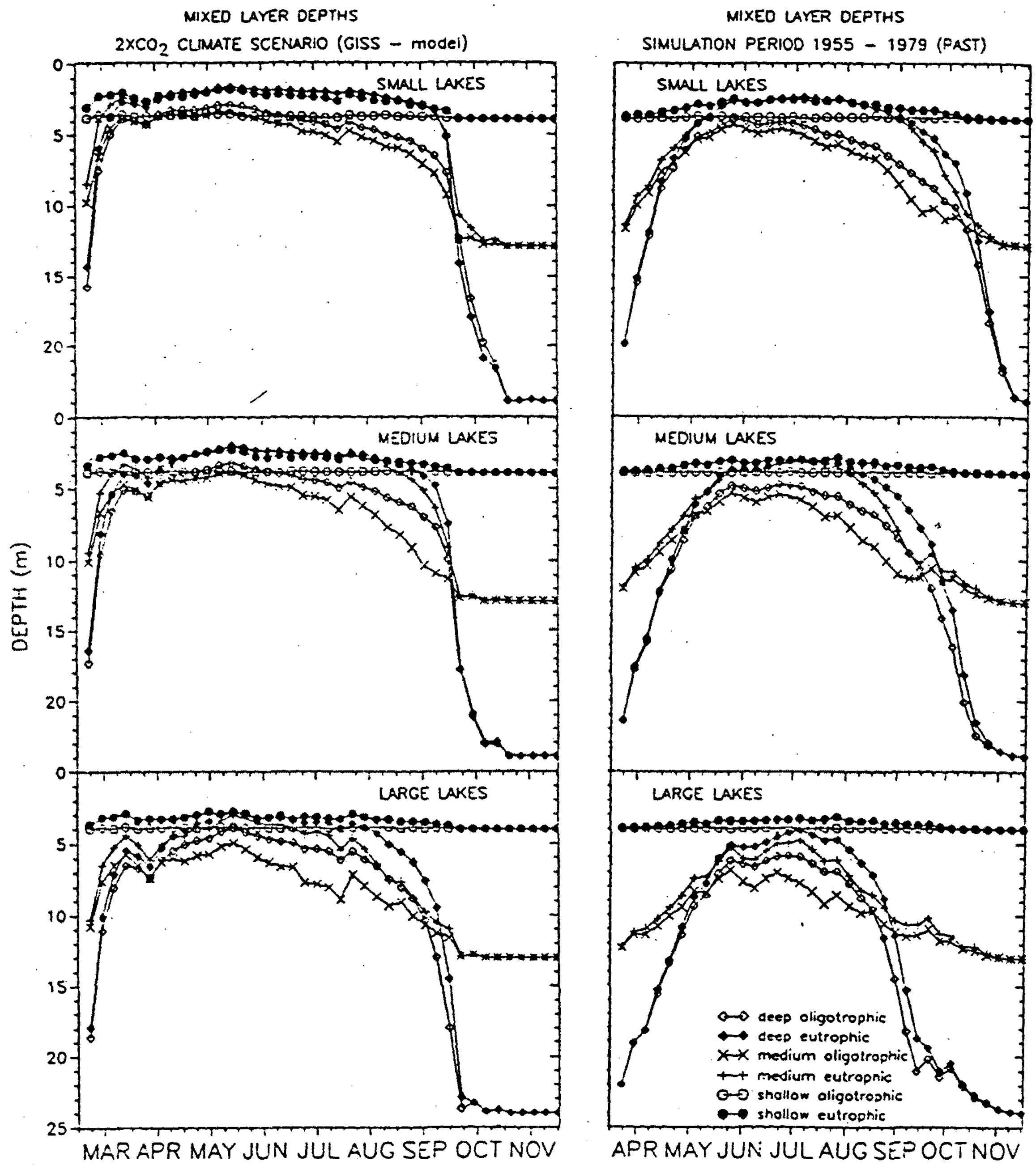

Fig. 5.14 Simulated weekly mixed layer depth.

The stabilizing effect of the density stratification and the destabilizing effect of the wind can be quantified using a Lake number (Imberger and Patterson, 1989):

$$L_n = \frac{g\, S_t(1 - z_t/z_m)}{\rho_0\, u_*\, A_o^{3/2}\, (1 - zg/zm)} \tag{5.2}$$

where g is acceleration due to gravity (m s^{-2}), z_t is height from the lake bottom to the center of the thermocline (m), z_m is maximum lake depth (m), z_g is the height of the center of volume of lake, A_0 is lake surface area (m^2), ρ_0 is hypolimnion density (kg m^{-3}), S_t is the stability of the lake (kg m; Hutchinson, 1957), u_* is surface shear velocity (m s^{-1}). Estimates for the different elements in the Lake number are obtained from daily lake water temperatures simulations, daily meteorological data, and lake geometry. Larger Lake number values indicate stronger stratification and higher stability i.e. forces introduced by the wind stress will have minor effect. Lake number dependence on lake area, depth, and trophic status, for different lake classes is given in Figure 5.15. Stability is higher for oligotrophic lakes than eutrophic lakes. Oligotrophic lakes had deeper thermoclines and required greater wind force in order to overturn the density structure of the water column. Climatic change caused higher lake numbers, i.e. more stable stratification among the same lake classes.

Seasonal stratification is defined herein as the condition when temperature difference between surface and deep water temperature is greater than 1°C. Although 1°C is an arbitrary criterion, it is useful to identify a possible stratification shift with climate change. With the above definition, stratification characteristics for southern Minnesota lakes are given in Table 5.5. A seasonal stratification ratio (SSR) is defined as the total number of days when stratification stronger than 1°C exists, divided by the period from the earliest to latest date of stratification. A SSR ratio less than 1.0 indicates a polymictic, typically shallow or a medium-depth large lakes. Other lake categories were dimictic since the seasonal stratification ratio was 1.0. In other words, once seasonal stratification was established, it lasted until fall overturn.

Climate change advanced the onset of seasonal stratification in the average by 50 days for shallow lakes, and 34 days for deep and medium deep lakes. Length of stratification was prolonged by 60 days for shallow and by 40 days for deep and medium deep lakes.

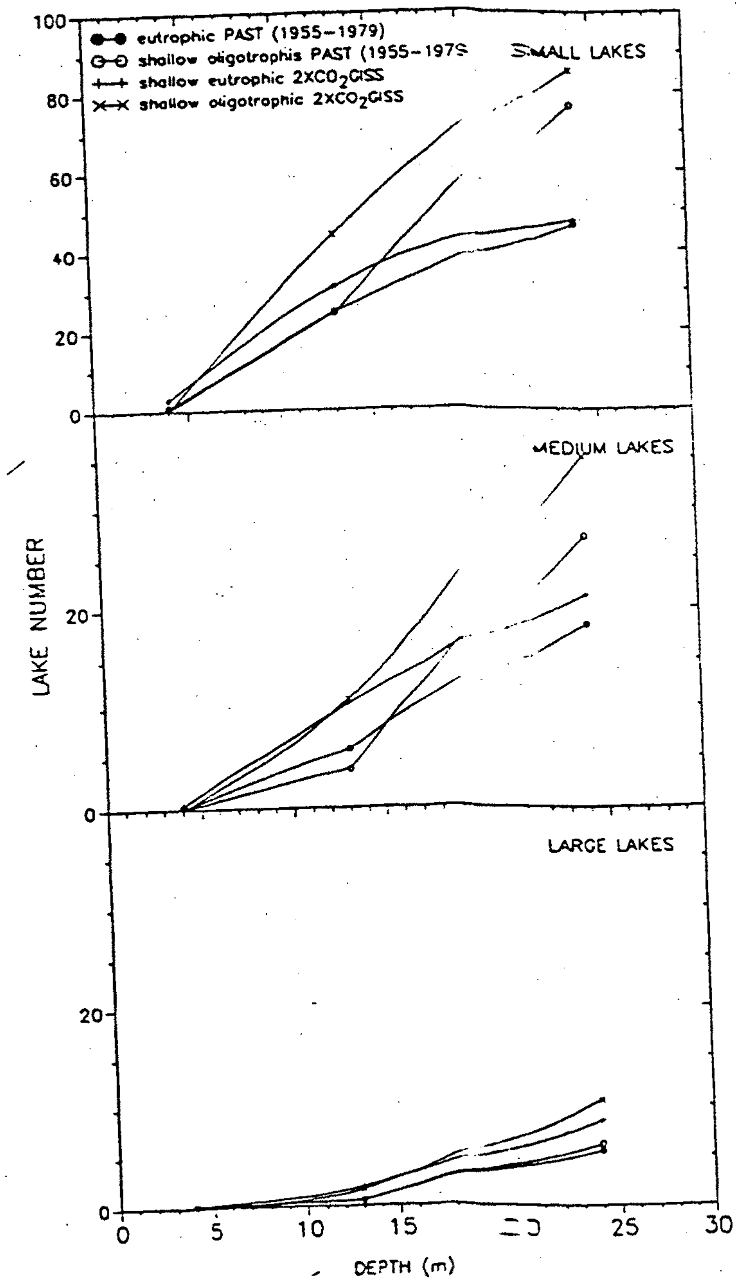

Fig. 5.15 Simulated lake numbers as a function of lake depth and trophic status.

Table 5.5 Seasonal stratification characteristics of southern Minnesota lakes

LAKE CHARACTERISTICS			PAST 1955–1979						GISS–2xCO_2						GISS – PAST			
MAXIMUM DEPTH m	SURFACE AREA km^2	TROPHIC STATUS	BSS day	ESS day	LSS day	SSR –	MAXSD m	MINSD m	BSS day	ESS day	LSS day	SSR –	MAXSD m	MINSD m	BSS day	ESS day	LSS day	SSR –
SHALLOW	SMALL	Eutrophic	118	269	152	0.89	1.7	0.1	68	271	204	0.98	1.7	0.1	–50	2	52	0.09
(4.0)	(0.2)	Mesotrophic	134	241	108	0.12	1.9	0.2	85	246	162	0.54	2.1	0.1	–49	5	54	0.42
		Oligotrophic	0	0	0				0	0	0							
	MEDIUM	Eutrophic	132	244	113	0.63	1.6	0.1	76	255	180	0.84	1.9	0.1	–56	11	67	0.22
	(1.7)	Mesotrophic	0	0	0				116	138	23	0.22	1.3	0.4				
		Oligotrophic	0	0	0				0	0	0							
	LARGE	Eutrophic	133	240	108	0.19	1.8	0.1	85	255	171	0.54	1.3	0.1	–48	15	63	0.35
	(10.0)	Mesotrophic	0	0	0				116	137	22	0.14	0.9	0.3				
		Oligotrophic	0	0	0				0	0	0							
MEDIUM	SMALL	Eutrophic	100	293	194	1.00	5.0	0.2	68	288	221	1.00	5.3	0.2	–32	–5	27	0.00
(13.0)	(0.2)	Mesotrophic	100	290	191	1.00	4.5	0.2	69	287	219	1.00	6.7	0.1	–31	–3	28	0.00
		Oligotrophic	101	268	168	1.00	7.0	0.2	70	276	207	1.00	9.1	0.1	–31	8	39	0.00
	MEDIUM	Eutrophic	105	262	158	1.00	4.9	0.4	69	274	206	1.00	5.9	0.4	–36	12	48	0.00
	(1.7)	Mesotrophic	106	256	151	1.00	4.9	0.4	69	270	202	1.00	4.0	0.4	–37	14	51	0.00
		Oligotrophic	106	241	136	0.99	6.1	0.4	70	251	182	1.00	5.3	0.4	–36	10	46	0.02
	LARGE	Eutrophic	106	241	136	0.86	3.5	0.4	70	250	181	0.99	2.9	0.4	–36	9	45	0.13
	(10.0)	Mesotrophic	106	233	128	0.87	4.5	1.0	72	250	179	0.97	4.3	0.4	–34	17	51	0.10
		Oligotrophic	124	210	87	0.99	5.5	1.0	73	247	175	0.90	5.3	0.4	–51	37	88	–0.10
DEEP	SMALL	Eutrophic	101	312	212	1.00	9.0	0.4	69	301	233	1.00	5.8	0.4	–32	–11	21	0.00
(24.0)	(0.2)	Mesotrophic	101	313	213	1.00	10.0	0.4	70	302	233	1.00	6.7	0.4	–31	–11	20	0.00
		Oligotrophic	101	312	212	1.00	13.0	0.4	70	302	233	1.00	8.6	0.4	–31	–10	21	0.00
	MEDIUM	Eutrophic	104	295	192	1.00	10.0	0.4	70	290	221	1.00	7.7	0.4	–34	–5	29	0.00
		Mesotrophic	104	295	192	1.00	10.0	0.4	71	290	220	1.00	8.6	0.4	–33	–5	28	0.00
		[illegible]	[illegible]	[illegible]	188	1.00	12.0	0.4	72	290	219	1.00	10.6	0.4	–33	–2	31	0.00
	[illegible]	[illegible]	[illegible]	[illegible]	159	0.99	8.0	0.4	72	275	204	1.00	11.5	0.4	–34	11	45	0.01
	[illegible]	[illegible]	[illegible]	[illegible]	[illegible]	[illegible]	9.0	0.4	71	275	205	1.00	13.4	0.4	–35	11	46	0.00
		[illegible]	[illegible]	[illegible]	[illegible]	[illegible]	[illegible]	[illegible]	72	273	202	1.00	9.6	0.4	–34	13	47	0.00

BSS Beginning seasonal stratification, i.e. first julian day when difference between surface and deep water temperature is greater than 1°C.

ESS End seasonal stratification, i.e. last julian day when difference between surface and deep temperature is less than 1°C.

LSS Length of seasonal stratification (ESS–BSS)+1

SSR Seasonal stratification ratio, i.e. total number of days when difference between surface and deep water temperature is greater than 1°C divided by LSS

MAXSD Maximum stratification depth, MINSD – Minimum stratification depth

5.5 Conclusions

A regional simulation study was conducted for 27 classes of lakes in Minnesota. Lakes were classified according to area, maximum depth, and trophic level. A validated, one-dimensional, unsteady lake water quality model was linked to global climate model output in order to quantify potential thermal changes in inland lakes due to climate change. Water temperatures were simulated on a daily time base for past weather conditions, 1955–1979 and the $2xCO_2$ GISS model climate scenario.

The main findings are as follows:

(1) Simulated epilimnetic temperatures were predominantly related to weather and secondarily to lake morphometry. Weekly average epilimnetic temperatures were raised by climate change for all lake classes. The seasonally averaged water temperature rise was 3°C, compared to 4.4°C air temperature increase caused by the climate change. The largest differences in water temperatures occurred in April and September, and were 7.2°C and 4.9°C, respectively. The seasonal daily maximum of epilimnetic temperatures rose only about 2°C with climate change.

(2) Hypolimnetic temperatures were predominantly related to lake morphometry and mixing events in spring, and only secondarily to weather in summer. The highest temperatures were calculated for large, shallow, eutrophic lakes. After climate change, hypolimnetic water temperatures were as follows: shallow lakes, warmer by an average 3.1°C; deep lakes, cooler by an average 1.1°C; small–area, medium depth lakes, cooler by 1.7°C; and large–area medium–depth lakes, warmer by 2.0°C.

(3) Simulated evaporative heat and water losses increased by about 30 percent for the $2xCO_2$ GISS climate scenario. Evaporative water losses increased by about 300 mm, making the total water loss 1200 mm.

(4) Net heat flux at the lake surface increased with changed climatic conditions. The largest difference in calculated cumulative net heat storage between past and future climate was 100,000 kcal m^{-2} and occurred in April and September with climate change.

(5) Simulated mixed layer depths decreased about 1 m in the spring and summer, and increased in the fall.

(6) With climate change, lakes stratify earlier, and overturn later in the season. Length of the stratification period was increased by 40 to 60 days.

(7) Climate change caused greater lake stability in spring and summer. In fall lakes were driven faster towards isothermal conditions.

6. Summary

As a result of the research described here, a better understanding of how freshwater inland lakes respond to variable atmospheric conditions has been gained.

Chapter 2 describes how a specific lake water temperature model was generalized to simulate the seasonal (spring to fall) temperature stratification over a wide range of lake morphometries and meteorological conditions. Model coefficients related to hypolimnetic eddy diffusivity, light attenuation, wind sheltering and convective heat transfer were generalized using theoretical and empirical model extensions. The proposed regional lake water temperature model simulates the onset of stratification, mixed layer depth, and water temperatures well.

Hypolimnetic eddy diffusivity was estimated as a function of lake surface area and stability frequency. Although the proposed relationship is a simplification of the turbulent diffusion processes taking place in the hypolimnion, it was found to be useful in seasonal lake water temperature modeling. Heat exchange between water and lake sediments, a process commonly neglected in previous work, was found to be important for the analysis of vertical hypolimnetic eddy diffusivity (Appendix A). Estimates of hypolimnetic eddy diffusivity made without sedimentary heat flux were up to one third smaller than those made with the heat flux. Effects of errors in temperature measurements and sediment heat flux estimates on the estimated vertical eddy diffusivity were evaluated as well.

Chapter 3 describes a first order analysis of uncertainty propagation in lake temperature modeling. The output uncertainty is defined as the result of deviations of the meteorological variables from their mean values. The analysis was applied to systems with correlated and uncorrelated meteorological variables. Surface water temperatures are strongly affected by uncertain meteorological forcing. Air temperature and dew point temperature fluctuations have a significant effect on lake temperature uncertainty. Long–term average water temperature structure in lakes can be estimated by computer model simulations for just one year when the results from the statistical analysis of meteorological variables are used as input. This analysis presents a useful alternative for the study of long–term averages and the variability of temperature structures in lakes due to variable meteorological forcing. In addition, the analysis revealed the separate contribution of each meteorological variable to water temperature uncertainty.

The analysis described in Chapter 4 was a first step in quantifying potential thermal changes in inland lakes due to climate change. Rather than using global climate change predictions, this analysis looked at the changes in heat balance and temperature profiles in a particularly warm year (1988) compared to a "normal" year (1971). A comparison was made for three morphometrically different lakes located in north central US. Simulated water temperatures were daily values driven by daily weather parameters and verified against several sets of measurements. The results show that in the warmer year, epilimnetic water temperatures were higher; evaporative water loss increased; and summer stratification occurred earlier in the season.

Rather than analyzing particular years and particular lakes, emphasis in Chapter 5 is on long term behavior and a wide range of lake morphometries and trophic levels. The regional lake water temperature model was linked to a daily meteorological data base to simulate daily water temperature profiles over a period of twenty–five (1955–1979) years. Twenty seven classes of lakes which are characteristic of the north–central US were investigated. Output from a global climate model (GISS) was used to modify the weather data base to account for the doubling of atmospheric CO_2. The simulations predict that after climate change epilimnetic temperatures will be higher but increase less than air temperature; hypolimnetic temperatures in seasonally stratified dimictic lakes will be largely unchanged or even lower than at present; evaporative water loss will be increased by as much as 300 mm for the season, onset of stratification will occur earlier and overturn later in the season; and overall lake stability will become greater in spring and summer.

References

Adams, E.E., Scott, S.A. and Ho, E. K. (1987). "Vertical diffusion in a stratified cooling lake, *Journal of Hydraulic Engineering,* ASCE, Vol. 113(3), pp. 293–307.

Adams, E.E., D.J. Cosler, and K.R. Helfrich (1990). Evaporation from heated water bodies: Predicting combined forced plus free convection, *Water Resources Research*, Vol. 26(3), pp. 425–435.

Aldama, A.A, D.R.F. Harleman, and E.E. Adams (1989). Hypolimnetic mixing in a weakly stratified lake, *Water Resources Research*, Vol. 25(5), pp. 1014–1024.

Andricevic, R. (1990). Cost–effective network design for groundwater flow monitoring, Stochastic Hydrology and Hydraulics, Springer International, Berlin, Germany, 4(1), pp. 27–41.

Baker, D.G., Kuehnast, E.L., and Zandlo, J.A (1985). Climate of Minnesota, Part 15 – Normal temperatures (1951–1980) and their application, Agricultural Experimental Station University of Minnesota, AD–SB–2777.

Bannister, T.T. (1974). Production equations in terms of chlorophyll concentration, quantum yield, and upper limit to production, *Limnology and Oceanography,* 19(1), pp. 1–12.

Bannister, T.T. (1979). Quantitative description of steady state, nutrient–saturated algal growth, including adaptation, *Limnology and Oceanography*, Vol. 24(1), pp. 76–96.

Birge, E.A., Juday, C. and March, H.W. (1927). The temperature of the Bottom deposits of Lake Mendota; A chapter in the heat exchange of the lake," *Transactions of the Wisconsin Academy of Sciences,* Arts and Letters, Vol 23, pp. 187–231.

Bloss, S., and Harleman, D.R.F. (1979). "Effect of wind–mixing on the thermocline formation in lakes and reservoirs," Tech. Rep. 249, Ralph M. Parsons Lab. for Water Resour. and Hydrodyn., Dep. of Civ. Eng., Mass. Inst. of Technol.

Bolin, B. and B.R. Doos (1986). *The Greenhouse Effect, Climate Change and Ecosystems*, John Wiley and Sons, New York, p. 541.

Canale, R. P., and S. W. Effler (1989). Stochastic phosphorus model for Onondaga Lake, *Water Research.*, 23(8), 1009–1016.

Carlson, R.E.(1977). 'A trophic state index for lakes', *Limnology and Oceanography*, Vol.22, pp. 361–369.

Carslaw, H.S. and Jaeger, J.C. (1959). *Conduction of heat in solids,* Oxford University Press, N.Y.

Chang, L.H., S.F. Railsback, and R.T. Brown (1992). Use of reservoir water quality model to simulate global climate change effects on fish habitat, *Climatic Change*, Vol. 20, pp. 277–296.

Colman, J.A., and Armstrong, D.E. (1987). Vertical eddy diffusivity determined with ^{222}Rn in the benthic boundary layer of ice–covered lakes, *Limnology and Oceanography,* 32(3), pp. 577–590.

Coutant, C.C. (1990). Temperature–oxygen habitat for freshwater and coastal striped bass in a changing climate, *Transactions of the American Fisheries Society*, Vol. 119(2), pp. 240–253.

Dake, J.M.K. and D.R.F. Harleman (1969). Thermal stratification in lakes: Analytical and laboratory studies, *Water Resources Research*, Vol. 5(2), pp. 404–495.

Dake, J.M.K. (1972). Evaporative cooling of a body of water, *Water Resources Research*, Vol. 8(4), pp. 1087–1091.

Dettinger, M. D., and J. L. Wilson (1981). First order analysis of uncertainty in numerical models of groundwater flow, 1, Mathematical development, *Water Resour. Res.*, 17(1), 149–161.

Dhamotharan, S., (1979). A mathematical model for temperature and turbidity stratification dynamics in shallow reservoirs, Ph.D. thesis, University of Minnesota, p. 319.

ERLD/MNDNR: (1990). Minnesota Department of Natural Resources Fisheries Division Lake Data Base, expanded by US Environmental Protection Agency Environmental Research Laboratory Duluth.

Ellis, C. and H.G. Stefan (1991). Water temperature dynamics and heat transfer beneath the ice cover of a lake, *Limnology and Oceanography*, Vol. 36(2), pp. 324–335.

Ford, D.E. (1976). Water temperature dynamics of dimictic lakes: Analysis and prediction using integral energy concepts, Ph.D. thesis, University of Minnesota, p. 432.

Ford, D.E. and H.G. Stefan (1980a). Thermal predictions using integral energy model, Jour. Hydraulics Division, ASCE, Vol. 106, HY1, pp. 39–55.

Ford, D. E., and H. G. Stefan (1980b). Stratification variability in three morphometrically different lakes under identical meteorological forcing, *Water Resour. Bull.*, AWRA, 16(2), 243–247.

Gardner, R.H., R.V., O'Neill, J.B., Mankin, J.H., Carney (1981). A comparison of sensitivity analysis and error analysis based on a stream ecosystem model, *Ecol. Modeling*, 12, 173–190.

Gargett, A.E. (1984). Vertical eddy diffusivity in the ocean interior, *Journal of Marine Research*,42(2), pp. 359–393.

Gargett, A.E. and Holloway, G. (1984). Dissipation and diffusion by internal wave breaking, *Journal of Marine Research*, 42(1), pp. 15–27.

Gerhard, H., J. Imberger, and M. Schimmele (1990). Vertical mixing in Uberlinger See, western part of Lake Constance, *Aquatic Sciences*, Vol. 53(3), pp. 256–268.

Gorham, E., and Boyce, F.M. (1989). Influence of lake surface area and depth upon thermal stratification and the depth of the summer thermocline, *J. Great Lakes Res.*, Vol. 15, pp. 233–245

Gu, R. and H. G. Stefan (1990). Year–round simulation of cold climate lakes, *Cold Regions Science and Technology* 18, pp. 147–160.

Harbeck, G.E. Jr. (1962). A practical field technique for measuring reservoir evaporation utilizing mass–transfer theory, U.S. Geol. Surv. Prof. Pap., 272E, pp. 101–105.

Harleman, D.R.F., and K.A. Hurley (1976). Simulation of the vertical thermal structure of lakes under transient meteorological conditions, *Dynamics of Stratification and of Stratified Flows in Large Lakes: Proceedings of Workshop of the Committee on Lake Dynamics* (Winsdor, Ontario: International Joint Commission, Regional Office), pp. 79–96.

Heiskary, S.A., Wilson, C.B., and Larsen, D.P. (1987). Analysis of regional patterns in lake water quality: Using ecoregions for lake management in Minnesota, *Lake and Reservoir Management*, Vol 3, pp. 337–344.

Heiskary, S.A. and C.B. Wilson (1988). Minnesota lake water quality assessment report, Minnesota Pollution Control Agency, St. Paul, p. 49.

Henderson–Sellers, B. (1988). Sensitivity of thermal stratification models to changing boundary conditions, *Applied Mathematical Modelling*, Vol 12, pp. 31–43.

Horsch, G. M. and H. G. Stefan (1988). Convective circulation littoral water due to surface cooling, *Limnology and Oceanography*, Vol. 33(5), pp. 1068–1083.

Houghton, J. T. et al. editors (1990). *Climatic Change: The IPCC Scientific Assessment.* Cambridge University Press.

Idso, S.B. and R. D. Jackson (1969). Thermal radiation from the atmosphere, *Jour. of Geophysical Research*, 74(23), pp. 5397–5403.

Idso, S.B. and R.G. Gilbert (1974). On the universality of the Poole and Atkins Secchi disk–light extinction equation, *J. Appl. Ecol.*, Vol. 11, pp. 339–401.

Imberger, J. (1985). The diurnal mixed layer, *Limnology and Oceanography*, Vol 30(4), pp. 737–770.

Imberger, J., and Patterson, J.C. (1989). Physical Limnology, in *Advances in Applied Mechanics*, edited by J.W. Hutchinson and T.Y. Wu, Academic Press, Vol 27, pp. 303–475.

Imboden, D.M., Lemmin, U., Joller, T., and Schurter, M. (1983). Mixing processes in lakes: mechanisms and ecological relevance, Schweiz. *J. Hydrol.*, 45(1), pp. 11–44.

Jassby, A. and Powell, T. (1975). Vertical patterns of eddy diffusion during stratification in Castle lake, California, *Limnology and Oceanography,* 20(4), pp. 530–543.

Jones, P.D., Wigley, T.M.L., and Wright, P.B. (1986). Global temperature variations between 1861 and 1984, *Nature,* Vol 332(31), pp. 430–434.

Keijman, J. Q. (1974). The estimation of energy balance of a lake from simple weather data, *Boundary–Layer Meteorology,* Vol. 7, 399–407.

Kerr, R.A. (1989). 1988 ties for warmest year, *Science,* Vol 243(17), pp. 891–892.

Lewis, W.M. (1982). Vertical eddy diffusion in a large tropical lake, *Limnology and Oceanography,* Vol. 27(1), pp. 161–163.

Lewis, W. M., Jr., (1983). Temperature, heat, and mixing in Lake Valencia Venezuela, *Limnology and Oceanography,* Vol. 28(2), pp.273–286.

Likens, G.E., and Johnson, N.M. (1969). Measurement and analysis of the annual heat budget for the sediments in two Wisconsin lakes. *Limnology and Oceanography,* Vol. 14(1), pp. 115–135.

Magnuson, J.J, J.D. Meisner, and D.K. Hill (1990). Potential changes in thermal habitat of Great Lakes fish after global climate warming *Transactions of the American Fisheries Society,* Vol. 119(2), pp. 254–264.

McCormick, M. J. (1990). Potential changes in thermal structure and cycle of Lake Michigan due to global warming, *Transactions of the American Fisheries Society,* Vol. 19(2), pp. 183–194.

McKinney, D. C. (1990). Predicting groundwater contamination: uncertainty analysis and network design, Ph.D. thesis, Cornell University, 256 pp

McLaughlin, D. (1985). A distributed parameter state space approach to evaluating the accuracy of the groundwater predictions, Ph.D. thesis Dep. of Civ. Eng., Princeton Univ., Princeton, N. J., 1985.

[illegible] R.O., W.S. Combs, Jr., P.D. Smith, and A.S. Knoll (1979). Attenuation of light and daily integral rates of photosynthesis attained by planktonic algae, *Limnology and Oceanography,* Vol. 24(6), pp. 1038–1050.

[illegible] J.D., J.L. Goddier, H.A. Regier, B.J. Shuter, and W.J. Christie (1987). An assessment of the effects of climate warming on Great Lakes Basin fishes, *Journal of Great Lakes Research,* Vol. 13(3), pp. 340–352.

National Research Council (1982). Carbon Dioxide/Climate Review Panel. Carbon Dioxide and Climate: A Second Assessment. National Academy Press, Washington, D.C., p. 72.

National Research Council (1983). Changing climate: report of the Carbon Dioxide Assessment Committee. National Academy Press, Washington, D. C., p. 496.

NCAR (1990). National Center for Atmospheric Research – data support section, Personal communication Roy Jenne and Dennis Joseph, Boulder, Colorado.

N[illegible]eler, U.P., Schindler, P.W., Wirz, U.E. and Imboden, D.M. (1983). Chemical and geochemical studies of Lake Biel II. A chemical approach to lake mixing. *Schweiz. Z. Hydrol.*, Vol. 45(1), pp. 45–61.

Osgood, R.A. (1984). A 1984 study of the water quality of 43 metropolitan area lakes, Metropolitan Council, St. Paul, MN, Publ. No. 10–84–172, p. 40.

Osgood, R.A. (1989). An evaluation of the effects of watershed treatment systems on summertime phosphorus concentration in metropolitan area lakes, Metropolitan Council, St. Paul, MN, Publ. No. 590–89–062, p. 85.

Osgood, R.A. (1990). Personal communication, Metropolitan Council, St. Paul, Minnesota.

Patankar, S. V. (1988). Numerical heat transfer and fluid flow, McGraw–Hill, New York, N.Y., 197 pp..

Poole, H.H. and W.R.G. Atkins (1929). Photo–electric measurements of submarine illumination throughout the year, *J. Mar. Biol. Assoc. U.K.*, Vol. 16, pp. 297–324.

Priscu, J.C., Spigel, R.H., Gibs, M.M., and Downes, M.T. (1986). A numerical analysis of hypolimnetic nitrogen and phosphorus transformations in Lake Rotoiti, New Zealand: A geothermally influenced lake, *Limnology and Oceanography,* Vol. 31(4), pp. 812–831.

Protopapas, A. L. (1988). Stochastic hydrologic analysis of soil–crop–climate interactions, Ph.D. thesis, Parsons Lab., Dep. of Civ. Eng., Mass. Inst.of Technol., Cambridge, 239 pp.

Protopapas, A.L., and R.L. Bras (1990). Uncertainty propagation with numerical models for flow and transport in the unsaturated zone, *Water Resour. Res.*, 26 (10), 2463–2474, 1990.

Quay, P.D., W.S. Broecker, R.H. Hesslein, and D.W. Schindler (1980). Vertical diffusion rates determined by tritium tracer experiments in the thermocline and hypolimnion of two lakes, *Limnology and Oceanography,* Vol. 25(2), pp. 201–218.

Richardson, C. W. (1981). Stochastic simulation of daily precipitation, temperature, and solar radiation, *Water Resour. Res.*, 17(1), 182–190, 1981.

Riley, M.J. and H.G. Stefan (1987). Dynamic lake water quality simulation model "Minlake", University of Minnesota, St. Anthony Falls Hydraulic Laboratory, Report No. 263, p. 140.

Robertson, D.M. (1989). The use of lake water temperature and ice cover as a climatic indicators, Ph.D. thesis, University of Wisconsin–Madison, p. 330.

Robertson, D.M., and R.A. Ragotzkie (1990). Changes in the thermal structure of moderate to large size lakes in response to changes in air temperature, *Aguatic Sciences,* Vol. 52(4), pp. 362–379.

Robinson, P.J., and Finkelstein, P.L. (1990) Strategies for the development of climate scenarios for impact assessment: Phase I final report, USEPA Atmospheric Research and Exposure Assessment Laboratory EPA/600/53–90/026.

Sadhyram, Y., P. Vethamony, A. Suryanarayana, G. N. Swamy, and J. S Sastry (1988). Heat energy exchange over a large water body unde stable atmospheric conditions, *Boundary–Layer Meteorology*, Vol. 44, p 171–180.

Scavia D., W. F. Powers, R. P. Canale, and J. L. Moody (1981). Comparis of first order error analysis and Monte Carlo simulation time–dependent lake eutrophication models, *Water Resour. Res.*, 17 1051–1059.

Schindler, D.W., K.G. Beaty, E.J. Fee, D.R. Cruikshank, E.R. DeBruyn, I Findley, G.A. Londsey, J.A. Sherer, M. Stainton, M.A. Turner (19 Effects of climatic warming on lakes of the Central Boreal For *Science*, Vol. 250(16), pp. 967–970.

Shapiro, J. and H. Pfannkuch (1973). The Minneapolis chain of lake study of urban drainage and its effects 1971–1973, Limnological Res Center, University of Minnesota, Minneapolis, Report No. 9.

Smith, C.R. and K.S. Baker (1981). Optical properties of the cl natural waters, *Applied Optics*, Vol. 20(2), pp. 177–184.

R.H., J. Imberger, and K.N. Rayner (1986). Modeling the diurnal mixed layer, *Limnology and Oceanography*, 31, pp. 533–556.

R.E., and Armstrong, D.E. (1983). Lake mixing and its relationship to epilimnetic phosphorus in Shagawa lake, Minnesota, *Can. J. Fish. Aquat. Sci.*, Vol. 41(1), pp. 57–69.

H.G. and D.E. Ford (1975). Temperature dynamics in dimictic lakes, *Journal of the Hydraulics Division, ASCE*, Vol. 101(HY1), pp. 97–114.

H.G., M.J. Hanson, D.E. Ford, and S. Dhamotharan (1980a). Stratification and water quality predictions in shallow lakes and reservoirs, *Proc. Second Int'l Symp. on Stratified Flows*, International Association for Hydraulic Research, pp. 1033–1043.

H.G., J. Gulliver, M.G. Hahn, and A.Y. Fu (1980b). Water temperature dynamics in experimental field channels: Analysis and modeling, University of Minnesota, St. Anthony Falls Hydraulic Laboratory, Report No. 193.

Stefan, H.G., S. Dhamotharan, and F.R. Schiebe (1982). Temperature/ *sediment model for a shallow lake, Journal of Environmental Engineering Division, ASCE,* Vol. 108(EE4), pp. 750–765.

Stefan, H.G., J.J. Cardoni, F.R. Schiebe, and C.M. Cooper (1983). Model of light penetration in a turbid lake, *Water Resources Research*, Vol. 19(1), pp. 109–120.

Strub, P. T. and T. M. Powell (1987). The exchange coefficients for latent and sensible heat flux over lakes: dependence upon atmospheric stability, *Boundary Layer Meteorology*, 40, 349–361.

Sweers, H.E. (1976). A monogram to estimate the heat–exchange coefficient at the air–water interface as a function of wind speed and temperature; a critical survey of some literature, *Journal of Hydrology*, Vol. 30, pp. 375–401.

Townley, L. R., and J. L. Wilson (1985). Computationally efficient algorithms for parameter estimation and uncertainty propagation in numerical models of groundwater flow, *Water Resour. Res.*, 21(12), 1851–1860.

US Army Corps of Engineers (1986). CE–QUAL–R1: A numerical one–dimensional model of reservoir water quality user's manual, Waterways Experiment Station, Corps of Engineers, Vicksburg, Mississippi, Report E–82–1, 1986.

Waggoner, P. E. (1990). *Climate Change and U.S. Water Resources*, Wiley series in climate and the biosphere, John Wiley & Sons. Inc., pp. 496.

Wanner, H. and U. Siegenthaler (1988). Long and short term variability of climate, Lecture Notes in Earth Sciences, Springer–Verlag Berlin/Heidelberg, pp. 175.

Welander, P. (1968). Theoretical forms for the vertical exchange coefficients in a stratified fluid with application to lakes and seas, Acta Regiae Societatis Scientiarum et Litterarum Gothoburgensis, *Geophysica 1*, pp. 1–26.

Wu, J. (1969). Wind stress and surface roughness at air–sea interface, *Jour. Geophysical Research*, 74, 2, 444–455.

Ward, P.R.B. (1977). *Diffusion in Lake Hypolimnia, Proceedings 17th Congress*, International Association for Hydraulic Research, Baden–Baden, IAHR, pp. 103–110.

Willis, R. and W.W-G. Yeh (1987). *Groundwater Systems Planning and Management*, Prentice–Hall, Englewood Cliffs, NJ 07632, p. 415.

Winter, T. (1980). Personal communication, U.S. Geological Survey, Denver Federal Center, Lakewood, CO 80225.

Wright, D., R. Lawrenz, W. Popp, and M. Danks (1988). Acid precipitation mitigation program, Progress report Thrush Lake Minnesota, Minnesota Department of Natural Resources Division of Fish and Wildlife Ecological Services Section, p. 177.

Appendices

APPENDIX A

Vertical diffusion in a small stratified lake: Data and error analysis

Water temperature profiles were measured at 2 minute intervals in a stratified temperate lake with a surface area of 0.06 km^2 and a maximum depth of 10 m from May 7 to August 9, 1989. The data were used to calculate the vertical eddy diffusion coefficient (K_z) in the hypolimnion. The depth is representative of a large number of lakes in the north central United States. (K_z) was calculated over time intervals of 1 to 15 days and varied from 10^{-3} to 10^{-1} cm^2s^{-1}. A numerical model was developed for heat conduction in the sediments, and heat flux between water and sediments was incorporated into the relationship from which eddy diffusivity was estimated. Heat flux between water and lake sediments, a term commonly neglected, was found to be important in the K_z estimation. K_z values were related to stratification stability as measured by the Brunt–Vaisala frequency N using Welander's expression of the form $K_z = a(N^2)^{\gamma}$. Values of a were on the order of 10^{-4} and γ varied from $-$ 0.36 to $-$ 0.45 when K_z was given in cm^2s^{-1} and N is in s^{-1}. An error analysis was conducted and the effects of different choices of sampling intervals in time and depth on the eddy diffusivity estimates were evaluated. The longest time interval (15 days) and the smallest depth increment (1 m) used in this study were found to give the best K_z estimation.

A.1 Introduction

Density stratification due to vertical temperature gradients inhibits vertical mixing in lakes and reservoirs, and mixing in turn affects the distribution of phytoplankton, nutrients, and other water quality constituents. Quantifying turbulent transport phenomena is one of the major challenges in lake and reservoir hydrothermal and water quality analysis. Specification of vertical turbulent (eddy) diffusion coefficients in one–dimensional water quality models, which are often used for decision–making, is particularly difficult.

In the analysis of vertical turbulent mixing by one–dimensional wind energy models, the depth of the surface mixed (epilimnetic) layer is calculated by an integral entrainment model while the vertical transport in the hypolimnion is taken into account by a diffusion equation (Stefan and Ford 1975; Bloss and Harleman 1979; Ford and Stefan 1980). Although the hypolimnion is isolated from the epilimnetic layer by the thermocline and its associated density gradient, strong and sporadical local mixing events have been observed in the hypolimnion (Jassby and Powell 1975; Imberger 1985; Imberger and Patterson 1989). Such mixing events can originate from oscillating boundary layers induced by seiche motions on the bottom of lakes, internal wave interaction and breakdown, shear instabilities in the thermocline (billows), epilimnetic turbulent kinetic energy leakage to the hypolimnion and double diffusion processes. Scales for such events range from the Kolmorgorov scale to the lake basin scale. Eddy diffusion dependence on stratification strength as measured by buoyancy frequency has been pointed out consistently (Colman and Armstrong 1987; Gargett 1984; Gargett and Holloway 1984; Imboden et al. 1983; Jassby and Powell 1975; Quay et al. 1980; Welander 1968).

Direct measurements of vertical turbulent diffusion in lakes are not easy because of the 3–D nature of the diffusion field, and the spatial and temporal scales. To estimate diffusion values, one can rely on measurements of water temperatures or concentrations of natural tracers present in the water. Water temperature measurement is the most commonly used method because of its simplicity; however, a careful assessment of all external and internal heat sources is required.

The purpose of this study was to estimate vertical eddy diffusion from water temperature measurements in a typical inland shallow lake. Sediment heat exchange, commonly neglected along with error analysis, is also included in the estimation. Lastly, criteria for measurement intervals in space and time that minimize the error in eddy diffusivity estimation are proposed. The latter uses principles which are also used in groundwater monitoring network design (Andricevic 1990).

A.2 Study Site

Ryan Lake, located in Minneapolis, Minnesota, has a surface area of 0.06 km^2, mean depth of 5 meters and maximum depth of 10.5 m (Fig. A.1). The lake, located in a flat terrain, suburban residential area, is highly eutrophic, and regularly experiences winterkill of fish. The maximum depth of 10 m is equal to the median maximum depth of 779 statistically analyzed lakes in Minnesota. The depth of Ryan Lake can be considered as typical for the north central United States.

Lake water temperatures were measured every two minutes at 1 m intervals from the lake surface to the 10 m depth. Every 20 minutes, the previous ten measurements were averaged and recorded. The measurement scheme was adopted to reduce the "high frequency" electronic and measurement noise, while retaining the fluctuations expected at timescales of hours and days. The probes are rubber coated thermisters with a time constant of 10 seconds. They were calibrated in a water bath prior to installation. Absolute accuracy (values measured by two adjacent probes at known temperatures) was $\pm$ 0.05°C (95% confidence interval), while relative accuracy (the difference between successive measurements by the same probe) was 0.01°C. A Campbell Scientific CR10 datalogger installed on a small raft recorded the water temperatures. Hypolimnetic data for the period from May 7 to August 9, 1989, were selected for analysis because this period was characterized by stable seasonal lake stratification. In 1990 measurements were extended to sediment temperatures using probes identical to those in the water. The sediments were soft, organic material and poorly consolidated, as

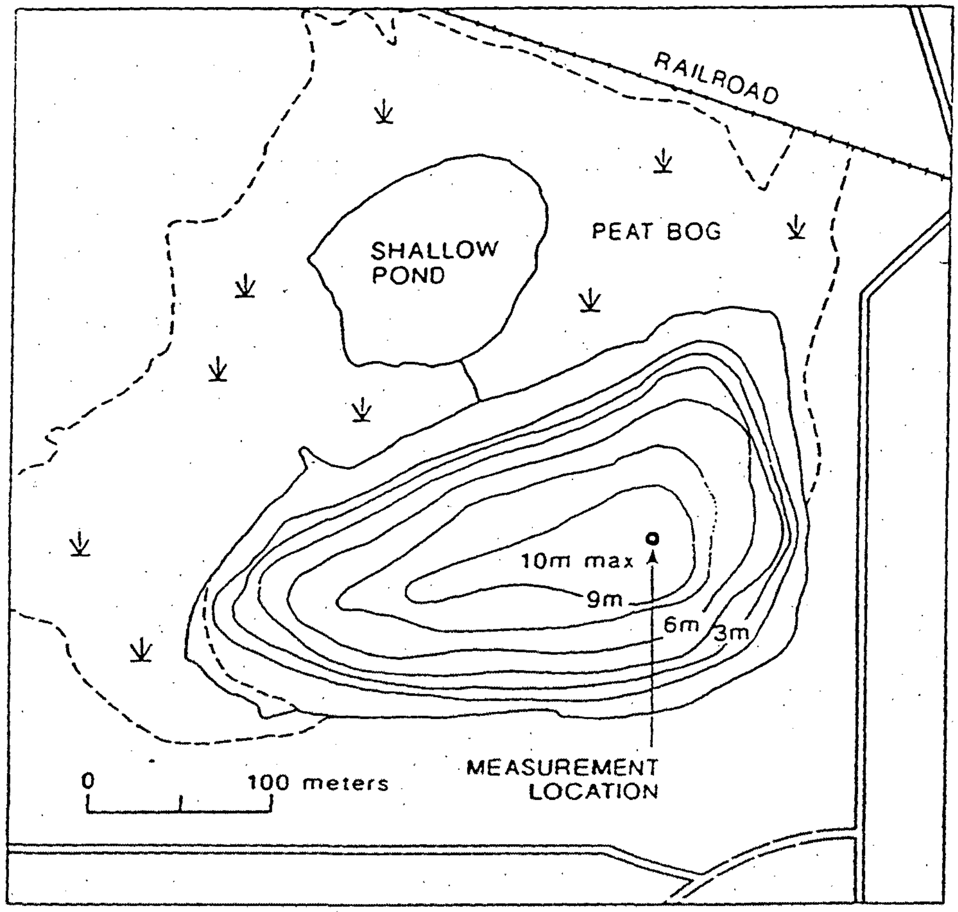

Fig. A.1 Ryan Lake bathymetry.

indicated by the ease with which the thermister probe support rod was installed.

A.3 Vertical Eddy Diffusivity

Many studies have assumed lake basins to be closed systems and have estimated an average vertical eddy diffusion coefficient over the whole basin (Adams et al. 1987; Gargett 1984; Imboden et al. 1983; Jassby and Powell 1975; Lewis 1983; Nyffeler et al. 1983; Priscu et al. 1986; Quay et al. 1980). One of the methods for such estimation is through the budgets of scalar quantities such as temperature (Gargett 1984).

The one-dimensional, unsteady heat transport equation applied along the vertical axis of a water column is:

$$\frac{\partial T}{\partial t} = - w \frac{\partial T}{\partial z} + \frac{\partial}{\partial z} (K_z \frac{\partial T}{\partial z}) + S \tag{A.1}$$

The flux-gradient method for the computation of K_z reduces this equation to the form

$$K_z = \left[\frac{\partial T}{\partial z} \right]^{-1} \left\{ \frac{\partial}{\partial t} \int_0^z T(\zeta)d\zeta + wT\Big|_0^z - \int_0^z S dz \right\} \tag{A.2}$$

It is assumed that there is no vertical advection ($w = 0$) of water anywhere. There is, however, a conductive heat flux H_{sed} from the sediment into the water at the lake bottom ($z = 0$) and a radiation (penetrative) heat flux H_{sol}. A heat balance for the water column between $z = 0$ and z therefore leads to a replacement for equation (A.2).

$$K_z = \left[\frac{\partial T}{\partial z} \right]^{-1} \left\{ \frac{\partial}{\partial t} \int_0^z T(\zeta)d\zeta - \frac{H_{sed}}{\rho c_p} - \frac{H_{sol(z)}}{\rho c_p} \right\} \tag{A.3}$$

Vertical kinematic thermal eddy diffusivity can be explicitly expressed as:

$$K_z = \frac{\frac{\partial}{\partial t} \left[\int_0^z T(\zeta)\, d\zeta \right] + w\, T\Big|_0^z - \int_0^z S\, dz}{\frac{\partial T}{\partial z}} \tag{A.4}$$

where $T(z,t)$ = measured water temperature distribution, z = upward coordinate starting at the lake bottom, t = time, w = vertical component of velocity, and S = internal source term. At the time scale of 1 to 15 days at which K_z is computed, and without significant inflow or outflow to or from the lake, net vertical velocity w is customarily small enough to be neglected. Short term effects during storms and turnovers will show up implicitly in the value of K_z. The source term "S" in Eq. A.4 accounts for solar short wave radiation absorbed in the water and heat flux through the water column to or from the sediments at the bottom. For shallow inland lakes, the source term can be particularly significant.

As pointed out by Gargett (1984), the budget method has two advantages. First, few additional assumptions are needed to estimate K_z from Equation A.4. Second, time averaging is implicit in the estimate of K_z. With the exception of the surface mixed layer, turbulence in lakes occurs in patches and intermittently. Turbulent "bursts" involve small volumes of water (tens of cubic meters) and last on the order of minutes (Imberger 1985). Therefore, time averaging for such systems appears to be essential to capture the long-term behavior.

Eddy diffusion dependence on buoyancy frequency was pointed out by Welander (1968) and others. Welander derived an expression relating K_z to the square of the Brunt–Vaisalla frequency (N) as $K_z = \alpha\,(N^2)^{\gamma}$, where $N^2 = -\frac{\partial \rho}{\partial z}\frac{g}{\rho}$, ρ = density of water and g = acceleration of gravity. If turbulence is generated by the dissipation of energy from large-scale motions, $\gamma = -1.0$; otherwise, if it is generated by shear flow, $\gamma = -0.5$. Welander's analysis was very informative, but it was based on several assumptions: steady state, no boundary effects, and a linear dependence of density on temperature. Such assumptions are only marginally valid for lakes. The results to be presented herein will show that Welander's theory fits lake data reasonably well.

A.4 Sediment Heat Storage

Few previous analyses include heat flux to or from the sediments in the eddy diffusivity estimation for summer conditions. A notable exception is Stauffer and Armstrong's (1983) study of Shagawa Lake's western basin (maximum depth 14 m). In principle, sediment heat flux is related to the water temperature gradient at the sediment/water interface (Nyffeler 1983); however, unknown turbulent heat transfer coefficients relating the flux to the gradient as well as exceedingly small temperature gradients in the near-sediment water limit the usefulness of the relationship. Relying on measurements and computer simulations, Priscu et al. (1986) assumed that the heat flux from the sediments to the water was constant. This was physically justified for the geothermally influenced lake which they studied. In the more general situation, conductive heat flux through the sediments is variable in depth as well as with time (Birge et al. 1927; Likens and Johnson 1969).

In this study, a numerical model was developed to simulate sediment heating or cooling by the overlying water. A one-dimensional, unsteady heat conduction equation was applied since conduction into and out of the sediments is essentially a 1-D process. The unsteady heat conduction equation for the sediments is a simplified version of Eq. A.1. Vertical velocity, w, is zero because there is no advection and S = 0 because there are no internal heat sources or sinks in the sediments. K_z in Eq. A.1 is replaced by K_{zs} = sediment thermal diffusivity, and T is replaced by T_s =

sediment temperature. So $\partial T_s/\partial t = K_{zs}(\partial^2 T_s/\partial z^2)$ is the heat conduction equation applied to the sediments. The partial differential equation was discretized using a control volume method (Patankar 1988) and solved by a tridiagonal matrix algorithm. The boundary conditions are: (1) measured water temperatures at the water/sediment interface and (2) no flux (adiabatic boundary) at z_d = 6 m depth below the sediment surface. It could be shown by unsteady heat transfer analysis of a semi-infinite slab that seasonal heat storage did not penetrate significantly beyond 6 m depth in an annual cycle. Heat flux (H_{sed}) through the sediment/water interface is calculated as the rate of change in sediment heat storage given by integration of computed sediment temperature profiles T(z,t):

$$H_{sed} = \rho_s \, c_{ps} \frac{\partial}{\partial t} \int_0^{z_d} T_s(z,t) \, dz \tag{A.5}$$

where ρ_s = bulk sediment density, c_{ps} is sediment specific heat and ($\rho_s \, c_{ps}$) is bulk specific heat of the sediments per unit volume.

Time series of measured sediment and overlying water temperatures are given in Fig. A.2 down to depths of 1.5 m into the sediment. No probes were placed at any greater depths. These temperatures were recorded from April 3 to July 9, 1990. In the early part of this season, temperature gradients, and hence heat fluxes into the sediments, are at a maximum. High fluctuations of water and sediment surface temperatures correspond to the spring overturn. Water temperatures at 0.5 m above the sediments and at the sediment surface plotted in Fig. A.2 were almost identical, indicating the presence of significant turbulent mixing in the water boundary layer. The differences between 20 minute readings at the two elevations had an average of 0.00845°C and a standard deviation of 0.088°C. The square of the correlation coefficient (R^2) was 0.98.

The unsteady sediment heat conduction model was calibrated for thermal diffusivity. A sediment thermal diffusivity of 0.0022 $cm^2 sec^{-1}$ applied uniformly over depth (Gu and Stefan 1990) simulated measured sediment temperatures well (Fig. A.3). The maximum difference between calculated and measured temperatures was 0.2°C in a range of 1.7 °C. Accuracy of the measurements was 0.05°C. The maximum discrepancy was observed at 0.5 m below the sediment surface in April. For the rest of the period the difference was less than 0.1 °C. Since sediment thermal properties do not change with season, the calibrated values should hold for year-round simulation.

Using the calibrated model and measured deep water temperatures from the 1989 data as the boundary condition at the water sediment interface, the sediment temperatures for the period of lake eddy diffusivity studies (May to August 9, 1989) could be simulated. Heat flux from the sediments was calculated using the simulated sediment temperatures in equation (2). Likens and Johnson (1969) used values of ρ_s=1.2 g cm^{-3} and c_{ps}=0.8 cal $g^{-1} \, {}^{\circ}C^{-1}$ for soft bottom sediments, giving ($\rho_s \, c_{ps}$) = 0.96 cal $cm^{-3} \, {}^{\circ}C^{-1}$. A water to solids ratio of 3:1 corresponded to the calibrated thermal diffusivity (Carslaw and Jaeger 1959), and hence values of 0.8 cal $g^{-1} {}^{\circ}C^{-1}$ for specific heat and

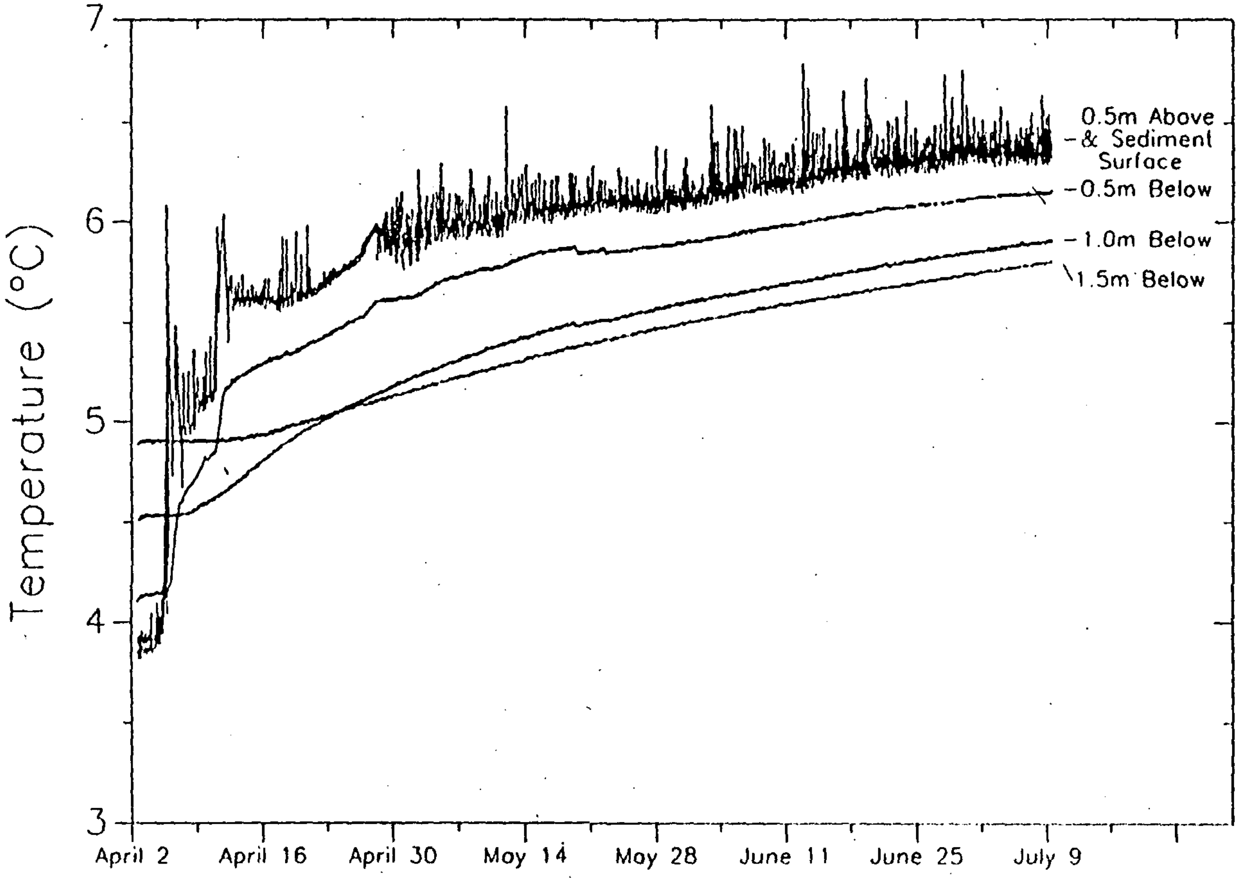

Fig. A.2 Temperatures recorded in lake sediments and overlying water, 1990.

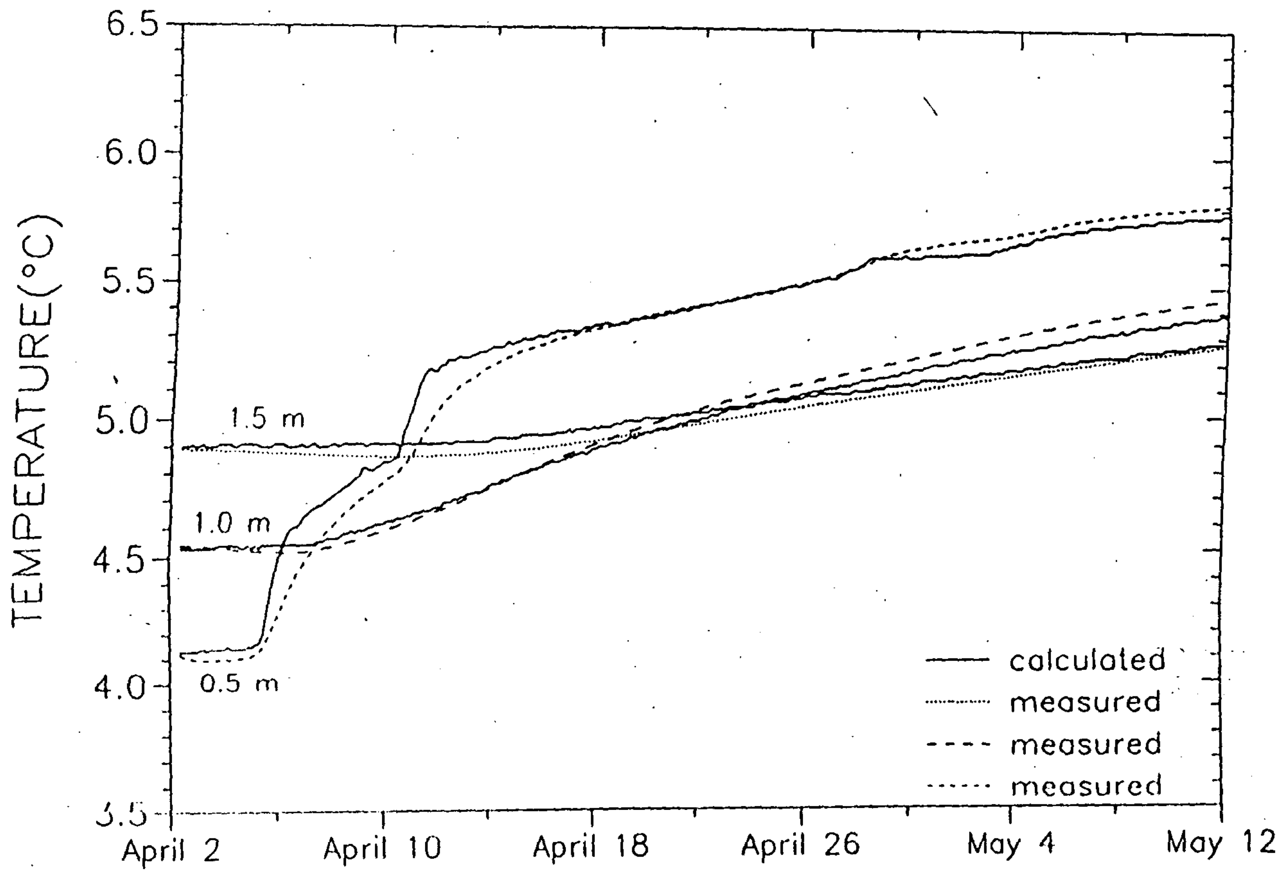

Fig. A.3 Calculated and measured temperatures in lake sediments, 1990.

gcm^{-3} for density of the sediment (ρ_s c_{ps} = 1.1 cal cm^{-3}) were applied uniformly in equation (2). It is estimated that the error on this ρ_s c_{ps} value is less than ± 20%. The absolute accuracy of the sediment heat flux from equation (2) is estimated to be 2 kcal m^{-2}day^{-1}.

A.5 Water temperature observations

Measured hypolimnetic water temperatures based on 20 minute averages are plotted in Fig. A.4. Depths are below the water surface which fluctuated by less than 0.1 m. There were no spatial variations of water temperatures to speak of, other than in the vertical direction. For the entire period of record, stratification was stable. Above 6 m depth, water temperatures were influenced by the deepening thermocline. The rise in water temperature at the 4 m depth in July was due to epilimnetic warming associated with increased solar radiation and deepening of the mixed layer.

Daily time series of on site incident solar radiation, air temperature, wind speed, and epilimnetic water temperature are given in Fig. A.5. Following standard weather bureau procedure, solar radiation is a daily total, wind speed is an average of three–hourly readings, and air temperature is the mean of a daily maximum and minimum reading. The strong rise of surface water temperature from May 7 to 17 coincides with high solar radiation and low wind. Water temperature fluctuations from May 17 to June 23 are the result of high fluctuations in solar radiation and air temperatures. From June 12 to the end of the observation period, high solar radiation and air temperatures increased water surface temperatures.

The entire stratification dynamics are put in perspective in Fig. A.6. The isotherms were developed from the water temperature records such as plotted in Fig. A.4. The window of data analyzed for vertical eddy diffusivities is shown in Fig. A.6.

A.6 Vertical eddy diffusion estimates

With temperature T(z,t) given by discrete measured values T_{ij} at increments Δz and Δt in depth and time, respectively, Equation (A.4) must be discretized numerically to yield the eddy diffusion coefficient estimator in the form:

$$K_z = \frac{\frac{1}{\Delta t}\sum_{i=1}^{N}(\Delta T_t\ \Delta z)_i - \left(\frac{H_{sol}}{\rho c_p} + \frac{H_{sed}}{\rho c_p}\right)}{\frac{1}{2\Delta z}\ \Delta T_z} \qquad (A.6)$$

where i and N are the bottom and topmost layer of the lake, respectively, ΔT_t = water temperature difference over a time interval Δt at a fixed depth z, H_{sol} = solar radiation heat flux at depth z, H_{sed} = water/sediment interface heat flux, and ΔT_z = temperature difference over a vertical distance Δz averaged over the time interval Δt, ρ = density of water and c_p = specific heat of water.

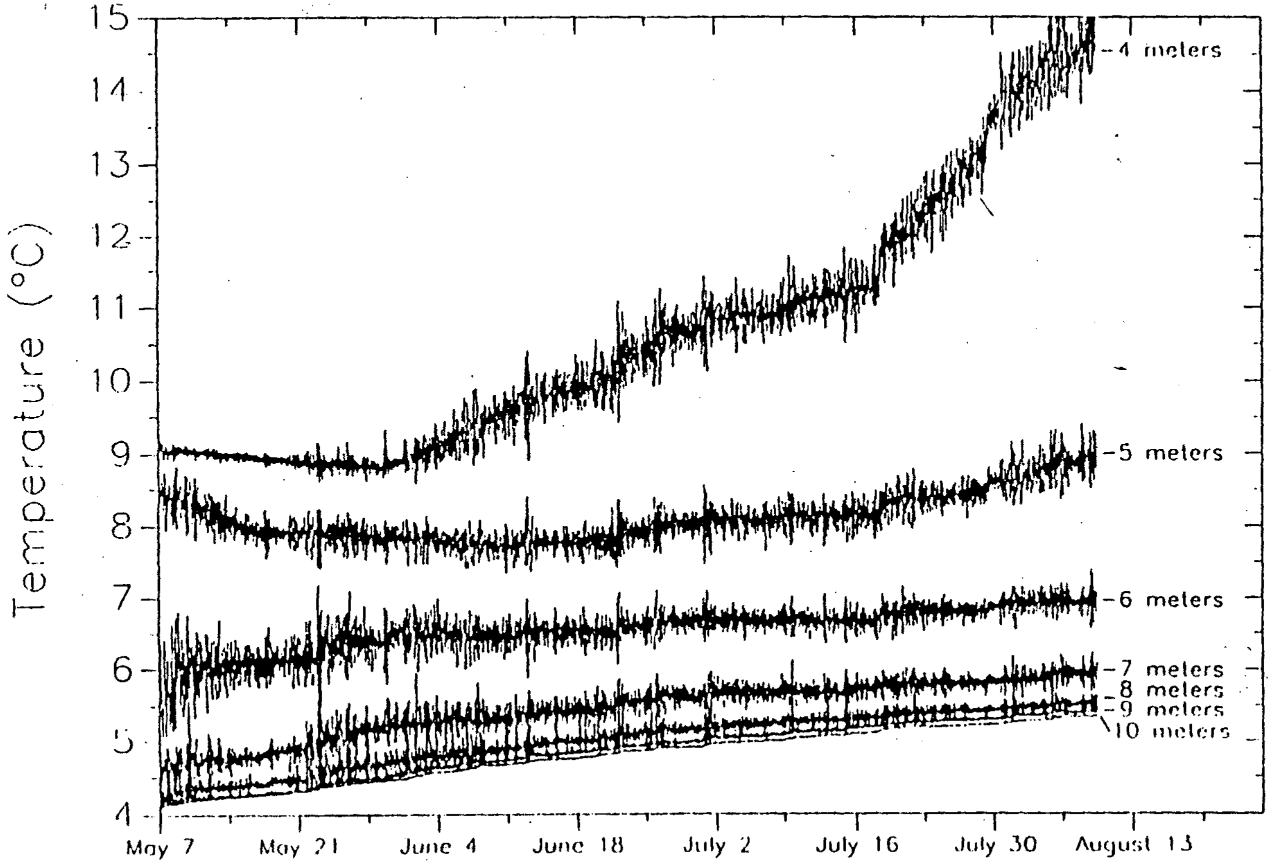

Fig. A.4 Hypolimnetic lake water temperatures recorded at 2 min interval in Ryan Lake, May 7 to August 9, 1989.

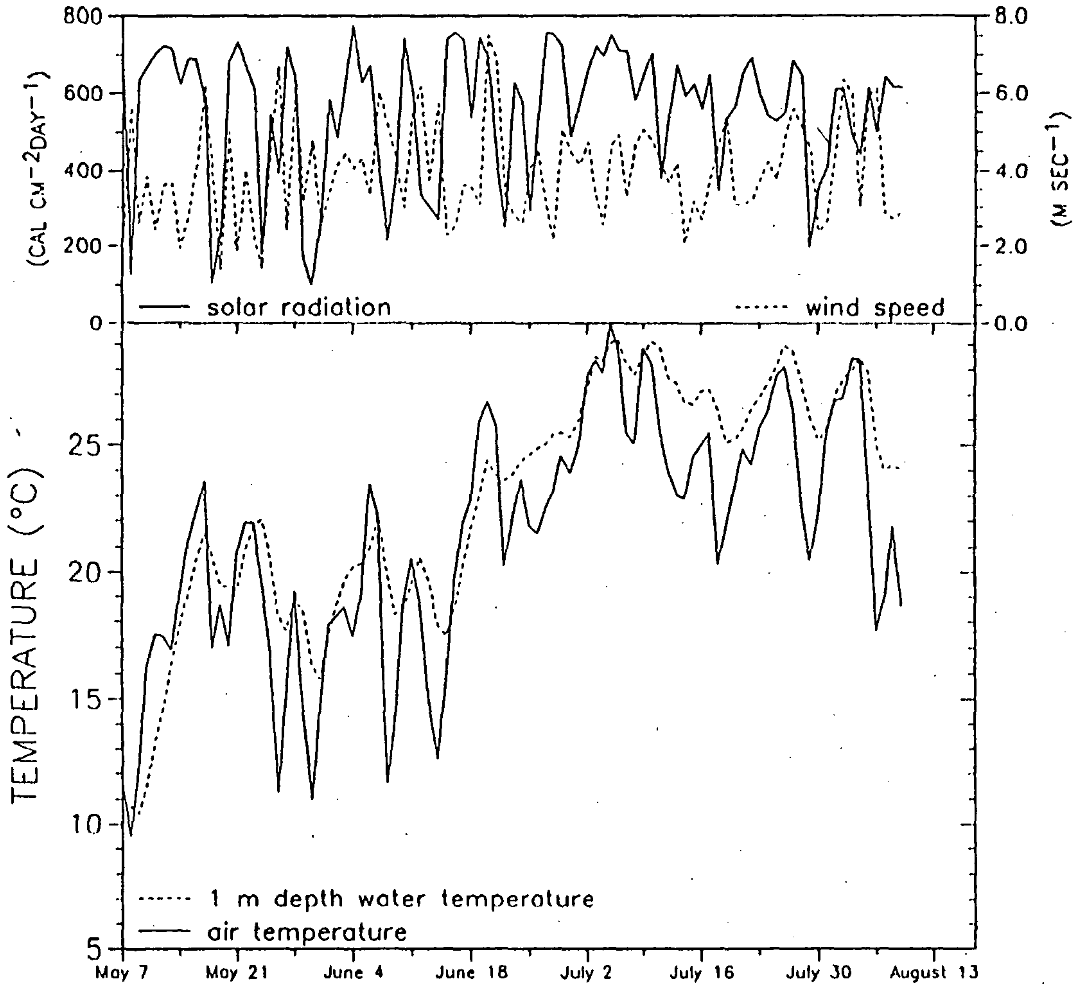

Fig. A.5 Meteorological conditions (solar radiation, wind speed and air temperatures) during the period of investigation.

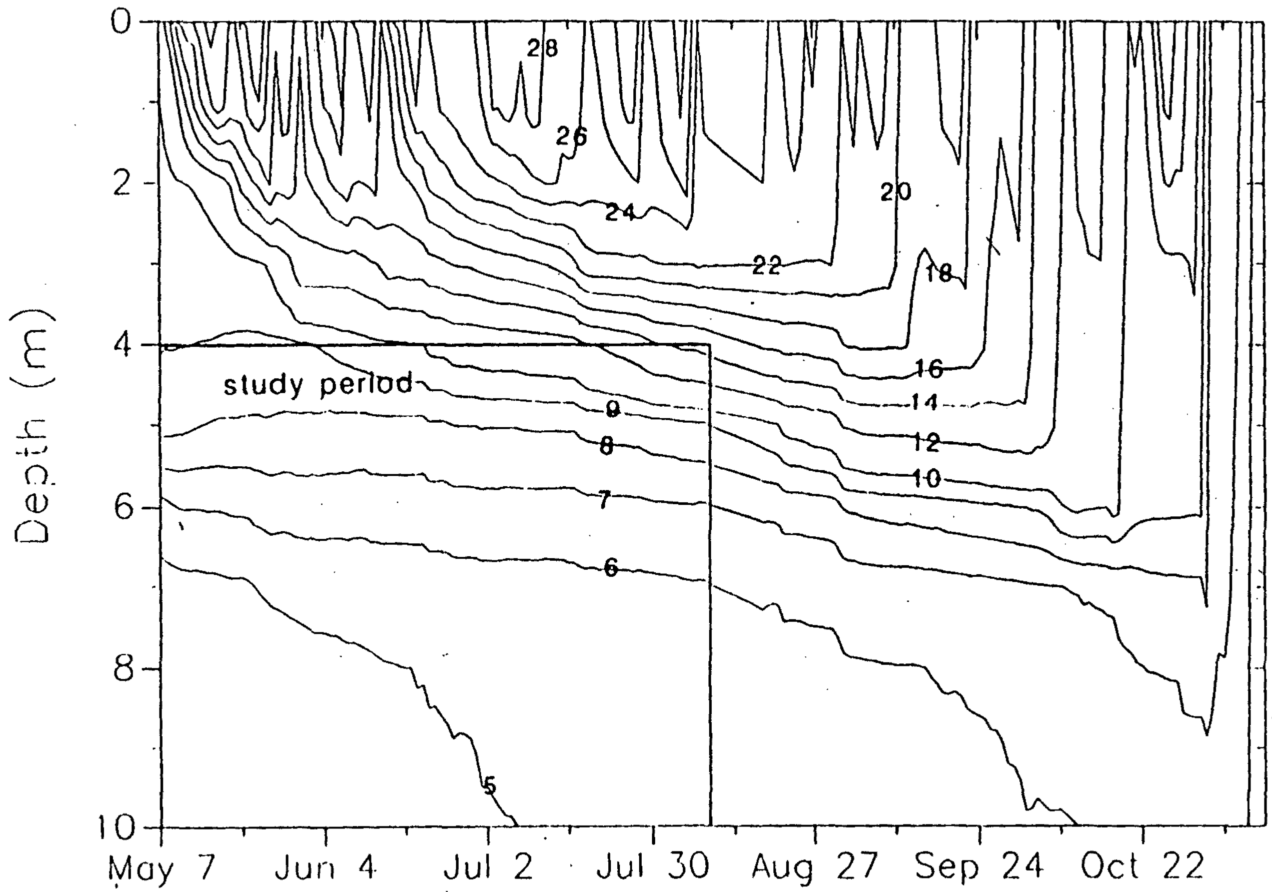

Fig. A.6 Seasonal lake temperature structure. Isotherms (°C) shown in this figure are derived from measurements at 20 minute and 1 m depth intervals.

Heat flux through the water–sediment interface was calculated by Equation (A.5). The average heat flux was 7.0 kcal m^2 day^{-1}, and the actual time series is shown in Fig. A.7. The heat flux was from the water into the sediment, i.e. the sediment acted as a heat sink throughout the period of investigation (May 7 – August 9).

Internal solar radiation absorption was calculated for each depth from measured radiation at the lake surface and an attenuation coefficient (Eq. 1.4). Bi–weekly Secchi depths varied from 0.8 m to 1.25 m during the period of analysis (May 7 to August 9, 1989) with a mean of 1.0 m. Relationship between total attenuation coefficient and Sechi disk depth translates a Secchi depth of 1.0 m into an attenuation coefficient of 1.8 m^{-1} which was used throughout the analysis (Fig. 2.4). Solar radiation adsorbed at the 4 m depth amounted to about one third of the sediment heat flux (see Fig. A.7) and was less at greater depth. In general, if an internal heat source due to solar radiation exists but is neglected, the eddy diffusion coefficient will be overestimated. Although not shown in Fig. A.7, solar radiation and water to sediment heat flux had different signs in Equation (A.6) because absorbed solar radiation is an input to the water and heat flux to the sediments is a loss from the water during the period of study.

Vertical eddy diffusion coefficients calculated for sampling intervals of five days and depth increments of 1 m (Fig. A.8) show decreasing values with time as seasonal stratification progresses. High variability in space and time is apparent. Vertical eddy diffusivity coefficient values ranged from approximately 0.001 to 0.1 cm^2s^{-1} with an average near 0.01 cm^2s^{-1}. The highest eddy diffusivity was found at the greatest depth (near the lake bottom) while the 4 m depth had the lowest values. Eddy diffusivity near the lake sediments is produced mainly by the interaction of internal waves with the lake bottom resulting in internal breaking waves and by turbulence induced by bottom shear during internal seiche motion. All of these are contributing to an intensely mixed lake bottom boundary layer, as previously shown by the temperature records in Fig. A.2. One result of this mixing is the decrease in stratification intensity with greater depth in the hypolimnion. There is also a positive feedback because shear–induced turbulence is dampened by density stratification conditions.

Eddy diffusion coefficient estimates versus static density stability (N^2) for different sampling periods with and without consideration of the sedimentary heat source term are given in Fig. A.9. A least squares linear regression was used to estimate coefficients α and γ in the relationship $K_z = \alpha(N^2)^\gamma$. As expected, an inverse relationship between K_z and N^2 was observed. When the sediment heat flux term was omitted, eddy diffusivity was underestimated. The error was up to one third of the estimated values. It is noteworthy that a stronger dependence of K_z on N^2 was observed when the sedimentary heat source term was considered (Fig. A.9).

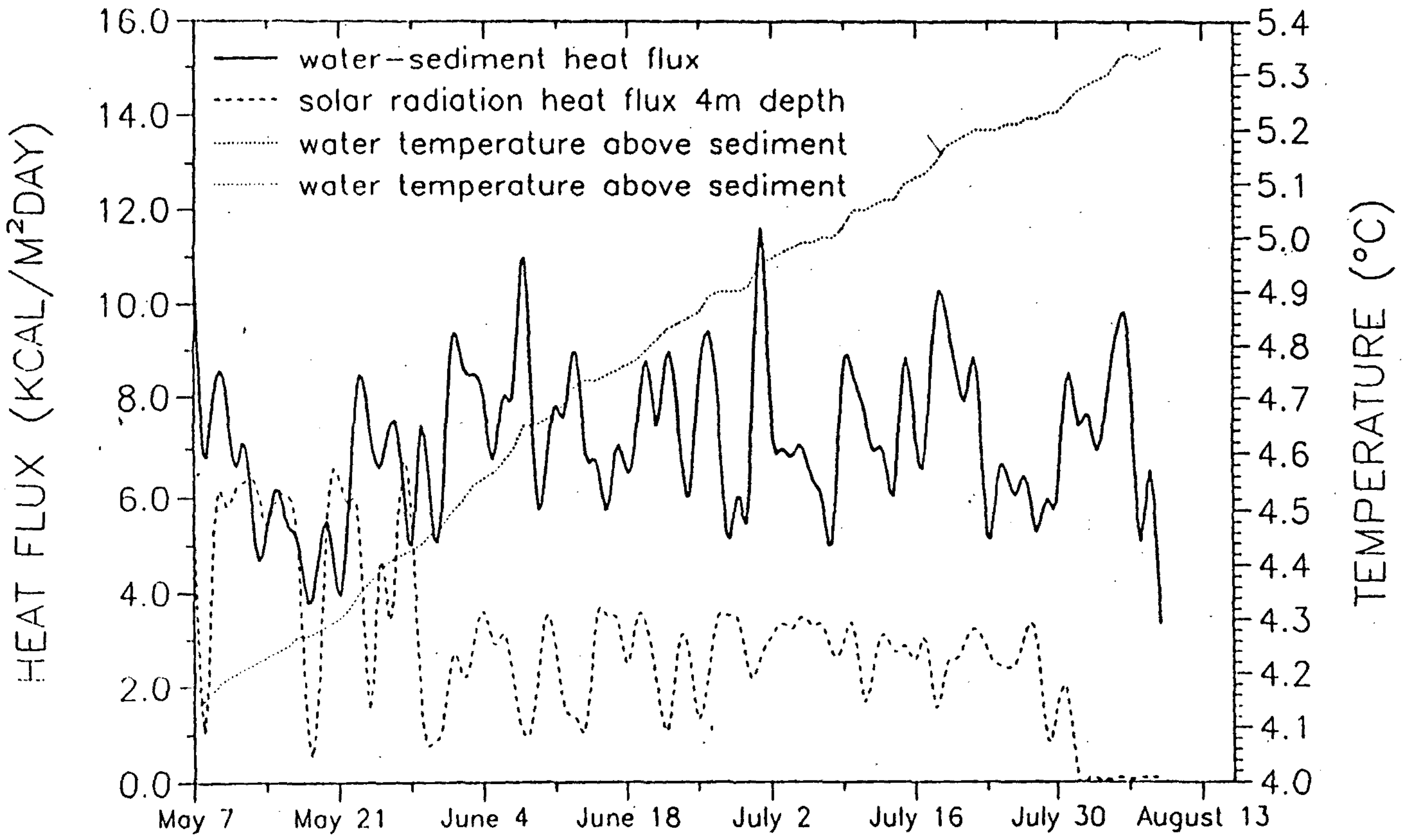

Fig. A.7 **Heat flux through the sediment–water interface and solar shortwave radiation received at the 4m depth, May 7 to August 10, 1989.**

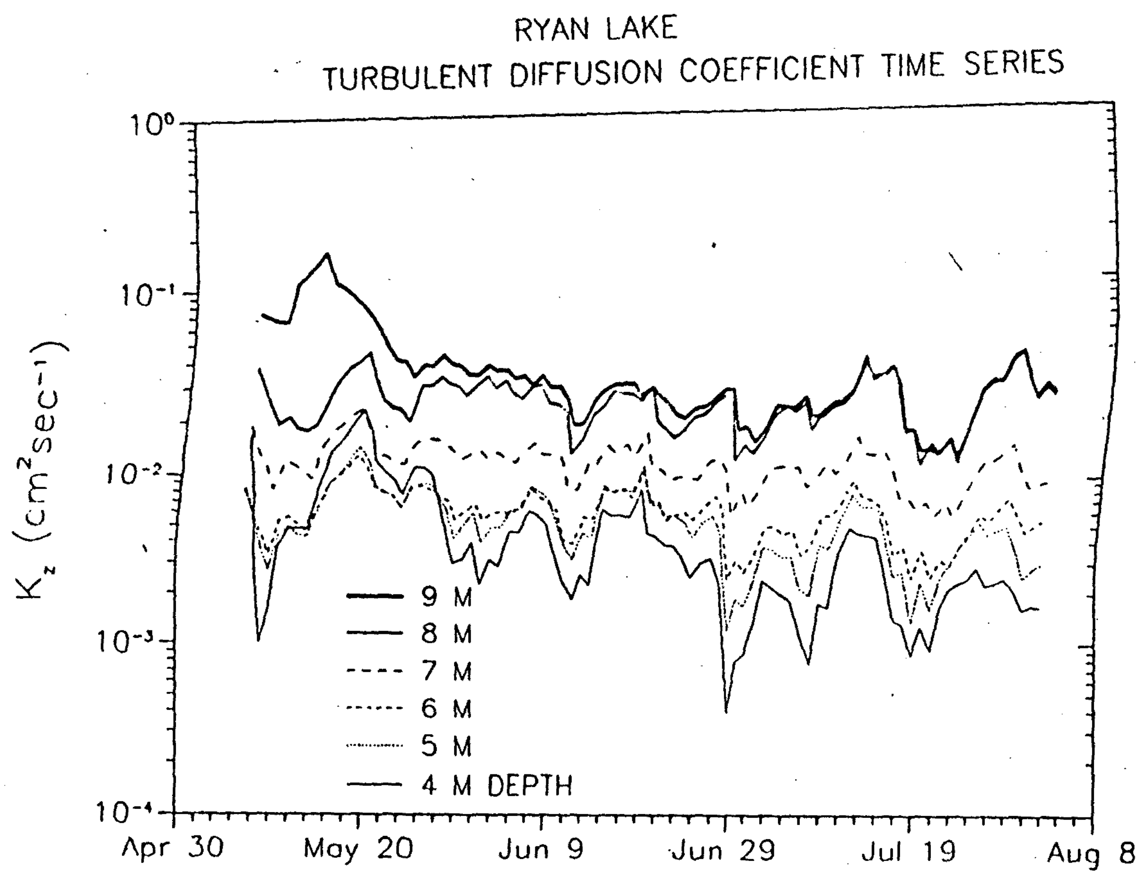

Fig. A.8 Vertical turbulent diffusion coefficient time series in Ryan Lake.

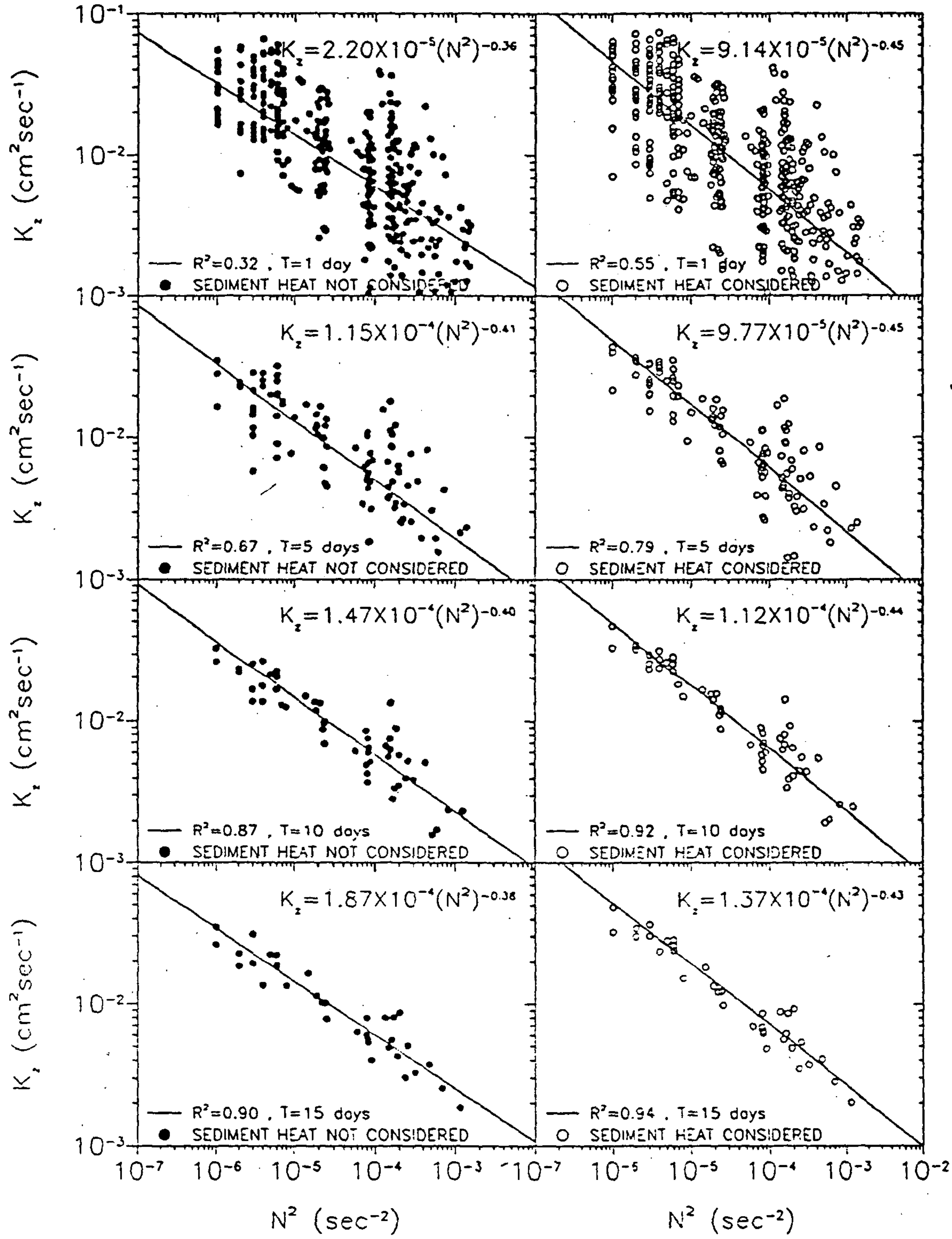

Fig. A.9 Calculated vertical eddy diffusion coefficients for time intervals of 1, 5, 10, and 15 days, with and without sediment heat flux.

Table A.1 Regression coefficients for $K_z = \alpha(N^2)^{\gamma}$

Sampling Interval (days)	$H_{sed} \neq 0$		$H_{sed} = 0$	
	α	γ	α	γ
1	$9.14*10^{-5}$	-0.45 ± 0.017	$2.20*10^{-5}$	-0.36 ± 0.041
5	$9.77*10^{-5}$	-0.45 ± 0.022	$1.15*10^{-4}$	-0.41 ± 0.028
10	$1.12*10^{-4}$	-0.44 ± 0.018	$1.47*10^{-4}$	-0.40 ± 0.03
15	$1.37*10^{-4}$	-0.43 ± 0.018	$1.87*10^{-4}$	-0.38 ± 0.02

K_z is a bulk estimate of the diffusivity over a time interval rather than an estimate of an instantaneous value. Variability of the eddy diffusivity was the highest for a sampling interval of one day. Different regression lines could be fitted to the one day results without changing the regression coefficient R^2. By increasing the sampling interval, the effects of variable meteorological conditions and mixing events were averaged out over longer and longer periods. With a longer sampling interval, the linear regression fit was better. Regression coefficients with standard errors are summarized in Table A.1.

A.7 Error Analysis

Uncertainties in the estimated K_z values are introduced by water temperature measurement errors, model parameter valucs, and model formulation. Magnitudes of errors for key variables in Equation (A.3) are listed in Table A.2. The first three of these errors are measurement errors. The last value is based on uncertainty in estimates of specific heat and soil temperature measurements. 2.0 kcalm^{-2} day^{-1} is about 30% of the average net heat flux value of 7 kcal m^{-2}day^{-1}.

Table A.2 Errors

Variable	Symbol	Error
Temporal temperature differential ΔT_t (measured)	ϵ_t	0.01 (°C)
Depth temperature differential ΔT_z (measured)	ϵ_z	0.05 (°C)
Depth increment Δz (measured)	$\epsilon_{\Delta z}$	0.01 (m)
Source heat flux ΔH (calculated)	ϵ_s	2.0 (kcalm^{-2}day^{-1})

To assess the estimation error of eddy diffusivity, a small perturbation ϵ of the variables in Table A.2 is introduced into equation (A.6). Temporal and depth temperature differentials, depth increments, and source heat fluxes are considered random variables and represented by the mean value plus a perturbation term. The perturbation terms have zero mean, and standard deviations equal to one-half the values given in Table A.2. Mean (denoted by overbar) and perturbation (denoted by ϵ) were expressed as:

$$K_z = \overline{K_z} + \epsilon_{kz} \tag{A.7}$$

$$\Delta T_t = \overline{\Delta T_t} + \epsilon_t \tag{A.8}$$

$$\Delta z = \overline{\Delta z} + \epsilon_{\Delta Z} \tag{A.9}$$

$$\Delta T_z = \overline{\Delta T_z} + \epsilon_Z \tag{A.10}$$

$$S = \overline{S} + \epsilon_S \tag{A.11}$$

with the statistical properties

$$E(\epsilon) = 0 \text{ (mean of } \epsilon) \tag{A.12}$$

$$E(\epsilon^2) = \sigma_\epsilon^2 \text{ (variance of } \epsilon) \tag{A.13}$$

It is assumed that perturbations (errors) are not correlated. Substituting equations A.8–A.11 into (A.6) and dropping overbars, the mean and the variance for the eddy diffusivity are obtained as:

$$E(K_z) = K_z = \frac{\frac{1}{\Delta t} \sum_{j=1}^{n} \Delta T_j \; \Delta z_j - \frac{S}{\rho c_p}}{\frac{1}{2\Delta z} \; (\Delta T_z)} \tag{A.14}$$

$$\mathrm{VAR}(K_z) = \sigma^2_{K_z} = \left\{ \frac{1}{\Delta t^2} \sum_{j=1}^{N} \sum_{i=1}^{N} \left[\Delta z_i \Delta z_j \epsilon_t^2 + \Delta T_i \Delta T_j \epsilon_{\Delta z}^2 \right] + \frac{N^2}{\Delta t^2} \right.$$

$$\left. \epsilon_t^2 \epsilon_{\Delta z}^2 + \frac{\epsilon_S^2}{\rho^2 c_p^2} \right\} \left\{ 1 + \frac{4 \Delta z^2}{\Delta T_z^2} \left[\frac{4 \epsilon_Z^2}{\Delta z^2} + \frac{\Delta T_z^2 \, \epsilon_{\Delta z}}{4 \Delta z^2} + \frac{4 \epsilon_{\Delta z}^2 \epsilon_Z^2}{\Delta z^4} \right] \right\}$$

$$\left(\frac{4 \Delta z^2}{\Delta T_z^2} \right) + \frac{16 \Delta z^4}{\Delta T_z^4} \left[\frac{1}{\Delta t} \sum_{j=1}^{N} T_j \Delta z_j - \frac{S}{\rho c_p} \right]$$

$$\left\{ \left[\frac{4 \epsilon_Z^2}{\Delta z^2} + \frac{\Delta T_z^2 \quad \epsilon_{\Delta z}^2}{4 \Delta z^2} + \frac{4 \epsilon_{\Delta z}^2 \epsilon_Z^2}{\Delta z^4} \right] \left[\frac{1}{\Delta t} \sum_{j=1}^{N} T_j \Delta z_j - \frac{S}{\rho c_p} \right] \right.$$

$$\left. + \frac{16}{\Delta t \Delta z^3} \sum_{i=1}^{N} \epsilon_Z^2 \, \epsilon_{\Delta z} \, \Delta T_i \right\} \qquad \text{(A.15)}$$

where i or j designate the depth under consideration, Δz = depth increment, ΔT_i or ΔT_j = temporal temperature difference at the depth i or j, respectively. N = total number of measuring points below the flux surface under consideration, ΔT_z = temperature difference over the depth increment Δz averaged over the time interval Δt, S is source term. Other variables are given in the main text (Table A.2).

Vertical profiles of the mean eddy diffusion coefficient plus or minus two standard deviation intervals are given in Fig. A.10. These profiles are for five day sampling intervals and depth increments of 1 m. The error in K_z estimation increased with depth mainly due to the smaller temperature gradient near the lake bottom.

The dependence of calculated K_z values on the frequency and spacing of the water temperature measurements is illustrated in Figs. A.11 and A.12. If sampling intervals exceeded four days, the error in estimated K_z values did not change significantly, regardless of depth. Sampling intervals of three days or less increased the error.

The tradeoff between depth and time intervals with regard to the error in K_z estimation is illustrated in Fig. A.12 by isolines of equal $2\sigma_{kz}$ values. Three regions can be distinguished on the graph: (1) up to a sampling interval of three days the error was a function of the time increment only. The bigger errors correspond to the smaller sampling time increments. (2) From 5 to 10 days sampling interval, errors were a function of both Δz and Δt. That was the region where trade–off between space and time was possible in order to obtain the same estimation error. In general, errors were

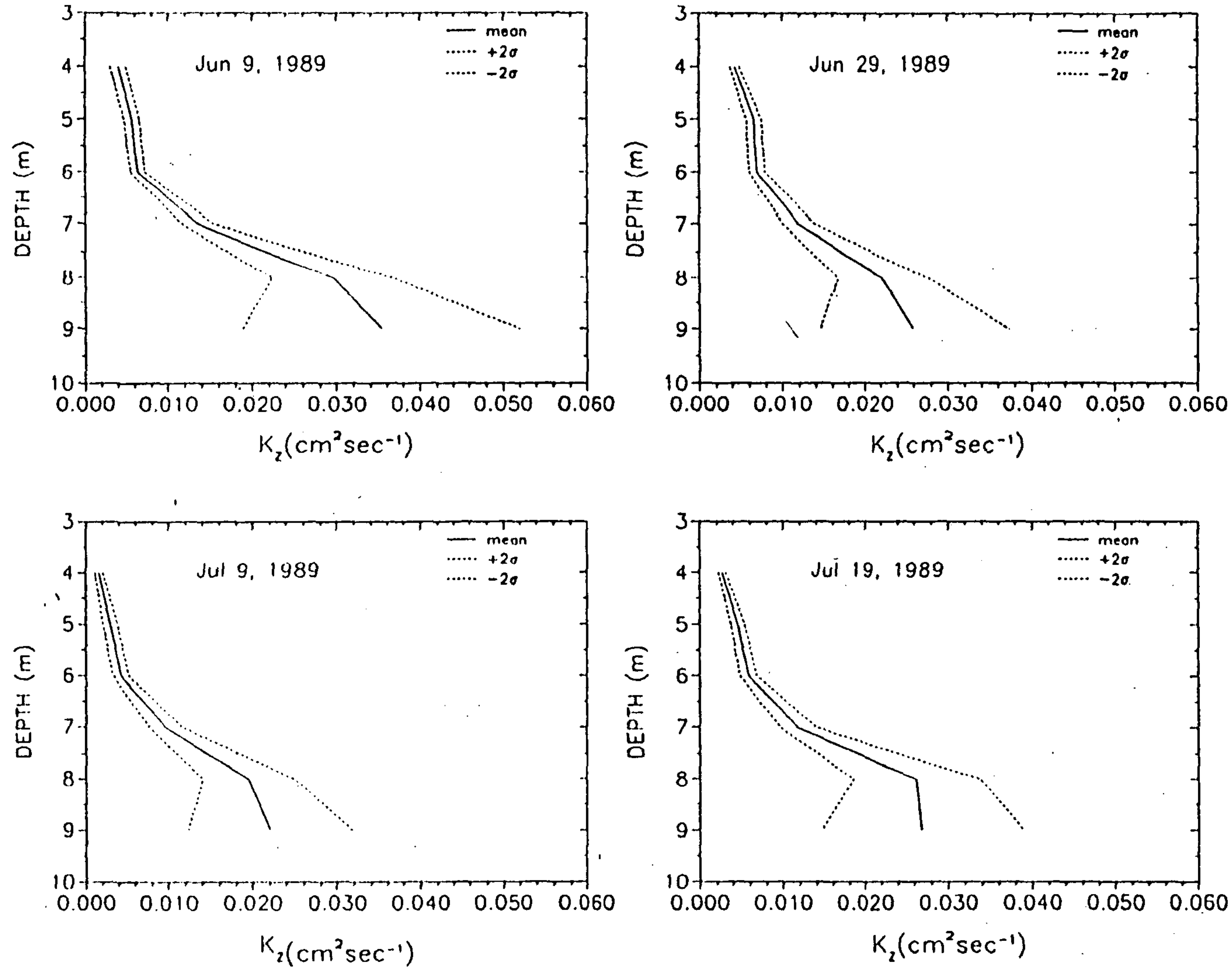

Fig. A.10 Mean values plus or minus two standard deviations of eddy diffusion coefficient as a function of depth.

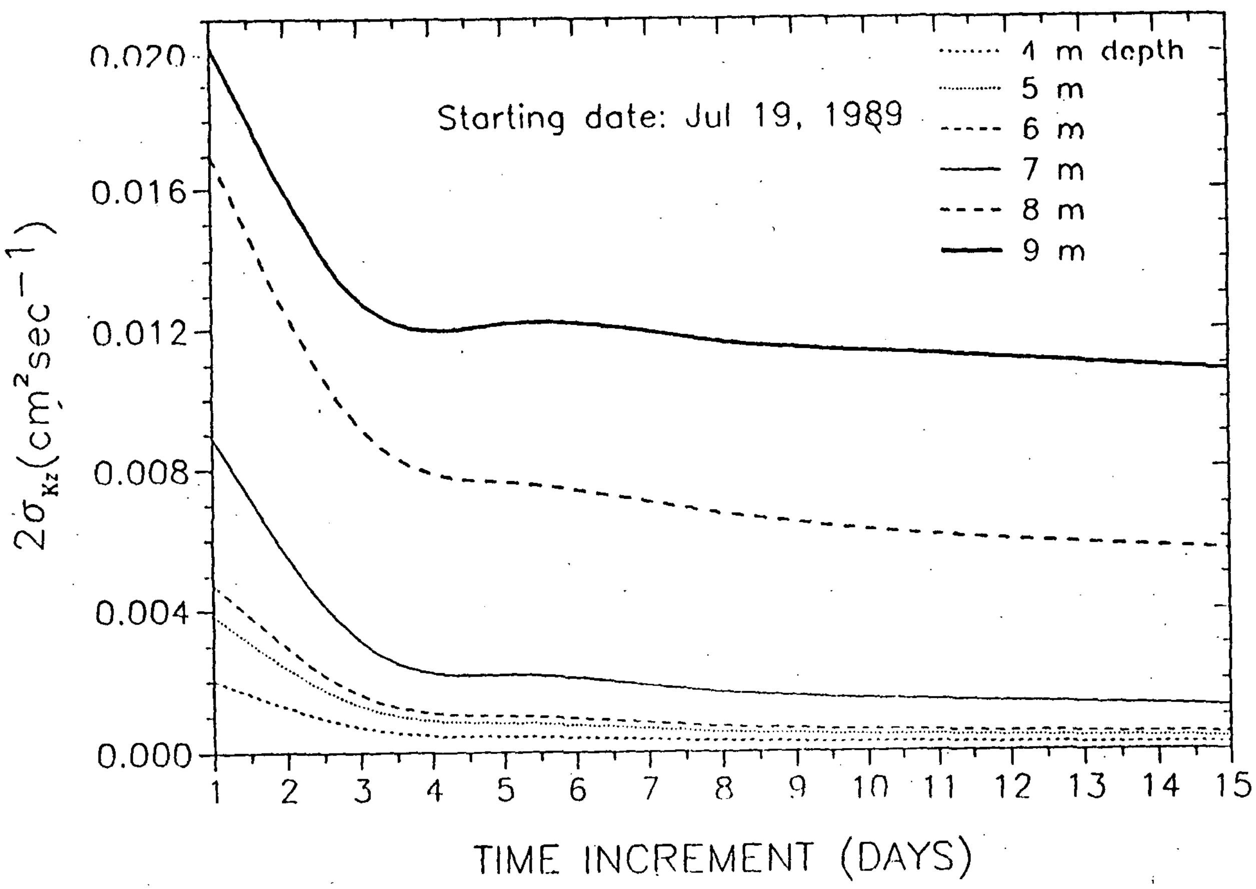

Fig. A.11 **Estimated eddy diffusion errors ($2\sigma_{K_z}$) for different sampling intervals.**

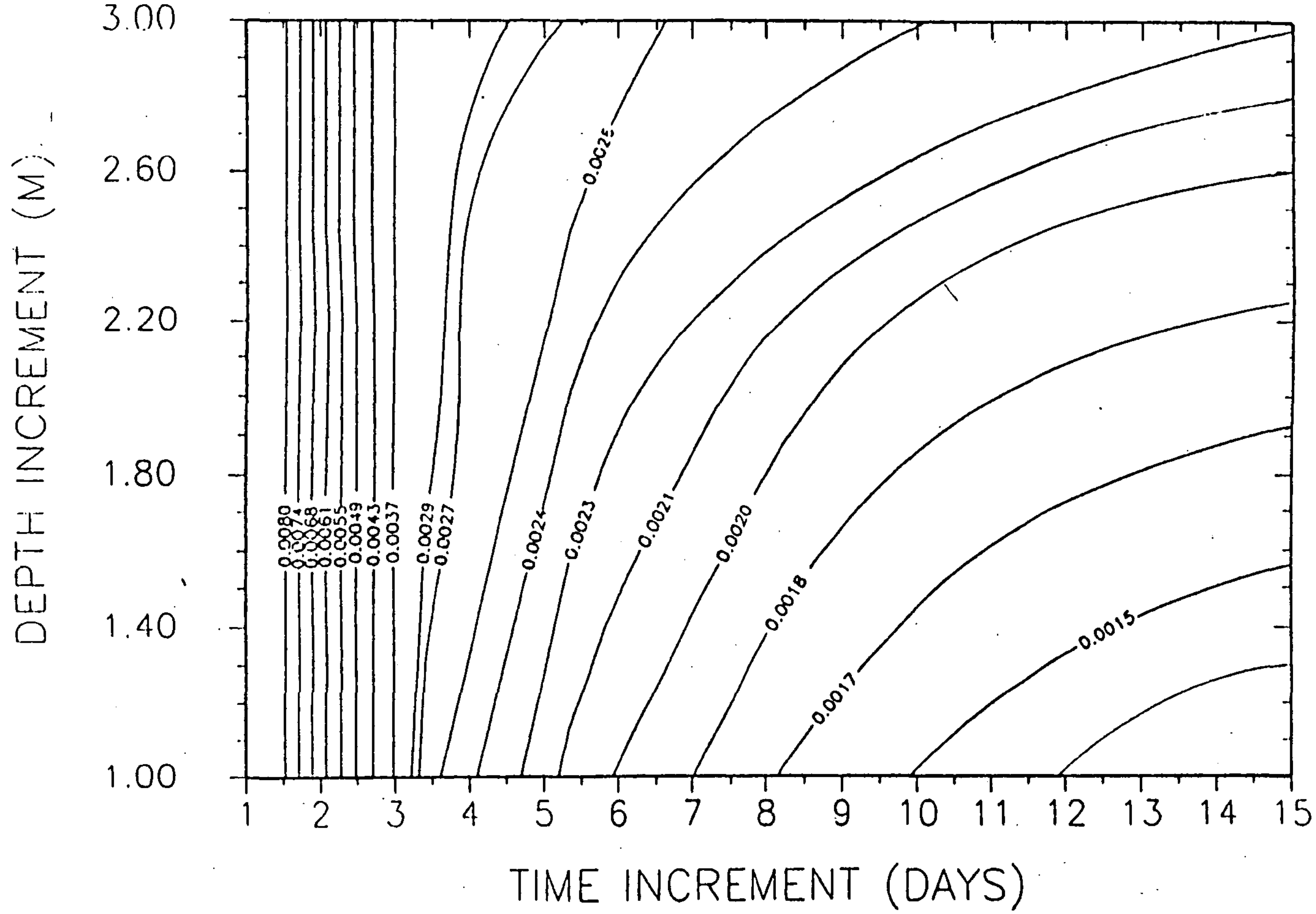

Fig. A.12 **Estimated eddy diffusion errors $2\sigma_{K_z}$(cm^{2}s^{-1}) space–time tradeoff, 7 m depth Jul 19.**

decreasing for smaller Δz and larger Δt. (3) For sampling intervals larger than 10 days the estimation error became primarily a function of Δz, i.e. the more measuring points used in a profile, the smaller the error in K_z.

A.7 Conclusions

The vertical turbulent eddy diffusion coefficients in the hypolimnion of a temperature stratified temperate lake with a depth typical of the north central United States were evaluated from water temperatures measured at 2 minute intervals from May 7 to August 9, 1989. K_z values typically increased by a factor of 10 between 4 m depth and 9 m depth. Eddy diffusion coefficients K_z were computed for periods from 1 to 15 days and varied from 0.001 to 0.1 cm^2/s for the 1–day intervals and from 0.002 to 0.04 cm^2/s for 15–day intervals. K_z also varied with stratification stability measured by the Brunt–Vaisala frequency N. The relationship $K_z = \alpha(N^2)^\gamma$ produced the best fit when $\alpha = 0.00014$ and $\gamma = -0.43$ for periods of 15 days, where K_z is in cm^2s^{-1} and N in s^{-1}. As the time step was shortened to one day, the fit became poorer and γ values changed slightly (Fig. A.9). The value $\gamma = -0.43$ fits Welander's (1969) model for shear driven thermocline erosion. The α value is related to lake size (Fig. 2.2).

The water temperatures measured and recorded every 20 minutes at the sediment/water interface and at 0.5 m above showed a mean difference of only 0.008°C and nearly identical responses in time (Fig. A.2) over a period of three months. This is indicative of a well–mixed boundary layer near the lake bed.

Heat exchange between water and lake sediments was found to be important to the analysis of vertical thermal diffusivity. A numerical model was used to estimate sedimentary heat flux for incorporation into the eddy diffusivity estimation. A mean value of sedimentary heat fluxes during the summer period (May – August) was 7 kcal $m^{-2}day^{-1}$. Estimates of K_z made without sedimentary heat flux were up to one third smaller than those made with that heat flux. Heat input by solar radiation through the water surface also influences the estimates of K_z, but this influence diminishes with depth.

Effects of errors in temperature measurements and sediment heat flux estimations on calculated vertical eddy diffusion coefficients were evaluated. Estimation errors were much larger near the lake bottom (in the hypolimnion) than in the thermocline region (Fig. A.10). The smallest estimation errors of the eddy diffusivity were obtained for sampling intervals of 15 days and depth increments of 1.0 m. At the 7 m depth, the error was about 0.0011 cm^2/s relative to a value on the order of 0.010 or 11 percent (see Figs. A.8 and A.11). The error doubled when the depth increment was trippled to 3.0 m or when the sampling interval was reduced from 15 days to 5 days (Fig. A.12). At the shorter sampling interval the error was, however, insensitive to the depth increment. When the sampling interval was reduced to 1.5 days, the estimation error increased to 0.008 cm^2/s or nearly 80% of the estimated value calculated at the 7 m depth. Thus the recommendation is to sample at longer time intervals (several days) and at finer depth resolution (order of 1 m).

APPENDIX B

Temperature equation discretization

Temperature equation (1.1) is discretized using the control volume method. For intermediate control volumes (i = 2, m–1).

$$\left(-\frac{A_{i-0.5}}{A_i} K^{k}_{i-0.5}\right) T^{k+1}_{i-1} +$$

$$\left[\frac{(\Delta z)^2}{\Delta t} + \frac{A_{i-0.5}}{A_i} K^{k}_{i-0.5} + \frac{A_{i+0.5}}{A_i} K^{k}_{i+0.5}\right] T^{k+1}_{i} -$$

$$\left(\frac{A_{i+0.5}}{A_i} K^{k}_{i+0.5}\right) T^{k+1}_{i+1} = \frac{(\Delta z)^2}{\Delta t} T^{k}_{i} + \frac{(\Delta z)^2 H}{\rho_w c_p} \tag{B.1}$$

where Δt is time step, Δz is control volume width (constant) , k stands for time, i stands for control volume location. Source term H, is described by equation 1.4. System matrix of the deterministic model $A_c(k)$ contains terms on the left hand side of equation (B.1).

For the surface control volume (i=1) equation (B.1) will differ: eddy diffusivity $K_{i-0.5}$ is zero, the first entry in the matrix is term multiplied by T^{k+1}_{i}, source terms are equations (1.2), (1.3), (1.6), (1.7), (1.8) and (1.9). For the bottom control volume (i=m) insulation is imposed by setting $K_{i+0.5}$ equal zero. Diagonal entry in the matrix is term multiplied by T_i^{k+1}.

Eddy diffusivities at the control volume interfaces are defined as harmonic mean

$$K_{i-0.5} = \frac{2 K_i K_{i-1}}{K_{i-1} + K_i} \tag{B.2}$$

APPENDIX C

Temperature equation linearization

Matrix $\hat{A}_c(k)$ has the same entries as the system matrix $A_c(k)$ given in Appendix B. Matrix B(k) is tridiagonal, and contains derivatives with respect to lake water temperature at time step k. For the intermediate control volumes :

$$\frac{A_{i-0.5}}{A_i}\left[\frac{\partial \hat{K}_{i-0.5}}{\partial \hat{T}^{k}_{i-1}}\hat{T}^{k+1}_{i-1} - \frac{\partial \hat{K}_{i-0.5}}{\partial \hat{T}^{k}_{i-1}}\hat{T}^{k+1}_{i}\right] T'^{k}_{i-1} +$$

$$\frac{A_{i-0.5}}{A_i}\left[\frac{\partial \hat{K}_{i-0.5}}{\partial \hat{T}^{k}_{i}}\hat{T}^{k+1}_{i-1} - \frac{\partial \hat{K}_{i-0.5}}{\partial \hat{T}^{k}_{i}}\hat{T}^{k+1}_{i}\right] T'^{k}_{i} +$$

$$\left(\frac{A_{i+0.5}}{A_i}\left[\frac{\partial \hat{K}_{i+0.5}}{\partial \hat{T}^{k}_{i}}\hat{T}^{k+1}_{i+1} - \frac{\partial \hat{K}_{i+0.5}}{\partial \hat{T}^{k}_{i}}\hat{T}^{k+1}_{i}\right] + \frac{(\Delta z)^2}{\Delta t} + \delta_i H_{ad}\right) T'^{k}_{i} +$$

$$\frac{A_{i+0.5}}{A_i}\left[\frac{\partial \hat{K}_{i+0.5}}{\partial \hat{T}^{k}_{i+1}}\hat{T}^{k+1}_{i+1} - \frac{\partial \hat{K}_{i-0.5}}{\partial \hat{T}^{k}_{i+1}}\hat{T}^{k+1}_{i}\right] T'^{k}_{i+1}$$

where $\delta_i = 1$ if $i = 1$ else $\delta_i = 0$

For the surface control volume matrix $\hat{B}(k)$ will slightly differ. First, terms which are multiplied by T_i are the first entry (b_{11}). Secondly, eddy diffusivity $K_{i-0.5}$ is equal to zero. Thirdly, additional terms which take into account boundary conditions have to be added (Equations 1.6, 1.8, and 1.9). These equations have to be differentiated and evaluated with respect to the water temperature in the first control volume.

$$H_{ad} = \left[\frac{\partial H_{br}^{\,k}}{\partial \hat{T}^{k}_{1}} + \frac{\partial H_{c}^{\,k}}{\partial \hat{T}^{k}_{1}} + \frac{\partial H_{e}^{\,k}}{\partial \hat{T}^{k}_{1}}\right]\frac{\Delta z}{\rho_w c_p} T'^{k}_{i} \tag{C.1}$$

For the bottom control volume matrix $\hat{B}(k)$ will also slightly differ. Diagonal term (b_{mm}) is the one which is multiplied by T_i. Eddy diffusivity $K_{i+0.5}$ is zero.

Eddy diffusivity vector K(z,k) contains epilimnion and hypolimnion diffusivities. Epilimnetic diffusivities are a function of wind speed, thus their partial derivative with respect to lake temperature is zero entry. This is not the case for the hypolimnetic eddy diffusivity.

$K = \alpha\ (N^2)^b$ where N^2 is Brunt–Vaisala frequency $N^2 = \left(\frac{\partial\rho(T)}{\partial z}\right)\frac{g}{\bar{\rho}}$

$$\frac{\partial K_{i-0.5}}{\partial T_i} = 2\,\frac{K_i^2}{(K_{i-1} + K_i)^2}\,\frac{\partial K_i}{\partial N_i}\,\frac{\partial N_i}{\partial T_i} \tag{C.2}$$

Matrix $\hat{F}(k)$ contains terms which require evaluation of first order derivatives with respect to uncertain meteorological variables. Equations 1.3, 1.4, 1.6, 1.8, and 1.9 have to be differentiated and evaluated at the nominal values of those variables. Entries in the matrix are grouped with respect to the perturbed meteorological parameters. Matrix dimensions are m x m+3

$$\left[\,\hat{F}_1(k) \vdots \hat{F}_2(k) \vdots \hat{F}_3(k) \vdots \hat{F}_4(k)\right]$$

where air perturbation temperature vector $\hat{F}_1(k)$ is:

$$H_{c1} = \left(\frac{\partial \hat{H}_a}{\partial T_a^k} + \frac{\partial \hat{H}_c}{\partial T_a^k}\right)\frac{\Delta z}{\rho_w c_p}\,T'^{\,k}_{a_i} \tag{C.3}$$

dew point temperature perturbation vector $\hat{F}_2(k)$ is:

$$H_{c2} = \left(\frac{\partial \hat{H}_e}{\partial e_a^k}\,\frac{\partial \hat{e}_a}{\partial T_d^k}\right)\frac{\Delta z}{\rho_w c_p}\,T'^{\,k}_{d_i} \tag{C.4}$$

wind speed perturbation (mxm) matrix $\hat{F}_3(k)$ is:

$$\frac{A_{i-0.5}}{A_i}\left[\frac{\partial \hat{K}_{i-0.5}}{\partial \hat{W}s^k_{i-1}}\,\hat{T}^{k+1}_{i-1} - \frac{\partial \hat{K}_{i-0.5}}{\partial \hat{W}s^k_{i-1}}\,\hat{T}^{k+1}_{i}\right] Ws'^{\,k}_{i-1} +$$

$$\frac{A_{i-0.5}}{A_i}\left[\frac{\partial \hat{K}_{i-0.5}}{\partial \hat{W}s^k_{i}}\,\hat{T}^{k+1}_{i-1} - \frac{\partial \hat{K}_{i-0.5}}{\partial \hat{W}s^k_{i}}\,\hat{T}^{k+1}_{i}\right] Ws'^{\,k}_{i} +$$

$$\left(\frac{A_{i+0.5}}{A_i}\left[\frac{\partial \hat{K}_{i+0.5}}{\partial \hat{W}_{s_i}^{k}}\hat{T}_{i+1}^{k+1}-\frac{\partial \hat{K}_{i+0.5}}{\partial \hat{W}_{s_i}^{k}}\hat{T}_{i}^{k+1}\right]+\delta_i H_{c3}\right) W_{s_i}'^{\,k} +$$

$$\frac{A_{i+0.5}}{A_i}\left[\frac{\partial \hat{K}_{i+0.5}}{\partial \hat{W}_{s_{i+1}}^{k}}\hat{T}_{i+1}^{k+1}-\frac{\partial \hat{K}_{i-0.5}}{\partial \hat{W}_{s_{i+1}}^{k}}\hat{T}_{i}^{k+1}\right] W_{s_{i+1}}'^{\,k}$$

where

$$H_{c3} = \left(\frac{\partial \hat{H}_c}{\partial W_s^k} + \frac{\partial \hat{H}_e}{\partial W_s^k}\right)\frac{\Delta z}{\rho_w c_p} W_{s_i}'^{\,k} \qquad \text{(C.5)}$$

First and last control volume have interface diffusivities $K_{i+0.5}$ and $K_{i-0.5}$ equal to zero, and the additional term H_{c3} is present only in the first control volume.

Solar radiation perturbation vector $\hat{F}_4(k)$ is

$$H_{c4} = \left(\frac{\partial \hat{H}_{sn}}{\partial H_s^k}\right)\frac{\Delta z}{\rho_w c_p} H_{s_i}'^{\,k} \qquad \text{(C.6)}$$

APPENDIX D

Cross–term evaluations

Air and dew point temperature have significant correlation. The covariance matrix between successive days for these two parameters has been evaluated according to Protopapas (1988):

$$\mathrm{Cov}\,[\,C'(n)\;C'(k)\,] = S(n)\; M_c\; S(k)^T \tag{D.1}$$

where

$$S(n) = \begin{matrix} \sigma_{ta}(n) & 0 & 0 & 0 \\ 0 & \sigma_{td}(n) & 0 & 0 \\ 0 & 0 & 0 & 0 \\ 0 & 0 & 0 & 0 \end{matrix}$$

$$M_c = \begin{matrix} \rho_{ta}(n,k) & \rho_{tatd}(n,k) & 0 & 0 \\ \rho_{tdta}(n,k) & \rho_{td}(n,k) & 0 & 0 \\ 0 & 0 & 0 & 0 \\ 0 & 0 & 0 & 0 \end{matrix}$$

$$S(k) = \begin{matrix} \sigma_{ta}(k) & 0 & 0 & 0 \\ 0 & \sigma_{td}(k) & 0 & 0 \\ 0 & 0 & 0 & 0 \\ 0 & 0 & 0 & 0 \end{matrix}$$

where σ_{ta} is air temperature standard deviation, σ_{td} is dew point temperature standard deviation, $\rho_{ta}(n,k)$ is air temperature correlation between two days, $\rho_{td}(n,k)$ is dew point temperature correlation, $\rho_{tatd}(n,k)$ is air temperature - dew point temperature correlation.

Replacing index n by index k leads to the form of the covariance matrix M(k,k) for the zero time lag. In addition, the diagonal terms are [illegible] equal to one in the correlation matrix M_c. They are equal to the standard deviations of air temperature $\sigma_{at}(k)$, dew point temperature $\sigma_{td}(k)$, wind speed $\sigma_{ws}(k)$, and solar radiation $\sigma_{sr}(k)$ in the matrices S(k), and S(n).

If meteorological perturbations are not cross-correlated covariance matrix $M_{uc}(k,k)$ is

$$M_{uc}(k,k) = \begin{matrix} \sigma_{ta}^2(k) & 0 & 0 & 0 \\ 0 & \sigma_{td}^2(k) & 0 & 0 \\ 0 & 0 & \sigma_{ws}^2(k) & 0 \\ 0 & 0 & 0 & \sigma_{sr}^2(k) \end{matrix}$$

APPENDIX E

Regional lake water temperature simulation model

LAKE INPUT DATA FILE

TITLE	
SEKI	Secchi depth reading
NDAYS	Number of days for output
NPRNT	Dates for output
DZLL DZUL BETA EMISS WCOEF WSTR	Heat budget and mixing coefficient
WCHANL WLAKE DBL ST S FT	Initial stage & Outflow channel
ELCB ALPHA BW	

Initial conditions

MBOT NM NPRINT INFLOW DY MONTH ISTART MYEAR
Z(1)...Z(MBOT)
T(1)...T(MBOT)

Field data section

NF NPRFLE	Number of depths & parameters
NFLD	Parameter code (1)
DEPTH(1)...DEPTH(NF)	Depths
FDATA(1)...FDATA(NF)	Temperatures

.
.
.

NDAYS

EXAMPLE INPUT DATA.FILE

```
 LAKE CALHOUN 1971  ** from APRIL through december **
2
9
520 608 629 719 802 824 913 1011 1028
0.15 1.00 .4 .97 24.5 0.4
100. 100. 200 224.0 .001 .035
205 18 100
24 8 1 0 91 4 1 1971
0.5 1.5 2.5 3.5 4.5 5.5 6.5 7.5 8.5 9.5 10.5 11.5
12.5 13.5 14.5 15.5 16.5 17.5 18.5 19.5 20.5 21.5 22.5 23.5
4. 4. 4. 4. 4. 4. 4. 4. 4. 4.
4. 4. 4. 4. 4. 4. 4. 4. 4. 4.
4. 4. 4. 4.
11 1
1
0.   2.   4.   6.   7.   8.   10. 12. 15. 20. 23.
13.1 12.8 12.5 12.5 12.5 10.4 8.6 7.9 7.4 7.  6.9
14 1
1
0. 1. 2. 3. 4. 5. 6. 7. 8. 10. 12. 15. 20. 25.
20.4 20.3 20.1 19.8 15.1 13.6 12.3 11.7 11. 9.2 8.1 7.3 7.1 6.9
12 1
1
0. 1. 2. 3. 4. 5. 6. 8. 10. 12. 15. 20.
24.4 24.6 24.6 24.3 23.5 19. 15.1 11.5 10. 8.8 7.2 7.
14 1
1
0. 1. 2. 3. 4. 5. 6. 7. 8. 10. 12. 15. 20. 24.
23.1 23.1 23.1 23. 22.9 22.8 17.6 12.4 11.4 10.2 9. 8.2 7.8 7.7
14 1
1
0. 1. 2. 3. 4. 5. 6. 7. 8. 10. 12. 15. 20. 24.
21. 21. 20.8 20.8 20.8 20.6 19.4 14.7 11.3 9.8 9. 8.2 7.5 7.4
11 1
1
0. 1. 2. 3. 4. 5. 6. 7. 8. 10. 12. 15. 20.
22.7 22.7 22.7 22.7 22.6 22.6 20.5 15.7 12. 10.2 9.2 8.1 7.7
15 1
1
0. 1. 2. 3. 4. 5. 6. 7. 8. 9. 10. 12. 15. 20. 25.
21.7 21.7 21.5 21.5 21.5 21.3 21.1 18.5 13.3 10.6 10. 9. 7.9 7.6 7.5
13 1
1
0. 1. 2. 4. 6. 8. 10. 12. 14. 16. 18. 20. 22.
14.5 14.5 14.3 14.3 14.2 14.2 14.2 11.1 10.1 9.3 8.6 8.4 8.3
7 1
1
0. 12. 13. 14. 15. 20. 23.
12.7 12.7 10.5 9.0 8.4 7.9 7.8
```

LAKE INPUT DATA VARIABLES

SEKI	=	Secchi depth reading (m)
NDAYS	=	Number of particular dates selected for output
NPRNT	=	Dates selected for output
DZLL	=	Minimum layer thickness (m)
DZUL	=	Maximum layer thickness (m)
BETA	=	Surface absorption factor for solar radiation
EMISS	=	Emissivity of water
WCOEF	=	Wind coefficient for convective heat loss
WSTR	=	Wind sheltering coefficient
WCHANL	=	Width of the inlet channel (m)
WLAKE	=	Width of lake (m)
DBL	=	Elevation of the bed in the bottom layer (m)
ST	=	Stage of the lake on the first day of simulation (m)
S	=	Bed slope at inlet channel
FT	=	Roughness coefficient at inlet channel
ELCB	=	Elevation of the bottom of the outlet channel (m)
ALPHA	=	Side slope of outlet channel
BW	=	Bottom width of outlet channel (m)
MBOT	=	Total number of layers in the initial conditions
NM	=	Number of months to be simulated
NPRINT	=	Interval between days for tabular output
INFLOW	=	Number of inflow and outflow sources
DY	=	Julian day of first day of simulation
MONTH	=	First month of simulation
ISTART	=	Day of the month that simulation starts
MYEAR	=	Year of simulation
Z	=	Depths in the initial conditions (m)
T	=	Temperatures in the initial conditions (°C)
NF	=	Number of depths in field data profile
NPRFLE	=	Number of profiles in the field data
NFLD	=	Parameter code to match field data profiles to state variables 1 = Temperature (°C)
DEPTH	=	Field data depths (m)
FDATA	=	Field data temperatures (°C)

METEOROLOGICAL DATA FILE

MONTH KDAYS MYEAR
TAIR TDEW WIND DRCT RAD CR PR
.
.
.
KDAYS

where

MONTH	=	Month
KDAYS	=	Total number of days in the month
MYEAR	=	Year
TAIR	=	Average air temperature (oF)
TDEW	=	Dew point temperature (oF)
WIND	=	Average wind speed (mph)
DRCT	=	Wind direction
CR	=	Percent of sunshine
PR	=	Precipitation (inches)

EXAMPLE METEOROLOGICAL DATA FILE

4	30	1971				
32	22	22.4	320	203	9	13
21.5	10	19.3	320	324	8	6
26	14	13.9	310	514	93	0
32.5	12	7.6	280	568	100	0
34	14	3.9	310	558	100	0
39.5	23	6.7	30	489	100	0
53	29	9.3	80	533	100	0
55	32	13.5	50	398	94	0
49	27	13	290	553	100	3
54	28	15.3	80	527	100	0
54	34	13.5	340	432	62	0
50	25	6.8	280	373	78	0
39	20	9.7	280	389	73	1
40	23	4.3	50	471	79	0
55	32	13.9	100	531	99	0
61	46	12.9	40	347	79	2
55	36	6.6	190	565	97	0
52.5	37	11.7	140	76	7	11

.
.
.
KDAYS

```
123456789
$LARGE
    PROGRAM REGIONAL

C
C       THIS PROGRAM IS MODIFIED VERSION OF THE MINLAKE
C       MODEL (RILEY & STEFAN, 1987, UNIVERSITY OF MINNESOTA
C       SAFHL PROJECT REPORT # 263). THE COMPUTER CODE
C       IS ADDAPTED FOR THE REGIONAL LAKE WATER TEMPERATURE
C       SIMULATION IN A LAKE. ATTATCH USER SUBROUTINE DURING
C       LINKING.
C
    COMMON/MTHD/TAIR(31),TDEW(31),RAD(31),CR(31),WIND(31),
   + PR(31),DRCT(31)
    COMMON/RESULT/T2(40),CHLATOT(40),PA2(40),PTSUM(40),BOD2(40),
   +DSO2(40),C2(40),CD2(40),XNO2(40),XNH2(40),CHLA2(3,40),
   +PC2(3,40),XNC2(3,40),T20(40),SI2(40)
    COMMON/FLOW/HMK(41),QE(40),FVCHLA(5),PE(5,41)
    COMMON/VOL/ZMAX,DZ(40),Z(40),A(40),V(40),TV(40),ATOP(41),DBL
    COMMON/SUB/SDZ(60),SZ(60),LAY(40),AVGI(4,60),SVOL(60)
    COMMON/CHOICE/MODEL,NITRO,IPRNT(6),NDAYS,NPRNT(30),NCLASS,PLT(30)
    COMMON/WATER/BETA,EMISS,XK1,XK2,HKMAX,WCOEF,WSTR
    COMMON/CHANEL/WCHANL,ELCB,ALPHA,BW,WLAKE
    COMMON/STEPS/DZLL,DZUL,MBOT,NM,NPRINT,MDAY,MONTH,ILAY,DY
    COMMON/STAT/SUMXY(10),SUMX(10),SUMY(10),XSQ(10),
   +YSQ(10),RSQ(10),RMS(10),RELM(10),MTHREL(10),MDAYREL(10),ZREL(10),
   +ZRELM(10),RS(10),REL(10),MTHRMS(10),MDAYRMS(10),ZRS(10),ZRMS(10)
    COMMON/INFLOW/QIN(5),TIN(5),PAIN(5),BODIN(5),DOIN(5),CIN(5),
   +CDIN(5),XNHIN(5),XNOIN(5),CHLAIN(3,5)
    COMMON/SOURCE/RM(3,40),PROD(40),XMR(3,40),PRODSUM(40)
    COMMON/FIELD/ IFLAG(10),FLDATA(10,50),DEPTH(50),NFLD(10)
    COMMON/FILE/ DIN,MET,FLO,TAPE8,TAPE1,IREC
    COMMON/TITL/ TITLE
    DIMENSION B(10),STATVAR(80),ICX(4)
    CHARACTER*64 TITLE
    CHARACTER*16 DIN,MET,FLO,TAPE8,TAPE1
    CHARACTER*1 T8(16),FF,CX1,CX2,CX3,CX4,XS
    EQUIVALENCE (STATVAR(1),SUMXY(1)),(TAPE8,T8(1))
    EQUIVALENCE(CX1,ICX(1)),(CX2,ICX(2)),(CX3,ICX(3)),(CX4,ICX(4))
    DATA IPAN,PCOEFF/0,0.65/
    DATA ICX/16 #1B, 16#5B, 16#32, 16#4A/
    FF=CHAR(12)
990 FORMAT(1X,4A1)
    YSCHL=30.
    HSCSI=0.03
    CONST=.5
    CHLMAX=0.0
    DO 995 I=1,6
995 IPRNT(I)=0
    DO 996 I=1,10
996 IFLAG(I)=0
    DO 997 I=1,80
997 STATVAR(I)=0.0
     WRITE(*,1001)
     READ(*,'(A)') DIN
     WRITE(*,1000)
     READ(*,'(A)') MET
    WRITE(*,1002)
    READ (*,'(A)') TAPE8
    DO 405 I=1,16
      II=16-I+1
      IF(T8(II).NE.' ') THEN
          T8(II+1)='.'
          T8(II+2)='D'
          T8(II+3)='A'
          T8(II+4)='T'
          GOTO 406
      ENDIF
405   CONTINUE
406 OPEN (7,FILE=DIN)
     OPEN (8,FILE=TAPE8)
     OPEN (9,FILE=MET)
C
C THESE ARE OUTPUT DATA FILES
C
     OPEN(21,FILE='EPIL.PRN')
     OPEN(22,FILE='HYPOL.PRN')
     OPEN(28,FILE='TEMPER.PRN')
C
     READ(7,'(A)') TITLE
```

```
505  FORMAT(' REQUEST CHANGE OF TITLE (Y/N) ?',8X,/)
506  FORMAT(' ENTER NEW TITLE :')
     WRITE(*,505)
     READ(*,'(A)') XS
     IF(XS.EQ.'Y' .OR. XS.EQ.'y') THEN
      WRITE(*,506)
      READ(*,'(A)') TITLE
     ENDIF
     WRITE(8,999) FF
     WRITE(8,1900)
     WRITE(8,'(A)') TITLE
 999 FORMAT(1X,A1)
1001 FORMAT(' ENTER INPUT DATA FILE NAME :',10X,/)
1002 FORMAT(' ENTER FILE NAME FOR TABULAR OUTPUT :  ',/)
1000 FORMAT(' ENTER METEOROLOGICAL DATA FILE NAME : ',/)
1003 FORMAT(' ENTER INFLOW DATA FILE NAME :',9X,/)
1900 FORMAT(//,8X,/)
C
     CALL START(ST,S,FT,ISTART,INFLOW,MYEAR,IRUN,ILSEKI)
C
C***** Call LAKE routine to change or add input quantities ***

     ZMAX=ST-DBL
     CALL SETUP
     I=1
  11 IF(DZ(I).GT.DZUL.AND.MBOT.LT.40) THEN
      CALL SPLIT(I,ILAY)
      GO TO 11
     ENDIF
     I=I+1
     IF(I.GT.MBOT.OR.I.GT.40) GOTO 12
     GOTO 11
  12 CALL SETZ(MBOT)
     CALL VOLUME(MBOT)
     CALL AREA
     CALL ABOUND
     CALL TVOL(MBOT)
C_DETERMINATION OF INITIAL MIXED LAYER DEPTH
     ILAY=1
     DO 7 I=1,MBOT-1
     IF(T2(I).GT.T2(I+1)+CONST) GO TO 8
   7 ILAY=ILAY+1
   8 DMIX=Z(ILAY)+DZ(ILAY)*0.5
     DO 9 I=1,10
      RELM(I)=0.
   9  RMS(I)=0.0
     NDAYS=1
     MP=0
     IPRNT(1)=1
     KDAYS=0
     IPRNT(5)=IPRNT(5)-1
     MDAY=0
     WRITE(8,999) FF
     CALL PTABLE
     IPRNT(5)=IPRNT(5)+1
C_ Start simulation for each month
     EDAY=365.
     YEAR=REAL(MYEAR)
     IF(AMOD(YEAR,4.0).EQ.0.0) EDAY=366.
     ETSUM=0.
     HTSUM=0.
C
     DO 100 J=1,NM
     CALL MTHDATA(MONTH,KDAYS,MYEAR)
     EDAY=365.
     YEAR=REAL(MYEAR)
     IF(AMOD(YEAR,4.0).EQ.0.) EDAY=366.
C_START SIMULATION FOR EACH DAY
     DO 200 MDAY=ISTART,KDAYS
     NFLOW=INFLOW
     CALL LAKE(0.,0.,0.5)
     IF(MDAY.EQ.KDAYS.OR.MP/NPRINT*NPRINT.EQ.MP) IPRNT(1)=1
     IF(MONTH*100+MDAY.EQ.NPRNT(NDAYS)) IPRNT(1)=1
C
     P=PR(MDAY)*0.0254
     MP=MP+1
     TMIX=T2(1)
C_CALCULATION OF KINETIC ENERGY FROM WIND STRESS
     CALL WINEN(TAU,VC,WIND(MDAY))
     RKE=TAU*VC*ATOP(1)*WSTR*86400.
```

```
C
C..DETERMINATION OF WIND MIXING ORDER
C..HEAT IS ABSORBED FIRST, THEN WATER COLUMN IS MIXED BY THE WIND
C
    CALL HEBUG(ILAY,TMIX,QNET,HS,HA,HBR,HE,HC,
   +TAIR(MDAY),TDEW(MDAY),CR(MDAY),RAD(MDAY),WIND(MDAY),
   +IPAN,PCOEFF,SEKI)
    CALL CONMIX(ILAY,TMIX,MBOT)
C..CALCULATION OF EVAP. IN TERMS OF VOLUME
C..CALCULATES LATENT HEAT OF VAPORIZATION ALV
    HED=HE/((597.31-0.5631*T2(1))*RHO(T2(1),C2(1),CD2(1)))
    HEV=HED*ATOP(1)
    CALL WINMIX(RKE,TMIX,ILAY,MBOT)
    DMIX=Z(ILAY)+0.5*DZ(ILAY)
C
 35  CALL LAKE(0.,0.,0,13)
C
     IF(IPRNT(1).EQ.1) THEN
C..Output tabular data on tape8.DAT
     CALL PTABLE
C..Output meteorological data on tape8.DAT
     CALL PMETE(HS,RAD(MDAY),HA,WIND(MDAY),HBR,
   + P,HE,TAIR(MDAY),HC,TDEW(MDAY),HED,HEV,QNET,DMIX,ZEUPH,SEKI)
    ENDIF
C..Output to plot file (tape8.PLT)
    IF(MDAY+MONTH*100.EQ.NPRNT(NDAYS)) THEN
C..Access and output field data
      CALL FDATA(NF)
      WRITE(*,3020)
      READ(*,99) XS
 99   FORMAT(A1)
 3020  FORMAT(///,' DO YOU WANT TO VIEW GRAPHICAL RESULTS: (Y/N)',
   +     3X\)
C..Call plotting routines
      IF(XS.EQ.'Y' .OR. XS.EQ.'y') THEN
       CALL SUBPLOT(NF,MYEAR)
      ENDIF
      ENDIF
    DY=DY+1.
    IPRNT(1)=0
 200 CONTINUE
    ISTART=1
 100 CONTINUE
C..Compute and list statistics:
C..   1)relative and absolute maximum deviations between
C..     model and field data and day of occurrence
C..   2) slope of regression of field data on simulation results
C..   3) regression coefficient
C..   4) standard error of the regression
    WRITE(8,3000)
    DO 101 I=1,10
     IF(XSQ(I).GT. 0.) B(I)=SUMXY(I)/XSQ(I)
     IF(IFLAG(I).GT.2) THEN
      SUMXY(I)=(YSQ(I)-SUMXY(I)*SUMXY(I)/XSQ(I))/(IFLAG(I)-2)
      RSQ(I)=1.-SUMXY(I)*
   +    IFLAG(I)*(IFLAG(I)-1)/(IFLAG(I)*YSQ(I)-SUMY(I)*SUMY(I))
      SUMXY(I)=SQRT(SUMXY(I))
     ENDIF
 101 CONTINUE
    WRITE(8,3001)
    WRITE(8,3013)(RELM(J),J=1,10)
    WRITE(8,3014)(MTHREL(J),MDAYREL(J),J=1,10)
    WRITE(8,3015)(RMS(J),J=1,10)
    WRITE(8,3016)(MTHRMS(J),MDAYRMS(J),J=1,10)
    WRITE(8,3017)(B(J),J=1,10)
    WRITE(8,3018)(RSQ(J),J=1,10)
    WRITE(8,3024)(SUMXY(I),I=1,10)
    WRITE(*,3000)
    WRITE(*,3019)
    WRITE(*,3013) RELM(1)
    WRITE(*,3015) RMS(1)
    WRITE(*,3017) B(1)
    WRITE(*,3018) RSQ(1)
    WRITE(*,3024) SUMXY(1)
 4000 FORMAT(///1X,'PRODUCE TIME SERIES PLOTS (Y/N) ? '\)
 3000 FORMAT(///5X,'ANALYSIS OF ERRORS BETWEEN FIELD DATA AND MODEL')
 3001 FORMAT(/42X,'TEMP',5X,'CHLA',7X,'PA',7X,'PT',6X,'BOD',7X,'DO',
   +6X,'TSS',6X,'TDS',6X,'N03',6X,'NH4'/)
 3013 FORMAT(1X,'MAXIMUM RELATIVE ERROR (%)',10X,10(5X,F4.0))
 3014 FORMAT(1X,'DATE OF MAX. REL. ERR.',14X,10(4X,I2,'/',I2))
 3015 FORMAT(1X,'MAXIMUM ABSOLUTE ERROR',14X,10(2X,F7.3))
```

```
3016 FORMAT(1X,'DATE OF MAX. ABS. ERR.',14X,10(4X,I2,'/',I2))
3017 FORMAT(1X,'SLOPE: MODEL TO DATA REGRESSION',5X,10(2X,F7.2))
3018 FORMAT(1X,'REGRESSION COEFFICIENT (R**2)',7X,10(2X,F7.2))
3019 FORMAT(1X,/42X,'LAKE WATER TEMPERATURE STATISTICS')
3024 FORMAT(1X,'STANDARD ERROR OF ESTIMATE',10X,10(2X,F7.3))
     END
C
     SUBROUTINE FDATA(NF)
C*****
C***** Subroutine to read field data from the input data
C***** and compute statistics and deviations between field
C***** data and simulation
C*****
     COMMON/FILE/ DIN,MET,FLO,TAPE8,TAPE1,IREC
     COMMON/RESULT/ T2(40),CHLATOT(40),PA2(40),PTSUM(40),BOD2(40),
    +DSO2(40),C2(40),CD2(40),XNO2(40),XNH2(40),CHLA2(3,40),
    +PC2(3,40),XNC2(3,40),T20(40),SI2(40)
     COMMON/STAT/SUMXY(10),SUMX(10),SUMY(10),XSQ(10),
    +YSQ(10),RSQ(10),RMS(10),RELM(10),MTHREL(10),MDAYREL(10),ZREL(10),
    +ZRELM(10),RS(10),REL(10),MTHRMS(10),MDAYRMS(10),ZRS(10),ZRMS(10)
     COMMON/VOL/ZMAX,DZ(40),Z(40),A(40),V(40),TV(40),ATOP(41),DBL
     COMMON/STEPS/DZLL,DZUL,MBOT,NM,NPRINT,MDAY,MONTH,ILAY,DY
     COMMON/CHOICE/MODEL,NITRO,IPRNT(6),NDAYS,NPRNT(30),NCLASS,PLOT(30)
     COMMON/FIELD/ IFLAG(10),FLDATA(10,50),DEPTH(50),NFLD(10)
     DIMENSION COMP(40,10)
     EQUIVALENCE (T2(1),COMP(1,1))
     CHARACTER*16 DIN,MET,FLO,TAPE8,TAPE1
     DO 303 I=1,10
       RS(I)=0
303   REL(I)=0
     DO 304 J=1,20
       DO 304 I=1,10
304   FLDATA(I,J)=0.0
     READ(7,*)NF,NPRFLE
     NDAYS=NDAYS+1
     IF(NF.GT.0) THEN
       READ (7,*)(NFLD(I),I=1,NPRFLE)
       READ(7,*)(DEPTH(I),I=1,NF)
       DO 305 I=1,NPRFLE
         READ(7,*)(FLDATA(NFLD(I),J),J=1,NF)
305     CONTINUE
       LL=1
C_Locate simulation values corresponding to sampled
C_constituents and depth of field data
       DO 310 KK=1,NF
         L=LL
         DO 315 LL=L,MBOT
           ZX=Z(LL)+0.5*DZ(LL)
           IF(ZX.LT.DEPTH(KK)) GOTO 315
           IF(LL.EQ.1) THEN
            DO 320 I2=1,NPRFLE
             I=NFLD(I2)
             IF(FLDATA(I,KK).GT.0)THEN
              XX=COMP(LL,I)
              CALL STATS(FLDATA(I,KK),XX,IFLAG(I),DEPTH(KK),I)
             ENDIF
320         CONTINUE
           ELSE
            DO 330 I2=1,NPRFLE
             I=NFLD(I2)
             IF(FLDATA(I,KK).GT.0) THEN
              XX=COMP(LL-1,I)+(DEPTH(KK)-Z(LL-1))/(Z(LL)-Z(LL-1))
    +          *(COMP(LL,I)-COMP(LL-1,I))
              CALL STATS(FLDATA(I,KK),XX,IFLAG(I),DEPTH(KK),I)
             ENDIF
330         CONTINUE
           ENDIF
           GOTO 310
315       CONTINUE
310     CONTINUE
C_Store statisitcal results in the consol and tape8.DAT
       WRITE(8,3009) MONTH,MDAY
266    FORMAT(1X,F9.2,2X,F9.4)
       WRITE(*,3010)
       WRITE(*,3013) REL(1)
       WRITE(*,3014) ZREL(1)
       WRITE(*,3015) RS(1)
       WRITE(*,3016) ZRS(1)
       WRITE(8,3010)
       WRITE(8,3013) (REL(I),I=1,10)
       WRITE(8,3014) (ZREL(I),I=1,10)
```

```
      WRITE(8,3015) (RS(I),I=1,10)
      WRITE(8,3016) (ZRS(I),I=1,10)
C_Store data on plot file (tape8.PLT)
      IF(IPRNT(5).GT.0) THEN
        WRITE(1,REC=IREC) REAL(NF)
        IREC=IREC+1
        WRITE(1,REC=IREC) REAL(NPRFLE)
        IREC=IREC+1
        DO 500 I=1,NF
         WRITE(1,REC=IREC) DEPTH(I)
500      IREC=IREC+1
        DO 501 I=1,NPRFLE
         WRITE(1,REC=IREC) REAL(NFLD(I))
501      IREC=IREC+1
        DO 502 I2=1,NPRFLE
        DO 502 I=1,NF
         WRITE(1,REC=IREC) FLDATA(NFLD(I2),I)
502      IREC=IREC+1
        IF( NFLD(1).NE.1) THEN
          X=0.0
        ELSE
C_Mixed layer depth in field data taken at dT/dZ=1.0
          DO 503 J2=2,NF
            X=(FLDATA(1,J2-1)-FLDATA(1,J2))/
     +                      (DEPTH(J2)-DEPTH(J2-1))
            IF(X.GT.1.0) GOTO 504
503          CONTINUE
504        X=(DEPTH(J2)+DEPTH(J2-1))*0.5
           IF(J2.GE.NF) X=ZMAX
        ENDIF
        WRITE(1,REC=IREC) X
        IREC=IREC+1
      ENDIF
     ELSE
      NF=0
      IF(IPRNT(5).GT.0) THEN
       WRITE(1,REC=IREC) REAL(NF)
       IREC=IREC+1
      ENDIF
     ENDIF
2999 FORMAT(1X,I4,3X,I5)
3009 FORMAT(///5X,'DATE: ',I2,' / ',I3,//5X,
    +'SUM OF ERRORS BETWEEN MODEL AND FIELD DATA')
3010 FORMAT(5X,43('-'),/42X,
    +'LAKE TEMPERATURE STATISTICS',/)
3013 FORMAT(1X,'MAXIMUM RELATIVE ERROR (%)',10X,10(5X,F4.0))
3014 FORMAT(1X,'DEPTH OF MAX. REL. ERR. (M)',9X,10(5X,F4.1))
3015 FORMAT(1X,'MAXIMUM ABSOLUTE ERROR',14X,10(2X,F7.3))
3016 FORMAT(1X,'DEPTH OF MAX.ABS. ERR. (M)',9X,10(5X,F4.1),///)
3020 FORMAT(/42X,'TEMP',5X,'CHLA',7X,'TP',7X,'DO')
     RETURN
     END
C
     SUBROUTINE PTABLE
C*****
C***** Send simulation results to the tabular
C***** output file (tape8.DAT)
C*****
     COMMON/RESULT/ T2(40),CHLATOT(40),PA2(40),PTSUM(40),BOD2(40),
    +DSO2(40),C2(40),CD2(40),XNO2(40),XNH2(40),CHLA2(3,40),
    +PC2(3,40),XNC2(3,40),T20(40),SI2(40)
     COMMON/VOL/ZMAX,DZ(40),Z(40),A(40),V(40),TV(40),ATOP(41),DBL
     COMMON/STEPS/DZLL,DZUL,MBOT,NM,NPRINT,MDAY,MONTH,ILAY,DY
     COMMON/CHOICE/MODEL,NITRO,IPRNT(6),NDAYS,NPRNT(30),NCLASS,PLT(30)
     IF(MDAY.NE.0) THEN
      WRITE(8,3000)
     ELSE
      WRITE(8,2999)
     ENDIF
     IF(IPRNT(4).LT.1) THEN
      WRITE(8,3008)
      WRITE(28,7777) MONTH,MDAY
      DO 200 I=1,MBOT
CM
       WRITE(28,3009) Z(I),T2(I)
7777   FORMAT(I3,2X,I5)
200  CONTINUE
      RETURN
     ENDIF
     IF(NCLASS.EQ.1)THEN
     ELSE
```

```
      IF(NITRO.GT.0) THEN
      ELSE
      ENDIF
      WRITE(8,3006)
      IF(NITRO.GT.0) THEN
      ELSE
      ENDIF
    ENDIF
1200 FORMAT(///5X,'ZOOPLANKTON PARAMETERS',/,5X,22('-'),/,6X,
   + 'CONC. (#/M3)',2X,'PREDATION(#/M3)',3X,'GRAZING(MG/M3)',3X,
   + ' DAYDEPTH(M)',/,9X,F7.0,9X,F7.1,9X,F6.4,11X,F4.1,//)
1201 FORMAT(F11.4)
2999 FORMAT(//5X,'INITIAL CONDITIONS',/5X,18('-'),/)
3000 FORMAT(///5X,'INFORMATION ON LAKE QUALITY',/5X,27('-'),/)
3001 FORMAT(5X,'Z(M)    T(C) SS(PPM) TDS(PPM)  CHLA(PPM)  PC(PPM)',
   +' P(PPM)  PT(PPM)   BOD(MG/L)  DO(MG/L)  DZ(M)',
   + '  AREA(M2)     VOL(M3)')
3002 FORMAT(5X,3(F5.2,2X),1X,F5.1,4X,4(2X,F6.4),6X,F6.2,6X
   +F5.2,4X,F4.2,2(2X,E10.4))
3003 FORMAT(5X,'Z(M)    T(C) SS(PPM) TDS(PPM)  PA(PPM)    PT(PPM)',
   +' BOD(MG/L)  DO(MG/L)  NO3(MG/L)  NH4(MG/L)  DZ(M)',
   + '  AREA(M2)     VOL(M3)')
3004 FORMAT(5X,3(F5.2,2X),1X,F5.1,2(4X,F6.3),4X,F6.2,5X,F5.2,4X,
   +2(F6.3,6X),F4.2,2(2X,E10.4))
3005 FORMAT(5X,3(F5.2,2X),1X,F5.1,2(4X,F6.3),4X,F6.2,5X,F5.2,25X,F4.2,
   +2(2X,E10.4))
3006 FORMAT(///5X,'BIOLOGICAL PARAMETERS',/5X,21('-'),/,5X,'Z(M)',9X,
   +'CHLOROPHYLL',6X,'TOTAL',6X,'INERNAL P',11X,'INTERNAL N',/16X,
   +'1',6X,'2',6X,'3',5X,'CHLA',4X,'1',6X,'2',6X,'3',6X,'1',6X,'2',
   +6X,'3',/,5X,10('       ',2X))
3007 FORMAT(5X,F5.2,2X,10(F5.3,2X))
3008  FORMAT(///,5X,' TEMPERATURE PROFILES',/,5X,'Z(M)',4X,'T(C)',
   +6X,'AREA (M2)',5X,'VOL (M3)')
3009 FORMAT(5X,2(F5.2,2X),2(2X,E10.4))
    RETURN
    END
    SUBROUTINE SUBPLOT(NF,MYEAR)
C*****
C***** Produce profile of state variables and
C***** field data (if available)
C*****
    CHARACTER*1 XS,CH1,CH2,CH3,CH4
    CHARACTER*32 TITLE(1)
    CHARACTER*4 MNTH(12)
    COMMON/SOURCE/RM(3,40),PROD(40),XMR(3,40),PRODSUM(40)
    COMMON/STEPS/DZLL,DZUL,MBOT,NM,NPRINT,MDAY,MONTH,ILAY,DY
    COMMON/RESULT/ T2(40),CHLATOT(40),PA2(40),PTSUM(40),BOD2(40),
   +DSO2(40),C2(40),CD2(40),XNO2(40),XNH2(40),CHLA2(3,40),
   +PC2(3,40),XNC2(3,40),T20(40),SI2(40)
    COMMON/FIELD/IFLAG(10),FLDATA(10,50),DEPTH(50),NFLD(10)
    COMMON/VOL/ZMAX,DZ(40),Z(40),A(40),V(40),TV(40),ATOP(41),DBL
    DIMENSION ZD(23),FD(23),VTM(43),ZV(43),VAR(40,10)
    DIMENSION FCT(10),LEN(10),ISCAL(10),ICX(4)
    EQUIVALENCE (T2(1),VAR(1,1)),(ZD(1),PROD(1)),(FD(1),PRODSUM(1)),
   +(VTM(1),RM(1,1)),(ZV(1),XMR(1,1))
    EQUIVALENCE (CH1,ICX(1)),(CH2,ICX(2)),(CH3,ICX(3)),(CH4,ICX(4))
    DATA ICX/16#1B,16#5B,16#32,16#4A/
    DATA ISCAL/1,3*-1,3*1,3*-1/
    DATA FCT/1,3*1000,4*1,2*1000/
    DATA MNTH/'JAN ','FEB ','MAR ','APR ','MAY ','JUN ','JUL ','AUG ',
   +'SEP ','OCT ','NOV ','DEC '/
    DATA TITLE /'TEMPERATURE  (C)'/
    DATA LEN /16,27,28,25,23,4*24,25/
1000 WRITE(*,109) CH1,CH2,CH3,CH4
 109 FORMAT(1X,4A1,/)
C...list and select desired state variable for plotting
    DO 100 I=1,1
 100   WRITE(*,101) I,TITLE(I)
 101 FORMAT(1X,I2,' = ',A32)
    WRITE(*,99)
  99 FORMAT(/1X,'CHOOSE (1) DESIRED PLOT (ENTER  Q  TO QUIT) :  ',\)
    READ(*,*,ERR=1001) IC1
    X=0.
C...change depth to negative values for plotting with depth
    DO 110 I=1,MBOT
    ZV(I)=-Z(I)
    VTM(I)=VAR(I,IC1)
    IF(X.LT.VAR(I,IC1)) THEN
     X=VAR(I,IC1)
     IND=IC1
    ENDIF
```

```
 110 CONTINUE
    I2=0
C_if field data is available, locate field data corresponding
C_to selected state variables
     IF(NF.GT.0) THEN
       DO 111 I=1,NF
       IF(FLDATA(IC1,I).GT.0) THEN
         I2=I2+1
         FD(I2)=FLDATA(IC1,I)
         ZD(I2)=-DEPTH(I)
         IF(X.LT.FD(I2)) THEN
          X=FD(I2)
          IND=-1
         ENDIF
       ENDIF
 111   CONTINUE
      ENDIF
      NPEN=1
      NPEN1=1
      IPORT=99
      MODL=99
      ZV(MBOT+1)=0.
      ZD(I2+1)=0.
      VTM(MBOT+1)=0.
      FD(I2+1)=0.
      FCTOR=0.72
C_begin plotting sequence
 990  CALL PLOTS(0,IPORT,MODL)
      CALL SIMPLX
      CALL FACTOR(FCTOR)
      CALL NEWPEN(NPEN)
C_determine maximum x & y values either in simulated
C_state variables or in field data
      IF(IND.GT.0) THEN
        I3=MBOT+1
        CALL SCALE(VTM,10.,I3,1)
        DX=VTM(MBOT+3)
      ELSE
        I3=I2+1
        CALL SCALE(FD,10.,I3,1)
        DX=FD(I2+3)
      ENDIF
      IF(ZV(MBOT).LT.ZD(I2)) THEN
        I3=MBOT+1
        CALL SCALE(ZV,6.,I3,-1)
        YSC=-ZV(MBOT+3)
      ELSE
        I3=I2+1
        CALL SCALE(ZD,6.,I3,-1)
        YSC=-ZD(I2+3)
      ENDIF
      ZV(MBOT+2)=YSC
      ZD(I2+2)=YSC
      VTM(MBOT+2)=DX
      FD(I2+2)=DX
      DAXIS=DX*FCT(IC1)
      YD=ANINT(6.*YSC)
      CALL STAXIS(.2,.25,.2,.15,ISCAL(IC1))
C_draw x-axis
      CALL AXIS(1.,7.,TITLE(IC1),LEN(IC1),-10.,0.,0.,DAXIS)
      CALL STAXIS(.2,.25,.2,.15,1)
C_draw y-axis
      CALL AXIS(1.,1.,'DEPTH  (M)',10,-6.,90.,YD,-YSC)
      XMDAY=MDAY
      XMYEAR=MYEAR
C_print title to diagram
      CALL SYMBOL(4.5,.5,.25,MNTH(MONTH),0.,4)
      CALL NUMBER(999.,999.,.25,XMDAY,0.,-1)
      CALL SYMBOL(999.,999.,.25,', ',0.,2)
      CALL NUMBER(999.,999.,.25,XMYEAR,0.,-1)
      CALL NEWPEN(NPEN1)
      CALL PLOT (1.,7.,-3)
C_plot simulated profiles as a line
      CALL LINE(VTM,ZV,MBOT,1,0,1)
C_plot field data with a symbol
      IF(I2.GT.0)  CALL LINE(FD,ZD,I2,1,-1,4)
      CALL PLOT(0.,0.,999)
      WRITE(*,130)
 130 FORMAT(1X,'SEND TO HARDCOPY DEVICE ?  (Y/N)   ',\)
      READ(*,'(A)',//') XS
      IF(XS.EQ.'Y' .OR. XS.EQ.'y') THEN
```

```
      WRITE(*,140)
      READ(*,*) IPORT,MODL
 140  FORMAT(/1X,'ENTER PLOT88 IOPORT AND MODEL : ',\)
      WRITE(*,143)
      READ(*,*) NPEN,NPEN1
 143  FORMAT(/1X,'ENTER LINE WEIGHT (AXIS,DATA) : ',\)
      WRITE(*,141)
      READ(*,*) FCTOR
 141  FORMAT(/1X,'ENTER REDUCTION FACTOR ( >1.0 ) : ',\)
      GOTO 990
      ENDIF
      GOTO 1000
1001  RETURN
      END
      SUBROUTINE ABOUND
C*****
C***** Computes the surface area of each layer (ATOP)
C***** using the depth area relationship in LAKE.
C*****     ATOP(1) = surface area of the lake
C*****     ATOP(MBOT+1) = 0.0
C*****
      COMMON/STEPS/DZLL,DZUL,MBOT,NM,NPRINT,MDAY,MONTH,ILAY,DY
      COMMON/VOL/ZMAX,DZ(40),Z(40),A(40),V(40),TV(40),ATOP(41),DBL
      DUM=0.
      DO 100 I=1,MBOT
      ZDUM=ZMAX-DUM
      DUM=DUM+DZ(I)
      CALL LAKE(ZDUM,ADUM,0,1)
 100  ATOP(I)=ADUM
      ATOP(MBOT+1)=0.
      RETURN
      END
      SUBROUTINE AREA
C*****
C***** Compute the area through the middle of each layer
C***** using the depth-area relationship in LAKE
C*****
      COMMON/STEPS/DZLL,DZUL,MBOT,NM,NPRINT,MDAY,MONTH,ILAY,DY
      COMMON/VOL/ZMAX,DZ(40),Z(40),A(40),V(40),TV(40),ATOP(41),DBL
      DUM=0.
      DO 100 I=1,MBOT
      ZDUM=ZMAX-DUM-DZ(I)/2.
      DUM=DUM+DZ(I)
      CALL LAKE(ZDUM,ADUM,0,1)
 100  A(I)=ADUM
      RETURN
      END
       SUBROUTINE COEF(MODEL,MBOT,NCLASS)
C*****
C***** Compute some coefficients used in the constant
C***** volume and finite difference solutions
C*****
        COMMON/COEFF/ DUM2(40),DUM3(40)
        COMMON/VOL/ ZMAX,DZ(40),Z(40),A(40),V(40),TV(40),ATOP(41),DBL
        COMMON/FLOW/ HMK(41),QE(40),FVCHLA(5),PE(5,41)
       DO 100 I=2,MBOT-1
        DUM1= 2./(A(I)*DZ(I))
        DUM2(I)=DUM1*ATOP(I)*HMK(I)/(DZ(I)+DZ(I-1))
 100    DUM3(I)=DUM1*ATOP(I+1)*HMK(I+1)/(DZ(I)+DZ(I+1))
      KK=2
      IF(MODEL.GT.1) KK=1
      DO 200 K=KK,NCLASS+1
       DO 200 I=2,MBOT
       X=FVCHLA(K)*(DZ(I-1)+DZ(I))*.5/HMK(I)
C------ PE=(1.0-.1*ABS(X))**5/X ----------------
       A0=1.0-.1*ABS(X)
       A1=A0*A0
       PE(K,I)=A1*A1*A0/X
      PE(K,1)=0.0
 200  PE(K,MBOT+1)=0.0
      RETURN
      END
      SUBROUTINE CONMIX(ILAY,TMIX,MBOT)
C*****
C***** Remove density instabilities by mixing unstable
C***** layers downward and merging with lower layers.
C*****
      COMMON/RESULT/ T2(40),CHLATOT(40),PA2(40),PTSUM(40),BOD2(40),
     +DSO2(40),C2(40),CD2(40),XNO2(40),XNH2(40),CHLA2(3,40),
     +PC2(3,40),XNC2(3,40),T20(40),SI2(40)
      COMMON/VOL/ZMAX,DZ(40),Z(40),A(40),V(40),TV(40),ATOP(41),DBL
```

```
      DIMENSION RHOT(40)
      DO 100 I=1,MBOT
100   RHOT(I)=RHO(T2(I),0.,0.)
6     IFLAG=0
      I=0
      M=MBOT-1
1     I=I+1
      IF(I.EQ.M) GO TO 5
      IF(RHOT(I).LE.RHOT(I+1)) GO TO 1
      IFLAG=1
      IB=I
      TVDUM=T2(I)*V(I)
      VDUM=V(I)
      TDUM=TVDUM/VDUM
      RHODUM=RHO(TDUM,0.,0.)
      J=I-1
3     J=J+1
      IF(RHODUM.LE.RHOT(J+1)) GO TO 2
      IFLAG=1
      TVDUM=TVDUM+T2(J+1)*V(J+1)
      VDUM=VDUM+V(J+1)
      TDUM=TVDUM/VDUM
      RHODUM=RHO(TDUM,0.,0.)
      IF(J.EQ.M) GO TO 2
      GO TO 3
2     IE=J
      IF(J.EQ.M) IE=IE+1
      IF(IB.EQ.IE) GO TO 4
      DO 200 K=IB,IE
      T2(K)=TDUM
200   RHOT(K)=RHODUM
4     IF(I.NE.M) GO TO 1
5     IF(IFLAG.EQ.1) GO TO 6
C...DETERMINE MIXED LAYER DEPTH...
      DO 700 I=1,MBOT-1
      IF((T2(I)-T2(I+1)).LE..001) GO TO 700
      ILAY=I
      GO TO 10
700   CONTINUE
10    TMIX=T2(1)
      RETURN
      END
      SUBROUTINE MERGE(I,MBOT,LW)
C*****
C***** Merge layers that are either low volume (V < 500 m3) or
C***** too thin (DZ < DZLL).  Negative layers are also handled
C***** by reducing the volume of the next lower layer by the
C***** negative volume.
C*****
      COMMON/VOL/ZMAX,DZ(40),Z(40),A(40),V(40),TV(40),ATOP(41),DBL
      COMMON/RESULT/ T2(40),CHLATOT(40),PA2(40),PTSUM(40),BOD2(40),
     +DSO2(40),C2(40),CD2(40),XNO2(40),XNH2(40),CHLA2(3,40),
     +PC2(3,40),XNC2(3,40),T20(40),SI2(40)
      COMMON/CHOICE/MODEL,NITRO,IPRNT(6),NDAYS,NPRNT(30),NCLASS,PLOT(30)
      IF(V(I).LE.0.) THEN
        IF(I.EQ.MBOT) THEN
          II=MBOT
2         V(II-1)=V(II-1)+V(II)
          MBOT=MBOT-1
          IF(V(II-1).LE.0.0) THEN
            II=II-1
            GOTO 2
          ENDIF
          RETURN
        ENDIF
       V(I+1)=V(I)+V(I+1)
       DZZ=DZ(I)
       KK=I
       MBOT=MBOT-1
      ELSE
       II=I
       IF(I.EQ.MBOT) II=I-1
       KK=II+1
       VC=V(II)+V(KK)
       VCOMB=1./VC
       T2(II)=(T2(II)*V(II)+T2(KK)*V(KK))*VCOMB
       C2(II)=(C2(II)*V(II)+C2(KK)*V(KK))*VCOMB
       CD2(II)=(CD2(II)*V(II)+CD2(KK)*V(KK))*VCOMB
       DO 55 K=1,NCLASS
55       CHLA2(K,II)=(CHLA2(K,II)*V(II)+CHLA2(K,KK)*V(KK))*VCOMB
```

```
      IF(MODEL.EQ.3) THEN
       DO 57 K=1,NCLASS
57      PC2(K,II)=(PC2(K,II)*V(II)+PC2(K,KK)*V(KK))*VCOMB
      ENDIF
     PA2(II)=(PA2(II)*V(II)+PA2(KK)*V(KK))*VCOMB
     BOD2(II)=(BOD2(II)*V(II)+BOD2(KK)*V(KK))*VCOMB
     DSO2(II)=(DSO2(II)*V(II)+DSO2(KK)*V(KK))*VCOMB
       IF(NITRO.EQ.1) THEN
        XNH2(II)=(XNH2(II)*V(II)+XNH2(KK)*V(KK))*VCOMB
        XNO2(II)=(XNO2(II)*V(II)+XNO2(KK)*V(KK))*VCOMB
        DO 56 K=1,NCLASS
56        XNC2(K,II)=(XNC2(K,II)*V(II)+XNC2(K,KK)*V(KK))*VCOMB
       ENDIF
     V(II)=VC
     DZ(II)=DZ(II)+DZ(KK)
     Z(II)=Z(II)+DZ(KK)*0.5
     DZZ=0.0
     MBOT=MBOT-1
     IF(LW.GT.1) LW=LW-1
     IF(L.EQ.MBOT) GO TO 3
    END IF
    DO 100 K=KK,MBOT
    T2(K)=T2(K+1)
    C2(K)=C2(K+1)
    CD2(K)=CD2(K+1)
    DO 150 KI=1,NCLASS
150 CHLA2(KI,K)=CHLA2(KI,K+1)
    PA2(K)=PA2(K+1)
    BOD2(K)=BOD2(K+1)
    DSO2(K)=DSO2(K+1)
    IF(MODEL.EQ.3) THEN
     SI2(K)=SI2(K+1)
     DO 151 KI=1,3
151  PC2(KI,K)=PC2(KI,K+1)
    IF(NITRO.EQ.1) THEN
      DO 152 KI=1,3
152   XNC2(KI,K)=XNC2(KI,K+1)
      XNH2(K)=XNH2(K+1)
      XNO2(K)=XNO2(K+1)
     ENDIF
    ENDIF
    V(K)=V(K+1)
    DZ(K)=DZ(K+1)
    Z(K)=Z(K+1)-DZZ
100 CONTINUE
3   ZMAX= Z(MBOT) + 0.5*DZ(MBOT)
    RETURN
    END
    SUBROUTINE HEBUG(IL,TS,ON,HS,HA,HBR,HE,HC,
   +TAIR,TDEW,CR,RAD,WIND,IPAN,PCOEFF,SEKI)
C*****
C***** Compute the temperature profile using routines FLXOUT and
C***** FLXIN for the surface heat exchange. Solution is by the
C***** implicit central difference formulation. CONMIX called to
C***** check for and resolve density instablities between layers.
C*****
     COMMON/VOL/ZMAX,DZ(40),Z(40),A(40),V(40),TV(40),ATOP(41),DBL
     COMMON/RESULT/ T2(40),CHLATOT(40),PA2(40),PTSUM(40),BOD2(40),
    + DSO2(40),C2(40),CD2(40),XNO2(40),XNH2(40),CHLA2(3,40),
    + PC2(3,40),XNC2(3,40),T20(40),SI2(40)
     COMMON/TEMP/PARIO(4),PCDUM(3,40),XNHD(40),XNOD(40),
    + CHLADUM(3,40),XNCD(3,40),PADUM(40),SID(40)
     COMMON/STEPS/DZLL,DZUL,MBOT,NM,NPRINT,MDAY,MONTH,ILAY,DY
     COMMON/FLOW/HMK(41),QE(40),FVCHLA(5),PE(5,41)
     COMMON/WATER/BETA,EMISS,XK1,XK2,HKMAX,WCOEF,WSTR
     COMMON/SOLV/ AK(40),BK(40),CK(40),DK(40)
     DIMENSION Q(40)
C...CALCULATION OF THE HEAT ABSORPTION FROM METEOROLOGICAL PARAMETERS
C...IN A COLUMN OF WATER
C...CALCULATION OF HEAT FLUXES INTO THE WATER BODY
     CALL FLXIN(HS,HA,TAIR,RAD,CR,C2)
     CALL FLXOUT(TS,HBR,HE,HC,TAIR,TDEW,WIND,IPAN,PCOEFF,WCOEF)
     HQOUT=HBR+HE+HC
C...CALCULATION OF EXTINCTION COEFF. (ETA) AS A FUNCTION OF SUSPENDED
C...SEDIMENT CONCENTRATION
      ETA=1.84*(1/SEKI)
C...CALCULATION OF HEAT ABSORBED IN EACH LAYER
      HQ=(1.-BETA)*HS
     EX=EXP(-ETA*DZ(1))
     Q(1)=((BETA*HS+HA-HQOUT)*ATOP(1)+HQ*(ATOP(1)-EX*ATOP(2)))
    +                          /(1000.*V(1))
```

```
C_CONVERSION FACTOR OF 1000 USED FOR DENSITY*HEAT CAPACITY OF WATER
    HQ=HQ*EX
C_CALCULATE THE SOURCE TERM Q FOR EACH LAYER
    DO 10 I=2,MBOT
     ETA=1.84*(1/SEKI)
      EX=EXP(-ETA*DZ(I))
      Q(I)=HQ*(ATOP(I)-ATOP(I+1)*EX)/(1000.*V(I))
      HQ=HQ*EX
 10  CONTINUE
    CALL SETAMK(WIND,HKMAX,ILAY,MBOT)
C_SET-UP COEFFICIENTS FOR TRI-DIAGONAL MATRIX
    DO 100 I=2,MBOT-1
      D1= 2/(A(I)*DZ(I))
      D2=D1*ATOP(I)*HMK(I)/(DZ(I)+DZ(I-1))
      D3= D1*ATOP(I+1)*HMK(I+1)/(DZ(I)+DZ(I+1))
      AK(I)=-D2
      BK(I)=1.0+D2+D3
      CK(I)=-D3
      DK(I)=T2(I)+Q(I)
100   CONTINUE
    DK(1)=T2(1)+Q(1)
    DK(MBOT)=T2(MBOT)+Q(MBOT)
    AK(1)=0.
    CK(1)=-2.*ATOP(2)*HMK(2)/(A(1)*DZ(1)*(DZ(1)+DZ(2)))
    BK(1)=1.-CK(1)
    I=MBOT
    AK(I)=-2.*ATOP(I)*HMK(I)/(A(I)*DZ(I)*(DZ(I)+DZ(I-1)))
    BK(I)=1.-AK(I)
    CK(I)=0.0
C
    CALL SOLVE(T2,MBOT)
    TS =T2(1)
    CALL CONMIX(IL,TS,MBOT)
    DO 90 I=1,IL
    T2(I)=TS
 90  CONTINUE
C
C KEEP 4oC WATER TEMPERATURE
C
    IF(T2(1).LT.4.) THEN
    DO 9467 I=1,MBOT
    T2(I)=4.
 9467 CONTINUE
    ENDIF
C
    QN=HS+HA-HQOUT
    RETURN
    END
    SUBROUTINE FLXIN(HSN,HAN,TC,RAD,CC,C)
C_CALCULATION OF THE TOTAL RADIATION FLUX INTO A BODY OF WATER IN
C_FROM NET SOLAR RADIATION (HSR) AND NET ATMOSPHERIC RADIATION (HSN)
C_IN KCAL/M*M
C_IDSO JACKSON FORMULA USED FOR ATM. RADIATION
C_CONVERT AIR TEMPERATURE IN DEGREE C TO DEGREE ABSOLUTE
    TCA=TC+273.
    TCA=TCA*TCA
    HAN=1.171E-6*(1.-0.261*EXP(-7.77E-4*TC*TC))
    +*(TCA*TCA)*(1.+0.17*CC*CC)
C_CALCULATION OF NET SOLAR RADIATION AND CONVERSION TO KCAL/M*M/DAY
C_CALCULATION OF REFLECTED SOLAR RADIATION HSR
C_HSRW--- DUE TO CLEAR WATER USING KOBERGS CURVES
C_HSRS--- DUE TO SUSPENDED SEDIMENTS AT THE WATER SURFACE
    HSR=(0.087-6.76E-5*RAD+0.11*(1.-EXP(-0.01*C)))*RAD
    HSN=(RAD-HSR)*10.
    RETURN
    END
    SUBROUTINE FLXOUT (TT,HBR,HE,HC,TAIR,TD,WIND,IPAN,PCOEFF,WCOEF)
C_CALCULATES THE ENERGY FLUX OUT OF A BODY OF WATER FROM
C_EVAPORATIVE HEAT LOSS (HE), CONVECTIVE HEAT LOSS (HC), AND
C_BACK RADIATION (HBR) IN KCAL/M*M/DAY.
C_CONVERSION OF TEMP. VALUES FROM DEG. C TO DEG. ABSOLUTE
    TSK=TT+273.15
    TAK=TAIR+273.15
    FCN=WCOEF *WIND
    IF(IPAN.GT.0) GO TO 20
C_EVALUATES SATURATION VAPOR PRESSURE VALUES IN MB USING MAGNUS TETONS
C_FORMULA
    ESA=6.1078*EXP(17.2693882*TT/(TSK-35.86))
C_EVALUATES SATURATION VAPOR PRESSURE VALUE
    EA=6.0353*10.**(7.45*TD/(235.+TD))
C_CALCULATES EVAPORATIVE HEAT LOSS
```

```
      HE=FCN*(ESA-EA)
      GO TO 30
 20   HE=2.54*TD*PCOEFF*590.*10.
C_CALCULATES BACK RADIATION
 30   HBR=(1.171E-6*0.97*TSK*TSK*TSK*TSK)
C_CALCULATES CONDUCTIVE LOSS USING BOWENS RATIO
      HC=FCN*0.61793*(TSK-TAK)
      RETURN
      END
      SUBROUTINE SETAMK(W,HKMAX,ILAY,MBOT)
C*****
C***** Compute vertical diffusion coefficient in each layer.
C***** Diffusion coefficient between layers as the harmonic
C***** mean of the diffusion coefficients in adjacent layers.
C*****
      DIMENSION AMK(41)
      COMMON/FLOW/HMK(41),QE(40),FVCHLA(5),PE(5,41)
      COMMON/VOL/ZMAX,DZ(40),Z(40),A(40),V(40),TV(40),ATOP(41),DBL
      COMMON/RESULT/ T2(40),CHLATOT(40),PA2(40),PTSUM(40),BOD2(40),
     +DSO2(40),C2(40),CD2(40),XNO2(40),XNH2(40),CHLA2(3,40),
     +PC2(3,40),XNC2(3,40),T20(40),SI2(40)
      DIMENSION PSQN(40)
      AREA=(ATOP(1)/(10**6.))
      ALFA=8.17*0.0001*(AREA)**0.56
C_Vertical diffusion coefficient in the mixed layer
C_computed as a function of the wind speed
      DKM=28.*W**1.3
      IF(DKM.GT.HKMAX) THEN
      SQN=0.000075
      DKM=(ALFA/((SQN)**0.43))*8.64
      ENDIF
C
      DO 100 I=1,ILAY
      AMK(I)=DKM
 100  CONTINUE
C
C 929 FORMAT(1X,'HYPOLIMNION')
C_HMK TEMPORARILY USED TO STORE DENSITIES.
C_diffusion coefficient below the mixed layer computed as
C_a function of the square of the Brunt-Vasala frequency (SQN)
C_ SQN= (G/RHO) * d(RHO)/dZ
      DO 200 I=ILAY,MBOT
 200  HMK(I)=RHO(T2(I),C2(I),CD2(I))
C     WRITE(99,*)
      DO 300 I=ILAY+1,MBOT-1
      AVRHO=(HMK(I-1)+HMK(I+1))*0.5
      SQN=ABS(HMK(I-1)-HMK(I+1))/((Z(I+1)-Z(I-1))*AVRHO)*9.81
      PSQN(I)=SQN
      IF(SQN.LT. 0.000075) THEN
      SQN=0.000075
      ENDIF
      AMK(I)=(ALFA/((SQN)**0.43))*8.64
 300  CONTINUE
C——ASSUME AMK(MBOT-1) =  MAX AMK FOR SQN=0.000075
      AMK(MBOT)=AMK(MBOT-1)
      DO 400 I=2,MBOT
      HMK(I)=2.*AMK(I)*AMK(I-1)/(AMK(I)+AMK(I-1))
      HMK(1)=0.0
 400  CONTINUE
      RETURN
      END
      SUBROUTINE MTHDATA(MONTH,KDAYS,MYEAR)
C*****
C***** Read monthly meteorological data
C*****
      COMMON/FILE/ DIN,MET,FLO,TAPE8,TAPE1,IREC
      COMMON/MTHD/TAIR(31),TDEW(31),RAD(31),CR(31),WIND(31),
     +PR(31),DRCT(31)
      CHARACTER*16 DIN,MET,FLO,TAPE8,TAPE1
C_FIND MET DATA FOR FIRST MONTH OF SIMULATION
      IF(KDAYS.EQ.0) THEN
       MTH=MONTH
       MYR=MYEAR
       READ(9,*)MONTH,KDAYS,MYEAR
       IF(MONTH.EQ.MTH.AND.MYR.EQ.MYEAR) GO TO 20
      ELSE
      READ(9,*) MONTH,KDAYS,MYEAR
      ENDIF
C_READ IN MONTH, NO. OF DAYS IN THE MONTH AND YEAR
C_READ IN AIR TEMP. AND DEW PT. TEMP. IN CELSIUS, WIND VELOCITY IN
C_M.P.H., SOLAR RADIATION IN LANGELY/DAY AND CLOUD COVER IN TENTHS
```

```
20  CONTINUE
    DO 104 K=1,KDAYS
    READ(9,*) TAIR(K),TDEW(K),WIND(K),DRCT(K),RAD(K),CR(K),PR(K)
    PR(K)=PR(K)/100.
104 CONTINUE
    DO 100 K=1,KDAYS
     TAIR(K)=(TAIR(K)-32.)*0.5556
     TDEW(K)=(TDEW(K)-32.)*0.5556
100  CR(K)=(100.-CR(K))*.01
C
C MAKE CORRECTIONS FOR CLIMATE MODEL OUTPUT
C IF NEEDED. THESE ARE MONTHLY ADJUSTMENTS.
C
C     DO 1287 K=1,KDAYS
C     IF(MONTH.EQ.3) THEN
C     TAIR(K)=TAIR(K)+4.80
C     TDEW(K)=TDEW(K)+7.25
C     WIND(K)=WIND(K)*0.82
C     RAD(K)=RAD(K)*1.04
C     PR(K)=PR(K)*1.02
C     ENDIF
C     IF(MONTH.EQ.4) THEN
C     TAIR(K)=TAIR(K)+4.97
C     TDEW(K)=TDEW(K)+4.49
C     WIND(K)=WIND(K)*0.85
C     RAD(K)=RAD(K)*1.0
C     PR(K)=PR(K)*1.17
C     ENDIF
C     IF(MONTH.EQ.5) THEN
C     TAIR(K)=TAIR(K)+1.54
C     TDEW(K)=TDEW(K)+1.96
C     WIND(K)=WIND(K)*0.57
C     RAD(K)=RAD(K)*1.04
C     PR(K)=PR(K)*0.86
C     ENDIF
C     IF(MONTH.EQ.6) THEN
C     TAIR(K)=TAIR(K)+3.51
C     TDEW(K)=TDEW(K)+5.20
C     WIND(K)=WIND(K)*0.74
C     RAD(K)=RAD(K)*1.00
C     PR(K)=PR(K)*1.33
C     ENDIF
C     IF(MONTH.EQ.7) THEN
C     TAIR(K)=TAIR(K)+2.59
C     TDEW(K)=TDEW(K)+2.14
C     WIND(K)=WIND(K)*0.75
C     RAD(K)=RAD(K)*0.97
C     PR(K)=PR(K)*0.97
C     ENDIF
C     IF(MONTH.EQ.8) THEN
C     TAIR(K)=TAIR(K)+2.80
C     TDEW(K)=TDEW(K)+3.06
C     WIND(K)=WIND(K)*0.88
C     RAD(K)=RAD(K)*0.96
C     PR(K)=PR(K)*1.35
C     ENDIF
C     IF(MONTH.EQ.9) THEN
C     TAIR(K)=TAIR(K)+3.96
C     TDEW(K)=TDEW(K)+2.66
C     WIND(K)=WIND(K)*0.81
C     RAD(K)=RAD(K)*1.01
C     PR(K)=PR(K)*1.96
C     ENDIF
C     IF(MONTH.EQ.10) THEN
C     TAIR(K)=TAIR(K)+3.89
C     TDEW(K)=TDEW(K)+3.90
C     WIND(K)=WIND(K)*0.73
C     RAD(K)=RAD(K)*0.97
C     PR(K)=PR(K)*1.24
C     ENDIF
C     IF(MONTH.EQ.11) THEN
C     TAIR(K)=TAIR(K)+5.93
C     TDEW(K)=TDEW(K)+5.51
C     WIND(K)=WIND(K)*1.06
C     RAD(K)=RAD(K)*0.95
C     PR(K)=PR(K)*1.16
C     ENDIF
C 1287 CONTINUE
 1001 FORMAT(//,5X,70('*'),//,20X,'PROGRAM ABORTED.',/,10X,
   + 'METEOROLOGICAL DATA FILE DOES NOT',/,15X,
   + 'MATCH YEAR OF SIMULATION',//,5X,70('*'))
```

```
      RETURN
      END
      SUBROUTINE PMETE(HS,RAD,HA,WIND,HBR,P,HE,TAIR,HC,TDEW,HED,HEV,
     +QNET,DMIX,ZEUPH,SECCHI)
C*****
C***** Output table of meteorological and heat flux values
C*****
      COMMON/FILE/ DIN,MET,FLO,TAPE8,TAPE1,IREC
      CHARACTER*16 DIN,MET,FLO,TAPE8,TAPE1
      COMMON/STEPS/DZLL,DZUL,MBOT,NM,NPRINT,MDAY,MONTH,ILAY,DY
C
      WRITE(8,2000) HS,RAD,HA,WIND,HBR,P,HE,TAIR,HC,TDEW,HED,HEV,
     +QNET,DMIX,ZEUPH,SECCHI
C
2000  FORMAT(/,5X,26HMETEOROLOGICAL INFORMATION,/,5X,26(1H-),
     +/,7X,17HNET SOLAR RAD. = ,4X,F9.2,13H KCAL/M*M/DAY,
     +25X,13HSOLAR RAD. = , 9X,F6.1,8H LANGLEY,
     +/,7X,16HNET ATM. RAD. = ,5X,F9.2,13H KCAL/M*M/DAY,
     +25X,16HWIND VELOCITY = , 7X,F5.1,7H M.P.H.,
     +/,7X,12HBACK RAD. = , 9X,F9.2,13H KCAL/M*M/DAY,
     +25X,16HPRECIPITATION = , 8X,F6.3,13H METER(S)/DAY,
     +/,7X,19HEVAPORATIVE LOSS = ,2X,F9.2,13H KCAL/M*M/DAY,
     +25X,12HAIR TEMP. = ,12X,F5.2,10H DEGREES C,
     +/,7X,20HCONDENSATION LOSS = , 1X,F9.2,13H KCAL/M*M/DAY,
     +25X,16HDEW PT. TEMP. = , 8X,F5.2,10H DEGREES C,
     +/,7X,20HEV. HEAT TRANSFER = ,5X,F7.4,10H M/DAY OR ,E10.4,7H M**3/D
     +2HAY,/,7X,19HNET HEAT FLUX IN = , 2X,F9.2,9H KCAL/M*M,
     +/,7X,' MIXED LAYER DEPTH (M)=',2X,F5.2,
     +38X,'EUPHOTIC DEPTH (M) =',2X,F5.2,
     +/8X,'SECCHI DEPTH (M) =',7X,F5.2)
      RETURN
      END
      SUBROUTINE SETUP
C*****
C***** Determine the initial thickness, volume, and area of layers
C***** and the total volume of above each layer from the depths given
C***** in the input data file.
C*****
      COMMON/VOL/ZMAX,DZ(40),Z(40),A(40),V(40),TV(40),ATOP(41),DBL
      COMMON/STEPS/DZLL,DZUL,MBOT,NM,NPRINT,MDAY,MONTH,ILAY,DY
      DZ(MBOT)=ZMAX-(Z(MBOT)+Z(MBOT-1))*.5
      Z(MBOT)=ZMAX-DZ(MBOT)*.5
      CALL LAKE(DZ(MBOT),VDUM,0,3)
      V(MBOT)=VDUM
      AZ=DZ(MBOT)
      TV(MBOT)=V(MBOT)
      DO 10 I=1,MBOT-2
      II=MBOT-I
      DZ(II)=Z(II+1)-(DZ(II+1)+Z(II)+Z(II-1))*.5
      Z(II)=(DZ(II)+Z(II)+Z(II-1))*.5
      AZ=AZ+DZ(II)
      CALL LAKE(AZ,VDUM,0,3)
      TV(II)=VDUM
      V(II)=TV(II)-TV(II+1)
 10   CONTINUE
      DZ(1)=Z(2)-DZ(2)*.5
      AZ=AZ+DZ(1)
      CALL LAKE(AZ,VDUM,0,3)
      TV(1)=VDUM
      V(1)=TV(1)-TV(2)
      RETURN
      END
      FUNCTION RHO (T,C,CD)
C_CALCULATES THE DENSITY OF WATER AS A FUNCTION OF TEMPERATURE PLUS
C_DENSITY DUE TO TOTAL SOLIDS (SUSPENDED AND DISSOLVED)
      RHO=(.999878+T*(6.16606E-5+T*(-8.14577E-6+T*4.76102E-8)))*1000.
     + +(C+CD)*0.001
      RETURN
      END
      SUBROUTINE SETZ(MBOT)
C*****
C***** Compute Z from DZ for each layer
C*****
      COMMON/VOL/ZMAX,DZ(40),Z(40),A(40),V(40),TV(40),ATOP(41),DBL
      AZ=0.
      DO 100 I=1,MBOT
      Z(I)=AZ+DZ(I)*.5
      AZ=AZ+DZ(I)
 100  CONTINUE
      RETURN
      END
```

```
      SUBROUTINE SOLVE(VAR2,MBOT)
C*****
C***** Tri-diagonal matrix solving routine
C*****
      COMMON/SOLV/ AK(40),BK(40),CK(40),DK(40)
      DIMENSION VAR2(40),TX(40)
      DO 60 I=2,MBOT
        TT=AK(I)/BK(I-1)
        BK(I)=BK(I)-CK(I-1)*TT
 60     DK(I)=DK(I)-DK(I-1)*TT
C**********BACK SUBSTITUTION**************
      TX(MBOT)=DK(MBOT)/BK(MBOT)
      DO 70 I=1,MBOT-1
        J=MBOT-I
 70     TX(J)=(DK(J)-CK(J)*TX(J+1))/BK(J)
      DO  80 I=1,MBOT
 80   VAR2(I)=(TX(I))
      RETURN
      END
      SUBROUTINE SPLIT(I,LW)
C*****
C***** Routine to split thick layers (DZ > DZUL) into two or more
C***** layers of equal thickness. All state variables are the same in
C***** each new layer. Volume is adjusted later.
C*****
      COMMON/VOL/ZMAX,DZ(40),Z(40),A(40),V(40),TV(40),ATOP(41),DBL
      COMMON/CHOICE/MODEL,NITRO,IPRNT(6),NDAYS,NPRNT(30),NCLASS,PLOT(30)
      COMMON/RESULT/ T2(40),CHLATOT(40),PA2(40),PTSUM(40),BOD2(40),
     +DSO2(40),C2(40),CD2(40),XNO2(40),XNH2(40),CHLA2(3,40),
     +PC2(3,40),XNC2(3,40),T20(40),SI2(40)
      COMMON/STEPS/DZLL,DZUL,MBOT,NM,NPRINT,MDAY,MONTH,ILAY,DY
      DO 100 K=I,MBOT
      II=MBOT+I-K
      T2(II+1)=T2(II)
      C2(II+1)=C2(II)
      CD2(II+1)=CD2(II)
      DO 50 KI=1,NCLASS
 50   CHLA2(KI,II+1)=CHLA2(KI,II)
      PA2(II+1)=PA2(II)
      BOD2(II+1)=BOD2(II)
      DSO2(II+1)=DSO2(II)
      IF(MODEL.EQ.3) THEN
       SI2(II+1)=SI2(II)
       DO 51 KI=1,3
 51    PC2(KI,II+1)=PC2(KI,II)
       IF(NITRO.EQ.1) THEN
        DO 52 KI=1,3
 52     XNC2(KI,II+1)=XNC2(KI,II)
        XNO2(II+1)=XNO2(II)
        XNH2(II+1)=XNH2(II)
       ENDIF
      ENDIF
      DZ(II+1)=DZ(II)
 100  CONTINUE
      MBOT=MBOT+1
      DZ(I+1)=DZ(I)*0.5
      DZ(I)=DZ(I+1)
      IF(LW.GE.I) LW=LW+1
      RETURN
      END
      SUBROUTINE START(ST,S,FT,ISTART,INFLOW,MYEAR,IRUN,LEN&SEKI)
C*****
C***** Routine to read the input data file for initial
C***** conditions and input coefficients
C*****
      COMMON/RESULT/ T2(40),CHLATOT(40),PA2(40),PTSUM(40),BOD2(40),
     +DSO2(40),C2(40),CD2(40),XNO2(40),XNH2(40),CHLA2(3,40),
     +PC2(3,40),XNC2(3,40),T20(40),SI2(40)
      COMMON/TEMP/PARIO(4),PCDUM(3,40),XNHD(40),XNOD(40),
     + CHLADUM(3,40),XNCD(3,40),PADUM(40),SID(40)
      COMMON/CHOICE/MODEL,NITRO,IPRNT(6),NDAYS,NPRNT(30),NCLASS,PLOT(30)
      COMMON/CHANEL/WCHANL,ELCB,ALPHA,BW,WLAKE
      COMMON/WATER/BETA,EMISS,XK1,XK2,HKMAX,WCOEF,WSTR
      COMMON/STEPS/DZLL,DZUL,MBOT,NM,NPRINT,MDAY,MONTH,ILAY,DY
      COMMON/VOL/ZMAX,DZ(40),Z(40),A(40),V(40),TV(40),ATOP(41),DBL
      COMMON/FLOW/HMK(41),QE(40),FVCHLA(5),PE(5,41)
      COMMON/FILE/ DIN,MET,FLO,TAPE8,TAPE1,IREC
      CHARACTER*16 DIN,MET,FLO,TAPE8,TAPE1
      CHARACTER*1 T1(16)
      EQUIVALENCE (T1(1),TAPE1)
      IRUN=IRUN
```

```
      NITRO=0
      DO 200 I=1,30
200   NPRNT(I)=0
C********* INPUT MODEL OPTIONS AND INITIAL CONDITIONS ******
      READ(7,*) SEKI
       WRITE(*,1006)
       READ(*,'(A)') X
        IF(X.EQ.'Y' .OR. X.EQ.'y') THEN
        IPRNT(2)=1
        TAPE1=TAPE8
        T1(LEN8+2)='O'
        T1(LEN8+3)='U'
        OPEN(2,FILE=TAPE1,STATUS='NEW')
      ENDIF
      IPRNT(4)=0
1000 FORMAT(' PLOT FILE TO BE CREATED  (Y/N) ?      '\)
1001 FORMAT(A1)
1004 FORMAT(' ENTER UP TO 10 DEPTHS TO BE SAVED '/,
    +'  END WITH A CHARACTER (#,#,#,...,X) :  '\)
1006 FORMAT(' OUTFLOW FILE TO BE CREATED  (Y/N) ?    '\)
      READ(7,*) NDAYS
      IF(NDAYS.GT.0) READ(7,*)(NPRNT(I),I=1,NDAYS)
      READ(7,*)  DZLL,DZUL,BETA,EMISS,WCOEF,WSTR
      READ(7,*)  WCHANL,WLAKE,DBL,ST,S,FT
      READ(7,*)  ELCB,ALPHA,BW
*     READ(7,*)  MBOT,NM,NPRINT,INFLOW,DY,MONTH,ISTART,MYEAR
      READ(7,*)  (Z(I),I=1,MBOT)
      READ(7,*)  (T2(I),I=1,MBOT)
1500 FORMAT( /,  5X,
     +/,5X,41HMINIMUM THICKNESS OF EACH LAYER (DZLL) = ,F5.2,9H METER(S)
     +/,5X,41HMAXIMUM THICKNESS OF EACH LAYER (DZUL) = ,F5.2,9H METER(S)
     +/,5X,40HSURFACE ABSORPTION COEFFICIENT (BETA) = ,F5.2,
     +/,5X,30HEMISSIVITY OF WATER (EMISS) = ,F5.2,
     +/,5X,'EXTINCTION COEFF. OF WATER (XK1) = ',F5.2,3X,'M**-1',
     +/,5X,'EXTINCTION COEFF. OF CHLA  (XK2) = ',F5.2,3X,'L/MG/M',
     +/,5X,'MAX. HYPOLIMNETIC DIFFUSIVITY (HKMAX) = ',F7.4,' M**2/D',
     +/,5X,'WIND FUNCTION COEFFICIENT (WCOEF) = ',F6.3,
     +/,5X,'WIND SHELTERING COEFFICIENT (WSTR)= ',F6.3/,
     +/,5X,34HWIDTH OF INLET CHANNEL (WCHANL) = ,F6.2,9H METER(S))
1501 FORMAT(5X,'LONGITUDINAL LENGTH OF LAKE (WLAKE) =',F10.2,7H METERS,
     +/,5X,30HDEEPEST BED ELEVATION (DBL) = ,F8.2,17H METERS ABOVE MSL,
     +/,5X,26HINITIAL LAKE STAGE (ST) = ,F8.2,17H METERS ABOVE MSL,
     +/,5X,16HBED SLOPE (S) = ,F10.8,
     +/,5X,29HROUGHNESS COEFFICIENT (FT) = ,F6.4,
     +//,5X,48HELEVATION OF BOTTOM OF OUTFLOW CHANNEL (ELCB) = ,F6.2,
     +17H METERS ABOVE MSL,
     +/,5X,40HSIDE-SLOPE OF OUTFLOW CHANNEL (ALPHA) = ,F6.2,8H DEGREES,
     +/,5X,31HBOTTOM WIDTH OF CHANNEL (BW) = ,F6.2,7H METERS,
     +//,5X,34HINITIAL NUMBER OF LAYERS (MBOT) = ,I2,
     +/,5X,37HNUMBER OF MONTHS OF SIMULATION (NM) = ,I2,
     +/,5X,54HDAY OF MONTH OF THE FIRST DAY OF SIMULATION (ISTART) = ,I2
     +/,5X,53HINTERVAL AT WHICH RESULTS WILL BE PRINTED (NPRINT) = ,I3,
     +7H DAY(S))
C********** INPUT PARAMETERS FOR BIOLOGICAL ROUTINES *****
  2   FORMAT(//1X,'ENTER CHANGES: INTEGER,NEW VALUE'/,
     + 5X,'(ENTER ANY CHARACTER FOR NO CHANGES):  '\)
1950  FORMAT(/,2X,'BIOLOGICAL COEFFICIENTS'/,2X,23('-')//,10X,
     + 'CARBON-CHLOROPHYLL RATIO',5X,F5.0,/,10X,'MAX. NUTRIENT '
     + 'SATURATED PHOTOSYNTHETIC RATE',3X,F5.3,'  /DAY'/,10X,
     + 'MINIMUM CELL QUOTA FOR PHOSPHORUS',3X,F5.3,/,10X,
     + 'MORTALITY RATE',3X,F6.3,'  /DAY'/)
2000 FORMAT(//,4X,'BODK20',4X,'SB20',5X,'BRR',5X,'FVBOD',/,3X,
     +'(1/DAY)',2(2X,'(GM/M2)'),3X,'(M/S)'/,2X,5(F7.3,2X))
      RETURN
      END
      SUBROUTINE STATS(FLDATA,XX,IFLAG,DEPTH,I)
C*****
C***** Compute statistics and statisitical quantities with
C***** Y designating field data and X designating model results
C*****
      COMMON/STAT/SUMXY(10),SUMX(10),SUMY(10),XSQ(10),
     +YSQ(10),RSQ(10),RMS(10),RELM(10),MTHREL(10),MDAYREL(10),ZREL(10),
     +ZRELM(10),RS(10),REL(10),MTHRMS(10),MDAYRMS(10),ZRS(10),ZRMS(10)
      COMMON/STEPS/DZLL,DZUL,MBOT,NM,NPRINT,MDAY,MONTH,ILAY,DY
      SUMXY(I)=SUMXY(I)+FLDATA*XX
      SUMX(I)=SUMX(I)+XX
      SUMY(I)=SUMY(I)+FLDATA
      XSQ(I)=XSQ(I)+XX*XX
      YSQ(I)=YSQ(I)+FLDATA*FLDATA
      XX=XX-FLDATA
      X2=XX/FLDATA*100.
```

```
      X3=ABS(XX)
      IF(X2.GT.ABS(REL(I))) THEN
       REL(I)=X2
       ZREL(I)=DEPTH
      ENDIF
      IF(X2.GT.ABS(RELM(I))) THEN
       RELM(I)=X2
       MTHREL(I)=MONTH
       MDAYREL(I)=MDAY
       ZREL(I)=DEPTH
      ENDIF
      IF(X3.GT.ABS(RS(I))) THEN
       RS(I)=XX
       ZRS(I)=DEPTH
      ENDIF
      IF(X3.GT.ABS(RMS(I))) THEN
       RMS(I)=XX
       MTHRMS(I)=MONTH
       MDAYRMS(I)=MDAY
       ZRMS(I)=DEPTH
      ENDIF
      IFLAG=IFLAG+1
      RETURN
      END
      SUBROUTINE THICKNS(MBOT)
C*****
C***** Compute thickness of each layer from the depth
C***** area curve in LAKE.
C*****
      COMMON/VOL/ZMAX,DZ(40),Z(40),A(40),V(40),TV(40),ATOP(41),DBL
      AZ=0.
      AVOL=0.
      DO 100 I=1,MBOT
      II=MBOT+1-I
      AVOL=AVOL+V(II)
      CALL LAKE(ZDUM,AVOL,0,4)
      DZ(II)=ZDUM-AZ
      AZ=AZ+DZ(II)
  100 CONTINUE
      RETURN
      END
      SUBROUTINE TVOL(MBOT)
C*****
C***** Determine the volume of water above a layer
C*****
      COMMON/VOL/ZMAX,DZ(40),Z(40),A(40),V(40),TV(40),ATOP(41),DBL
      SUM=0.
      DO 100 I=1,MBOT
      SUM=SUM+V(I)
      TV(I)=SUM
  100 CONTINUE
       RETURN
      END
      SUBROUTINE WINEN(T,V,WIND)
C_
C_CALCULATION OF THE SHEAR VELOCITY AND THE WIND SHEAR STRESS
C_CONVERSION OF WIND SPEED FROM M.P.H. TO M/S
C_DENSITY OF WATER AND AIR ASSUMED TO BE 1000 AND 1.177 KG/M3
C_
      W=WIND*0.447
      CALL LAKE(FTCH,0,0,0,2)
      ZB=ALOG(FTCH)*0.8-1.0718
      W=W*1.666667*(ZB+4.6052)/(ZB+9.2103)
C_CALCULATION OF WIND SHEAR STRESS
      CZ=SQRT(W)*.0005
      IF(W.GE.15.) CZ=.0026
      T=1.177*CZ*W*W
C_ASSIGNMENT OF CHARACTERISTIC SURFACE VELOCITY
C_USING CALCULATION OF SHEAR VELOCITIES
      V=.0343*SQRT(CZ)*W
      RETURN
      END
      SUBROUTINE WINMIX(E,TS,IL,MBOT)
C_
C_CALCULATE THE AMOUNT OF ENTRAINMENT RESULTING FROM WIND MIXING.
C_USE THE DEPTH OF CENTER OF MASS OF MIXED LAYER TO DETERMINE THE
C_POTENTIAL ENERGY THAT MUST BE OVERCOME BY THE KINECTIC ENERGY
C_OF THE WIND FOR ENTRAINMENT TO OCCUR.
C_
      COMMON/VOL/ZMAX,DZ(40),Z(40),A(40),V(40),TV(40),ATOP(41),DBL
      COMMON/RESULT/ T2(40),CHLATOT(40),PA2(40),PTSUM(40),BOD2(40),
```

```
     +DSO2(40),C2(40),CD2(40),XNO2(40),XNH2(40),CHLA2(3,40),
     +PC2(3,40),XNC2(3,40),T20(40),SI2(40)
      IF(IL.GE.MBOT) GO TO 35
      SUM1=0.
      SUM2=0.
      DO 10 I=1,IL
      ILAY=I
      RV=RHO(T2(I),C2(I),CD2(I))*V(I)
      SUM1=SUM1+RV
 10   SUM2=SUM2+RV*Z(I)
      I=ILAY
 20   DCM=SUM2/SUM1
      TSTEP=T2(I+1)
C...CALCULATION OF POTENTIAL ENERGY OF MIXED LAYER
      PE=9.81*TV(I)*(Z(I)+(DZ(I)/2.)-DCM)*(RHO(TSTEP,C2(I+1),CD2(I+1))
     +-RHO(TS,C2(I),CD2(I)))
C...CRITERIA FOR ENTRAINMENT
      IF( E.LT.PE) GO TO 40
C...ENTRAINMENT OF LAYER I+1
      I=I+1
      TS=(TS*TV(I-1)+TSTEP*V(I))/TV(I)
      IF(I.GE.MBOT) GO TO 40
      RV=RHO(T2(I),C2(I),CD2(I))*V(I)
      SUM1=SUM1+RV
      SUM2=SUM2+RV*Z(I)
      GO TO 20
 35   I=IL
 40   IL=I
      DO 50 K=1,IL
 50   T2(K)=TS
      RETURN
      END
      SUBROUTINE VOLUME(MBOT)
C*****
C***** Compute the volume of each layer based on the depth-volume
C***** relationship found in LAKE.
C*****
      COMMON/VOL/ ZMAX,DZ(40),Z(40),A(40),V(40),TV(40),ATOP(41),DBL
      AZZ=0.
      CALL LAKE(ZMAX,VDUM,0,3)
      VZ=VDUM
      DO 100 I=1,MBOT-1
        AZZ=DZ(I)+AZZ
        Z2=ZMAX-AZZ
        CALL LAKE(Z2,VDUM,0,3)
        V(I)= VZ-VDUM
 100    VZ=VDUM
      V(MBOT)=VZ
      RETURN
      END
```

LAKE SPECIFIC SUBROUTINE

Area computation section
Depth-area functions of the form AREA=f(ZMAX-Z), written as DUM=f(ZD). AREA(m^2), Z(m).

Fetch computation section
The longest distance across the lake surface area in the wind direction (m).

Volume computation section
Volume-depth functions of the form VOLUME(below depth Z)=f(ZMAX-Z), written as ZD=f(DUM). VOLUME (m^3), Z(m).

EXAMPLE LAKE SPECIFIC SUBROUTINE

```
      SUBROUTINE LAKE(ZD,DUM,NFLOW,ID)
      COMMON/MTHD/TAIR(31),TDEW(31),RAD(31),CR(31),WIND(31),
     + PR(31),DRCT(31)
      COMMON/RESULT/ T2(40),CHLATOT(40),PA2(40),PTSUM(40),BOD2(40),
     +DSO2(40),C2(40),CD2(40),XNO2(40),XNH2(40),CHLA2(3,40),
     +PC2(3,40),XNC2(3,40),T20(40),SI2(40)
      COMMON/SOURCE/RM(3,40),PROD(40),XMR(3,40),PRODSUM(40)
      COMMON/FLOW/HMK(41),QE(40),FVCHLA(5),PE(5,41)
      COMMON/TEMP/PARIO(4),PCDUM(3,40),XNHD(40),XNOD(40),
     + CHLADUM(3,40),XNCD(3,40),PADUM(40),SID(40)
      COMMON/VOL/ZMAX,DZ(40),Z(40),A(40),V(40),TV(40),ATOP(41),DBL
      COMMON/SUB/SDZ(60),SZ(60),LAY(40),AVGI(4,60),SVOL(60)
      COMMON/CHOICE/MODEL,NITRO,IPRNT(6),NDAYS,NPRNT(30),NCLASS,PLT(30)
      COMMON/WATER/BETA,EMISS,XK1,XK2,HKMAX,WCOEF,WSTR
      COMMON/CHANEL/WCHANL,ELCB,ALPHA,BW,WLAKE
      COMMON/STEPS/DZLL,DZUL,MBOT,NM,NPRINT,MDAY,MONTH,ILAY,DY
      COMMON/STAT/SUMXY(10),SUMX(10),SUMY(10),XSQ(10),
     +YSQ(10),RSQ(10),RMS(10),RELM(10),MTHREL(10),MDAYREL(10),ZREL(10),
     +ZRELM(10),RS(10),REL(10),MTHRMS(10),MDAYRMS(10),ZRS(10),ZRMS(10)
      COMMON/INFLOW/QIN(5),TIN(5),PAIN(5),BODIN(5),DOIN(5),CIN(5),
     +CDIN(5),XNHIN(5),XNOIN(5),CHLAIN(3,5)
      COMMON/FIELD/ IFLAG(10),FLDATA(10,50),DEPTH(50),NFLD(10),SD
      COMMON/FILE/ DIN,MET,FLO,TAPE8,TAPE1,IREC
      COMMON/TITL/ TITLE
      CHARACTER*16 DIN,MET,FLO,TAPE8,TAPE1
      GOTO(100,200,300,400,500,600,700,800,900,1000,1100,1200,1300) ID
      NFLOW=NFLOW
C********* AREA COMPUTATION SECTION ***********
100   CONTINUE
      ASURF=1.71E6
      DUM=0.00896*ASURF*(ZD+1.)**1.46209
      RETURN
C********** FETCH COMPUTATION SECTION *********
 200  ZD=sqrt(4./3.1459*ASURF)
      RETURN
C********** VOLUME COMPUTATION SECTION *****
300   CONTINUE
1234  ASURF=1.71E6
      CONS=0.00364*ASURF
      DUM=CONS*(ZD+1.)**2.46209
      RETURN
C***** COMPUTE DEPTH FROM VOLUME *****
400   CONS=0.00364*ASURF
      DUM1=DUM/CONS
      ZD=(DUM1**0.40616)-1.
      RETURN
C***** WRITE ON THE SCREEN, DAY, MONTH ****
 500  WRITE(*,501) MONTH,MDAY
 501  FORMAT(2X,' month',i3,' day ',i2)
C***** WRITE EPILIMNION & HYPOLIMNION TEMPERATURES ****
      DO 11111 I=1,MBOT
      IF (I.EQ.2) THEN
      WRITE (21,871) MONTH,MDAY,Z(I),T2(I)
      ENDIF
      IF (I.EQ.22) THEN
      WRITE (22,871) MONTH,MDAY,Z(I),T2(I)
      ENDIF
 871  FORMAT(1X,I4,1X,I4,2X,F9.2,3X,F9.3)
11111 CONTINUE
      RETURN
 600  RETURN
 700  RETURN
 800  RETURN
 900  RETURN
 1000 RETURN
 1100 RETURN
 1200 CONTINUE
 1300 CONTINUE
      RETURN
      END
```